DISS. ETH NR. 23671

The Source for Ultracold Neutrons at the Paul Scherrer Institute
—
Characterisation, Optimisation, and International Comparison

ABHANDLUNG

zur Erlangung des Titels

DOKTOR DER WISSENSCHAFTEN

der

ETH ZÜRICH

(Dr. sc. ETH Zürich)

vorgelegt von

Dieter Achim Ries

MSc ETH Physik, ETH Zürich

geboren am 08.12.1986

aus Deutschland

Angenommen auf Antrag von

Prof. Klaus Kirch

Prof. Günther Dissertori

Dr. Bernhard Lauss

2016

Abstract

The source for ultracold neutrons (UCN) at the Paul Scherrer Institute (PSI) is in regular operation since 2011. This work describes characterisations and optimisations done since beginning of proton accelerator operation in 2012. A description of parts of the UCN source relevant to this work is given first, followed by several measurements of the performance of individual subsystems. These characterisation measurements are important in order to verify calculations and models of the source operation.

Since 2012 the number of UCN produced per unit time at the UCN source has approximately doubled. Multiple optimisations, both to the performance of the UCN source and to the environment for users are described in this thesis.

At the time of this writing, the PSI UCN source is one of five operating general purpose UCN sources. Prior to this work, no quantitative comparison of these sources had been done. A robust and mobile setup for the determination of UCN densities available to experiments at a given UCN source, one of the most important benchmark parameters of any UCN source, was developed and is described and characterised in this work. Using this setup, a world-wide comparison of all operating UCN sources was performed in 2015, which is also documented in this work.

Zusammenfassung

Die Quelle für ultrakalte Neutronen (UCN) am Paul Scherrer Institut (PSI) ist seit 2011 in Betrieb. In dieser Arbeit werden Charakterisierungen und Optimierungen seit Beginn des Beschleunigerbetriebs 2012 beschrieben. Zuerst wird eine Beschreibung von für diese Arbeit relevanten Teilen der UCN Quelle gegeben, gefolgt von der Beschreibung mehrerer Charakterisierungsmessungen individueller Subsysteme der Quelle. Diese Charakterisierungsmessungen sind wichtig um Berechnungen und Modelle des Quellenbetriebs zu verifizieren.

Seit 2012 hat sich die Anzahl der pro Zeit produzierbaren UCN der Quelle etwa verdoppelt. Mehrere Optimierungen, sowohl der Quelle selbst als auch der Benutzerumgebung der Quelle, werden in dieser Dissertation beschrieben.

Zur Zeit der Abfassung dieser Dissertation ist die UCN Quelle am PSI eine von fünf in Betrieb befindlichen, allgemein zugänglichen UCN Quellen. Vor dieser Arbeit ist kein quantitativer Vergleich dieser Quellen vorgenommen worden. Ein robuster und transportabler Aufbau zur Ermittlung der UCN Dichte, die an einer Quelle zur Verfügung steht wurde im Rahmen dieser Arbeit entwickelt, beschrieben und charakterisiert. Die UCN Dichte in experimenten ist eines der wichtigsten Vergleichskriterien von UCN Quellen. Mit diesem Aufbau wurden im Jahr 2015 alle in Betrieb befindlichen UCN Quellen weltweit verglichen. Diese Vergleichsmessungen sind auch in dieser Arbeit dokumentiert.

Contents

List of Figures

List of Tables

Chapter 1

Ultracold Neutrons

1.1   History

In 1946 Fermi and Zinn reported on measurements performed at the CP-3 reactor in 1944, where they for the first time observed total reflection of neutrons [Fermi, E. and Zinn, W.H., 1946].

They were using a collimated beam of thermal neutrons, which was reflected from polished surfaces of several materials under small angles of incidence. An example of their results is shown in Fig. 1.1.
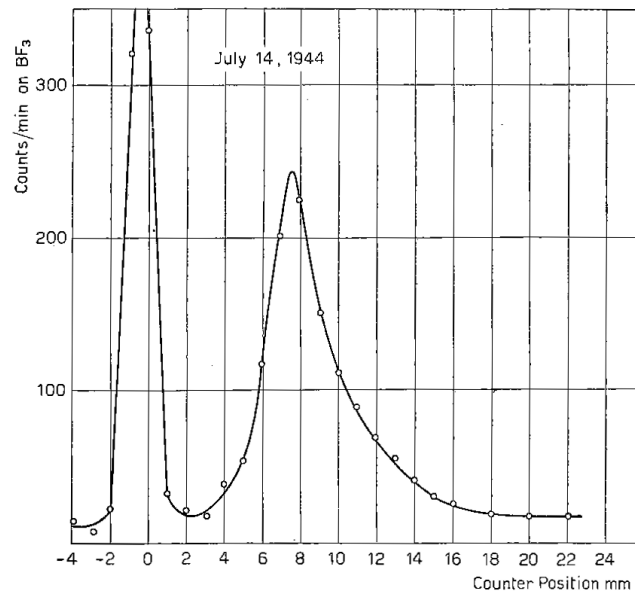
Fig. 1. – Graphite mirror. Glancing angle 3 minutes. Refected beam displaced 0.8 cm.

Figure 1.1: *Original measurement of Fermi and Zinn showing two peaks in the neutron counts plotted against the posistion of the neutron detector. The first peak originates from the not reflected neutron beam, the second corresponds to neutrons being reflected at an angle of 0.05° on a polished graphite mirror. Illustration from [Fermi, E. and Zinn, W, 1944] with written permission from Accademia Nazionale dei Lincei.*

Already in 1936 Fermi and Amaldi had predicted a material specific potential for slow neutrons in the vicinity of bound nuclei, which for certain materials could be repulsive [Fermi, E. and Amaldi, E, 1936]. This led Zel'dovich to propose the storage of very slow neutrons in material bottles in 1959. The neutrons would be surrounded by materials with high optical potentials (now also known as "Fermi potentials"), like carbon and beryllium. Like this, they could be trapped for several minutes if their kinetic energy was less than the repulsive Fermi potential, because they would be totally reflected from the walls under any angle of incidence [Zel'dovich, Z. B., 1959].

About ten years later, Lushchikov, Shapiro, and others measured that neutrons diffused through a hollow copper tube for approximately 200 s, and could therefore be considered stored [Lushikov et al., 1969].

Shapiro was the first to realise in 1968 that storable neutrons could open the door to more precise measurements of the free neutron lifetime and searches for a non-zero electric dipole moment of the neutron [Shapiro, 1968]. He was also responsible for coining the term "ultracold" neutrons.

1.2   Definition

Today, ultracold neutrons, or UCN, are typically defined as neutrons with kinetic energies below the Fermi potential of ^{58}Ni, V_F = 335 neV, which is the material with the highest Fermi potential in practical use. UCN can be totally reflected under any angle of incidence from surfaces made from or coated with ^{58}Ni, and can therefore be stored in material bottles for times up to their β-decay lifetime. This kinetic energy corresponds to a velocity of 8 m s^{-1}, which is extraordinarily slow for an elementary particle. Slow neutrons are typically named after the equilibrium temperature their velocities correspond to. For UCN this temperature can be calculated to be 3.9 mK.

1.3   Interactions

UCN interact with all four fundamental forces. They are subject to the Fermi potential, which originates in the *strong nuclear force* and leads to the reflection of UCN from certain materials. After approximately 880 s [Serebrov et al., 2005, Pichlmaier et al., 2010, Arzumanov et al., 2012], UCN β-decay into a proton, an electron, and an electron antineutrino due to the *weak nuclear force*. UCN are massive particles, and as such subject to *gravity*. A UCN with a velocity of 8 m s^{-1} pointing upwards will only rise 3.3 m before falling back down. The potential energy of UCN in the earth's gravitational field is ΔV = 102.5 neV m^{-1}. Although they are electrically neutral particles, neutrons interact *electromagnetically* through their magnetic dipole moment of μ_n = −60.3 neV T^{-1}. UCN can be spin-polarised by strong magnetic fields. Because of their small kinetic energy polarized UCN can also be trapped by strong magnetic fields.

1.4   Research

Today, UCN are valuable tools in fundamental precision physics. They allow for research on free neutrons with long observation times, because of the possibility to store them in suitable material or magnetic traps.

The two flagship experiments with UCN are the precise measurement of the *free neutron life-time* and the search for a non-zero *electric dipole moment* of the neutron. Both measurements have been pursued since the 1950s, long before UCN were available, and have been improved continuously since then.

1.4.1   The free neutron lifetime

The free neutron lifetime has been measured by experiments with beams of cold neutrons and with stored ultracold neutrons. While both methods appear at present to be consistent amongst themselves (and reach a precision on the order of one second) they disagree with each other by approximately 8 seconds [Olive et al., 2014]. This discrepancy needs to be resolved. Therefore several experiments aiming for a precision determination of the neutron lifetime are under way world-wide.

The correct value of the free neutron lifetime is of great importance for big bang nucleosynthesis models, where the error on the neutron lifetime currently dominates the uncertainty on the helium abundance in the early universe [Cyburt et al., 2016]. A precise measurement with sub-second accuracy would also allow for testing the unitarity of the CKM matrix [Marciano and Sirlin, 2006] . A detailed review on the neutron lifetime can be found in [Wietfeldt and Greene, 2011].

1.4.2   The electric dipole moment of the neutron (nEDM)

No non-zero neutron EDM has been measured yet. However, since the first experiments started to look for an nEDM with stored UCN in the 1980s, the upper limit on its magnitude has been improved by two orders of magnitude to a current value of $3.0 \times 10^{-26}\,e$ cm [Pendlebury et al., 2015]. Several experiments aiming for a more precise nEDM measurement are planned or already running at the moment. The nEDM experiment at the Paul Scherrer Institute is currently taking data and achieves a statistical sensitivity on the order of $1.0 \times 10^{-25}\,e$ cm per day.

A future measurement of a non-zero nEDM would greatly contribute to the understanding of the matter to anti-matter asymmetry during primordial baryogenesis, as non-zero electric dipole moments of elementary particles violate CP symmetry, which is necessary for such an asymmetry to occurr, according to [Sakharov, A. D., 1967].

Stricter upper limits on the magnitude of an nEDM would further constrain the parameter space of theories of CP violation beyond the Standard Model and be complementary to efforts at the high energy particle physics frontier [Engel et al., 2013]. Detailed reviews on the neutron EDM can be found in [Ramsey, 1982, Lamoreaux and Golub, 2009, Chupp and Ramsey-Musolf, 2015].

1.4.3   Other research utilising UCN

Apart from the two examples mentioned above, there are numerous projects working with UCN (non exclusively) on:

- Gravitational quantum states of neutrons: [Nesvizhevsky et al., 2002, Baessler et al., 2011, Jenke et al., 2011, Jenke et al., 2014]

- Neutron beta decay asymmetries: [Mendenhall et al., 2013, Broussard et al., 2013]

- Electrical charge of the neutron: [Plonka-Spehr et al., 2010]

- Tests of the weak equivalence principle: [Frank et al., 2009]

and many others.

1.5   Sources of Ultracold Neutrons

At the time of this writing, sources for ultracold neutrons are in operation at four institutions world-wide, namely at the Institute Laue Langevin in Grenoble, France; at Los Alamos National Laboratory, Los Alamos NM, USA; at Johannes Gutenberg University Mainz, Germany; and at the Paul Scherrer Institute, Villigen, Switzerland.

Several other groups are working towards new sources in the US, Canada, Europe, and Asia.

All existing sources are treated in this work, with the focus on the source at the Paul Scherrer Institute.

Chapter 2

The Source for Ultracold Neutrons at the Paul Scherrer Institute

2.1 Working Principle

The process of production of ultracold neutrons (UCN) in the source at Paul Scherrer Institute (PSI) can be described as follows:

2.1.1 Production of free neutrons

Although free neutrons have a limited lifetime of about 880 s, bound in nuclei neutrons are stable and abundant.

There are two processes technically available to produce free neutrons in large quantities:

- Nuclear *fission*: As discovered by [Hahn and Strassmann, 1939] and later explained by [Meitner and Frisch, 1939], certain heavy elements like ^{235}U or ^{239}Pu have large thermal neutron capture cross sections on the order of several 100 b. The products of a neutron capture process on these nuclei have such small binding energies that it is energetically favored for the nucleus to decay into two lighter nuclei with larger binding energies. Typically, up to four fast neutrons are released as well, which can be used to create a self sustainig chain reaction in a reactor, releasing large amounts of free neutrons.

- Nuclear *spallation*: First studied by [Seaborg, 1937], when heavy, neutron-rich nuclei are bombarded with high energy particles like protons (order 1 GeV), they disintegrate into fragments. Up to 20 free neutrons can be produced by a single incident proton.

2.1.2   Reducing the neutrons' energy

Free neutrons created either by fission or by spallation have kinetic energies which are up to 15 orders of magnitude higher than the energies of ultracold neutrons. Therefore the main task of a source for ultracold neutrons is to make the neutrons lose most of their kinetic energy as efficiently as possible.

In contrast to charged particles, neutrons cannot be accelerated (or decelerated) by electric fields. Instead, large numbers of light nuclei at a temperature equivalent to the target energy are used as a moderator. Neutrons elastically scatter from the nuclei, typically hydrogen or deuterium bound in the form of light or heavy water, and transfer a fraction of their energy in every scattering process.

After many collisions between the free neutrons and the moderator nuclei, the kinetic energy of both will approach equilibrium, given by the Maxwell-Boltzmann distribution of their velocities at the temperature of the moderator material. This process is called thermalisation (because the neutrons end up in thermal equilibrium with the surrounding material), and leads to a most probable neutron energy of about 25 meV at room temperature (290 K) , only about five orders of magnitude above the point where the neutrons could be called ultracold.

Although the unit of kinetic energy used here, meV, implies low energy, the fact that free neutrons are rather light objects manifests in the corresponding velocity of such a thermal neutron still exceeding 2 km/s.

2.1.3   From fighter jets to marathon runners

Unfortunately, thermalisation is not suitable to cool neutrons down until they can be considered ultracold, because this would require a large amount of an ideal moderator material at a temperature on the order of 1 mK.

However, in certain materials like solid deuterium or superfluid helium it is possible for slow neutrons to lose almost all of their kinetic energy when exciting a vibration in the solid deuterium or a soundwave-like excitation in the superfluid helium.

If the remaining kinetic energy is in the range between 0 and 335 neV, corresponding to velocities between 0 and $8\,\mathrm{m\,s^{-1}}$, an ultracold neutron was "produced" and is ready to be studied in an experiment.

In solid deuterium, the UCN can only travel for a few centimeters before being absorbed or reaccelerated by the deuterium molecules. Thus it has to be removed from the deuterium quickly. In superfluid helium, a UCN can survive for long times, therefore this is not necessary.

Neutrons which enter for example the solid deuterium at the speed of the fastest supersonic jets ever built are partially thermalised in the cold (5 K) deuterium to speeds around a few $100\,\mathrm{m\,s^{-1}}$, which is already less than former civil supersonic aircraft cruising speeds. Like this, the probability for the neutrons to downscatter to velocities below $8\,\mathrm{m\,s^{-1}}$ is approximately 10 times higher than without the additional moderation by the solid deuterium.

For reference, the average speed of the world record marthon runner is approximately 42 km/2 h or $5.83\,\mathrm{m\,s^{-1}}$.

2.1.4 Neutrons on tap - UCN storage and distribution

Once neutrons have been slowed down to such low speeds, they reflect from many materials (e.g. iron, nickel, or diamond) under any angle of incidence. This can be exploited in order to guide the neutrons away from where they are produced and towards experiments, which may be several meters away from the place of production.

It also offers the possibility to store the UCN for several minutes, e.g. until an experiment is ready to take them. Like this, multiple experiments can use neutrons from a single source.

Fig. 2.1 shows two examples from the UCN source at PSI where either just a UCN detector is connected to the beam port West-1, or multiple experiments are connected and one of the experiments just takes neutrons after the first is finished, which is after about 30 s.

For technical details on the features of Fig. 2.1 see later parts of this chapter.

Several million UCN can be provided to multiple experiments with a repetition frequency of typically one production every 5 min at PSI.
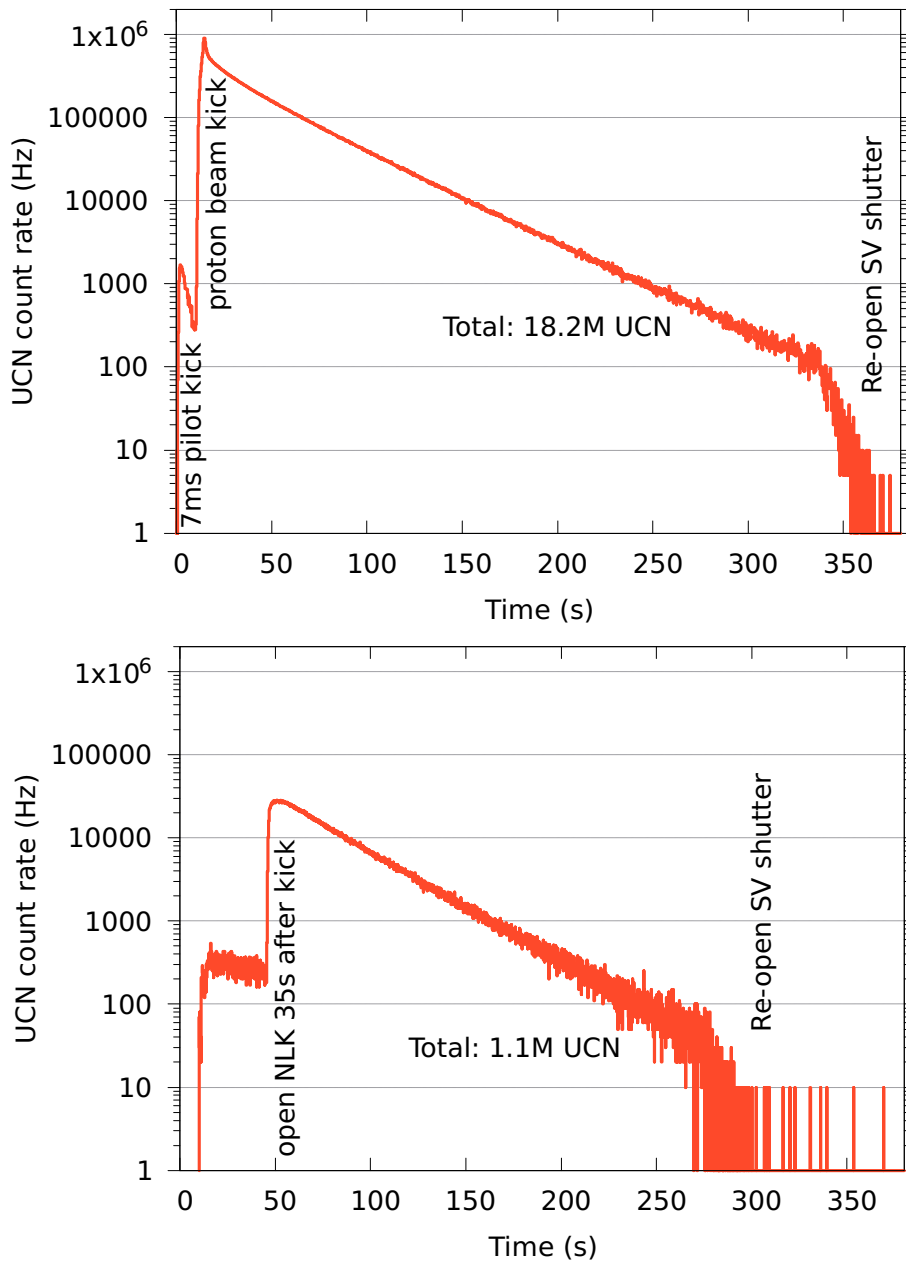
Figure 2.1: *Top: UCN arrival rate at beam port West-1. A UCN detector is connected directly to the beam port, the flap inside the guide (NLK), is open. The small peak in UCN rate at the beginning is due to UCN produced by a 7 ms long kick to the target, used to test if the beam is correctly centered on the target. The main proton beam kick (here: 4 s long) is sent to the target 10 s later. At the end of the kick, the large shutter inside the source, called central storage vessel (SV) shutter, is closed. It is re-opened about 320 s later to get ready for the next kick. In total, more than 18 million UCN were counted in the detector.*
Bottom: UCN arrival rate in an experiment at beam port West-1, only extracting UCN from the central storage vessel about 35 s after the beginning of the proton beam kick to the UCN spallation target. During the first 35 s, UCN were provided to a second experiment.

2.2   The UCN Source at the Paul Scherrer Institute

Only elements of the source which are relevant to this work are described here. For a more detailed description of all elements of the PSI UCN source see [Göltl, 2012].

An annotated drawing of the source is shown in Fig. 2.2.
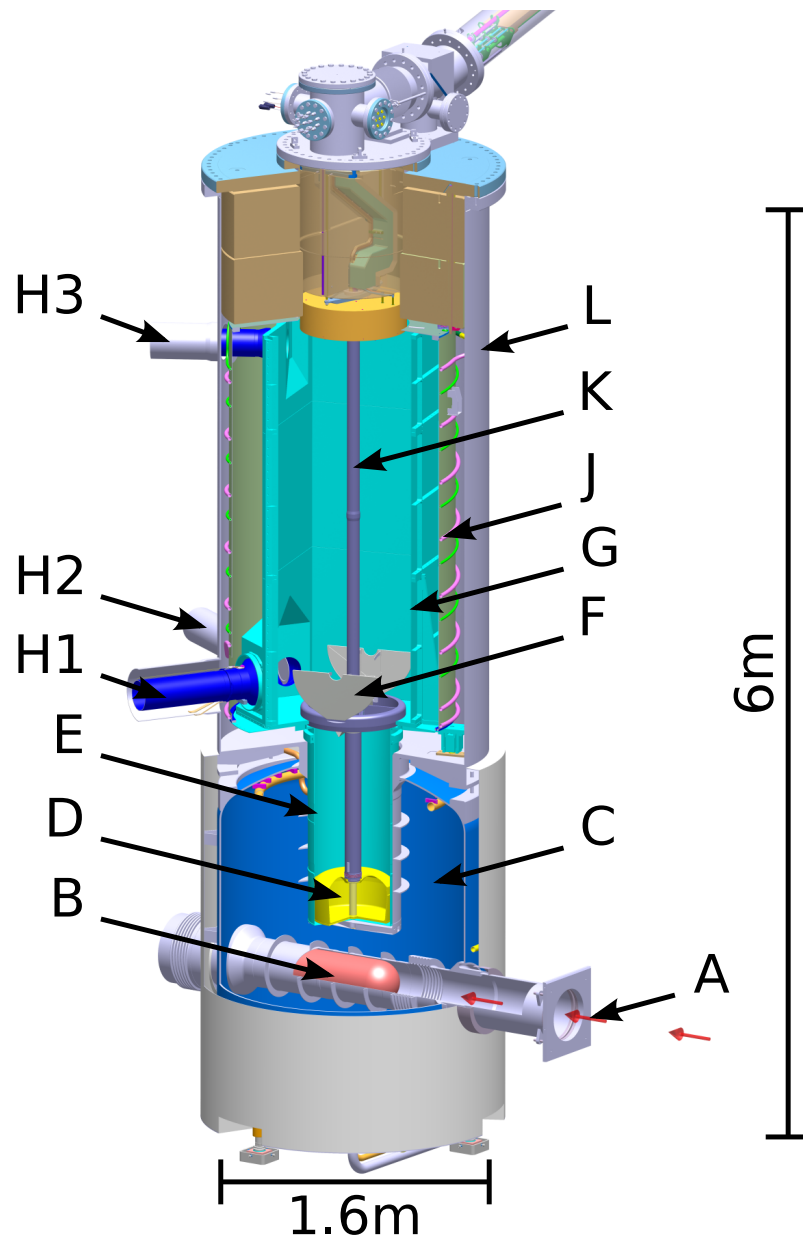
Figure 2.2: *Rendering of the central part of the UCN source from construction CAD files. A: Incoming proton beam; B: Spallation target; C: Heavy water tank; D: Solid deuterium moderator vessel; E: Vertical UCN guide; F: Central storage vessel flaps; G: Central storage vessel; H1-H3: Guides towards beamports "South", "West-1" and "West-2"; J: Thermal shield; K: Deuterium and helium supply lines; L: Vacuum vessel.*

2.2.1   From protons to hot neutrons

The High Intensity Proton Accelerator (HIPA) [Seidel et al., 2010] at PSI accelerates protons to an energy of 590 MeV wit a peak intensity of presently up to 2.4 mA.

The proton beam is guided to the dedicated spallation target for the UCN source for periods ranging from 7 ms up to 8 s. This is done by ramping the magnetic field of a fast kicker magnet, which is able to divert the full proton beam from the main beamline to the UCN source beamline within 3 ms [Anicic et al., 2005]. The incident proton beam is indicated by label A in Fig. 2.2.

The spallation target of the UCN source [Wohlmuther and Heidenreich, 2006] is mainly consisting of lead, which is contained in 756 Zircalloy tubes. Because of the thermal power introduced into the target by the proton beam, additionally heavy water is circulated between the Zircalloy tubes. The target is indicated by label B in Fig. 2.2.

While the proton beam is incident on the target, on average 7.27 neutrons per proton are released by spallation ([Becker et al., 2015]). These neutrons have kinetic energies on the order of 2 MeV and up to a few hundreds of MeV. Neutrons in this energy range are called "fast" neutrons.

Details about the optimisation of the proton beam spot's size and position on the target can be found in Sec. 4.1.

2.2.2   Thermalisation

The spallation target is surrounded by a vessel filled with heavy water (D_2O) at room temperature, which is indicated by label C in Fig. 2.2, except for its insertion tube along the proton beam axis, which is needed for the proton beam tube and periphery for the target itself.

In the heavy water the neutrons undergo "thermalisation", where they lose a significant part of their kinetic energy in elastic collisions with the deuterons in the water molecules.

The resulting thermal spectrum peaks at a neutron temperature of 313 K, corresponding to about 27 meV [Zsigmond, 2015].

Details about the characterisation of the thermal flux can be found in Sec. 3.1.

2.2.3   Cold moderation and downscattering into the ultracold regime

In the central upper part of the heavy water tank, the moderator vessel is located (indicated by label D in Fig. 2.2). Here up to 5 kg of purified (ortho-) deuterium (D_2)[1] is cooled to a temperature of 5 K using liquid helium. At this temperature two processes are possible in the solid D2:

1. In analogy to the thermal moderation in the heavy water, neutrons can lose energy in elastic collisions with the deuterium molecules and hence become cold neutrons.

---

[1]Solid deuterium has a mass density of about 0.2 g/cm^3. 5 kg of solid D_2 correspond to a volume of approximately 25 L. This amount of deuterium occupies about 28 m^3 under standard conditions.

2. Neutrons can lose almost all of their remaining kinetic energy by exciting one or more phonons in the deuterium crystal. This process is called downscattering, and it is heavily energy dependent. The downscattering cross section peaks at an incoming neutron energy of 9 meV, as measured by [Atchison et al., 2007a].

The solid deuterium crystal in the UCN source is typically about 15 cm high. Due to the short lifetime of UCN in solid deuterium, predominantly UCN from the upper layers can escape through the top surface, while the majority of the solid deuterium effectively acts as a cold moderator only.

Once a neutron has become ultracold by a downscattering process, the probability for the reversed process (upscattering) is suppressed by a factor of $e^{-\Delta E/k_B T}$ where ΔE is the difference of neutron kinetic energy before and after the down- or upscattering, k_B the Boltzmann constant and T the temperature. $k_B T$ at 5 K is equivalent to 0.43 meV. Thus, an excess of neutrons with energies below the thermal equilibrium is produced.

Such sources for UCN are therefore called "superthermal".

Characterisation measurements of the UCN production in thin films of solid deuterium are described in Sec. 3.2.

2.2.4 Intermediate storage of UCN

Once produced, UCN have to be extracted from the solid deuterium in order to prevent them from being lost due to nuclear capture or upscattering, which can occur by thermal deexcitation of a phonon as described above or by nuclear spin flips of the deuterium molecules from remanent paradeuterium molecules. Lifetimes UCN on the order of a few 10 ms can be achieved in solid deuterium, as shown by [Morris et al., 2002].

If a UCN exits the surface of the solid deuterium, it gets a boost in kinetic energy of 102 neV due to the Fermi potential of deuterium. This boost points normal to the surface at the point of exit, and as the ultracold neutrons are extracted towards the top, this typically points upwards.

To compensate for this boost in energy at the PSI UCN source, the central UCN storage vessel is located 1 m above the solid deuterium surface and UCN lose approximately this boost energy by gravity when traveling upwards. UCN are extracted from the solid deuterium to the top and pass through an aluminium lid of 0.5 mm thickness for safety reasons.

Above the 1 m long vertical guide, a 2 m³ large central storage vessel (SV) is located, indicated by label G in Fig. 2.2. Its walls are made from aluminium and coated with nickel and diamond-like carbon (DLC) on top. The used DLC has a high Fermi potential of about 235 neV (compatible with earlier measurements by [Atchison et al., 2007b]) and a very low neutron absorption cross section, and therefore is well suited for storage of UCN.

The vertical guide connects to an opening in the bottom plate of the central SV. The opening can be closed by two large half-circle shaped flaps, also coated with DLC, which are opened while the proton beam is on target and UCN are being produced. As soon as the neutron production is finished the flaps are closed and the UCN confined in the storage vessel. These flaps are indicated by label F in Fig. 2.2.

UCN can be stored in the central SV for several minutes. From there they are being distributed to up to three experiments.

The long term characteristics of UCN storage in the central storage vessel are described in Sec. 3.3.

Details about the optimisation of the central storage vessel flaps and their actuation timing can be found in Sec. 4.2.

2.2.5 Transport of UCN to experiments

Three horizontal UCN guides of between 6.5 m and 8.5 m length, mainly made of glass tubes of 180 mm inner diameter, coated with a mixture of nickel and molybdenum (NiMo) with a mass ratio of 85 to 15, connect the central storage vessel to beam ports outside the biological shielding, where UCN experiments can be connected.

Two guides are connected at the base of the central SV, with their central axes at heights of 152 mm (guide "West-1") and 209 mm (guide "South") above the bottom of the storage vessel, while one guide is connected at a height of 2235 mm. One of the lower guides (H1 in Fig. 2.2) exits the biological shielding at the south side, and is therefore called guide "South" or beam port "South". The other low guide (H2 in Fig. 2.2) as well as the elevated guide (H3 in Fig. 2.2) exit the biological shielding towards the west side and are called "West-1" for the low guide and "West-2" for the elevated guide.

Only UCN with kinetic energies above about 200 neV can reach the "West-2" guide, while UCN of all energies can enter the two lower guides "West-1" and "South". This results in similarly high UCN intensities at both low guides, and a reduced intensity in "West-2". The "West-2" guide is bent downwards by a 90° bend at the edge of the shielding.

All three guides are separated from the experimental area by a safety window made from a 100 μm thick foil of an aluminium alloy called AlMg3 at the end of the guide. The Fermi potential of Aluminium is 54 neV (see [Golub, R. and Richardson, D. and Lamoreaux, S.K., 1991]), which therefore causes a low-energy cut-off at this energy without further efforts.

Measurements of the in-situ transmission characteristics of the UCN guides are shown in Sec. 3.4.

2.2.6 Periphery

The whole central storage vessel complex is surrounded by a thermal shield which is cooled to a temperature of 70 K (J in Fig. 2.2).

Deuterium and helium are fed to the moderator vessel through a tube in the center of the central storage vessel and horizontal guide (K in Fig. 2.2).

Except for the spallation target and the heavy water tank, the whole source is contained in a large vacuum tank (L in Fig. 2.2).

The source is completely surrounded by several meters of iron and concrete as biological shielding.

2.2.7 UCN density

The density of UCN available to an experiment connected to a beam port, measured in units of UCN/cm^3, is one of the most important characteristics of any UCN source.

Multiple measurements of the UCN density at the PSI UCN source are shown in Sec. 3.6.

A world-wide comparison of UCN sources with respect to the UCN density is presented in Chap. 7.

2.2.8 Polarisation of UCN at beam port South

UCN can be spin-polarised by strong magnetic fields in vacuum or in magnetized foils.

As beam port "South" is dedicated for the nEDM experiment, which is conducted using polarised UCN, a superconducting 5 T solenoid was installed at the end of the UCN source vacuum vessel at beam port South, with the vacuum safety window in the highest field region.

UCN with one spin state are accelerated towards the highest magnetic field, while UCN with the other one are decelerated and finally reflected. As a magnetic field strength of 1 T is equivalent to kinetic UCN energies of 60 neV and the magnetic field inside the source before the magnet is very small, transmitted UCN have 300 neV more kinetic energy when transmitting the foil, and their transmission losses are therefore largely reduced. The energy cutoff due to the positive Fermi potential of the foil, which is present at all other beam ports, is avoided at beam port south as long as the magnet is on.

Details about the transmission of UCN through the polarising magnet can be found in Sec. 3.5.

2.2.9 Duty cycle

Except for shutdown and service periods, the HIPA accelerator is operated continuously. Protons are permanently used for production of Pions and Muons in two target stations and thermal and cold neutrons in the Swiss spallation neutron source SINQ at the end of the beam line.

The proton beam can be kicked to the UCN spallation target for up to 8 s, during which the other target stations receive no beam.

The original design and operating allowance of the UCN source was aimed at operation at an average proton beam current of 20 µA (the normal proton beam current used to be 2000 µA).

At 2000 µA proton beam current, this average beam current corresponds to a 1 % duty cycle in time.

The allowed average proton beam current was based on calculations of the radiation levels in the experimental areas, which have to stay safe for work during beam operation.

In 2015, a process of increasing the average proton beam current on the UCN target from 20 µA to 60 µA was started.

This is explained in detail in Chapter 4.3.

2.2.10   UCN production sequence

The full 590 MeV proton beam, typically operating at a beam current between 2200 μA and 2400 μA, can be steered onto the spallation target of the UCN source, using a fast kicker magnet located about 11 m downstream of the ring cyclotron. This magnet was developed especially for the UCN source and is described in detail in [Anicic et al., 2005].

In order to avoid damage to the beamline and target, which would be the inevitable if the control over this 1.3 MW proton beam were lost, every proton beam kick for UCN production is preceded by one or up to three short so-called "pilot" kicks.

These kicks have a duration of 7 ms and are used to verify that the beam is well centered throughout the whole beamline up to the target. If the automatic beam diagnostic systems detect a deviation from the set beam position, steering magnets are automatically adjusted to compensate for the measured deviation. An additional pilot kick is used to determine if the automatic adjustment was successful.

This process can be repeated several times until a long production kick is allowed. If the automatic centering system fails to determine a setting of the steering magnets with which a long kick would be safely possible, the kick sequence is aborted.

The long kicks for UCN production have a maximum duration of 8 s. Should this limit be exceeded, the power supply of the kicker magnet shuts off automatically and triggers an interlock, which stops the proton beam immediately for safety reasons.

Details about the production sequence and accompanying trigger signals can be found in Sec. 8.1.

2.3   Modes of UCN Production

The UCN source is typically operated in one of three distinct modes:

2.3.1   Production kicks "with Klappentrigger signal"

This is the standard mode of operation, resulting in the highest UCN yield per unit time. The time between successive kicks can be defined by the experimenters with the minimum time between two successive proton beam kicks given by the constraints on the average proton beam on target. For example the standard operation for the nEDM experiment is one kick every 300 s.

The duration of each kick is set to be maximal for the given repetition rate, such that the allowed average proton beam current on the UCN target does not exceed 40 μA (as of 05/2016).

For the example of the nEDM experiment, the maximal kick duration for a repetition every 300 s at a full proton beam current of 2200 μA is 5.45 s.

At a given time before the *end* of the proton beam kick, typically set to 2400 ms, the accelerator timing system sends a trigger signal to the source control electronics.

After an additional delay, which has to be optimised with respect to the UCN output per kick, the source control electronics closes the central storage vessel flaps.

During the proton beam kick UCN rates of approximately 1 MHz are observed, while immediately after the proton beam kick, UCN rates exceeding 500 kHz can be measured at beamports West-1 and South. This rate declines with a halflife of approximately 25 s, as given by the open guide and connected detectors as a sink, which results in count rates still exceeding 1 kHz 200 s later.

In total, up to 3×10^7 UCN can be measured at the beamports West-1 and South per proton beam kick, see Figs. 2.1 and 2.3.

The central storage vessel flaps are usually reopened about 30 s before the beginning of the next proton beam kick.

The dependence of UCN output to the length of the proton beam kick has been investigated and is presented in Sec. 3.7.

2.3.2   "Norm-kicks"

The simplest mode of operation is used to measure the UCN output in the most reproducible way, as no mechanical movements are involved and all parameters are kept the same.

The proton beam gets kicked towards the UCN target for 2 s, no trigger signal is sent to the central storage vessel flaps, which hence stay open. Thus the UCN lifetime in the central storage vessel is drastically reduced because UCN can fall back towards the moderator vessel where they are lost.

This results in a reduced amount of UCN per kick with respect to standard operation, the system is simplified and very reproducible.

This mode is used to assess the overall quality of the solid deuterium.

The total output of these "Norm-kicks" is measured at the West-1 beam port with the big Cascade detector (see Sec.2.4 below) attached to the beam port through an additional 1 m long UCN guide with an inner diameter of 180 mm, coated with NiMo.

UCN numbers about 4×10^6 UCN per Norm-kick are typically measured.

UCN rate spectra of a production kick and a Norm-kick are shown in Fig. 2.3.

2.3.3   "Splitter" mode

It is possible to shear off a small fraction of the proton beam from the very tails of its horizontal distribution and continuously produce UCN instead of the usual kicks of the full beam to the UCN target. This mode is only used for short times for testing purposes. UCN rates fluctuate in this mode by about 20 % and the UCN output is very low.

Permanent proton beam currents of up to 10 μA are possible, restricted by activation due to proton losses close to the kicker magnet. The UCN count rate measured with the big Cascade detector at beam port West-1 during continuous operation with a proton beam current of 5 μA is approximately 500 Hz.
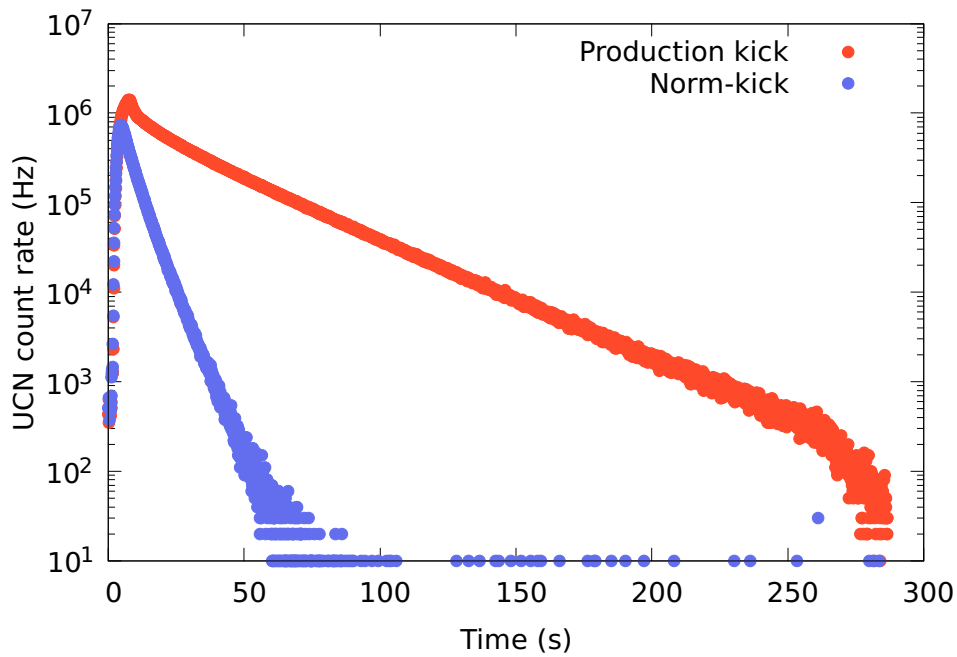
Figure 2.3: *Comparison of two UCN production types, Data measured at beam port West-1 in June 2016. The red points show UCN rates measured with a 5.4 s long production kick, which yielded in excess of 3×10^7 UCN in total. The blue points show a Norm-kick measured at the same day, which yielded approximately 4.5×10^6 UCN. The difference in the decay time of the UCN rate is obvious. While for the Norm-kick, the detected rate is on background level after about 100 s, UCN rates of almost 3 kHz are observed at the end of the production kick, when the re-opening of the central storage vessel flaps leads to a quick diminishing of the remaining rate.*

2.4   UCN Detectors

"Cascade-U" UCN detectors made by CDT[2] are used for source characterisation measurements and experiments at beam ports West-1 and West-2.

These detectors consist of

- an aluminium entrance window coated with a 200 nm thick layer of ^{10}B on the inside

- an ionisation volume filled with $Ar + CO_2$ gas mixture

- one GEM foil[3] for charge amplification

- a grid of 12.5×12.5 mm^2 readout pixels.

Incoming UCN are captured in the layer of ^{10}B in a ^{10}B$(n, \alpha)^7$Li reaction, resulting in a ^{7}Li$^+$ ion and an α particle being released. These fragments subsequently ionise the gas mixture, which results in a localised cloud of electrons and ions. The electrons drift towards the readout pixels, which are on positive potential (high voltage: 1300 - 1500 V), and pass through a GEM foil, where the charge is amplified up to 400-fold. This amplified electron cloud is then detected by the read-out pixels, the electric signals get processed in a custom ASIC and FPGA and are subsequently read out by a PC.

Two versions of these detectors exist at PSI:

- The "Big" detector

    - active area: 200 by 200 mm^2

    - 16 by 16 pixels

    - entrance window made of 100 μm thick AlMg3 foil optimised for UCN transmission, coated with 200 nm ^{10}B

    - electronics inside the detector housing

    - read out via optical fiber

- Three "Small" detectors

    - active area: 100 by 100 mm^2

    - 8 by 8 pixels

    - entrance window made of 100 μm thick Aluminium foil, coated with 200 nm ^{10}B

    - electronics in separate box

    - read out via USB

---

[2]http://n-cdt.com/products/cascade-detector-systems/cascade-u-systems/
[3]https://gdd.web.cern.ch/GDD/

Chapter 3

Characterisation of the UCN Source

3.1 Thermal Neutron Production

The first step towards UCN production (neglecting operation of the proton accelerator) is the production and thermalisation of neutrons in the target and the surrounding heavy water. This has been simulated using the MCNPX Monte Carlo (MC) transport code [D.B. Pelowitz, Ed., 2011].

In order to validate these calculations, measurements using gold activation were performed in order to directly measure the flux of (mainly) thermal neutrons around the heavy water container and the UCN source tank. Gold foils were positioned along a nylon rope in a vertical aluminium tube just outside the tank, where they were irradiated using short proton beam kicks to the UCN target. Afterwards their activity was measured and compared to simulation. After refining the model used in the calculations with respect to materials and shielding, MC calculations and measurements were very well in agreement. For a drawing of the setup and a comparison of measured data and simulation see Fig. 3.1.

The results of this measurement have been published in [Becker et al., 2015].
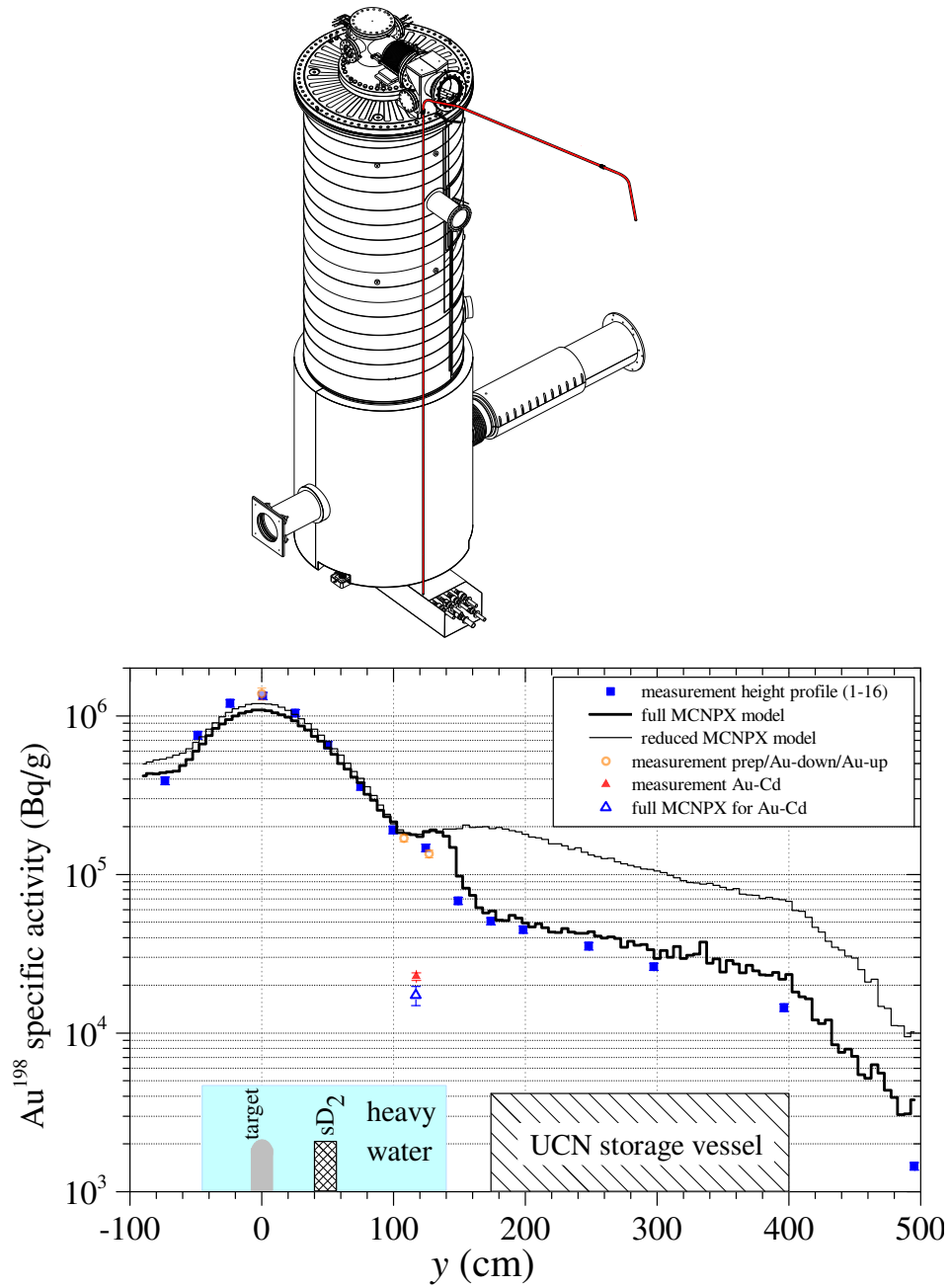
Figure 3.1: *Measurement of the thermal neutron flux at the UCN source. Top: Drawing of the UCN source tank, the external vertical tube where the gold activation measurement was conducted is indicated in red. Bottom: Comparison of measurement and MC simulation which are well in agreement. Source: [Becker et al., 2015]*

3.2   UCN Production in Thin Solid D2 Films

3.2.1   Motivation

Production of UCN in a large solid block of deuterium is a complex combination of many processes which contribute to the final production rate. Some of these processes are only relevant for thick bulks of deuterium:

- Cold moderation of the incoming neutron flux

- Loss of UCN through absorption by deuterium atoms

- Scattering of UCN on defects in the solid deuterium

- Thermal upscattering

- Upscattering via para- to ortho-deuterium spin-flips

All of these are governed by the total cross section of neutrons on solid deuterium, measured by [Seiffert, 1970] and [Atchison et al., 2005a] to be on the order of 10 b per molecule.

These processes are also related to the following relevant parameters in our system:

- Geometrical shape and thickness of the solid deuterium

- Structure of the solid deuterium

- Temperature distribution inside the deuterium

which cannot be easily assessed inside of the UCN source moderator vessel.

In order to simplify the interpretation of the measured UCN output, the largest part of the deuterium content of the moderator vessel was removed, and UCN were produced in only a few grams of solid deuterium in December 2013, December 2014 and December 2015. This was done in order to produce thin films of deuterium, where we estimated that the time the UCN needed to exit the film towards the vacuum was short compared to the UCN lifetime inside the deuterium, which was measured by [Morris et al., 2002] to be around 30 ms for temperatures of about 5 K and ortho-deuterium fractions above 95 %, which is comparable to the ortho-deuterium fraction in our system. Assuming a deuterium thickness of 1 mm and a UCN velocity of 3 m s^{-1}, the time to pass the deuterium film is on the order of 0.3 ms, which is much smaller than 30 ms. Additionally, using the total cross section σ on the order of 10 b [Atchison et al., 2005a] from above, and a molecular density N of 3×10^{22} cm^{-3} [Souers, 1986], the interaction probability of a neutron in the relevant energy range with a solid deuterium film with a thickness d of 1 mm can be calculated as

$$P = 1 - e^{-N \times d \times \sigma} \simeq 0.03 \tag{3.1}$$

Incidentally, such a film of solid deuterium coincides well with the first theoretical calculations for superthermal UCN sources using solid deuterium [Golub and Boenig, 1983, Yu et al., 1986].

In addition to limiting interactions between thermal or ultracold neutrons with the deuterium film as shown above, such thin films are also more likely to be cooled more homogeneously than thick bulks, and are more likely to be distributed evenly on the bottom or possibly the walls of the moderator vessel.

Simplifying the UCN production process also results in simpler models for simulations. As many other subsystems of the UCN source can already be modeled very well, using a such a production mode can lead to a "calibrated" source of UCN inside the source, which could then be used to determine the overall UCN transport efficiency from inside the moderator to the detector by comparing the measured number of UCN to the calculated number of produced UCN.

3.2.2 Experimental challenges

The position and shape of the thin film of deuterium inside the moderator vessel are not evident because the deuterium will freeze onto the surface which is cooled down below the triple point first. As the cold helium enters the moderator vessel in the middle of the bottom plate, and is then distributed radially outwards, it is likely that the film will be in this position as well. A sketch of the coolant flow is shown in Fig. 3.2.

3.2.3 Thin film preparation

In 2013 the measurements of UCN production in thin deuterium films were demonstrated after measurements using only deuterium gas in the moderator were finished. A small amount of about 5 g of deuterium gas was used to create a thin film, subsequently about half of that was
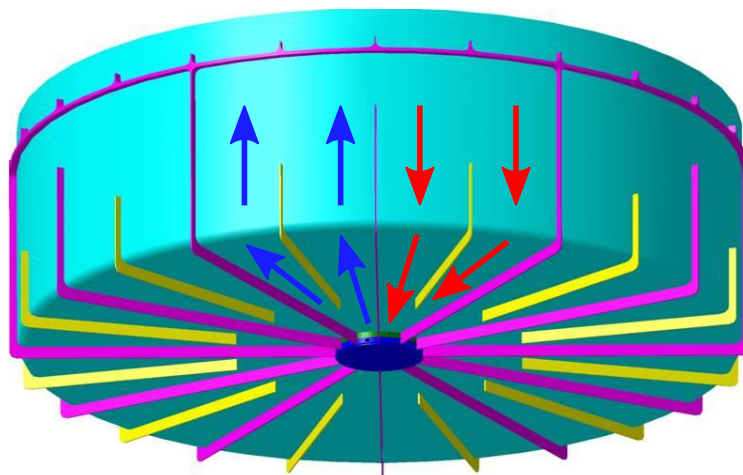
Figure 3.2: *Sketch of the coolant flow in the moderator vessel bottom and walls. The direction of flow of the helium is indicated by arrows. Helium is fed into the bottom of the moderator vessel from the center, flows outwards and up the side wall and then back down and inwards.*

released into the condenser vessel and the UCN output of a second thin film with about 2.5 g was measured. Promising results lead to dedicated measurement campaigns in December 2014 and December 2015.

In the deuterium handling system, the condenser vessel offers the best control over pressure and temperature, and therefore over deuterium content. There, the gas pressure can be measured precisely and the temperature of the vessel walls is measured directly using thermo sensors. Also the volume of the vessel is known precisely. Especially the possibility to directly measure the wall temperature and thus the equilibrium temperature of deuterium inside the vessel makes this vessel the better choice for estimating deuterium content than e.g. the moderator vessel. Therefore, for all thin film measurements except the first measurement of each campaign, the condenser vessel was used to either measure the total amount of deuterium in the system or to monitor incremental changes in the deuterium mass in the moderator vessel.

The first measurements of each campaign were done immediately after releasing the majority of the deuterium content to the external buffer tanks shortly before the end of proton accelerator operation at the end of the year. With the valves towards the buffer tanks opened and the moderator vessel at 24 K, after all deuterium was in the gas phase the system was in equilibrium with a final gas pressure of 850 mbar in 2014 and 870 mbar in 2015. Then all valves between buffer tanks, condenser vessel and moderator vessel were closed, and the moderator vessel cooled to 5 K.

The deuterium films with all other masses were prepared in two different ways for masses up to and above 75 g:

- Below 75 g:

  1. Initially, all deuterium was inside the condenser vessel.
  2. The UCN output with empty moderator vessel at 5 K was measured.
  3. Adjustment of the condenser vessel to 25 K, and the moderator vessel to 24 K.
  4. The valve between the condenser vessel and the moderator vessel was opened; the pressure reduction in the condenser vessel was monitored to estimate the mass flow.
  5. The valve between the condenser vessel and the moderator vessel was closed at the desired deuterium content inside the moderator vessel.
  6. The moderator vessel was cooled down to 5 K.
  7. UCN output was measured.
  8. The moderator vessel was warmed up to 24 K.
  9. Steps 4 to 9 were repeated with the next amount of deuterium.

- Above 75 g:

  1. Start with a certain amount of solid deuterium in the moderator vessel at 5 K.
  2. The valve to the condenser vessel at 24 K was opened and the mass flow was monitored via pressure reduction in the condenser vessel.

3. The valve to the condenser vessel was closed.

4. UCN output was measured.

(5. Additional conditioning in 2015 only: The moderator vessel was heated until a deuterium pressure of about 250-320 mbar was reached.)

(6. The moderator vessel was cooled down to 5 K.)

(7. UCN output was measured again.)

8. Steps 2 to 4 (or 7 in 2015) were repeated with the next amount of deuterium.

The separate treatment for higher deuterium masses was necessary as the system is not designed for operation at pressures exceeding 1000 mbar, which made total evaporation of more than about 75 g of deuterium inside the moderator vessel impossible.

Using the technique described above for higher masses was demonstrated with 158 g of deuterium in 2014 and allowed to measure with deuterium masses up to 254 g in 2015.

All measured thin films are listed in order of their measurement in Table. 3.1.

3.2.4   Experimental results

Thin films of deuterium were frozen from several different amounts of gas ranging from 2.5 g to 250 g. Measurements of the UCN output from the empty cold moderator vessel were done to be used as background, which can be interpreted as either UCN production in the cold aluminium of the moderator vessel material, or UCN production in the remaining deuterium gas.

The remaining deuterium pressures during the background measurements were < 0.01 Pa (in 2013), 0.07 Pa (in 2014), 0.15 Pa (in 2015), corresponding to 4923(98), 5411(116) and 4877(38) UCN counts.

The resulting UCN output of 3 s long proton beam kicks at 2.2 mA beam current can be seen in Fig. 3.3, they are also shown in Table 3.1. The storage vessel flaps were closed at the end of the proton beam kick.

The counts are integrated starting from 2 s after the end of the proton beam kick until 200 s later, which is just before the storage vessel flaps were opened for the next kick in 2014 and 2015. The background is treated the same way and subtracted from the data points.

A conservatively estimated error of only ±1 g on the mass of the deuterium in the moderator vessel can be assumed, as the volume, temperature, and pressure of the condenser vessel are known very precisely. As the measurements were spread over two years, and slight changes to the UCN transport, measurement system or detector efficiency cannot be excluded, an error of 2 % is assumed on the amount of counted UCN.

In the 2015 measurements, NLK south was open during the measurement of the data point at a deuterium mass of 58.9 g. Scaling this point upwards with a scaling factor determined later at a mass of 107 g yields a point which is in clear disagreement with earlier measurements. The point at 59 g has therefore been excluded from the fit to the data. Also the point at a high deuterium

mass of 254 g, where the UCN production clearly deviates from a linear behaviour, is excluded from the linear fit.

The remaining data has been fitted with a straight line, where the slope and y-intercept are free parameters of the fit.

The results are a slope of 4371.8(1173) UCN/g and a y-intercept of 5318(4852) UCN. The reduced χ^2 value of the fit is 6.3.

3.2.5 Interpretation

The UCN production rate seems to be linear in the mass of the deuterium film up to about 200 g, which corresponds to a film thickness of approximately 6 mm assuming a homogeneous layer of solid deuterium with a density of 0.197 g/cm^3 on the bottom of the moderator vessel. The data point at the highest D$_2$-mass can not be accomodated in the fit model.

mass (g)	date	pressure (Pa)	avg. UCN	σUCN	Comment
5.8	Dec 20, 2013	0.03	31448	1052	
2.8	Dec 20, 2013	0.01	20118	228	
0	Dec 20, 2013	0.00	4923	98	Background 2013
81	Dec 18, 2014	0.2	399415	1386	
158	Dec 19, 2014	2.76	620210	752	
0	Dec 19, 2014	0.07	5411	116	Background 2014
2.5	Dec 22, 2014	0.25	17576	88	
6	Dec 22, 2014	0.58	33998	131	
10	Dec 22, 2014	0.83	51943	289	
20	Dec 22, 2014	1.47	101375	424	
40	Dec 22, 2014	2.45	189240	558	
60	Dec 22, 2014	3.3	288733	2185	
75	Dec 22, 2014	3.96	372704	1300	
58.9	Dec 21, 2015	0.25	277059	807	NLK South open
106.7	Dec 21, 2015	1.5	448461	672	
106.7	Dec 21, 2015	1.5	332978	1046	NLK South open
106.7	Dec 21, 2015	1.39	642681	2468	Remelted
181.5	Dec 21, 2015	3.6	769698	2793	
181.5	Dec 22, 2015	3.5	1032751	3756	Remelted
253.8	Dec 22, 2015	6.0	964413	5122	
253.8	Dec 22, 2015	5.8	1374163	5236	Remelted
0	Dec 22, 2015	0.15	4877	38	Background 2015

Table 3.1: *Measured UCN production in thin solid deuterium films. Listed in order of measurements. Pressure: deuterium vapour pressure measured by the CP006 sensor. All measurements done with 3 s long proton beam kicks with KTR at nominal beam current of 2200 µA.*

The linear fit to the data seems to rather underestimate UCN output for data points up to a mass of 80 g, while it overestimates the points above. However, also the higher mass points are compatible with a linear fit without a zero-point offset.

Fitting only data points for films with masses up to 80 g to a linear function yields a slightly larger slope of 4846.2(690) UCN/g and a y-intercept of −1707(2379) UCN with a reduced χ^2 value of 0.68 when using the same 2 % error on the measured UCN intensity, or a slope of 4896.30(6849) UCN/g and a y-intercept of −2903(3154) UCN with a χ^2 value of 1.30 when using the standard deviation of the average as an error on the UCN intensity.

A comparison of the global and local fits and the measured data in 2014 is shown in Fig. 3.4.

While this may hint towards first effects due to non-negligible film thickness already at these masses, it is not conclusive. For masses larger than ~ 200 g of deuterium however, a deviation towards lower UCN output is visible.

3.2.6 Re-Liquefaction prior to high mass measurements

In 2015, each measurement with a deuterium mass higher than 80 g was done twice. Once right after adding deuterium and freezing it on top of the existing solid deuterium, and once after fully liquifying the content of the moderator vessel. The results are shown in Fig. 3.5.
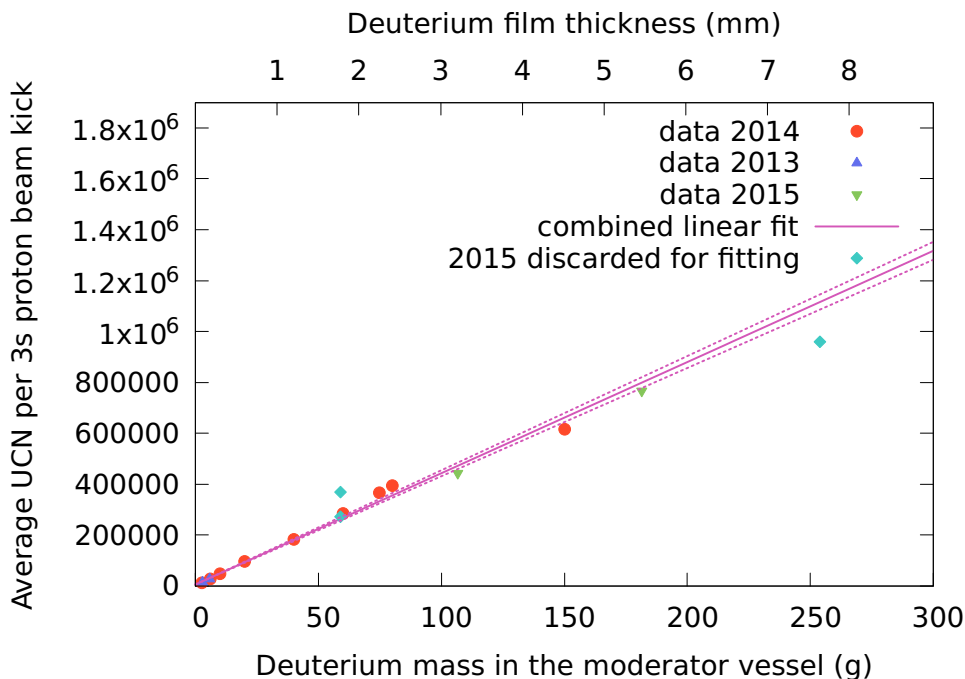
Figure 3.3: *UCN output with respect to D_2 mass in the moderator vessel. An error of 2 % on the UCN intensity is assumed. The fit indicated by the pink solid line is a linear fit to all data points but the ones indicated in turquoise. The dashed pink lines indicate the 1σ band around the fit result. Measured with 3 s long proton beam kicks with KTR at nominal beam current of 2200 µA. x and y error bars are on the order of the point size.*

The UCN output of thin films which have been liquefied before freezing is systematically higher by an average factor of 1.42(1) than for the same mass frozen from the gas phase without liquefaction.

This leads to the conclusion that already for deuterium masses above 80 g either the position at which the deuterium freezes or the shape of the films surface, are less than optimal when freezing from the gas phase. By liquefying the whole amount of deuterium and freezing from the liquid phase, a shape and position better for UCN production or extraction is realised. For example deuterium could also freeze to the moderator vessel walls when it is filled in gaseous form, and on later liquefaction said deuterium could flow down to the bottom of the vessel, where it would solidify later.

It has not yet been investigated if more than one cycle of liquifying the not-so-thin film deuterium and freezing it again further improves the UCN output further.

3.2.7 Outlook

The final goal of the thin film measurements is to understand the absolute UCN output of the source, namely to calculate the UCN production and compare the measured UCN counts at the beam port with the simulation.
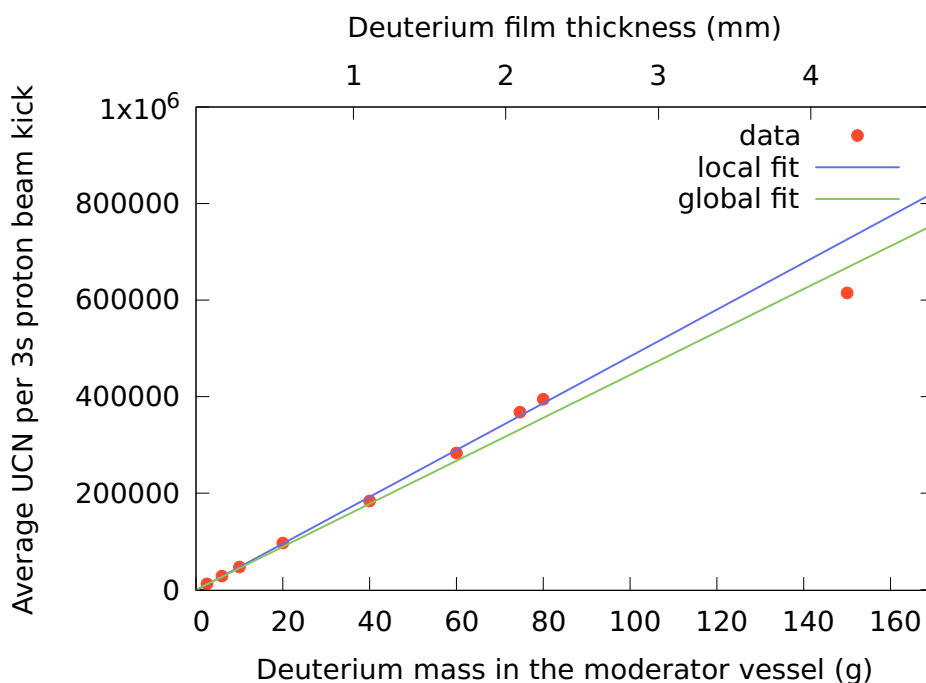
Figure 3.4: *UCN output with respect to D_2 mass in the moderator vessel. 2014 only. The local fit is a linear fit agains the data points with masses up to 80 g while the global fit includes all higher mass points measured in 2015 as well. x and y error bars are on the order of the point size.*

Taking the knowledge on UCN transport efficiency through the storage vessel and guide system from the "Ping-Pong" measurements (see Sec. 3.4) this comparison will allow us to determine the UCN extraction efficiency from the solid deuterium into the source storage vessel.

This can then be compared to extraction simulations done in [Brys, 2007].

The combination of all these inputs will then allow us to judge the quality of the solid deuterium.
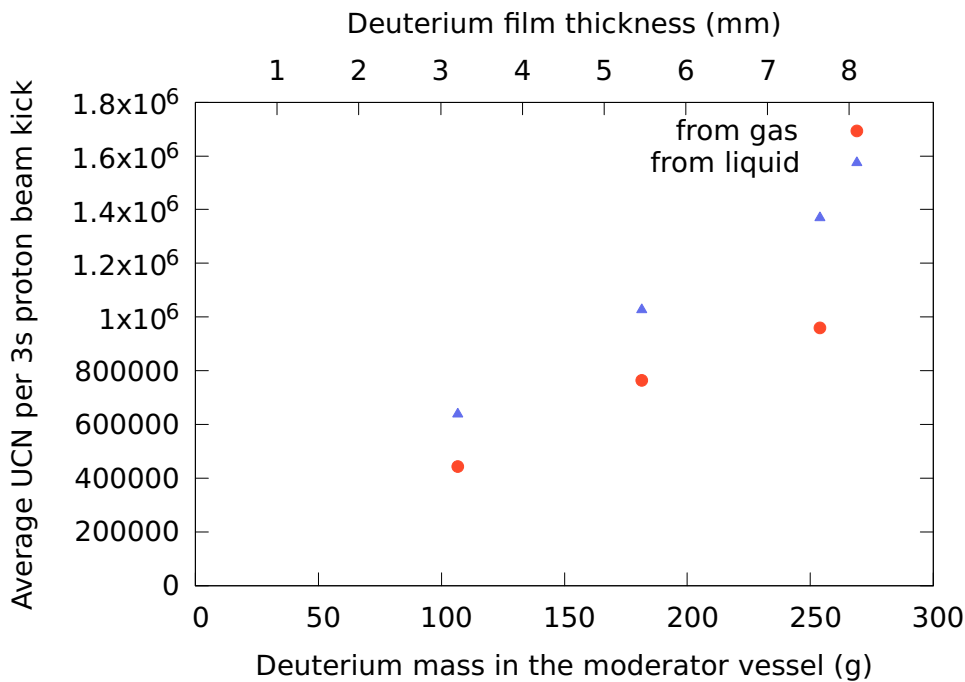
Figure 3.5: *UCN output with respect to D_2 mass in the moderator vessel. Large mass measurements made in December 2015. The red points correspond to measurements after additional deuterium was frozen onto the already existing solid from the gas phase. The blue points correspond to measurements where the deuterium was fully liquefied and then frozen again. A clear increase of UCN output can be observed for the measurements after liquefaction, while the addition of more deuterium from the gas phase onto the solid already present in the moderator vessel only results in small gains, or as in the case from 181.5 g to 253.8 g even leads to a reduction of the UCN production. x and y error bars are on the order of the point size.*

3.3   Storage Characteristics of the Source Storage Vessel

3.3.1   Motivation

As two measurements of the storage time constant of the UCN source's main storage vessel showed a deterioration in time, namely

- Oct 2011: 93.4(3) s [Göltl, 2012]

- Oct 2012: 89.2(2) s [Komposch, 2012]

a thorough check and measurements over a longer time period were done in order to corroborate that the vessel conditions stay comparable or to see if conditions deteriorate.

3.3.2   Setup

The storage time constant is deduced from a measurement at the West-1 beamline, while all UCN guide flaps (NLK West-1, NLK West-2, NLK South) are in their closed position. The central storage vessel flap's closing mechanism is triggered at the end of the proton beam pulse, such that the produced UCN are fully contained in the storage vessel. Like this, only a small percentage of UCN leaks out through the guide flap, travels along the UCN guide and is detected in a 200 mm Cascade UCN detector mounted directly at the West-1 beamport.

The rate of UCN leaking through the guide flap is assumed to be proportional to the total amount of UCN inside the storage vessel.

The length of the proton beam pulse as well as the general performance of the source at the time of measurement are not important for this determination of the storage time constant and only result in different absolute detection rates. Only a change in UCN spectrum correlated with the general performance of the source would have an influence.

3.3.3   Result

Fig. 3.6 shows the fitted storage curves. In 2011 and 2012 the measurements were done using time bins of 1 s, while at later times 100 ms were used. All data later than 2012 is rebinned to 1 s long bins. All data was treated in the same way and the storage time fitted in the same time window in order to make a correct comparison.

The 2011 data are identical to the data in [Göltl, 2012].

The 2012 data are identical to the data in [Komposch, 2012].

Both the position and the width of the fit window were chosen diffently though, because the default UCN production sequence was changed to shorter intervals between proton beam kicks starting in 2013. This results in the central storage vessel flaps opening only about 200 s to 350 s after any given proton beam kick, which in turn results in a drastic change of the storage time constant of the storage vessel as UCN are emptied towards the bottom through a large opening.

The reduced χ^2 values of the fits to single exponential decays vary between 0.98 and 1.19. The fit errors on the time constants are on the order of 1 s. There is no monotonous trend visible over time. Starting with 89 s in 2011, the storage time got worse until 2013 and recovered to 85 s in 2014. This is shown in Fig. 3.7.

Table 3.2 shows the tabulated results.

Candidates for an explanation of this behaviour could be:

- Changing vacuum conditions inside the source storage vessel

- Freeze out of residual gas on the inner storage vessel surface

- Variations in the slits of the UCN guide flaps, which could be caused by thermal expansion or contraction of the actuating steel wires

- Variations in the slits of the central storage vessel flaps

Changing vacuum conditions can be excluded after investigating the logged pressures of the vacuum gauge 2QNK12CP046. This gauge is the closest to the storage vessel. Its accuracy is limited, but a close correlation between the pressure in the storage vessel and the pressure measured by this gauge can be assumed.

There is no correlation between the pressure in the storage vessel and the measured storage time constant observable. Table 3.2 also lists the measured pressures.
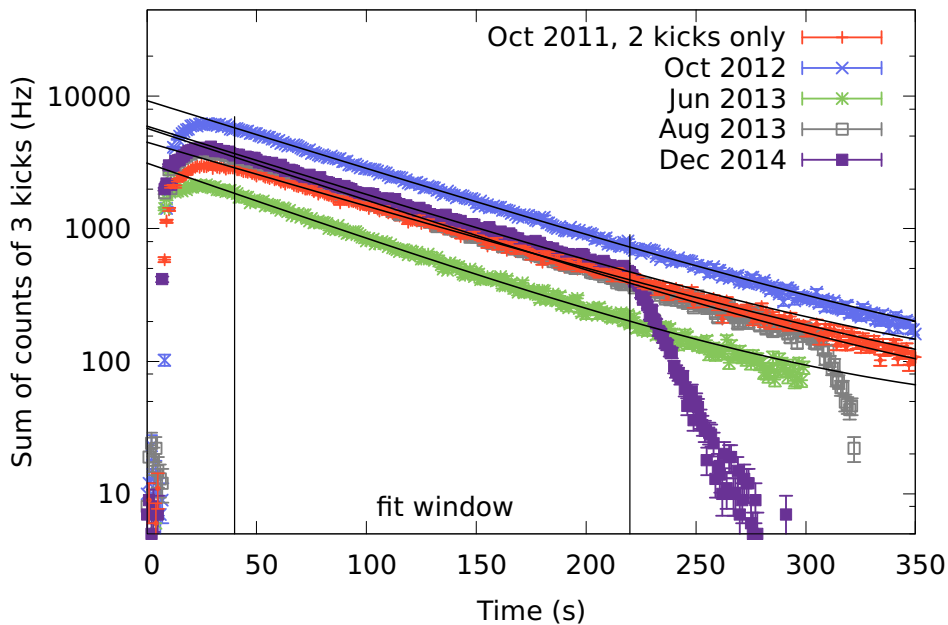
Figure 3.6: *UCN intensity spectra for four measurements of the source storage vessel storage time constant from Oct 2011 to Dec 2014, single exponential fits in the indicated time window are shown as well. The drastic reduction of UCN lifetime, e.g. at the end of the fit window in the 2014 data, is due to the reopening of the central storage vessel flaps in preparation for the next proton beam kick.*

Other causes which would result in a continuous degradation of the storage time constant, such as

- Contamination of the storage vessel surfaces

- Damage to the surface coating

can be excluded, because they cannot explain a growing storage time constant.

Large scale damage to the coating of the storage vessel has idependently been excluded by optical inspection using a remotely controlled camera in 2014.

3.3.4   Conclusion

From the lack of a clear trend towards longer or shorter storage time constants it can be concluded that no significant deterioration of the storage vessel is taking place.
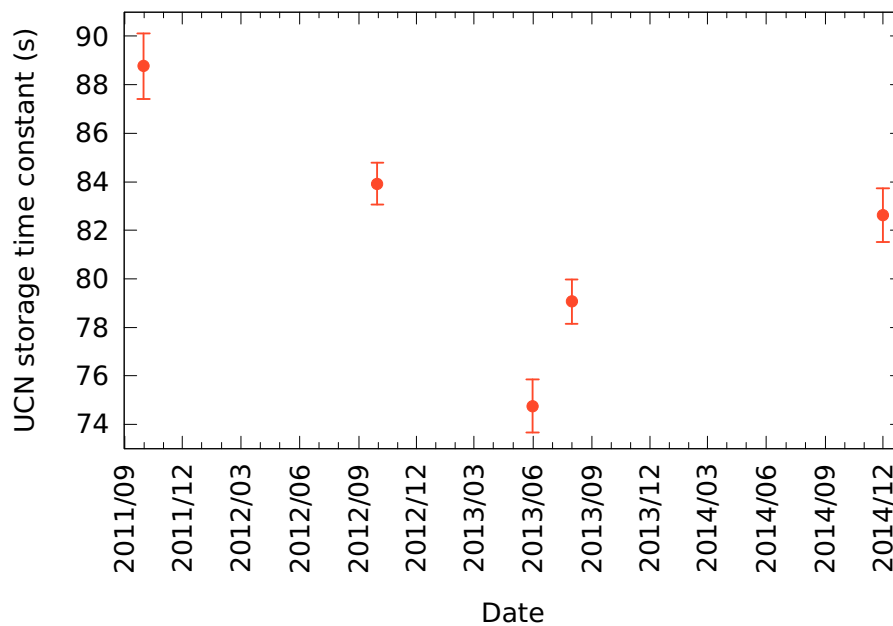
Figure 3.7: *UCN storage time constants in the source storage vessel. Error bars indicate fit errors using single exponential fits.*

Time of Measurement	Pressure at Sensor CP046	Storage Time Constant
Oct 09 2011, 09:30 - 11:00	1.6×10^{-7} mbar	89(1) s
Oct 01 2012, 13:13 - 13:51	1.2×10^{-7} mbar	84(1) s
Jun 03 2013, 10:18 - 10:46	0.5×10^{-7} mbar	75(1) s
Aug 19 2013, 13:10 - 13:26	0.6×10^{-7} mbar	79(1) s
Dec 12 2014, 17:57 - 18:20	0.2×10^{-7} mbar	83(1) s

Table 3.2: *Measured Storage time constants in the source storage vessel since 2011.*

3.4 UCN Transport — "Ping-Pong" Measurements

In order to measure the characteristics of UCN transport from the storage vessel inside the source to experiments located at the end of the three beam ports in situ, a test measurement dubbed "UCN Ping-Pong" was first conducted in 2012 and reported on in [Göltl, 2012]. Although all UCN guides had been tested for the UCN transport characteristics prior to commissioning of the UCN source [Göltl, 2012], this in situ measurement provides additional insights because it is sensitive to potential imperfections in the mounting of the guides as well as aging or contamination effects since the ex situ measurements. "Ping-Pong" measurements were repeated in 2013 using an automatic timing sequence for the central storage vessel flaps, using higher time resolution in the UCN detection and an inverted detector setup to increase counting statistics. Additionally, the measurements were also performed with the polarising magnet at beam port South ramped to multiple field strengths.

The idea of this measurement is to produce UCN inside the source storage vessel as usual, then fill an external storage vessel connected to one of the lower UCN guides. There the UCN are stored for 130 s, while the source storage vessel and guide system are cleansed of remaining UCN. This is done by opening the central storage vessel flaps, allowing UCN to fall back down towards the solid D2. When no UCN are left inside the source and guide system, the central storage vessel flaps are closed again to allow UCN to traverse from one guide into the other. Subsequently, UCN are released from the external storage vessel back towards the source's storage vessel. A detector mounted at the other lower UCN guide detects UCN which have traversed both UCN guides as well as the source storage vessel. In order to measure how many UCN started towards the source from the external storage vessel, UCN can also be extracted towards a Cascade detector mounted behind the shutter on the side pointing away from the source as a calibration. By using identical filling and storage times, the initial conditions for the "Ping-Pong" measurements can be established. The fraction of UCN released at one beam port and detected at the other beam port is then a measure for the cumulative losses occurring in guides, windows, and in the storage vessel. It also includes possible slits between individual components.

3.4.1 Setup

A 25 L external storage vessel made of a 1 m long piece of glass UCN guide (I.D. 180 mm, coated with NiMo) and two shutters coated with DLC is mounted at beam port West-1. It can be emptied in both directions, either towards a small Cascade UCN detector or back towards the UCN storage vessel of the source. A sketch is shown in Fig. 3.8. The shutters are actuated by pressurised air and take approximately 1 s to open or close, as described in [Göltl, 2012].

At beam port South, the big Cascade detector is mounted right outside the "Strahlwegventil" shutter, i.e. behind the 5 T polarising magnet.

Measurements with magnetic fields of 0, 1.5, 2, 3, and 5 T were conducted.
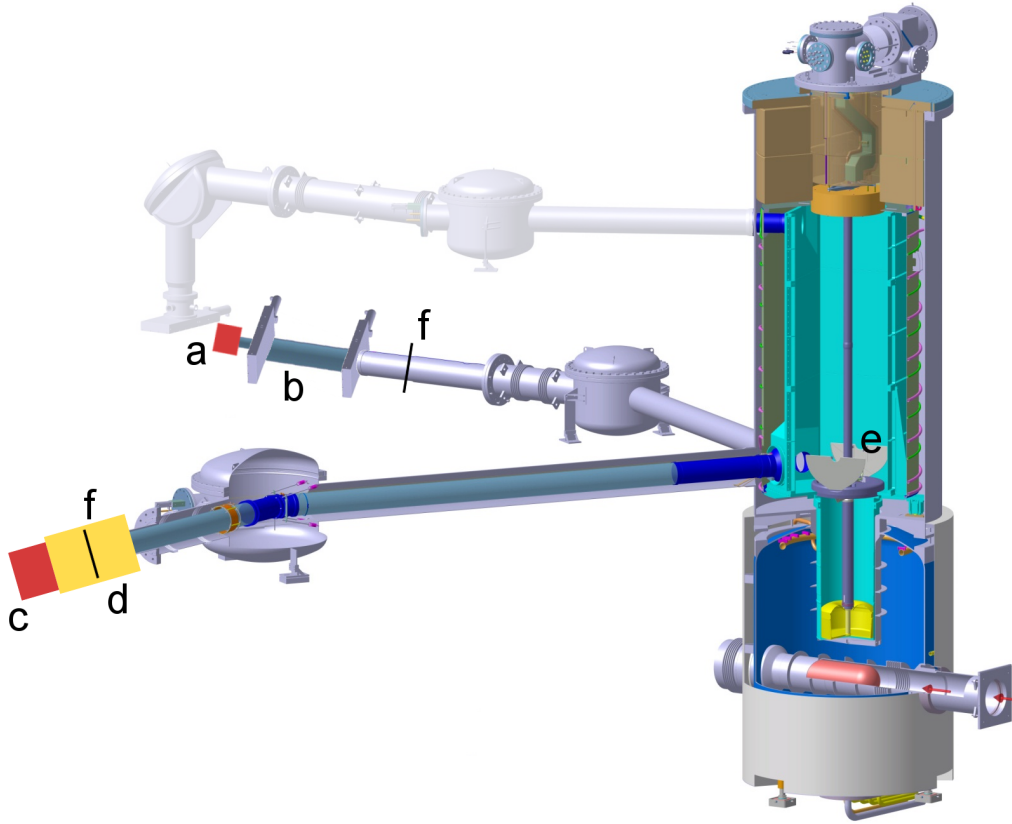
Figure 3.8: *Sketch of the installation used for the "Ping-Pong" measurements. a) small Cascade detector connected to the storage bottle at West-1 with a 300 mm long ID 100 mm guide. b) storage bottle made of a 1 m long glass UCN guide coated with NiMo and two DLC coated vacuum shutters. c) big Cascade Detector mounted at beam port South with a 150 mm long ID 180 mm guide. d) polarising magnet. e) central storage vessel flaps. f) AlMg3 vacuum separation foils.*

3.4.2 Measurement and timing

Three separate timing systems were used for the contol of the central storage vessel flaps and the external components like shutters or UCN detectors.

The central storage vessel flaps were controlled by the UCN source control system. As under normal operation conditions, the flaps are closed on a trigger from the accelerator system a constant time before the end of the proton beam kick. Instead of keeping the flaps closed until shortly before the next proton beam kick, the time to keep the flaps closed was reduced to 20 s, after which the flaps open again in order to drain the source from remaining UCN. The flaps are closed again another 110 s later by diverting the safety closedown timer of the flaps from its intended use. Typically in automatic UCN production mode, this timer is set to a large time on the order of 1×10^4 s, and closes the flaps if no trigger signals have occurred for this time.

When the flaps have been closed by the safety closedown timer, they are typically reopened only with the next occurring trigger, which results this first kick of a new production series being lost. In order to avoid that, we opened the flaps manually in a time window of 10 seconds. The only

conditions for the timing of this reopening are, that the measured UCN count rate is already at background level, and that the flaps are open and ready to close when the next trigger is received. As this time is not critical for the measurement, fluctuations in the final reopening time do not influence the measurements.

The shutter timing electronics (identical to the ones described in [Göltl, 2012]) are triggered by the falling edge of the WK signal, i.e. at the end of the proton beam kick. Both cascade detectors are triggered simultaneously on a signal created by delaying the WWK signal by approximately 8 s, which results in the time base of the Cascade data files starting at approximately 2 s before the beginning of the proton beam kick. They run on their internal clocks. Measurements with opening the pre-storage volume towards the source and directly to the detector were done in multiple groups of typically five measurements in order to avoid systematic effects due to drifts of the source performance.

The time sequence of the measurement is the following: After a 3 s beam-kick with trigger (i.e. with closing the main storage vessel flaps) the external storage vessel is filled with the outside shutter closed for 8.6 s. This filling time has been optimised beforehand. Then the source-side
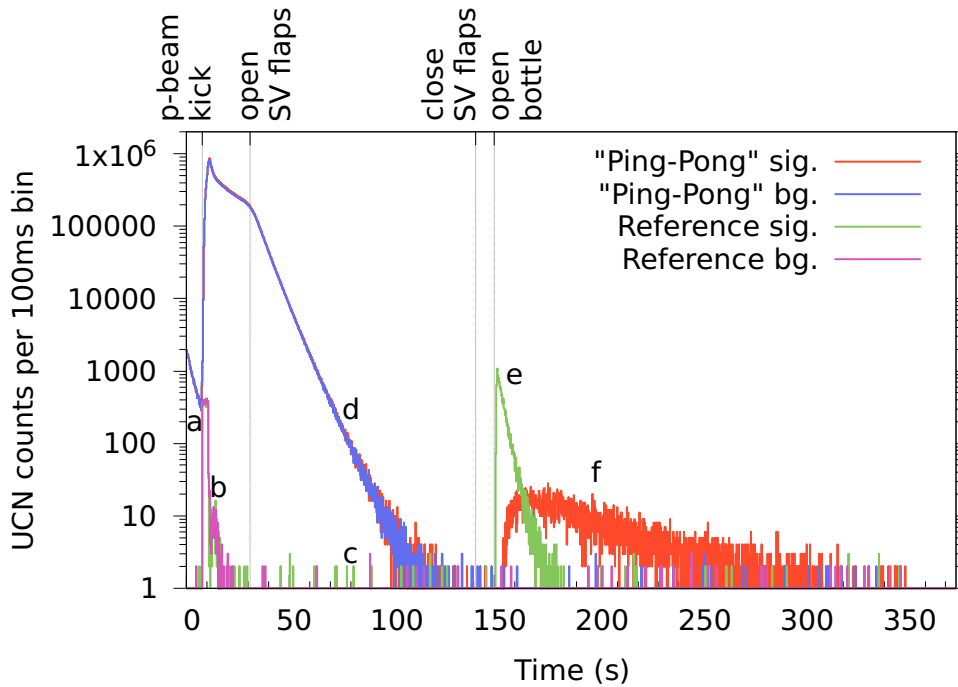
Figure 3.9: *Sum of UCN counts of 21 measurements opening the prestorage bottle (mounted at beam port "West-1") towards the UCN source and 20 measurements opening towards the external detector. a) UCN produced in the 7 ms long pilot beam kick. b) Increased background in the detector at West-1 through closed shutters during and shortly after the proton beam kick. c) Background level d) Quickly decaying UCN count rate at beamport South while SV flaps are opened. e) UCN peak after opening the prestorage bottle towards the directly attached detector. f) UCN peak after opening the prestorage bottle towards the source, measured at beam port South. The polarising magnet was switched off.*

shutter of the external vessel is closed. During that period, the storage time constant of the central storage vessel with NLK South and West-1 open is 22.1 s.

1.4 s later the main flaps of the UCN storage vessel to the moderator are opened and for 110 s the UCN can fall down towards the moderator, hence quickly emptying the storage vessel and connected guides. The UCN count rate in detector South drops rapidly after the central storage vessel flaps are opened and reaches the background level of < 1 Hz after about 100 s. The initial storage time constant with open central storage vessel flaps is approximately 6.0 s, marginally increasing once the source is almost empty. 110 s later, when the source and guides are emptied of all UCN, the main storage vessel flaps are being closed again.

After a storage time of 130 s one shutter of the external storage vessel is opened again, releasing the stored UCN. If the shutter pointing towards the detector at beam port West-1 is opened, a calibration measurement of the UCN still present in the prestorage vessel is done. If the shutter pointing back towards the UCN source is opened, a transport measurement to beamport south is done. After traversing the source guides and the central storage vessel, a certain fraction of the UCN reach the detector at beam port South. The observed number of UCN counts with respect to the time after the beam-kick is shown for both beam ports in Fig. 3.9.

The arrival peaks of UCN after opening the external storage bottle either towards the directly attached detector or back towards the source are well separated in time from UCN counted after the initial UCN production. This shows that the external storage time of 130 s is long enough such
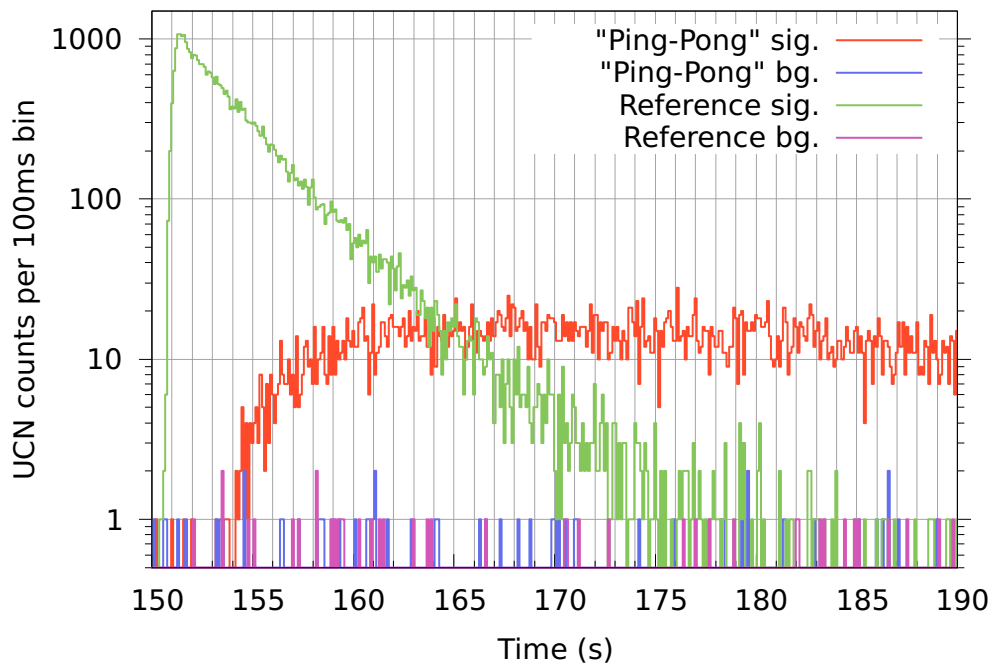
Figure 3.10: *Zoom into the region of interest. The first* 40 s *after opening the shutter of the prestorage vessel are shown. The arrival time difference of about* 4 s *between the first UCN detected in the directly connected detector (green line) and the first UCN detected at beamport South after traversing the source (red line) is well visible. The completely different peak shapes for the two settings are obvious.*

that the count rate of UCN which remained inside the source storage vessel reaches background levels before the external vessel is opened again.

A zoom into the region of interest is shown in Fig. 3.10.

The measurements were done with a proton beam kick repetition time of 360 s.

3.4.3   Results

The big and small Cascade detectors have different detection efficiencies, because different aluminium foils are used as entry windows. Their different sensitive areas also result in different UCN extraction efficiencies from the external storage bottle into the detector.

When measuring with directly attached detectors in identical conditions, i.e. only separated by the time it takes to unmount one and mount the other detector, we found that the small detector only counts 39(1) % of the amount of UCN with respect to the big detector in 3 s long proton beam kicks with SV flap trigger and 39.8(1) % in 2 s long proton beam kicks without trigger.

In order to calculate the transmission of UCN from the external storage vessel through the source guides and storage vessel to the detector at beam port South, the reference measurements with the small Cascade detector connected directly to the storage bottle have been scaled accordingly.

The measured fraction of UCN reaching the detector at beam port South is 0.10(1) with the polarising magnet switched off, and 0.07(1) for a field strength of 5 T in the polarising magnet (statistical errors only).

Results for all magnetic fields as well as the number of repetitions for both signal and background measurements are shown in Table. 3.3.

The transmission through the magnet decreases with higher field values as expected, as UCN with the "right" spin state are accelerated by the magnetic field and pass the magnet, while UCN with the "wrong" spin state are decelerated, and can only pass the magnet if their kinetic energy is higher than the repelling potential of ± 60.3 neV/T .

The maximum magnetic field strength of 5 T therefore results in a potential barrier which is higher than the Fermi potential of all walls in the source. This results in full polarisation of UCN by the magnet.

B	fraction	corr. fraction	sig. rep.	bg. rep.
0	0.25(2)	0.10(1)	21	20
1,5	0.19(1)	0.073(3)	15	6
2	0.17(1)	0.065(3)	14	9
3	0.17(2)	0.06(1)	17	8
5	0.18(1)	0.07(1)	28	11

Table 3.3: *Results for the pingpong measurements. The fraction of UCN counts at beam port South with respect to UCN counts at beam port West-1 and the same fraction corrected for detector efficiencies are given. The number of repetitions is given separately for signal measurements (opening towards beam port South) and background measurements (opening towards the detector at beam port West-1).*

However, the effective transmission rate of the magnet, taking into account the vacuum safety window made of a 100 μm thick AlMg3 foil mounted at the point of highest magnetic field inside the magnet, does not go down to 0.5. Instead, because UCN with the "right" spin state get accelerated in the magnetic field, their transmission through the foil is increased.

See also Chapter 3.5 for more details on UCN transmission through the magnet with respect to the magnetic field.

The measured fractions of UCN with respect to the magnetic field strength in the polarising magnet is shown in Fig. 3.11.

Fitting the emptying peak of the storage bottle into the directly attached detector yields a decay time constant of 3.08(2) s. Fitting the rate of UCN detected at beam port South after traversing the source, excluding the rising edge, yields a decay time constant of 35.0(14) s. This is compatible with measurements of the storage time constant of the central source storage vessel with both NLK West-1 and South opened, at times larger than 150 s after the proton beam kick, which is 35.8(2) s.

3.4.4   Additional measurements as MC input

Two quantities relevant as input for Monte Carlo calculations are the UCN transmission of the AlMg3 UCN guide end-windows as well as the UCN momentum distribution inside the 25 L
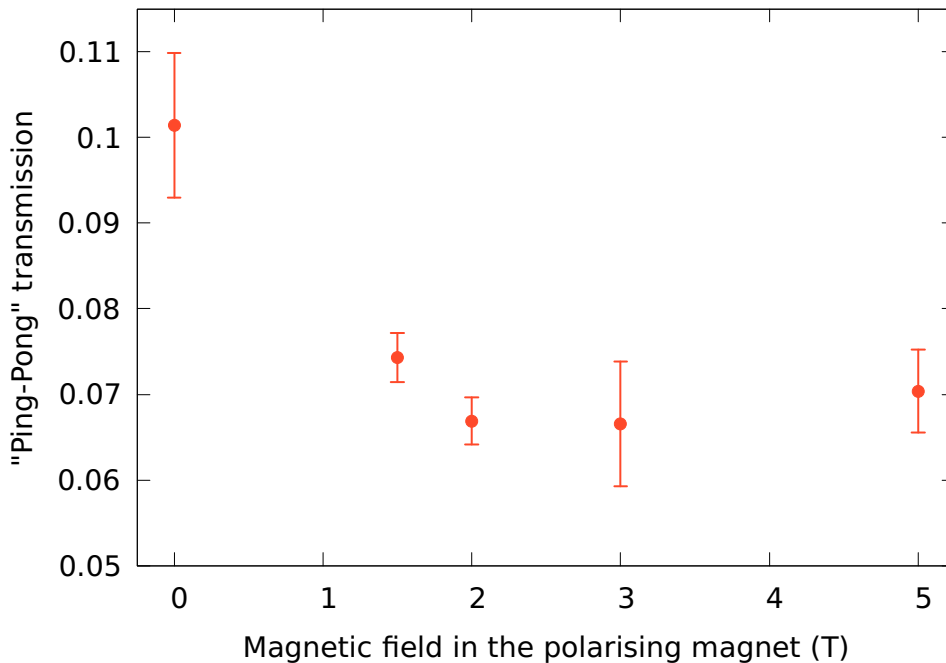
Figure 3.11: *"Ping-Pong" transmission, i.e. fraction of UCN exiting at beam port South with respect to beam port West-1, through the UCN guide system and storage vessel with respect to the magnetic field in the polarising magnet. The different detection efficiencies of small and big detectors are taken into account.*

vessel at the time of opening. Both are accessible by additional measurements, which were performed after the main measurements.

Momentum Distribution   To get a handle on the momentum distribution of UCN after 130 s of storage inside the 25 L storage vessel, a 2200 mm long, ID=180 mm UCN guide made of NiMo coated glass was installed between the storage vessel and the big detector at the West-1 beam port. Then the same shutter sequence as in the Ping Pong experiment itself was performed, opening towards the detector. All timing settings were identical to the ones used in the Ping-Pong measurements, e.g. the UCN were stored for the same 130 s. The detector was configured to use a time resolution of 25 ms per bin.

Fig. 3.12 shows a time spectrum of the UCN counts zoomed into the relevant first 50 s after shutter opening and a regular reference measurement of the Ping-Pong experiment (with a timing resolution of 100 ms). A delay of about 0.3 s of the arrival time through the 2.2 m long guide is visible with respect to the arrival time with the small detector connected via a 300 mm guide. The absolute heights of both curves are arbitrary, as the overall source performance was different, the binning is different and the amount of measurements which are summed over is different.

Transmission through End Windows
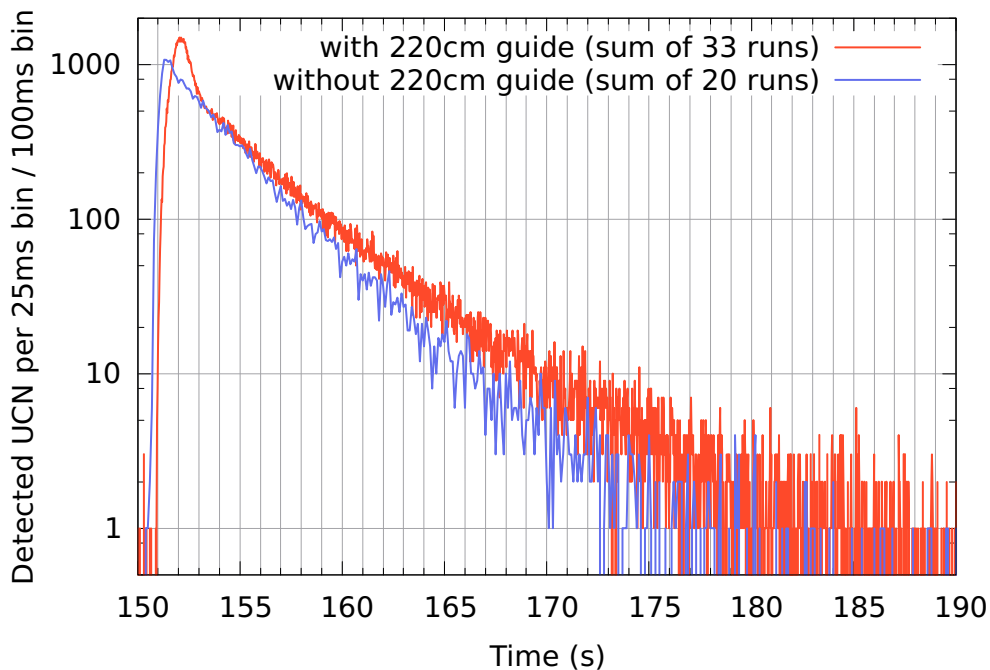
Figure 3.12: *Arrival time of UCN after traversing the* 2200 mm *UCN guide, bin size* 25 ms *(red), in comparison to Ping Pong reference measurements without the additional guide, bin size* 100 ms *(blue). The absolute heights of the curves are arbitrary, see text.*

The transmission through one and two foils from the same batch as the guide end windows and of the same geometry was measured in the same setup after 130 s of storage. Single foils or pairs with two foils placed at a distance of about 5 mm were mounted either close to the storage bottle or close to the detector.

The results of 0.70(3) are shown in Fig. 3.13. In the case of two foils, the second foil has a better UCN transmission than the first one, because UCN impinging on the first foil at small angles, which can therefore be reflected even though their kinetic energy is higher than the Fermi potential of the foil, do not contribute to the transmission of the second foil.

3.4.5 Conclusion

"Ping-Pong" type measurements of the UCN transmission through the guide system and central storage vessel have been done with high statistics and consistent timing, making sure signal and background regions were well separated.

The absolute transmitted fraction of UCN agrees well with both simple calculations ([Lauss, 2016]) and Monte Carlo simulations ([Zsigmond, 2015]).

In order to understand the distribution of UCN arrival times, further simulations taking into account more details have to be done.

Additional measurements which can be used to tune simulations to such details, like in situ foil measurements etc. have been done.
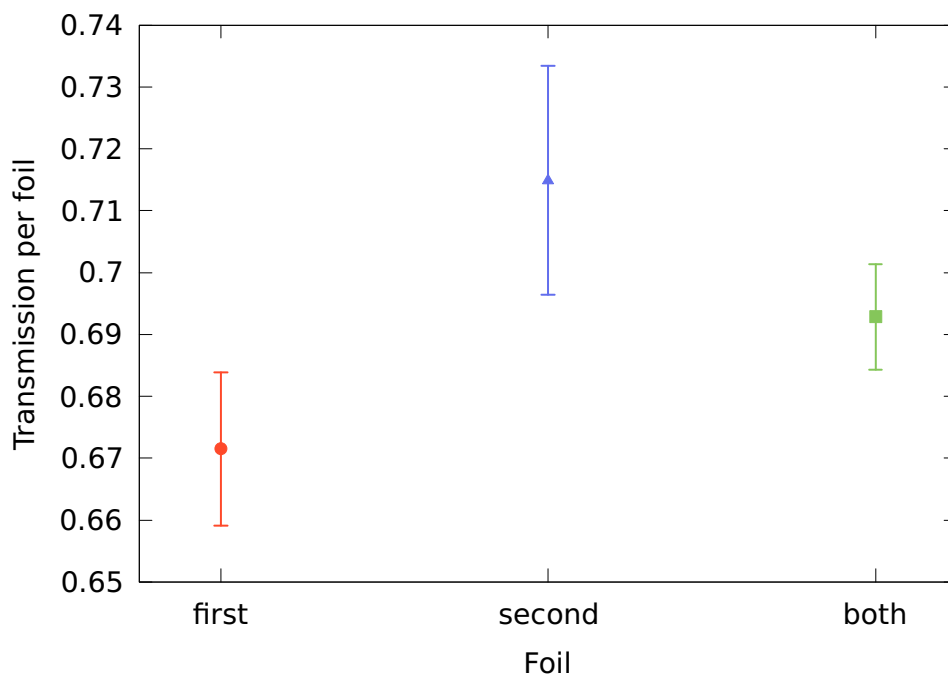
Figure 3.13: *UCN transmission of guide end window foils (*100 µm *AlMg3) measured with* 180 mm *diameter foils after* 130 s *of prestorage in the "Ping-Pong" setup.*

The fastest UCN reach the detector at beam port South about 4 s after being released from the pre-storage vessel at beam port West-1. The shortest possible path between the beamports is about 15.3 m long, which results in the maximum UCN velocity of about 3.8 m s^{-1} along the beam line after 130 s of pre-storage.

3.5   UCN Transmission through the Polarising Magnet

3.5.1   Setup

In the course of measuring the UCN transport through the UCN source guide system, the big Cascade detector was mounted at beam port south, behind the superconducting polarising magnet. No additional spin analysis system was used.

This setup was also used to investigate the time dependence of the UCN rate for various magnetic fields created by the magnet.

Due to the interaction of the neutron magnetic moment with magnetic fields, UCNs experience a change of potential of ±60.3 neV/T depending on their spin.

For magnetic fields in the range of 0 T to 5 T, multiple proton beam kicks, 3 s long and with active "Klappentrigger" as well as "Norm"-kicks, i.e. 2 s long kicks without "Klappentrigger", were recorded for each magnetic field magnitude. The proton beam current at the time of measurement was 2190 µA. Time bins of 100 ms were used.

It should be noted again that the safety foil of the UCN source vacuum at beam port South is located in the center of the magnet, at the highest field. This placement was chosen because the average kinetic energy of UCN with the transmitted spin is highest at this point, thus increasing the transmission probability through the foil and eliminating the reflection of low energy UCN with kinetic energies below the Fermi potential of the foil material (AlMg3, 54 neV).

3.5.2   Count rates

The averaged time spectra for magnetic fields from 0 T to 5 T, measured with "Klappentrigger" are shown in Fig, 3.14.

With the magnet turned off, the highest count rates were measured.

With increasing magnetic field magnitude, lower rates of UCN were registered in the detector. This is expected, as 50 % of the neutrons — one spin state — start to encounter a potential barrier increasing with magnetic field strength.

The integrated UCN counts for the different magnetic fields, measured with "Klappentrigger", are shown in Fig. 3.15 and are given with and without "Klappentrigger" in Tables 3.4 and 3.5. In both cases the lowest measurement at $B = 5$ T is lower than the measurement without magnetic field by a factor of 0.57.

The fraction is different from 0.5 because those UCN with the right spin to traverse the magnet even at high magnetic fields experience a corresponding raise in energy, which increases the transmission through the AlMg3 foil mounted in the center of the magnet. Also, possible loss of UCN spin polarization inside the source can lead to UCN returning to and passing the magnet after a first reflection. This would also lead to a fraction larger than 0.5.

3.5.3 Time Dependence

A zoom into the first 60 s as shown in Fig. 3.16 reveals several interesting features:

1. The peaks of the count rates, about 1 s after the end of the proton beam kick, are separated in intensity. UCN with forward momenta high enough to traverse the magnet at $B = 5\,$T are exiting the source.

2. Only about 1.5 s after the end of the kick, the UCN rates for $B = 4\,$T and $B = 5\,$T merge. This means, that no UCN with forward momenta high enough to traverse $B = 4\,$T magnetic fields are left in the source.

3. At about 5.5 s after the end of the kick, the same happens for UCNs which cannot traverse $B = 3\,$T.

4. At about 50 s after the end of the kick (not shown in Fig. 3.16), the same happens for UCNs which cannot traverse $B = 2\,$T.

3.5.4 Emptying times

A double exponential decay of the form
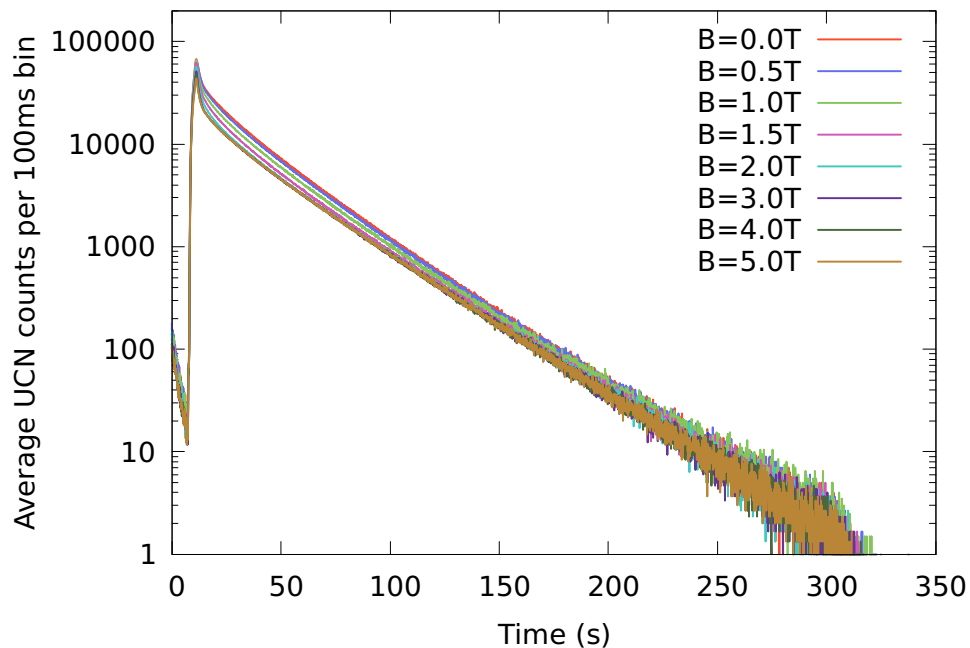
Figure 3.14: *UCN rates per* 100 ms *bin, averaged over 3 proton beam kicks with "Klappentrigger", for different magnetic fields in the polarising magnet.*

$$N(t) = a \times e^{-t/\tau_1} + b \times e^{-t/\tau_2} \qquad\qquad (3.2)$$

where $N(t)$ is the amount of UCN counted in a given time bin, a and b decay amplitudes for the short (τ_1) and long (τ_2) decay constants, was fitted to the time spectrum which reflects the emptying time of the source storage vessel. Both exponential decay times are shown in Fig. 3.17.

All fitted storage time constants are shown in Tab. 3.6. The fits are done in a time window from 15 s to 300 s, which corresponds to a 285 s long window starting about 4 s after the end of the proton beam kick.

The long time constant, on the order of 30 s, rises with the magnetic field strength and saturates at 3 T. This is likely caused by the fact that the magnetic field reflects UCN of the wrong spin state back into the source, where the UCN can change their spin e.g. in a wall collision and then come back to the magnet again after a diffuse reflection from a wall.

Like this, some UCN exit the source at later times than if there would not have been a magnetic field present, which leads to a longer emptying time.
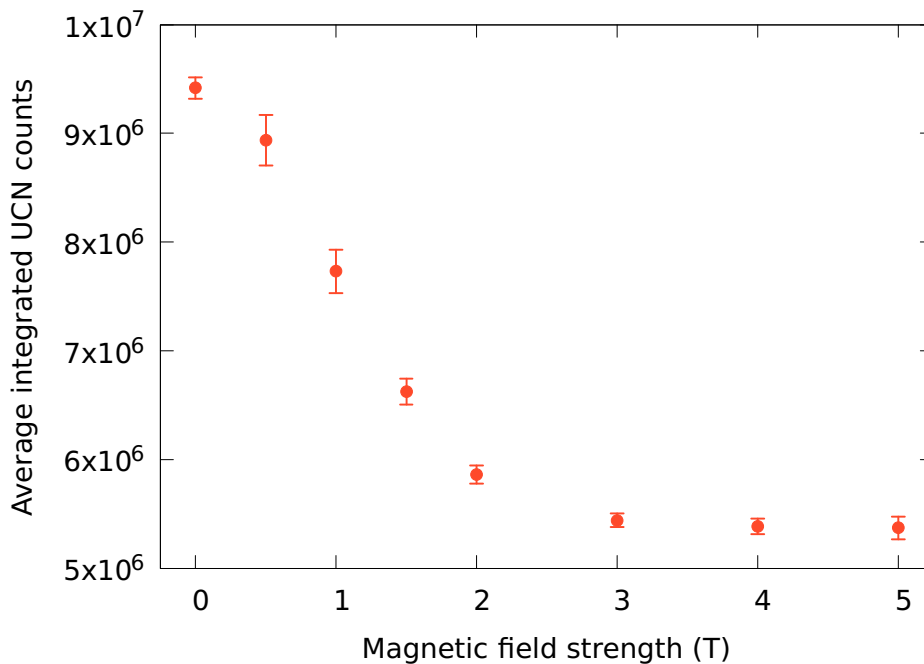
Figure 3.15: *UCN counts integrated from* 1 s *after the end of the proton beam kick up to* 300 s *, averaged over 3 proton beam kicks, for different magnetic fields in the polarising magnet.*
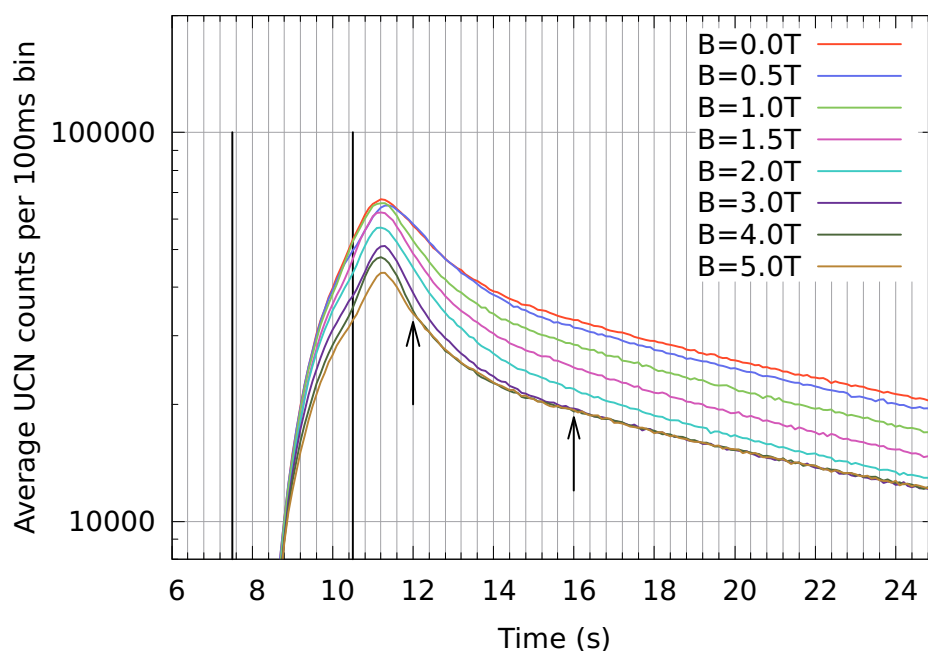
Figure 3.16: *UCN rates per* 100 ms *bin. The vertical black lines indicate start and end time of the* 3 s *long proton beam kick. The arrows indicate the times when no excess counts with respect to the next higher field value can be distinguished anymore (for 5, 4, and 3 T). The time dependence of the count rate at B = 0.5 T differs slightly at short times for unknown reason.*
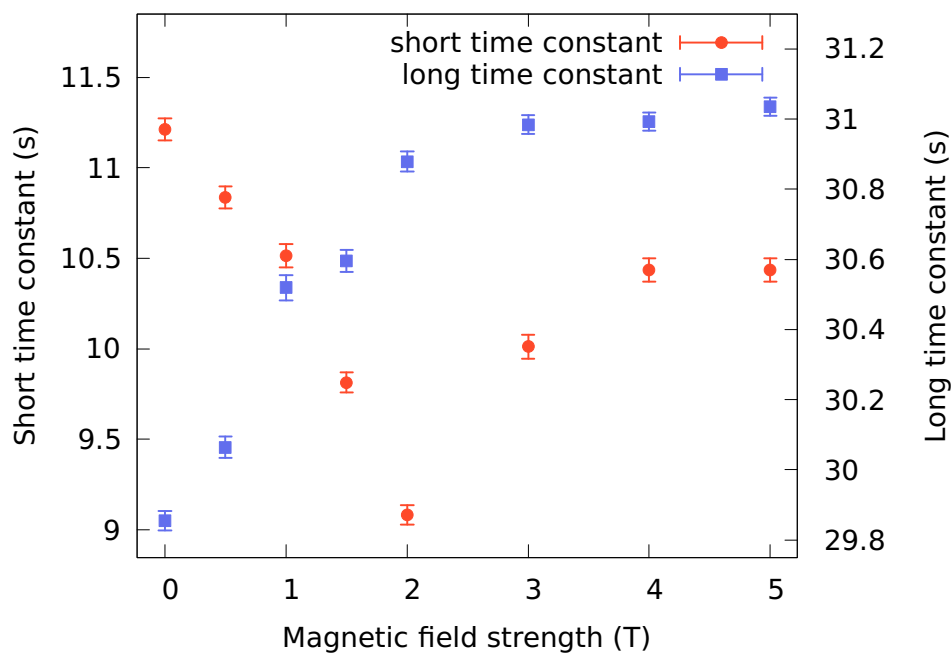
Figure 3.17: *Emptying times of the UCN source for different magnetic fields in the polarising magnet. The values and errors are extracted from fitting a double exponential decay to the data.*

B(T)	Avg. UCN per kick	Std. Dev.	Transmission
0.0	9 417 139	100 558	1.00
0.5	8 937 690	231 352	0.95(3)
1.0	7 732 001	199 624	0.82(2)
1.5	6 626 204	119 189	0.70(1)
2.0	5 863 190	83 587	0.62(1)
3.0	5 439 827	62 564	0.58(1)
4.0	5 383 889	72 511	0.57(1)
5.0	5 371 650	103 247	0.57(1)

Table 3.4: *Integrated UCN counts with respect to magnetic field strength, transmission relative to* 0 T. *Measured in* 3 s *long proton beam kicks at a proton beam current of* 2200 μA *with klappentrigger. Integrated from the end of the proton beam kick until the central storage vessel flaps were opened.*

B(T)	Avg. UCN per kick	Std. Dev.	Transmission
0.0	1 590 813	3047	1.00
0.5	1 523 938	3361	0.958(3)
1.0	1 353 955	7762	0.851(5)
1.5	1 183 752	9627	0.744(6)
2.0	1 043 948	4535	0.656(3)
3.0	923 201	3435	0.580(2)
4.0	900 786	5263	0.566(3)
5.0	898 481	3401	0.565(2)

Table 3.5: *Integrated UCN counts with respect to magnetic field strength, transmission relative to* 0 T. *Measured in* 2 s *long norm proton beam kicks at a proton beam current of* 2200 μA *without klappentrigger. Integrated from the end of the proton beam kick for* 300 s.

B(T)	τ_1(s)	τ_2(s)
0.0	11.21(6)	29.85(3)
0.5	10.84(6)	30.06(3)
1.0	10.52(6)	30.52(4)
1.5	9.81(6)	30.60(3)
2.0	9.08(5)	30.88(3)
3.0	10.01(7)	30.98(3)
4.0	10.44(7)	30.99(3)
5.0	10.44(7)	31.04(3)

Table 3.6: *Fitted storage time constants for various magnetic field strengths. Double exponential fit, fit window:* 15 s *to* 300 s *(for the timing relative to the proton beam kick see Fig. 3.16).*

3.6 UCN Density at Beam Port West-1

The density of UCN available at the beam port is one of the most distinctive quality factors of a UCN source. Section 7 gives a comparison of all operating UCN sources world-wide with respect to the UCN density.

The density available at the PSI UCN source was measured in two setups:

1. A 1 m long UCN guide made from glass, coated with NiMo (mass ratio 85/15), with an inner diameter of 180 mm, sandwiched between the West-1 "Strahlwegventil" and a second identical UCN and vacuum shutter made by VAT. The blades of both shutters are coated with DLC. The guide is made in the same way as the glass guides inside the UCN source. The two shutters are controlled with a LabView program through an electronics box containing 24 V control logic [Göltl, 2012]. This storage bottle has a volume of ~ 25.4 L, the Fermi potentials of the walls are 220 neV for the NiMo coating of the glass and 230 neV for the DLC coated shutter blades.

2. A ~ 32 L stainless steel storage bottle, described in detail in Section 6.

As the second setup does not include parts of the UCN source safety system, namely the so-called "Strahlwegventil" vacuum shutter, it's position is independent of the end of the beamport, it can be mounted at various positions and heights.

The height of the storage bottle above the beam port was varied using an S-shaped beam line made from electropolished stainless steel tubes complying with DIN 11865 (bends) and DIN 11866 (tube), consisting of two 45° bends and a 2 m long straight tube, all with an inner diameter of 200 mm and an outer diameter of 204 mm.

All parts[1] were specified as hygiene class H3, resulting in a roughness parameter $r_A < 0.8\,\mu m$. A drawing of the 45° bends is shown in Fig. 3.18. The specific measures are given in Table 3.7.

The first 45° bend was mounted directly behind the 1 m long glass guide coated with NiMo and a second VAT shutter, so basically behind the 25.4 L storage setup described above. Photographs of the 31.4 L storage bottle setup both directly at beamport West-1 and at greater height are shown in Fig. 3.22.

The idea behind varying the height of a storage experiment is first of all to adapt the storage vessel to the UCN energy spectrum delivered by the UCN source. At the West-1 beamport of the PSI UCN source, the energy spectrum is cut off at 54 neV at the lower end by the AlMg3 vacuum safety window located approximately 500 mm before the beamport shutter. As the maximum

---

[1]purchased from Herrli Ag, Kerzers, Switzerland, http://www.herrli.net

Dimension (mm)	R (mm)	l2 (mm)	l3 (mm)
204×2.0	300	224.3	100

Table 3.7: *Nominal measures of the 45° bends. For the meaning of the designations see Fig. 3.18*

storable UCN energy is given by the Fermi potential of the material of the storage bottle, such a lower cutoff effectively limits the phase space of UCN which can contribute to the UCN density. A rise in height shifts all UCN energies to lower values due to gravity, and thus can compensate for the energy cutoff caused by the safety window. If UCN losses in the guides from the beam port to the elevated storage bottle are low, the net density inside the bottle should be increased.

The height was adjusted by rotating the 2 m long stainless steel guide inbetween two 45° bends in order to keep the over all UCN guide length identical for all heights.

3.6.1 Density in a 25.4 L NiMo coated storage bottle at beam height

On July 12, 2013, measurements with the NiMo coated glass bottle were made at beamport West-1 using 6 s long proton beam kicks at a proton beam current of 2200 μA. After 2 s of storage, 535 000 UCN were measured in a big Cascade detector mounted directly behind the second VAT shutter.

Without any corrections for detector inefficiency or extrapolation to time zero, a UCN density of 21.0(1) UCN/cm^3 can be calculated, which is an improvement to the density of 16.8 UCN/cm^3 after 2 s using 7.7 s long proton beam kicks at a proton beam current of 2300 μA, as measured in [Göltl, 2012]. No full storage curve was recorded at this time.

On July 16, 2013, with the identical setup, a full storage curve was recorded, which is shown in Fig. 3.19. The measured UCN counts after a storage time of 2 s were 437 524(10938) , which
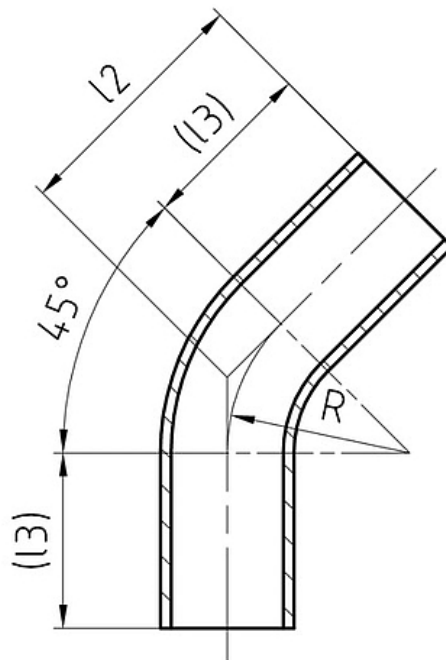
Figure 3.18: *Technical drawing of a DIN 11866 45° bend. Measures are given in Table 3.7. Source: Herrli AG, Kerzers, Switzerland.*

corresponds to a UCN density of 17.2(4) UCN/cm³. This was lower than four days earlier because of degradation of the UCN output with time, as there was no conditioning of the solid deuterium in between. 7 s long proton beam kicks were used, at a proton beam current of 2200 µA.

3.6.2 Density in a 32 L stainless steel storage bottle at various heights

In December 2015, density measurements with varying height above the beam port West-1 were conducted.

As the measurements were spread out over multiple days, and because the nEDM experiment was taking data 24/7, the UCN source performance varied strongly during the measurements. To compensate for this, all measurements were scaled to the same value of 2×10^6 UCN counts measured simultaneously directly at the West-2 beamport. In order to check if the normalisation to West-2 worked, most heights were measured twice and compared later.

Typically, every point was measured three times, while during repetition measurements for normalisation every point was measured less often.

All measurements were done using 5.4 s long proton beam kicks every 300 s, at the nominal proton beam current of 2200 µA.

In order to minimise leakage of UCN into the storage bottle, the second VAT shutter was closed together with the source-side storage bottle shutter.
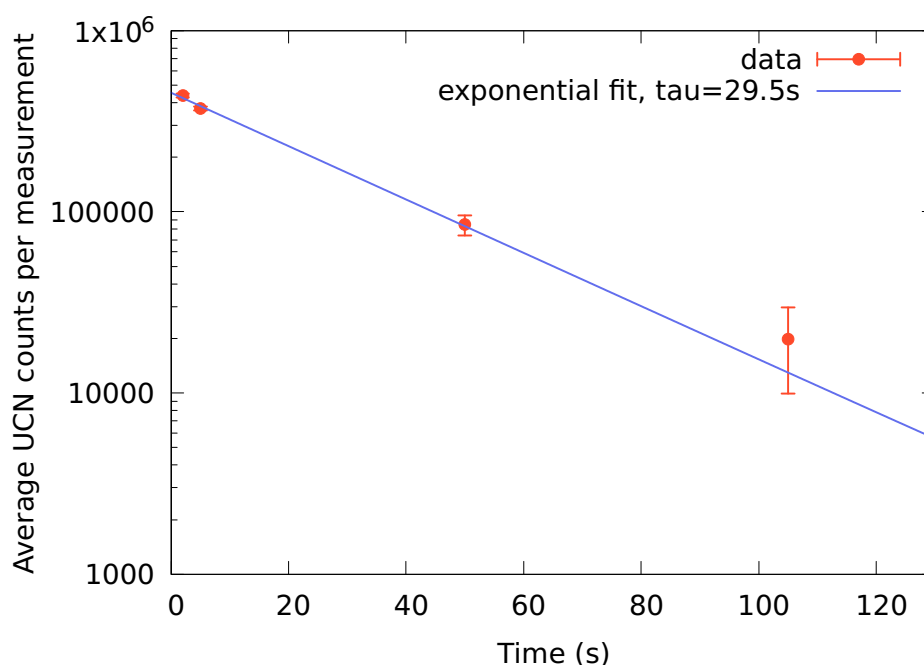
Figure 3.19: *Storage curve measured with a* 1 m *long* NiMo *coated glass guide of* 180 mm *inner diameter between two VAT vacuum shutters. Measured with the big Cascade detector connected directly to the second VAT shutter.*

The leakage from the enclosed volume between the second vacuum shutter and the storage bottle was measured for every height by keeping the source-side storage bottle shutter closed and the detector side shutter opened for the filling time, and measuring the content like for a regular 2 s storage time measurement.

The resulting height dependence of the UCN density after 2 s of storage is shown in Fig. 3.20. Measured UCN counts and leakage are given in Table. 3.8. Multiple data points for the same height indicate the goodness of the normalisation to West-2. Leakage counts were measured and subtracted for every height.

The height was measured from bottom of the UCN guide at the exit of the second VAT shutter to the bottom of the UCN guide at the bottle entrance. Given counts and densities are not corrected for detector inefficiency and beamline transmission, densities are not extrapolated to zero time.

UCN Densities between 6 UCN/cm^3 and 13 UCN/cm^3 were measured after 2 s of storage time.

The storage time constants depend on the average kinetic energy of the stored UCN, which in turn depends on the height above beam port of the storage bottle setup, as the UCN are slowed down by gravity.

Storage time constants were determined by measuring the leakage rate of UCN through the second storage bottle shutter during storage measurements with storage times of 100 s and fitting a model function of the form

$$N(t) \propto R(t) = A_1 \times e^{-t/\tau_1} + A_2 \times e^{-t/\tau_2} \tag{3.3}$$

where $N(t)$ is the total amount of UCN inside the storage bottle, $R(t)$ the rate of leaked UCN as measured in the detector, A_1 and A_2 population constants and τ_1 and τ_2 exponential decay time constants.

For an elevation of 1200 mm, such a double exponential fit didn't converge, so a single expoinential decay was fitted to the data.

The reduced χ^2 values of all fits were between 1.02 and 1.16

Table 3.9 shows the resulting storage time constants.

Height (mm)	UCN counts after storage	UCN counts at West-2	Leakage scaled to W2
1200(10)	321 876(114)	1 554 499	27 009
1200(10)	244 425(494)	1 224 614	27 009
1700(10)	78 276(158)	816 374	5037
1700(10)	164 740(392)	1 678 166	5037
400(10)	268 805(608)	1 171 547	47 334
−50(10)	141 879(313)	1 031 034	37 741
−50(10)	287 894(653)	2 025 039	37 741

Table 3.8: *Count data of density measurement with varying height above beam port West-1. The UCN counts after storage are corrected for UCN leakage through the closed source-side shutter. Leakage was only measured once and is thus scaled to 2×10^6 counts in West-2.*

Fig. 3.21 shows the storage curves measured for various heights, including repetitions at the same height with different normalisation due to changes in overall UCN source performance.

The transmission of the horizontally oriented 2 m long stainless steel guide and the two 45° bends, measured by comparing the horizontal storage measurement to a storage measurement without the parts in question, was found to be about 71.5(15) % for storage times from 2 s to 20 s. For even longer storage times, the transmission got even higher, which can be explained by the fact higher energy UCN are lost more likely in the beamline.

Fig. 3.22 shows photographs of the storage setup elevated to 1200 mm and directly attached to the second vacuum shutter.

After the measurements at various heights were finished, the storage bottle setup was mounted at a height of about 500 mm above the West-1 beam port using the identicel 45° stainless steel bends but only a 1 m long straight stainless steel guide. This measurement is described in detail in Sec. 7.9 and yielded a UCN density of 22.31(71) UCN/cm³ after 2 s of storage.

3.6.3 Conclusion and outlook

UCN densities of 21.0(1) UCN/cm³ and 22.31(71) UCN/cm³ have been measured at the West-1 beam port, using a NiMo coated glass storage bottle at beam port height and a stainless steel storage bottle elevated by 500 mm respectively.

As the UCN guides and bends used to reach the elevated position were made from stainless steel, their Fermi potential is identical to the Fermi potential of the stainless steel storage bottle. Therefore, significant loss of UCN with energies above 190 neV at beam port height during transport towards the bottle is to be expected.

In a future measurement, a UCN beam line and storage bottle with higher Fermi potentials should be used to measure the UCN density at an elevation $\gtrsim 500$ mm.

Height (mm)	τ_1 (s)	A_1	τ_2 (s)	A_2	χ^2/n_{df}
−50	14.9(20)	125(21)	41.5(21)	200(22)	1.14
400	23.8(45)	147(43)	70.9(100)	190(45)	1.02
1200	—	—	101.9(11)	225(1)	1.03
1700	—	—	92.2(12)	135(1)	1.16

Table 3.9: *Storage time constants for various heights above the West-1 UCN beam port.*
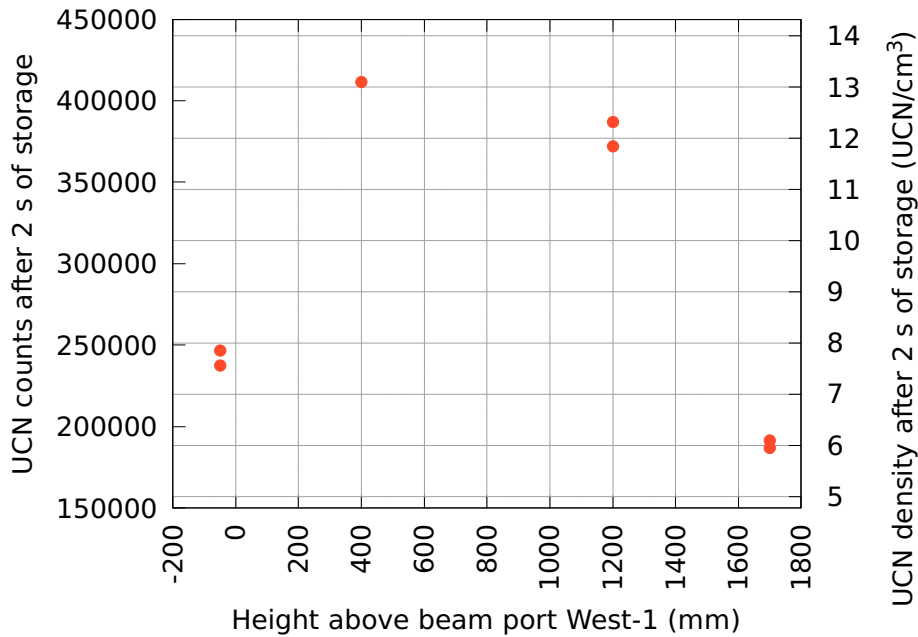
Figure 3.20: *UCN density after* 2 s *of storage in the stainless steel bottle, for various heights above the beam port. The height was adjusted by rotating a* 2 m *long stainless steel guide inbetween two 45° bends. Normalised to the total UCN counts in West-2. Leakage subtracted. Statistical error bars are smaller than the point size.*
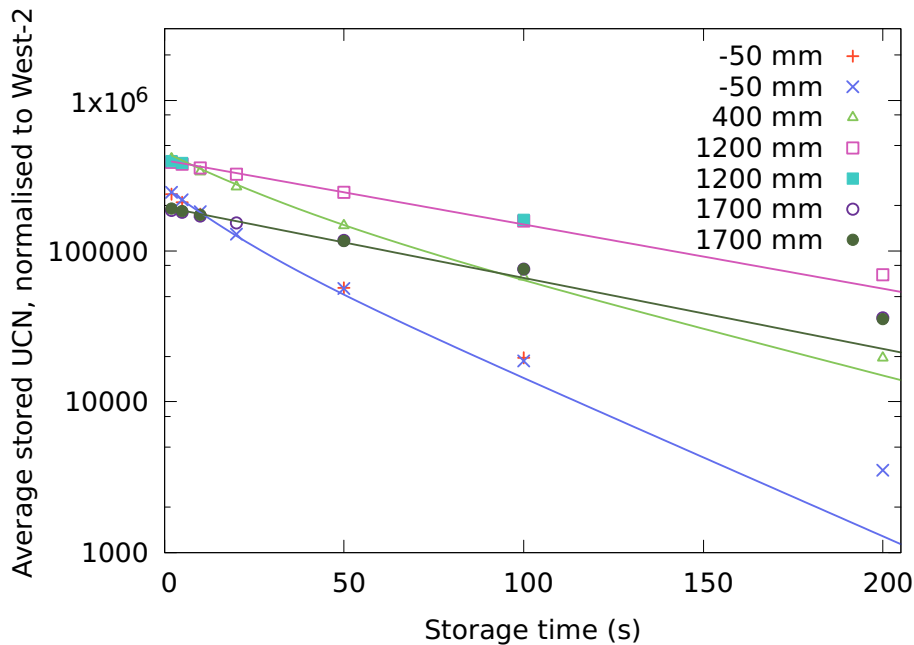
Figure 3.21: *Measured UCN counts (symbols) after various storage times, for various heights above West-1. Most height were measured multiple times and normalised to the total UCN output at the West-2 beam port. The lines indicate the fits to the UCN leakage rate through the second bottle shutter, scaled to the amount of stored UCN after* 2 s *of storage time. The storage time constants for an elevation of* 1700 mm *are the highest, as expected, as here the average kinetic UCN energy in the storage bottle is the lowest.*

Figure 3.22: *Setup at the West-1 beamport. Top: Storagebottle elevated by* 1200 mm. *Bottom: Storage bottle at the height of the beam port, without the* 2 m *guide and bends in order to measure calibration data needed to determine the transmission of the S-shaped beam line.*

3.7   UCN Output with Respect to Proton Beam Kick Length

A series of production type proton beam kicks with various kick lengths was conducted on December 15, 2014. The UCN output was recorded with a big Cascade detector connected directly to beamport West-1, a small Cascade detector connected directly to beamport West-2 and the nEDM apparatus in typical data taking configuration at beamport South.

Such measurements were done already previously [Göltl, 2012], but the timing jitter of the central storage vessel flap caused large fluctuations from one proton beam kick to the next. With the improved storage vessel flap timing (see Sec. 4.2) and at the time when permission to increase the proton beam duty cycle (see Sec. 4.3) was requested, it made a lot of sense to repeat these measurements.

3.7.1   Source status

The deuterium crystal had been in 24/7 operation for 9 days with 3.2 s long proton beam kicks every 340 s. In total about 2100 proton beam kicks had been performed prior to the start of this measurement series.

3.7.2   Measurement

In the beginning, several 2 s long "Norm-" kicks, i.e. kicks without closing the central storage vessel flaps, were recorded at beamports West-1 and West-2. Then, a series of kicks with SV flap trigger with kick durations increasing from 2 to 6 s in steps of about 1 s was measured, followed by six additional kicks with a kick duration of 6 s and two with a duration of 7 s. This series was then followed by several norm kicks again.

For the different types of UCN production kicks see Sec. 2.3.

3.7.3   Analysis

Data from the nEDM apparatus was used as-is from the so-called "Meta" datafile of run 009473. This file contains preprocessed counts for both detectors of the nEDM experiment, one measuring spin-up UCN, the other measuring spin-down UCN, after a storage time of 180 s during which the initially polarised UCN precessed inside the nEDM precession chamber. The sum of both values was used. The detection system is described in detail in [Afach et al., 2015].

Data from West-1 and West-2 are integrated over a time window from about 1.5 s after the end of the proton beam kick until 200.5 s after the end of the proton beam kick. This is done in order to cut away neutrons wich cannot be stored but are being guided out of the source shielding by the UCN guides anyway. The early end of the integration window is used because a rather short repetition time was used for the short kick durations. Like this, all datapoints are integrated over the same time window width in order to be comparable.

3.7.4   Results

The results of the measurement series are shown in Fig. 3.24.

While the increase in UCN output is steep at short kick lengths, it flattens out for longer ones. The integrated UCN counts at beamports West-1 and West-2 behave very similarly, while the UCN intensity inside the nEDM apparatus flattens out more. This might be caused by the fact that the filling time of the nEDM apparatus stayed constant at 28 s (which was found to be the optimal filling time for 3.2 s long kicks) in these measurements.

The saturation of UCN output with increasing proton beam kick length is also obvious when looking at the UCN detection rates during and shortly after the proton beam kick. This is expected, as the storage time constants of the UCN storage vessel inside the source, with open flaps towards the moderator vessel, are very short. A double exponential fit to the UCN rate in a "Norm-Kick" yields almost equally populated time constants of 2.9 s and 5.7 s with a reduced χ^2 value of 1.0 and negligible fit errors. Such a fit is shown in Fig. 3.23.

As a result of these short storage time constants, gains and losses start to cancel out for long kick durations.

Fig. 3.25 shows time spectra for all kick lengths, measured in the big Cascade detector at the West-1 beam port. The detection rate is growing rapidly during the kick, but it starts to flatten out around a kick length of 5 s, and only increases slightly afterwards.
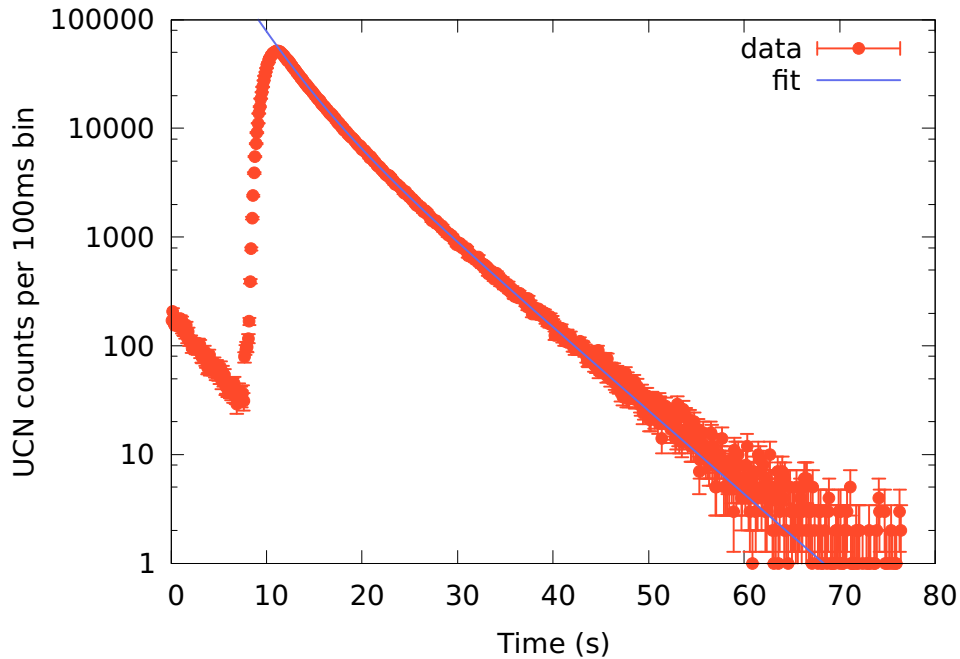
Figure 3.23: *UCN counts in a 2 s long "Norm-Kick", where the central SV flaps stay open. A double exponential fit is indicated in blue.*

This indicates that longer proton beam kicks than possible now (8 s is the maximum time the kicker magnet can be active) will not result in large improvements of UCN output, even if the proton beam kick duty cycle can be increased correspondingly.

3.7.5   UCN production increase during 6 s kick series

During a series of 6 s long proton beam kicks in December 2014, the total amount of UCN per kick was found to be increasing over time at all three beam ports. Even though the effect is only on the order of 3 % this is remarkable as it was never before observed. Comparing the norm kicks recorded at the West-1 and West-2 beamports before and after the whole measurement series, also here an increase in the total UCN output of 3.0(9) % in West-1 and 4.5(13) % in West-2 is observed. This might be caused by the combination of a larger heat load on the solid deuterium during the long pulses and the already bad state of the deuterium after more than 2000 pulses. Under these conditions, some annealing process during the longer beam kicks could e.g. repair defects in the solid deuterium surface structure (like snow), which could then result in higher UCN output.
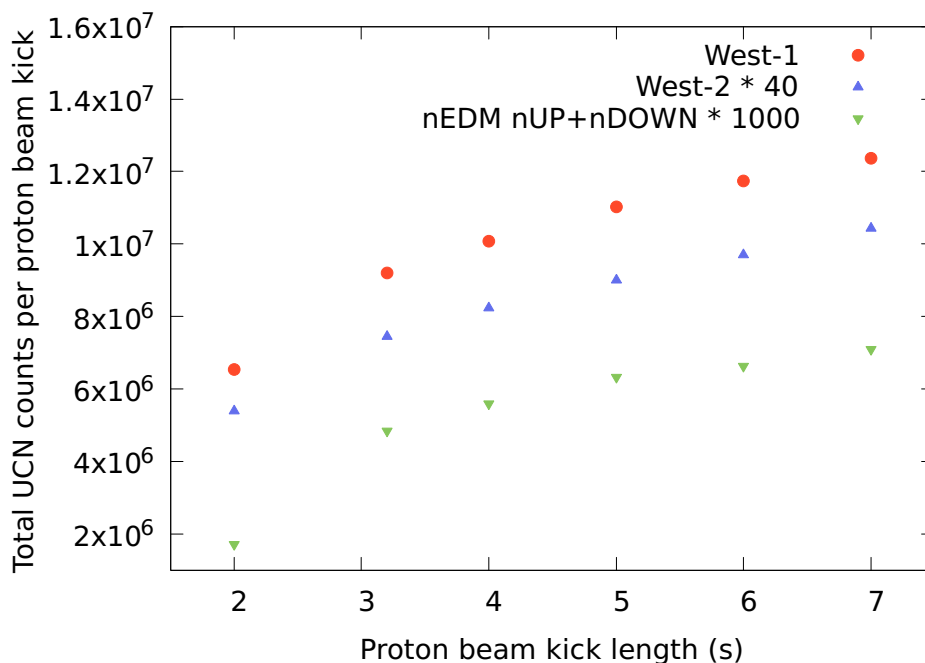
Figure 3.24: *Total integrated UCN counts at all beam ports for proton beam kick lengths from 2 to 7 s. West-2 scaled with a factor 40, nEDM counts scaled with a factor of 1000 for display. Statistical error bars are smaller than the point size.*

3.7.6 UCN intensity trend during 8 s kicks in December 2015

The indications that longer proton beam kicks are beneficial to the UCN output from the solid deuterium were further enhanced by results from the last week of nEDM data taking in 2015.

After the proton beam kick duty cycle had been increased throughout 2015, see Sec. 4.3, typically 5.4 s long kicks every 300 s were used for the nEDM experiment. On December 10 2015, this was changed to 8 s long kicks every 500 s, after the solid deuterium had been conditioned. Apart from a higher UCN yield per kick, a large difference in the decline of UCN intensity over time or over the amount of delivered kicks could be observed. Fig. 3.27 shows the amount of UCN measured in the nEDM experiment with respect to time, as well as with respect to the number of proton beam kicks to the UCN target.

The left hand side curve in both figures has been recorded with 5.4 s long kicks every 300 s, while the right hand side used 8 s long kicks every 500 s. All other parameters are identical. The isolated low outliers are due to a mispositioning of the UCN switch inside the nEDM experimental setup. It is obvious that both the decline of UCN output per unit time as well as of the UCN output with respect to the amount of proton beam kicks is slower with the longer kicks. The latter also directly shows that the decline is also slower with respect to the amount of protons delivered to the target, as this is even higher per kick with long kicks than with short kicks.
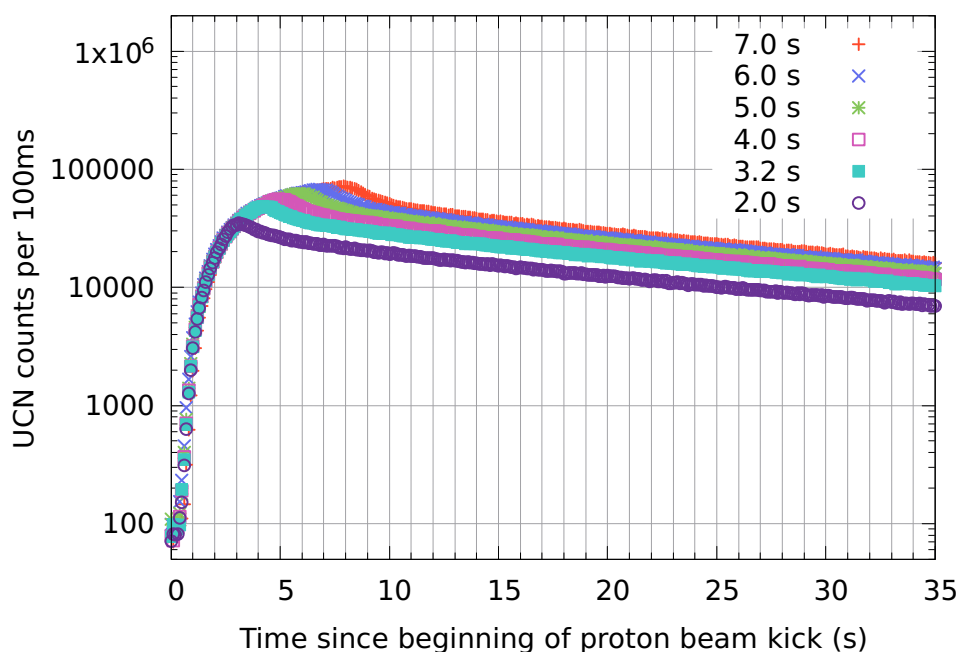
Figure 3.25: *UCN time spectra measured at the West-1 beam port for proton beam kick lengths from 2 to 7 s. Zoom into the first 35 s after the proton beam started to hit the target. It is well visible that for longer proton beam kicks the output UCN rate will go into saturation, but this saturation is not yet reached at 7 s long kicks.*
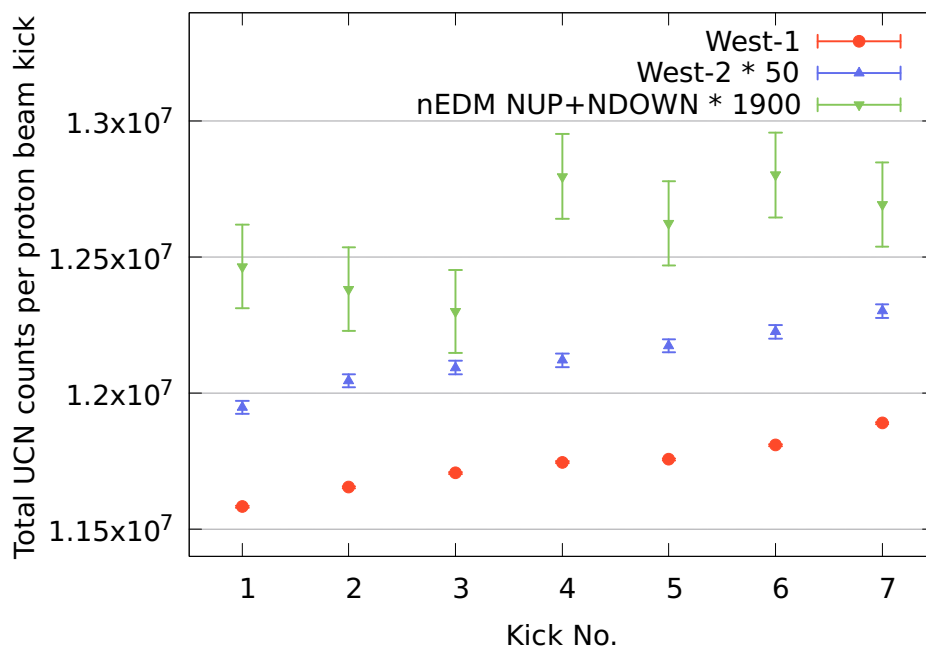
Figure 3.26: *Total UCN output during a series of 6 s proton beam pulses measured in December 2014. The total UCN output is increasing at all three beam ports, if only by a small amount. West-2 scaled with a factor 50, nEDM counts scaled with a factor of 1900 for display.*
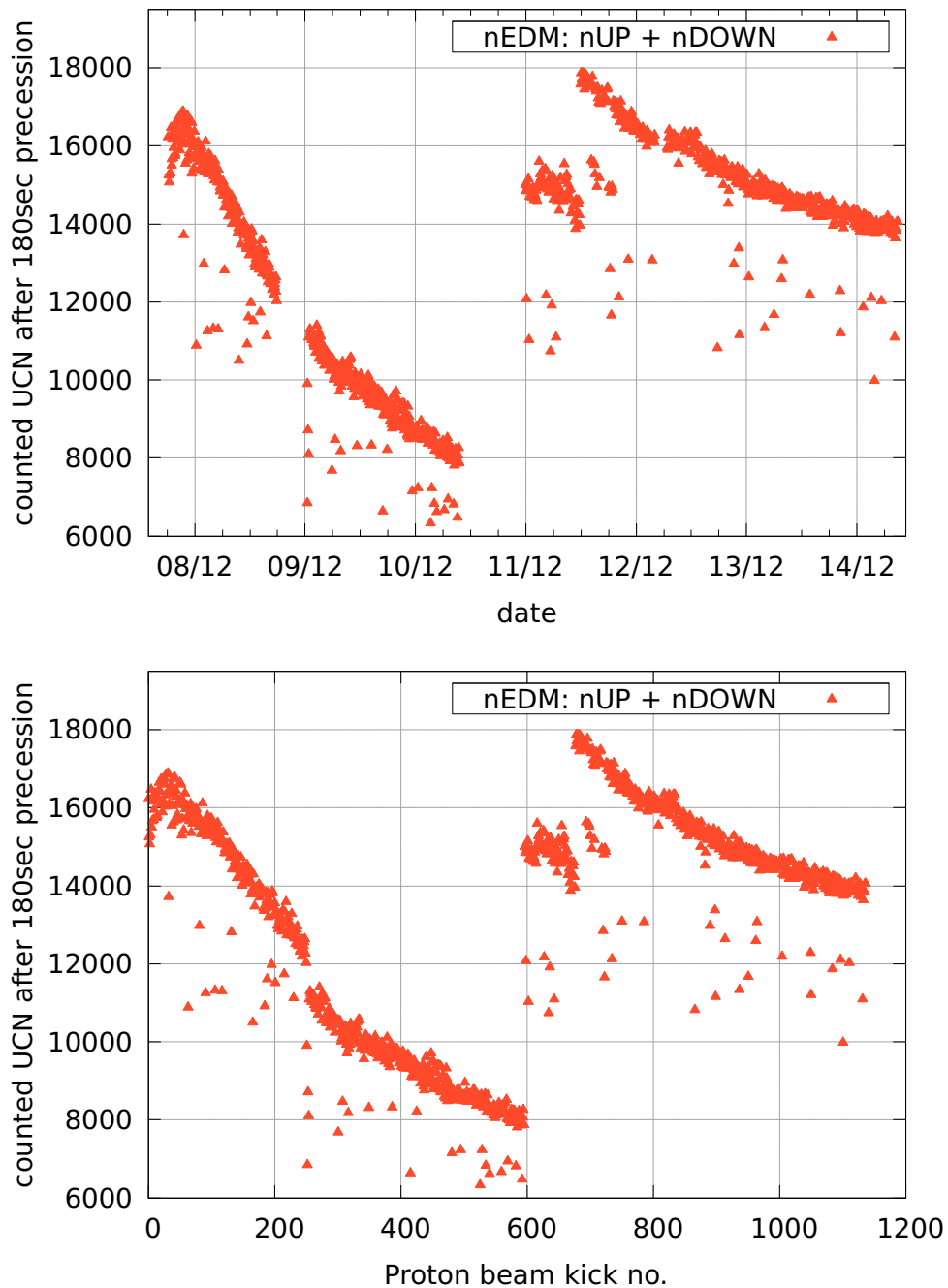
Figure 3.27: *Top: UCN counts per proton beam kick measured with the nEDM apparatus after* 180 s *of free precession with a repetition time of* 300 s. *Left hand side:* 5.4 s *long kicks, right hand side:* 8 s *long kicks. In the period with about* 15 000 *UCN per kick on early December 11th, the butterfly valve at the connection of beam port South to the source storage vessel, NLK South, was not opening fully, resulting in reduced UCN intensity. At late times on December 8th and 10th, no nEDM data was taken, but UCN production continued for peripheral characterisation measurements. Bottom: The same UCN counts plotted with respect to the proton beam kick number. Low outliers due to mispositioning of the nEDM UCN switch.*

Chapter 4

Optimisation of the Ultracold Neutron Intensity

4.1 Tuning the Proton Beam Shape and Position on the UCN Target

4.1.1 Shrinking the beam spot

The shape of the proton beam along its forward direction can be approximated as a 2-dimensional Gaussian. In order to measure and control the position of the beam center, the tails of these Gaussians are measured on so called harp monitors [Dölling et al., 2005]. These monitors are collimators which measure the stopped amount of charge. The beam tune used since start-up of the UCN source until June 2013 was such that 95.8 % of the proton beam current were impinging the UCN target, while 4.2 % were lost on the collimators / monitors.

On June 25th 2013, a new beam tune was introduced, with which only 1.4 % was lost on the collimators while 98.6 % hit the target. In both cases the simulated beam can be described as a 2-dimensional gaussian with the widths σ_x and σ_y. For the original beam tune, σ_x is 37.3 mm and σ_y is 36.3 mm while for the the optimised beam tune σ_x is 33.3 mm and σ_y is 33.1 mm. This is shown in Fig. 4.1. These numbers are based on simulations done by D. Reggiani using the PSI Graphic Turtle Framework by U. Rohrer based on a CERN-SLAC-FERMILAB version by K.L. Brown et al.

To measure the effect on UCN intensity, norm kicks were measured at the West-1 and West-2 beam ports.

The kick length was 2 s, the proton beam current was 2.17 mA. The central storage vessel shutter was kept open during the measurement, to minimize fluctuations due to moving parts. The big Cascade UCN detector was mounted after a 1 m long NiMo coated glass guide with an inner diameter of 180 mm and a vacuum shutter at beam port West-1, while a small Cascade UCN detector was mounted directly below the West-2 beam port. Two norm kicks were done with the old beam tune, then two kicks with the new beam tune.

Depending on when the integration of the UCN counts starts with respect to the proton beam kick, an increase in UCN intensity by between 4 % and 7 % was measured. The earlier the cut, the lower the gain. 4 % gain was with the beginning of the cut during the beam kick, so on the rising flank of the intensity, while 7 % was 4 s later and well after the peak.

4.1.2   Changing the height at which the beam hits the target

With a smaller beam spot, there was the possibility to steer the beam in such a way, that the center of mass is impinging not in the center of the target, but above. This should lead to an increased neutron flux in the moderator vessel for geometrical reasons.

An overview of the proton beam line from the accelerator to the UCN spallation target via a fast kicker magnet and two 45° bending dipoles is shown in Fig. 4.2, a more detailed view highlighting the complexity of the beamline instrumentation is shown in Fig. 4.3. The beam can be tilted from the horizontal plane using steering magnet SBA 6y located right before the second 45° bending magnet ABK2. It is tilted back using the last quadrupole (de-) focusing magnet QBB7 about 10 m upstream of the UCN target, which the proton beam traverses slightly off the central axis resulting in a vertical bending.

Test measurements, again on both beam ports West-1 and West-2, were done on June 28 2013. 2 s long norm kicks and the same detector configuration as described in Section 4.1.1,were used. The beam was lowered by about 5 mm and raised by about 4, 8, 13 and 17 mm. These heights are recorded at the "MBH2" harp beam monitor (about 1.5 m behind "QBB7").

Fig. 4.4 shows the resulting integrated UCN counts. Lifting the proton beam by about 13 mm yielded the highest UCN intensity and is used since then. The decline in UCN output for even
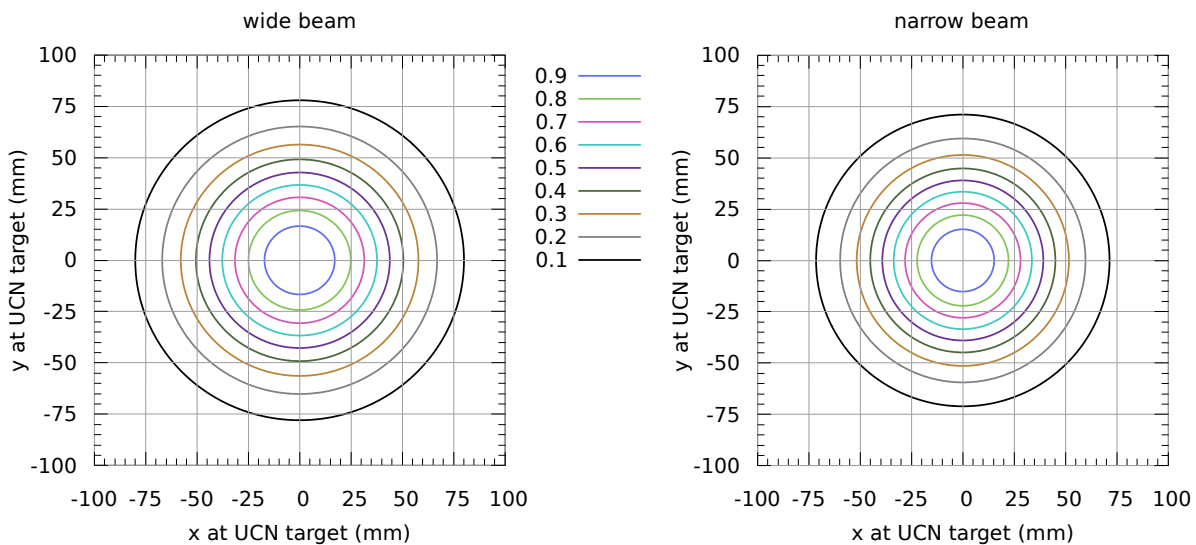
Figure 4.1: *Simulated proton beam profiles at the position of the UCN target before and after optimisation. Contour lines indicate relative proton beam intensities. Left: "Wide" beam tune, $(\sigma_x, \sigma_y) = (37.3\,mm, 36.3\,mm)$. Right: "Narrow" beam tune, $(\sigma_x, \sigma_y) = (33.3\,mm, 33.1\,mm)$.*

greater heights is caused by the last vertical collimator in front of the UCN target. For larger heights, losses at this collimator result in a reduced neutron and therefore UCN production.

The analysis was done for the total integrated UCN counts per proton beam kick as well as for an integration window starting 1.5 s after the end of the proton beam kick. The resulting improvement factors of the UCN output per kick was:

- West-1 full time integration: 1.027(1)

- West-1 time cut: 1.029(2)

- West-2 full time integration: 1.030(1)

- West-2 time cut: 1.032(3)

4.1.3   Conclusion

Profile and position of the HIPA proton beam on the UCN target during beam kicks have been optimised for maximum UCN production. The UCN yield was improved between 7 % and 10 %, depending on the time cut to the measured UCN spectra.
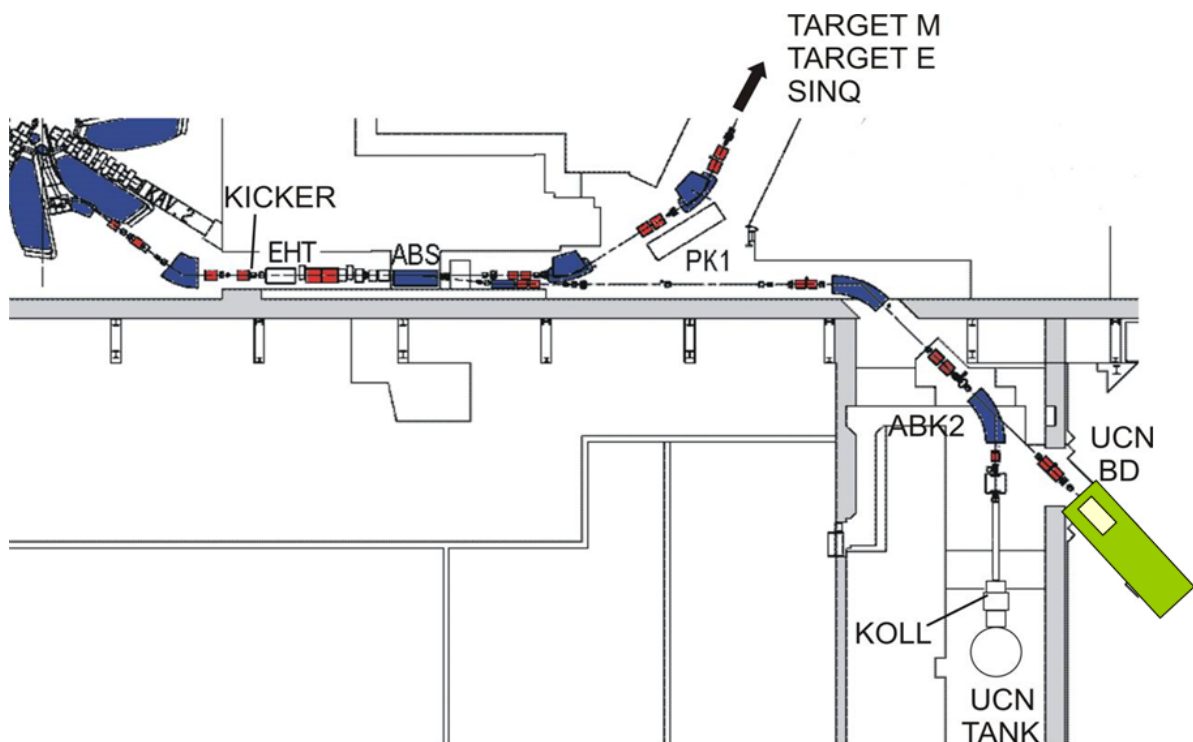
Figure 4.2: *Beamline overview from the* 590 MeV *proton accelerator (top left) to the UCN spallation target (bottom right). Image source: PSI.*
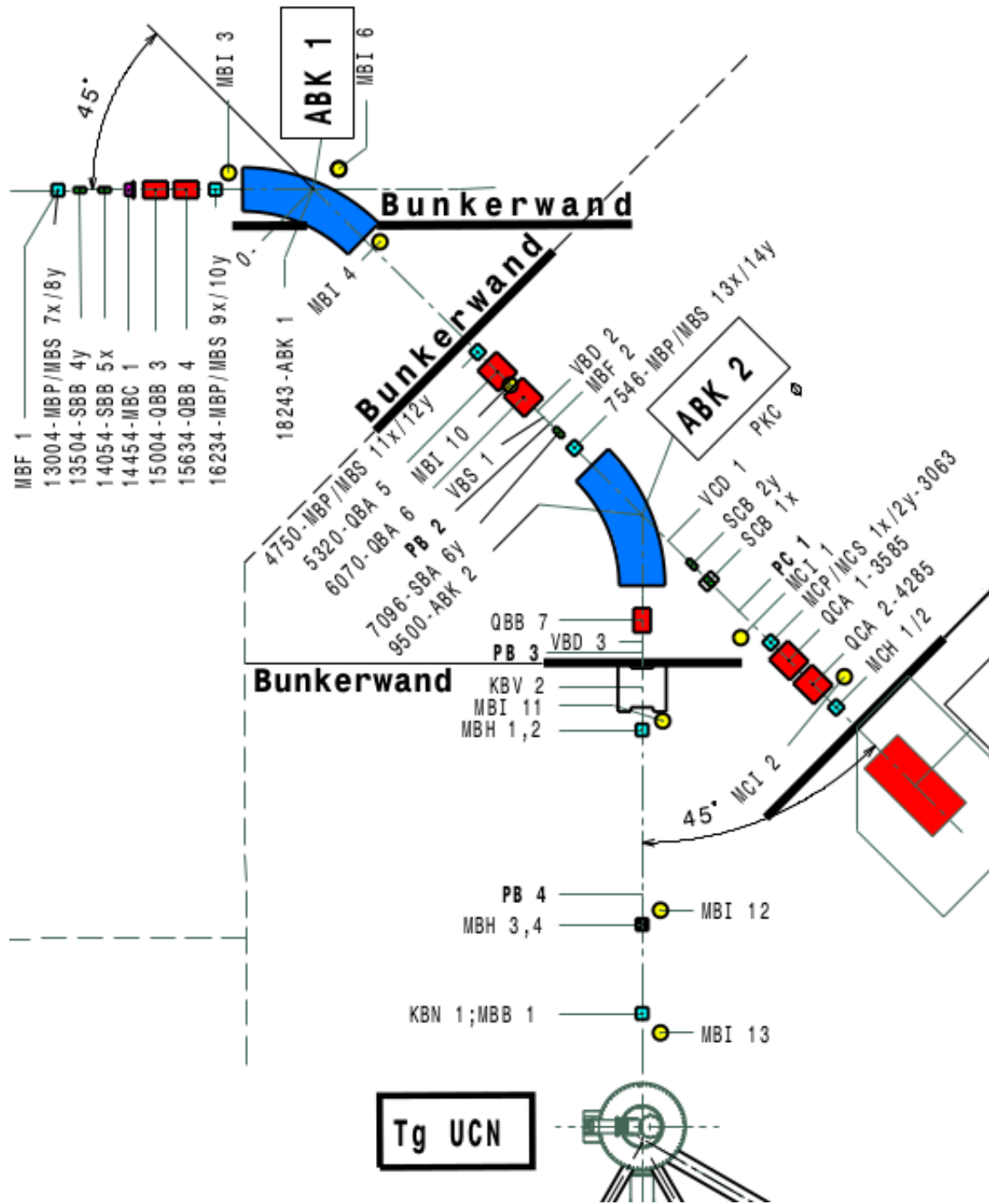
Figure 4.3: *Detailed view of the beamline elements. The proton beam enters from left to right on the top left corner, is then bent by two times 45° before it impinges on the UCN target on the bottom center of the drawing. Dipole magnets are indicated in blue, quadrupole magnets are indicated in red. On the right hand side, the beam dump used during commissioning of the beam line is shown. Image source: T. Rauber, PSI.*
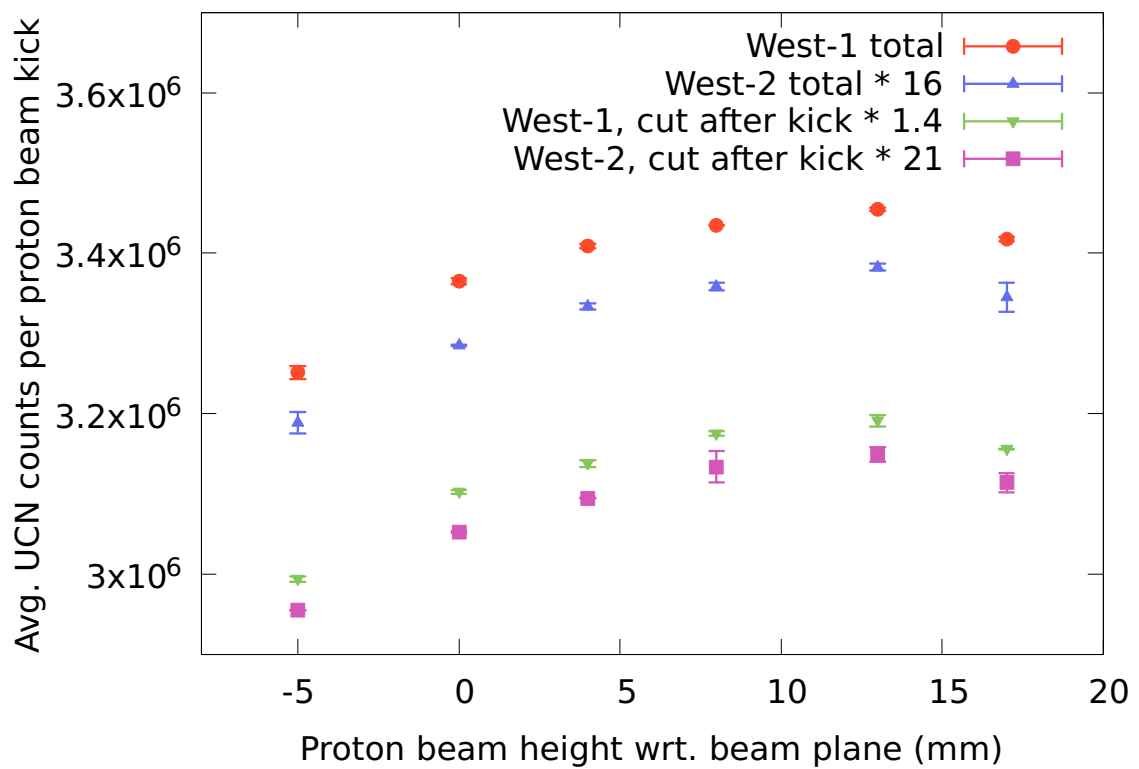
Figure 4.4: *Resulting UCN counts when changing the height of the proton beam.* 13 mm *above the beam plane was the best setting and is being used since then. Measured values for the detector at the West-2 beam port as well as for later time cuts in the integration are multiplied by arbitrary factors to fit the scale.*

4.2   Klappentrigger

4.2.1   UCN intensity fluctuation

Both the nEDM experiment at beam port South and test experiments at beam ports West-1 and West-2 observed large non-statistical fluctuations in UCN intensity from proton beam kick to proton beam kick in regular operation. This was first observed in 2013. Fig. 4.5 shows examples of these fluctuations.
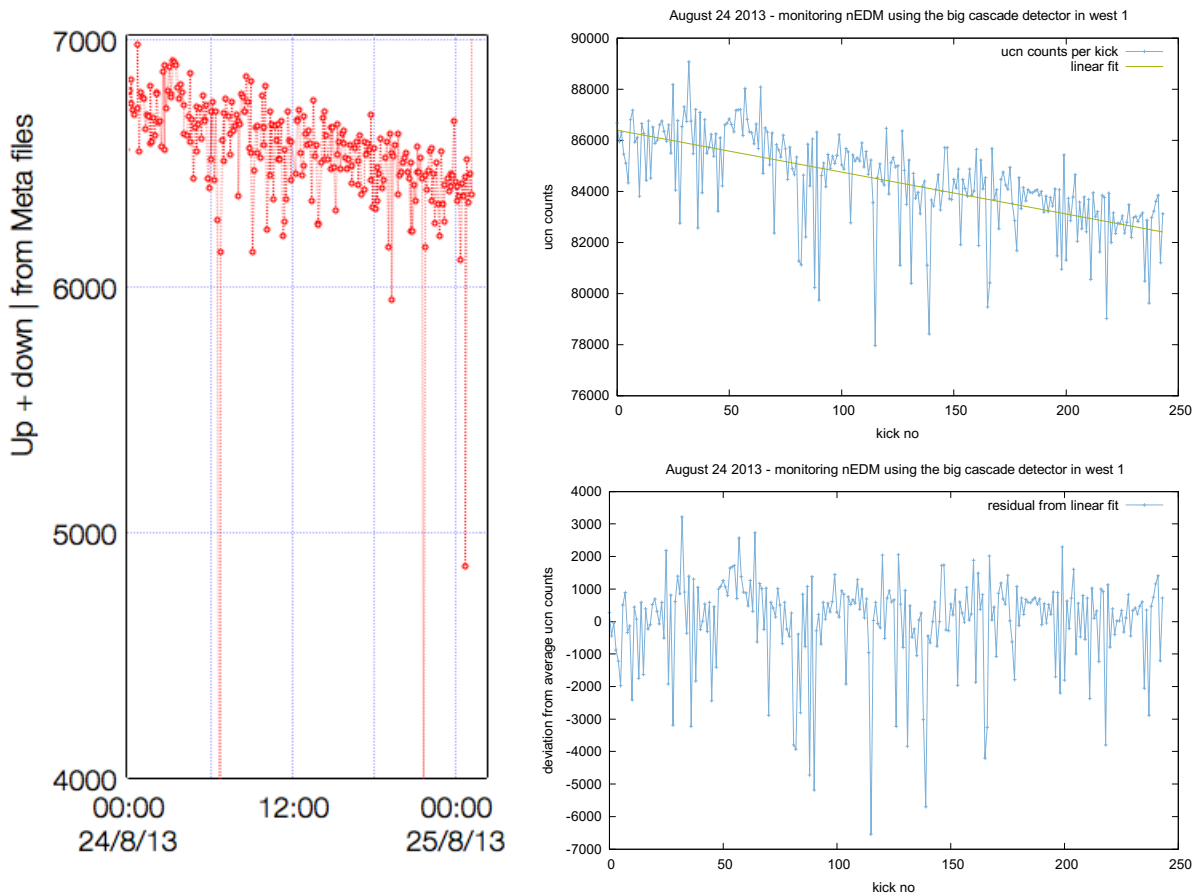
Figure 4.5: *Left: UCN intensity in various proton beam kicks on August 24th 2013. Right: UCN intensity measured with the big cascade detector at West-1 in the same period of time.*

The fluctuations were found to be as large as 10 % peak to peak, as shown in detail in Fig. 4.6.

4.2.2   The culprit

In December 2013, the following measurement was conducted during regular operation of the UCN source: Using a Raspberry Pi microcomputer, the relative timing between the KICK signal
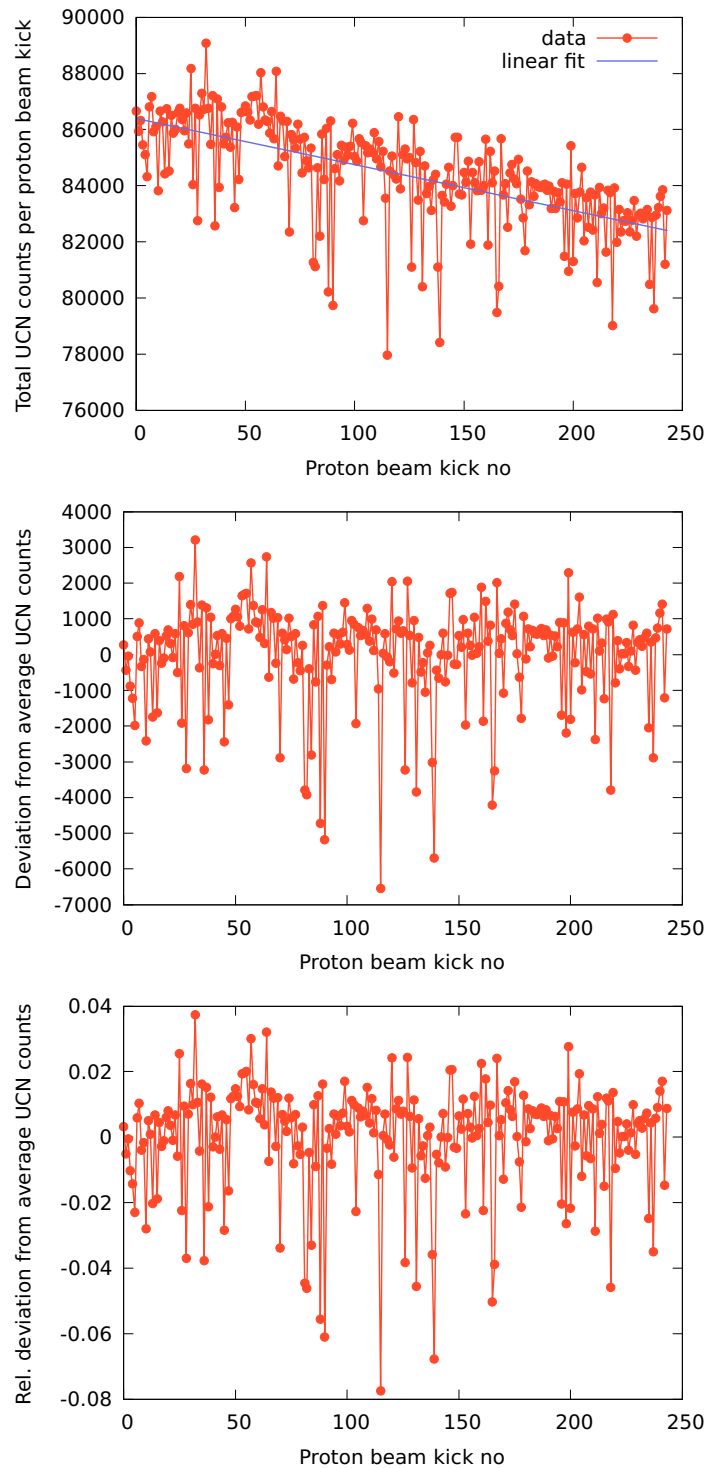
Figure 4.6: *Detailed UCN intensity fluctuations, measurements with a big Cascade detector connected to the West-1 beam port. Top: Raw measured data, linear fit. Middle: Fit subtracted from measured data. Bottom: Fit subtracted and deviation given relative to the fit value for every datapoint. Peak to peak fluctuations larger than 10 % are visible.*

sent by accelerator control and the 4 endswitches of the central storage vessel flap was recorded with sub-millisecond presision. Every event, i.e. every rising or falling flank of any of the 5 electrical signals was recorded together with a timestamp.

Correlating the measured time between the KICK signal and the event where flap "Villigen" starts moving and leaves the upper endswitch with the UCN counts measured at the West-2 beam port yielded a strong correlation, which is shown in Fig. 4.7. The timing between KICK signal and closing of the SV flap was fluctuating by more than 1 s, which caused UCN intensity fluctuations on the order of 10 %. Clearly visible for a given timing, the UCN intensity only fluctuates on the order of 2 % and a sharp optimum timing, placing the closing of the SV flap very close to the end of the (in this case 3 second long) proton beam kick, exists.

4.2.3   Tracing the problem

Investigations on where this problem originated lead to the understanding, that the signal path from the accelerator control room to the UCN source control was not optimised for fast and reproducible operation. As the trigger signal for the SV flap to close is calculated and generated in the accelerator control software, this signal has to be routed into the separate UCN source control system, which then reacts by closing the flaps. This signal is called "Klappentrigger", or WKT for short. The time when this signal is sent is calculated backwards from the time the proton beam kick onto the UCN target is supposed to end. The signals sent by the accelerator control program and their relative timing is shown in Fig. 4.8.
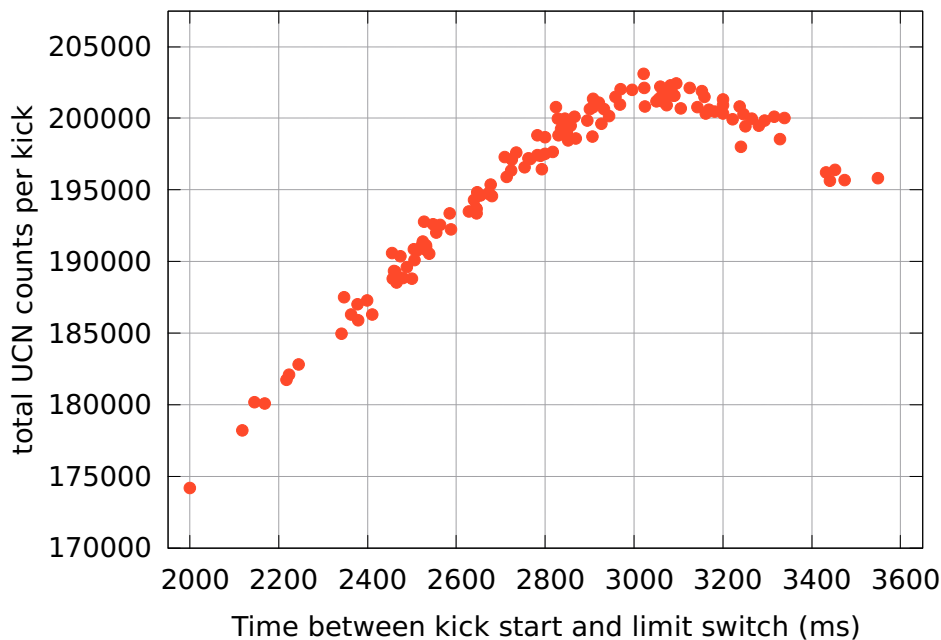
Figure 4.7: *Correlation between UCN counts measured at beamport West-2 in 3 second long pulses and SV-flap timing*

Before 2014, the signal from the accelerator was read from the EPICS accelerator control system in one Simatic device, then placed on a bus system and read by a second Simatic device, which then controlled the helium valves which actuate the SV flap. As each of the three devices in this chain could possibly have a jitter of several hundred milliseconds, this was the most likely candidate for the origin of the problem.

4.2.4   Optimisation of the signal path

Before operation started in 2014, the signalling path for the Klappentrigger signal was changed. In the new setup, the signal was electrically routed directly into the Simatic device where the SV flap helium valves are connected. Like this, the signalling path is simplified a lot, and better performance is to be expected.

Comparing timing measurements before and after yielded the results displayed in Fig. 4.9.

The average runtime of the signal had decreased by up to 1 s, but the jitter on the order of more than 1 s was still present.

4.2.5   Measurement of the Simatic switching time

To find the origin of the jitter, the time between a simulated WKT signal on the input side of the Simatic and the rising flank of one of the outputs which control the helium valves was measured with an oscilloscope. The results shown in Fig. 4.10 clearly show a jitter of about 1 s in the response time to the WKT signal.

The only devices in this setup are an optocoupler on the input side and the Simatic itself.

4.2.6   Investigation of the code inside the Simatic

The code which is responsible for controlling the SV flap in one of the Simatic devices was investigated together with an expert from Alpiq. The code is not originally written by Alpiq, but
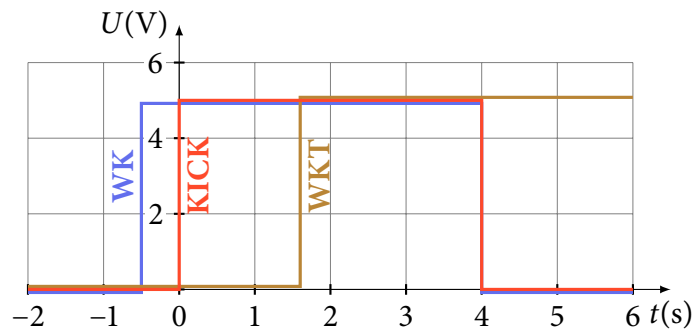
Figure 4.8: *Timing diagram of the voltage U on the signal lines WK, KICK, and WKT for a 4 s long proton beam kick starting at t = 0 s. WK goes HIGH at t = −1 s. KICK goes HIGH for 4 s at t = 0 s. WKT goes HIGH 2.4 s before the end of the proton beam kick. WK and KICK go LOW at t = 4 s when the kick is over. WKT stays high until it is reset at the beginning of the next kick sequence.*
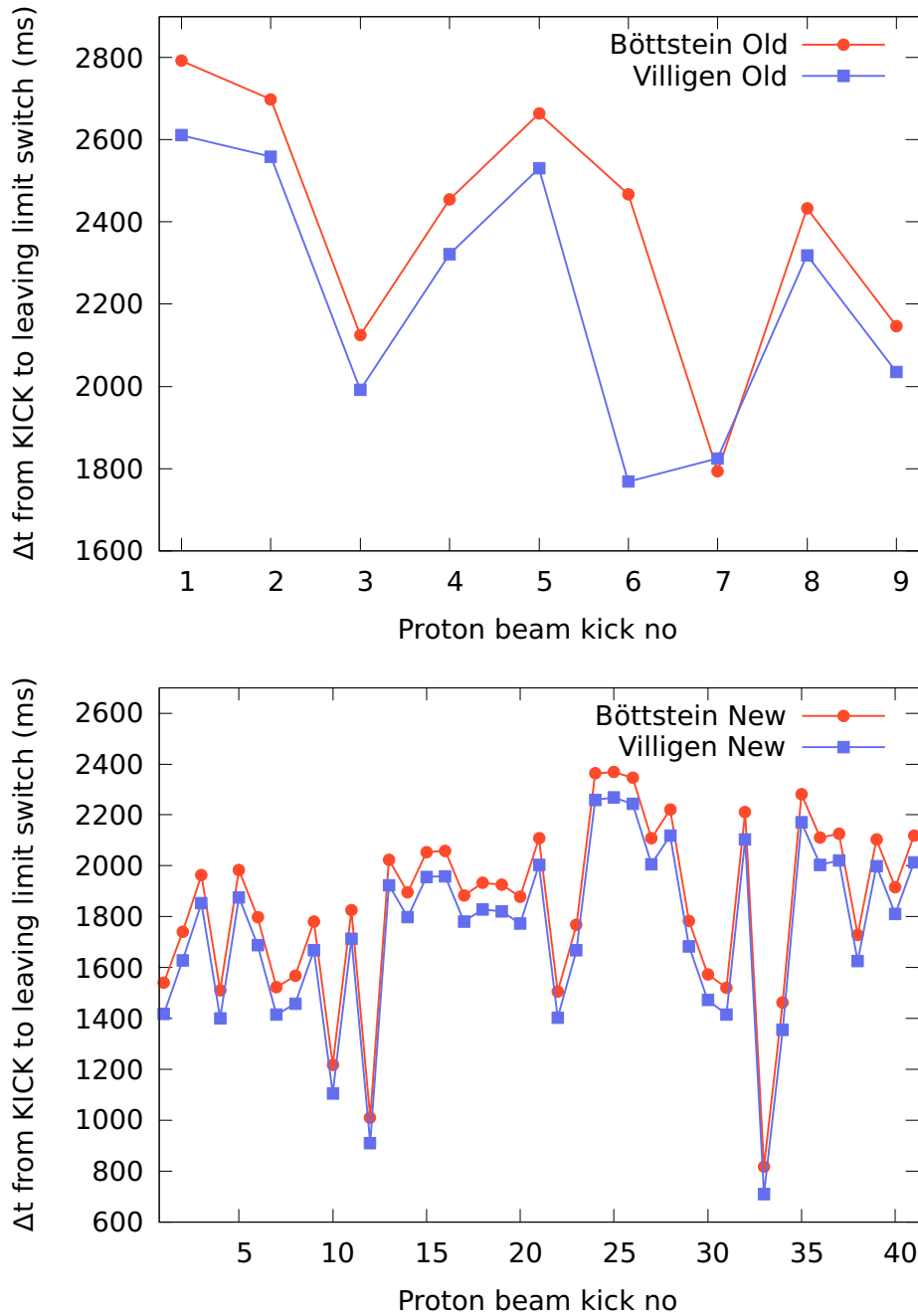
Figure 4.9: *Timing measurements of the SV flap endswitches with the old and new signalling path for the WKT signal. The absolute delay from signal to movement is reduced, but the timing jitter of about 1000 ms is still present.*

by Hauser Automation. No simple solution to the timing jitter was found. The code was found to be very monolithic and complex, and therefore hard to understand and debug. As the SV flap is a relatively independent subsystem of the UCN source, the control of the flaps is rather independent from other parts of the UCN source control system as well. It was therefore decided to completely decouple the SV flap control from the hardware of the UCN source control system, by using a dedicated device and optimised control software.

4.2.7 Test: Using a standalone Simatic SPS

4.2.7.1 Lab test

A new Simatic S7-1200 SPS was acquired to test if the problem could be solved by using a dedicated control mechanism of similar type as the hardware already present.

In a test setup in the lab a program was developed which enabled the SPS to:

- Control the 8 Helium valves used to open and close the 2 flaps manually

- Listen for a 5V TTL trigger

- Wait for a given time after a rising flank on that trigger input
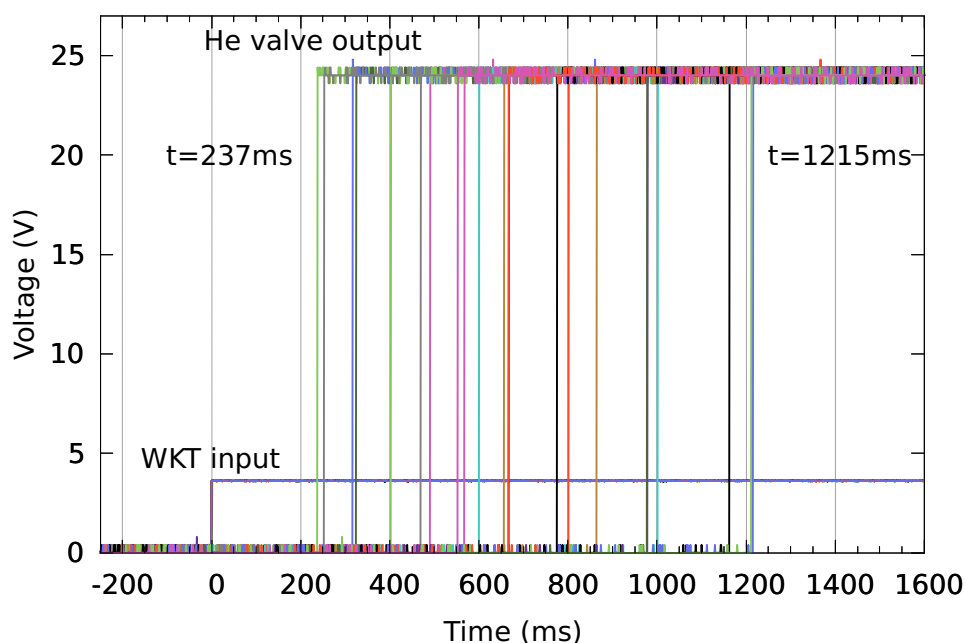
Figure 4.10: *Oscilloscope measurements of one He valve output of the Simatic, triggered manually on the WKT input. The trigger signal was always sent at t = 0. The variation of the time at which the 24 V signals transision from off to on demonstrates the jitter on the order of 1 s.*

- Close the flaps and open them again a defined time later

- Display the state and be controllable through a web frontend

All timing parameters were designed to be adjustable.

Using timing values scaled down from several 10 seconds between closing and opening the flaps (which are used in the real UCN source) to a few seconds, and using an external function generator as a trigger every 10 seconds, statistics on the time between trigger and opening / closing of the helium valves was recorded. A photo of the test setup is shown in Fig. 4.11. A screenshot of the oscilloscope is shown in Fig. 4.12.

2900 measurements were performed for the screenshot in Fig. 4.12. The statistical results are shown in Table 4.1. The jitter on the measured outputs is single digit milliseconds, which corresponds to the cycle time of 7 ms of the Simatic.

4.2.7.2   In-situ test

On October 1st 2014, the rack containing the SPS was installed in the UCN experiment area West. 8 cables matching the originally installed cables of the valves were prepared with the same plug, naming, and color scheme for the individual leads. The cables were temporarily routed from the West area up towards the rack containing the 8 valves 2QRM83AA101 - 2QRM83AA108. Photos can are shown in Figs. 4.13 and 4.14.
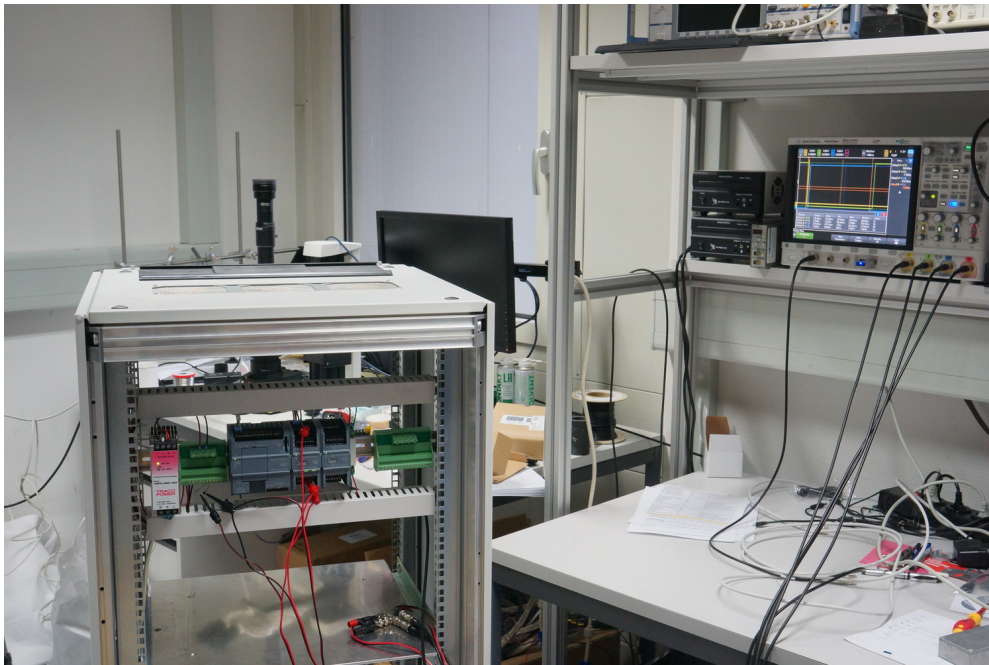
Figure 4.11: *Simatic SPS in the rack, connected to the oscilloscope in the lab. In this setup, timing jitter was measured with high statistics in a simulated environment.*

At 16:30h, the 8 plugs were unplugged from their original cables and plugged into the test cables one by one, while the corresponding error states in the UCN control system were monitored.

At 17:00 the new SPS was powered on for the first time with the valves connected. It was checked that all valves were in the right state for both flaps to be closed. Then first flap Boettstein and later flap Villigen were manually opened and closed from the control website of the new SPS. During all these tests, it was always made sure that all valves were working as expected.

At 17:30, a manual TTL trigger generator was connected to the cable normally providing the KICK signal to the source control system and to the new SPS as a trigger input. The KICK signal had to be used as this is the signal whis has been permanently recorded together with the endswitches of the two flaps during the last year. The new control system was set into automatic mode, reopening time set to 30 s and security closedown time to 1000 s. 19 triggers were manually given, at different times after the flap had automatically opened again. This was monitored on the output of the measurement program on the Raspberry Pi computer described in Section 4.2.2. The results are shown in Fig. 4.15.

A peak to peak jitter of about 85 ms can be observed. While manually providing trigger signals it seemed that the measured time depended on the amount of time between the last reopening of the flaps and the trigger pulse. Fig. 4.16 clearly shows this correlation.
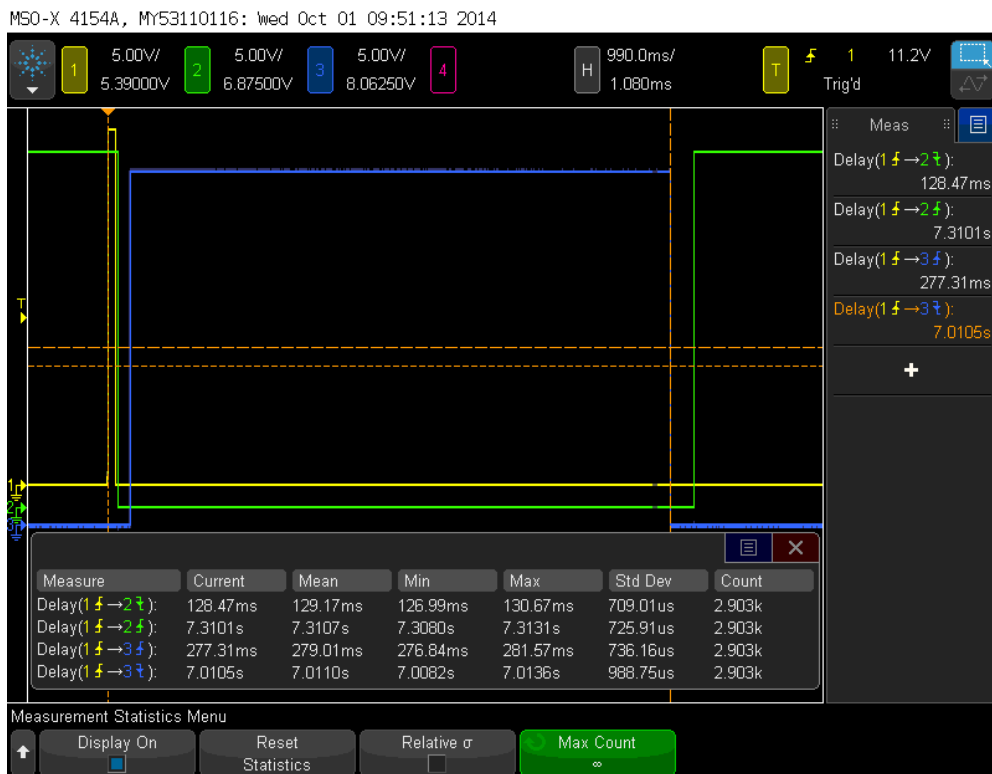
Figure 4.12: *Screenshot of the oscilloscope used in the lab setup. The values are given and described in table 4.1.*

After taking this into account, the peak to peak jitter for a constant trigger rate, as used under normal operation conditions, can be estimated as about 25 ms. The correlation between the waiting time and the closing time is assumed to be caused by the time it takes the pressure reservoirs in front of the pneumatic cylinders to refill. This assumption is backed by the following pressure readings for the time of this measurement, see Fig. 4.17.

In order to be able to compare the performance of the old system with the new SPS, on October 2 a series of 24 measurements was performed. The trigger signal was generated by a function generator in order to mimick the conditions under which the source operated in the last weeks, i.e. one kick every 300 s, and about 30 s between the time when the flaps reach the open endswitch and the next trigger.

The peak to peak jitter of each flap is about 25 ms. The result is shown in Fig. 4.18. Comparing this to a measurement of the jitter with the source in normal operation, which was recorded in the last week of September 2014, a significant decrease in jitter is evident as shown in Fig. 4.19.

A drastic reduction in UCN intensity fluctuation is achieved e.g. in the nEDM experiment. Fig. 4.20 shows two nEDM runs which had similar conditions, i.e. the same type of UCN production proton beam kicks, with the same waiting time in between.

4.2.8 Evaluation of the optimal timing for the storage vessel flaps

In order to optimise the UCN output per proton beam kick, the correct timing for the movement of the central storage vessel flaps is crucial. From the correlation measurements between UCN output and flap timing done when tracing the timing issues, shown in Fig. 4.7, it is obvious that for proton beam kicks with a length on the order of 3 s the correct time for the flaps to start moving is at the end of the proton beam kick. Empirically it has been measured that it takes the flaps approximately 1 s from the first trigger signal to the helium valves until the upper limit switch is released.

In order to keep the complexity of configuration done externally, e.g. by the accelerator control room shift crew, to a minimum, the typical configuration in 2015 using the interim solution was

Signal	Mean	Min	Max
Falling Channel 2	129.17 ms	126.99 ms	130.67 ms
Rising Channel 2	7310.7 ms	7308.0 ms	7313.1 ms
Rising Channel 3	279.01 ms	276.84 ms	281.57 ms
Falling Channel 3	7011.0 ms	7008.2 ms	7013.6 ms

Table 4.1: *Statistical evaluation of the lab tests of the Simatic. Measured with an Agilent MSO-X 4154A oscilloscope. Channels 2 and 3 were simulating the two helium valves used for closing and opening one side of the central storage vessel flaps. Following an external trigger simulating the WKT signal, after a short programmable delay the opening valve should be shut and the closing valve should be open. After a long programmable delay the reverse should happen. The recorded times are measured from the rising edge of the trigger signal until the designated edge of each channel.*

to keep the original WKT signal at 2400 ms before the end of the proton beam kick, which is the default value. Minor adjustments to the delay inside the Simatic are used to keep the flap closing tuned to the kick end. The correct delay value is typically fluctuating by ±30 ms around values of 1300 ms for flap "Böttstein" and 1400 ms for flap "Villigen". These values have been manually adjusted in intervals of roughly one week.

4.2.9 Conclusion

The non-statistical fluctuation of UCN intensity was found to be caused by timing jitter of the Siemens PLC based source control system responsible for closing and opening the central storage vessel flaps. Timing fluctuations on the order of 1 s were observed, and the highest UCN output was observed when the flaps started closing at the end of the proton beam kick.

Hardware for a dedicated control system for the SV flaps (Siemens Simatic S7-1200) was then acquired and programmed to replace the existing functionality of the UCN source control system. With the new hardware, timing with jitter below 10 ms was achieved in the lab.

As an interim solution, the dedicated control system was set up in a separate electronics rack in area West. Connected to the sources helium valves, a jitter in the movement of the storage vessel flaps of about 25 ms was observed. UCN intensity fluctuations from proton beam kick to proton beam kick were significantly reduced.

The interim solution was in permanenet operation during the beam-year of 2015 and has successfully handled more than 30 000 kicks to the UCN target.

During the proton accelerator shutdown 2015/2016, another Siemens PLC was acquired and installed in the electronics racks of the source control system. The software from the interim solution was enhanced and connected to the source control system in order to provide a central user interface. This system is in use since beginning of operations in 2016.
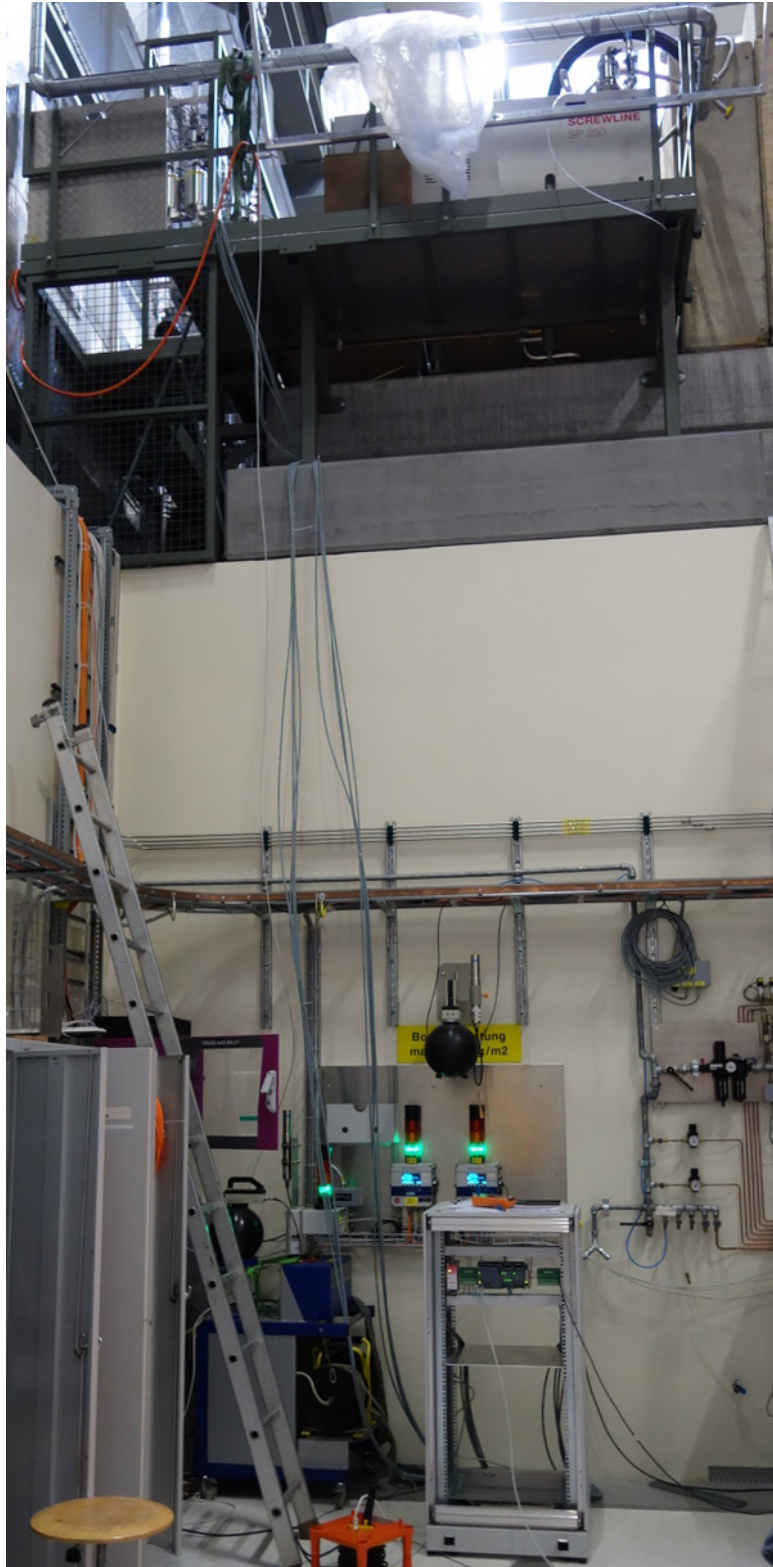
Figure 4.13: *Simatic SPS installed in the experimental area west and temporary cabling, view from below.*
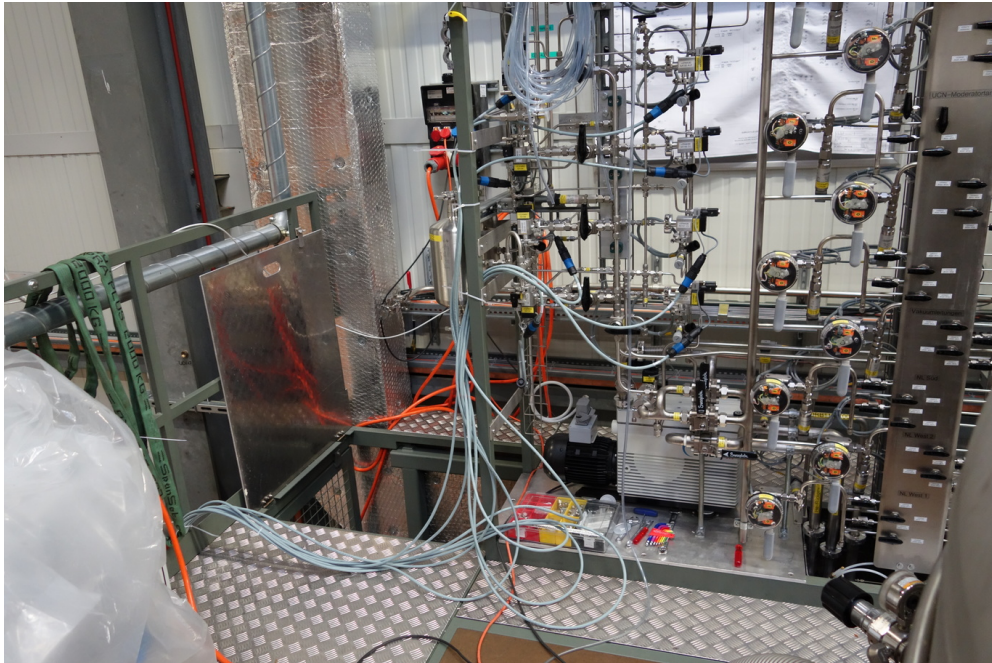
Figure 4.14: *Temporary cabling at the valve rack. In order to keep the original timing system operational as a back-up, additional temporary cables (light gray) were routed to the valves.*
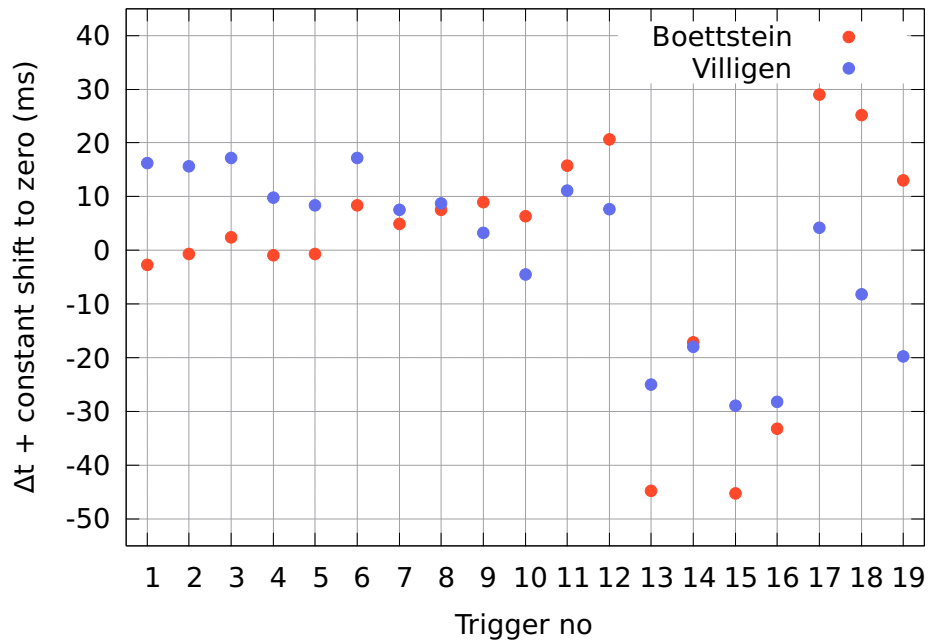
Figure 4.15: *Distribution of the time when the first open endswitch is left by each flap for the first 19 triggers.*
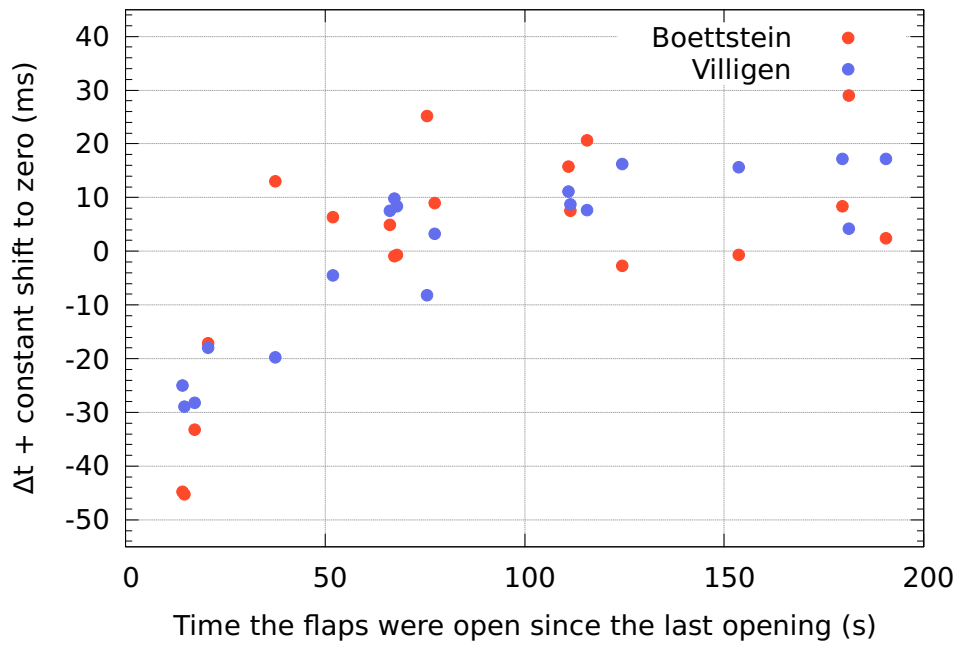
Figure 4.16: *Time when the first open endswitch is left by each flap with respect to the time between the last opening of the flaps and the trigger for the first 19 triggers.*
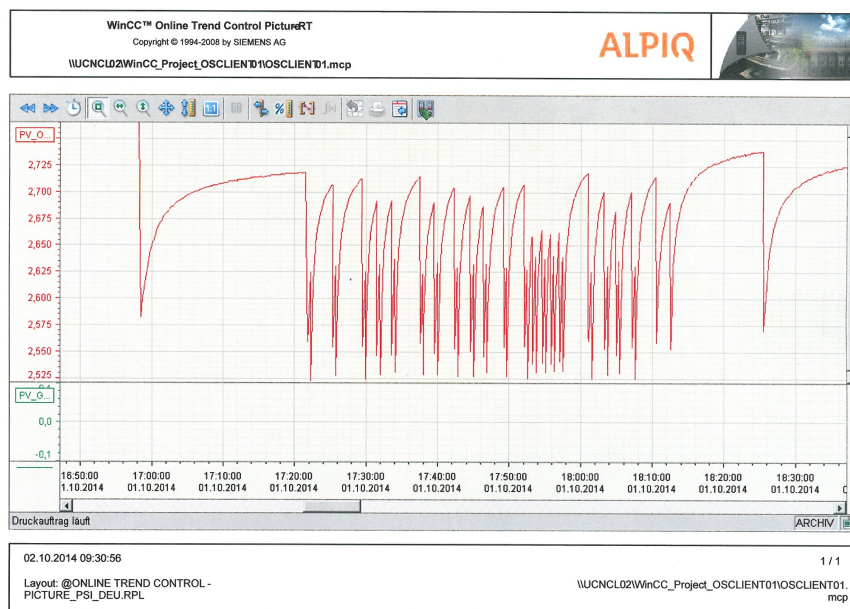
Figure 4.17: *Plot of the pressure in the gas reservoirs in front of the pneumatic cylinders which move the flaps for the time of this experiment*
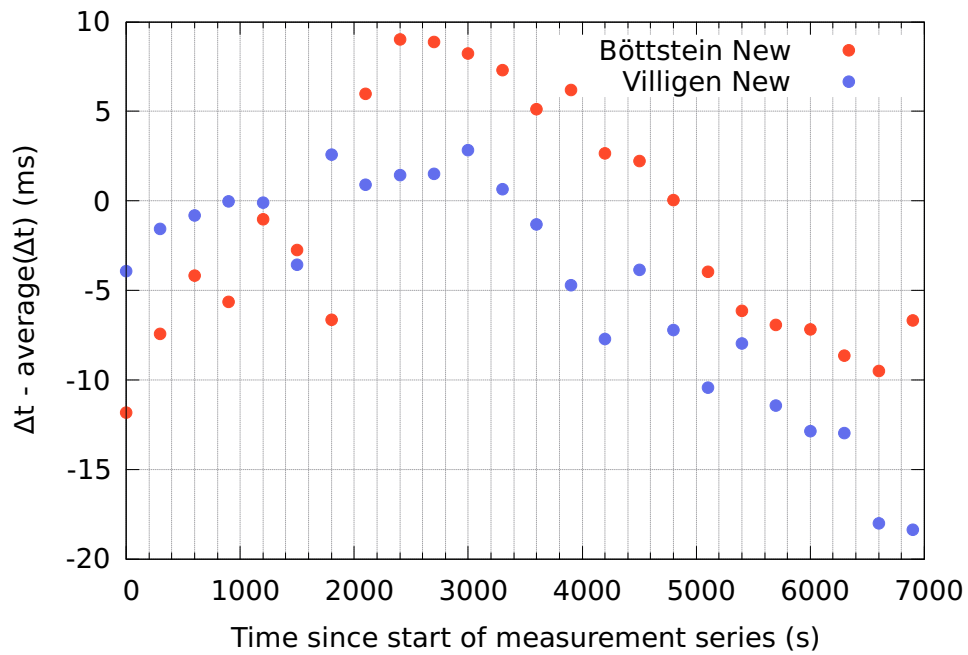
Figure 4.18: *Performance of the new Klappentrigger control system. Δt between trigger signal and the flaps leaving the limit switch installed at the fully opened position.*
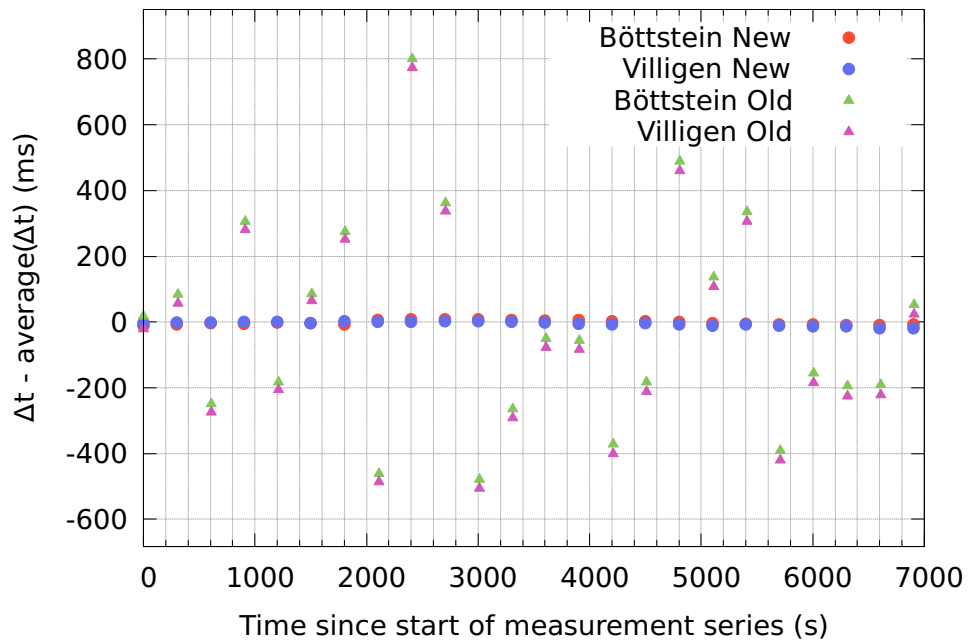
Figure 4.19: *Time distribution comparison of the old and new control system*
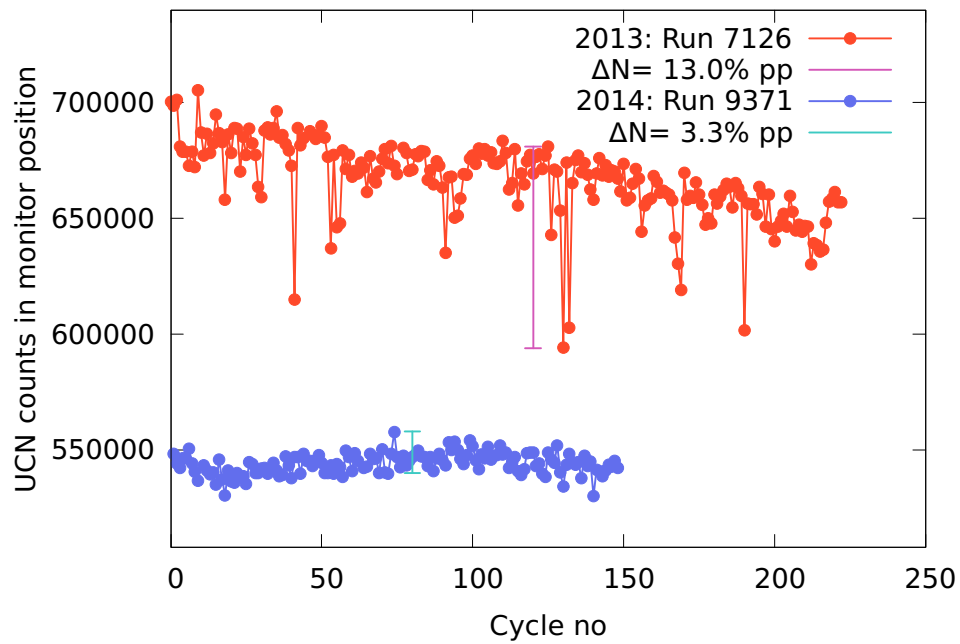
Figure 4.20: *Data recorded with the nEDM experiment under similar conditions before and after the change to the new storage vessel flap control. UCN counts observed in the monitor position per measurement cycle.*

4.3   Proton Beam Kick Duty Cycle

In regular operation, the 2.2 mA proton beam of the High Intensity Proton Accelerator (HIPA) [Seidel et al., 2010, Grillenberger et al., 2013] is being guided to the UCN target for intervals of up to 8 s, with long breaks on the order of several hundred seconds between these so-called beam kicks.

4.3.1   Original definition of the UCN production duty cycle

In the original permit of operation by the Swiss Federal Office of Public Health (BAG), it is stated, that the time-averaged proton beam current on the UCN target must not exceed 20 µA. This restriction is motivated by radiation safety. A cumulative dose of 50 mSv per three months may not be exceeded in the experimental area surrounding the UCN source. Dosimetry in the proximity of the UCN source showed no significant dose in correlation with 24/7 operation with the nominal duty cycle.

Based on these results, an increase of the permitted average proton beam current to 60 µA was requested by PSI radiation safety in September 2014.

4.3.2   Permission for a higher duty cycle

On October 17, 2014, permission to run the UCN source with an average proton beam current of up to 60 µA was granted by BAG, under the condition that:

(a) An intermediate report on the results of dosimetry measurements is given to BAG after increasing the average proton beam current to 40 µA.

(b) Radiation safety limits are still valid.

4.3.3   Increasing the duty cycle in 2015

During regular operation and nEDM data taking in autumn 2015, the average proton beam current was increased from 22 µA via 25 µA and 30 µA to 40 µA.

The measurements of the nEDM experiment were optimised to a repetition frequency of UCN production of 300 s. In order to keep the conditions for nEDM the same while increasing the duty cycle, only the proton beam kick length was modified in the following way:

- 22 µA: 3.0 s every 300 s

- 25 µA: 3.4 s every 300 s

- 30 µA: 4.1 s every 300 s

- 40 µA: 5.4 s every 300 s

4.3.4   UCN yield

As expected from the measurements described in Section 3.7, the UCN output per proton beam kick was increased by the longer kick lengths (see Fig. 3.24), which resulted in an increase in total UCN production per day.

It should be noted that with longer proton beam kicks at constant repetition time, the rate of UCN which can still be measured at the beamports when the central storage vessel flaps reopen to be ready for the next kick gets larger.

An example is shown in Fig. 4.21.

4.3.5   Response of the deuterium system

Although an increase of the proton beam kick length at constant repetition time causes an increasing heat load on the cryogenic system of the UCN source, no negative influence on the deuterium performance was visible. Fig. 4.22 shows a section of the recorded deuterium pressure in the moderator vessel as measured by sensor "CP006". Each peak in the pressure corresponds to a 5.4 s long proton beam kick to the UCN target.
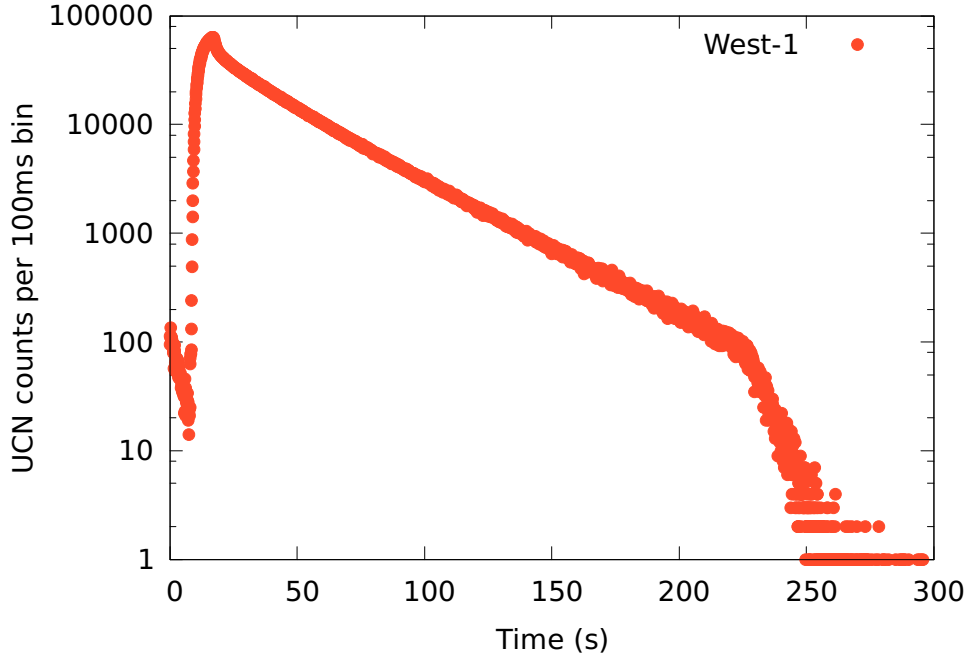
Figure 4.21: *Measured UCN count time spectrum with a* 5.4 s *long proton beam kick at a repetition rate of one kick every* 300 s*. The kink in the UCN rate at* 220 s *into the kick coincides with the reopening of the central storage vessel flaps. The UCN count rate is still on the order of* 1 kHz *when the flaps are opened. The total integrated counts in the shown pulse are* 1.7×10^7 UCN.

Fig. 4.23 shows the pressures of the deuterium for four different duty cycles. For any given average proton beam current, the first 48 h of permanent UCN production after the deuterium had been warmed up for conditioning is shown. The absolute pressure, between 1 and 5 Pa is a feature of the general state of the deuterium crystal. After about 24 h all four curves are essentially flat at a new equilibrium pressure, no further rise of the baseline deuterium pressure is visible.

Looking at the relative pressure curves for individual kicks of different length, Fig. 4.24, one observes a kick length dependent pressure increase, but for all duty cycles the pressure relaxes back towards its equilibrium value quite rapidly.

4.3.6   Radiation safety

When the source was operated with an average proton beam current of more than 30 µA, a small increase in radiation background in the experimental area became measurable.

Three hot spots were found, where the measured radiation was highest. Two were in close vicinity of the positions where the UCN guides of beam ports West-1 and West-2 penetrate the shielding, a third one where the cryogenic periphery is connected to the source vacuum tank by a 300 mm wide tube which also penetrates the shielding.

In all positions, additional shielding was installed during and after the 2015/2016 shutdown of the UCN source. Radiation levels at these positions were brought down significantly.
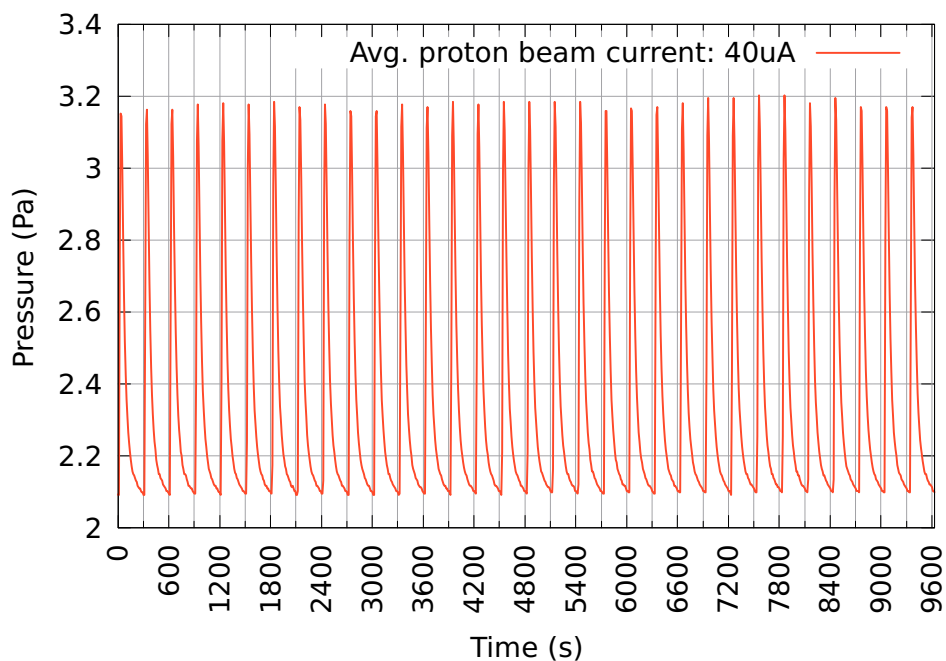
Figure 4.22: *Deuterium vapour pressure in the moderator vessel measured with sensor "CP006" for an average proton beam current of* 40 µA.
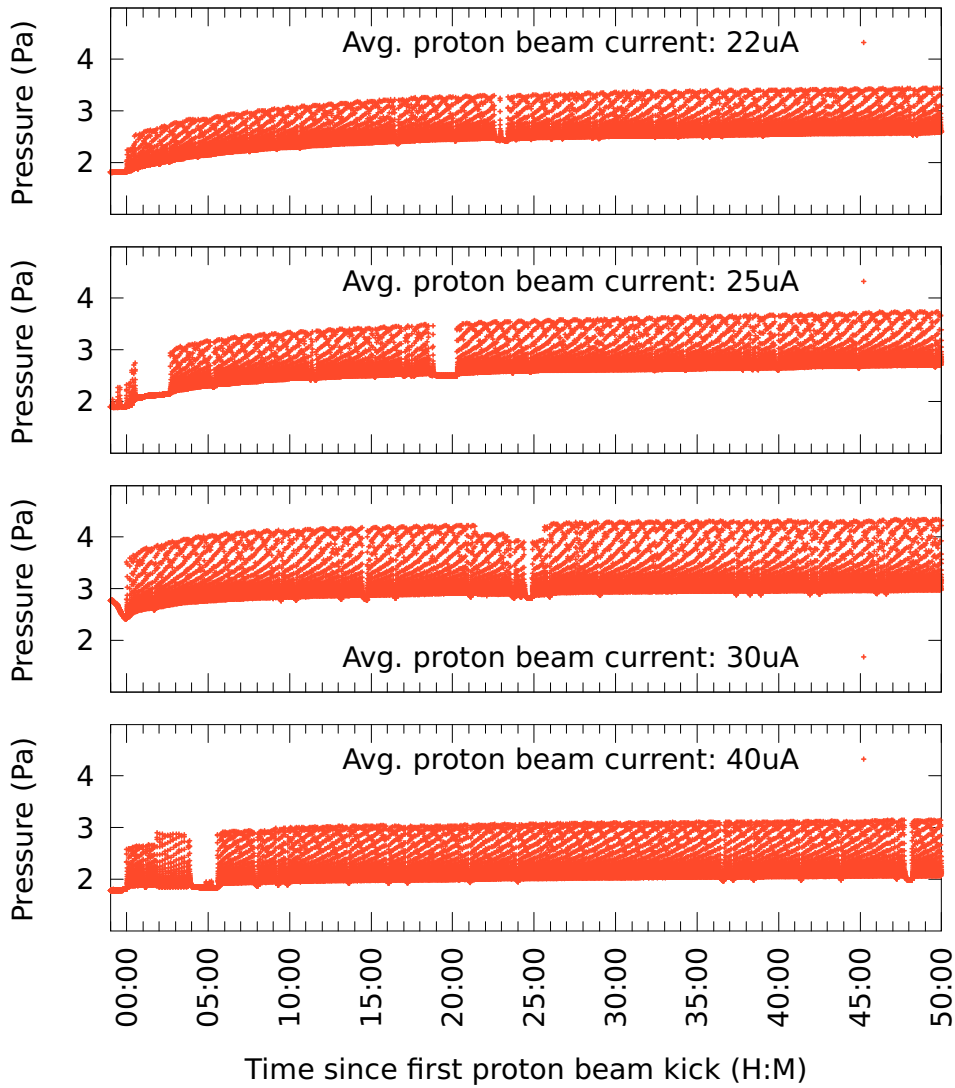
Figure 4.23: *Deuterium vapour pressure in the moderator vessel ("CP006") for four different proton beam kick duty cycles. The given time is measured from starting a series of proton beam kicks every* 300 s *following a conditioning of the deuterium.*

4.3.7 Conclusion and outlook

In the original design of the UCN source, an averaged proton beam current to the UCN target of maximal 20 µA was foreseen. After an in-depth evaluation of dosimetry measurements in the experimental areas, permission to increase this current was granted by the BAG. By the end of HIPA operations in 2015, the UCN source was running regularly with an averaged proton beam current of 40 µA. This corresponds to a 5.4 s long proton beam kick every 300 s.

The resulting increase in UCN output confirmed the expecations from test measurements at different kick lengths in 2014.

Comparing the vapour pressure rise for the various duty cycles we did not observe a deuterium temperature increase that significantly influenced the UCN output and would prevent a further increase of duty cycle. The deuterium system handled the doubling of heat load very well, and it is planned that the average proton beam current will be increased further towards 60 µA in 2016.
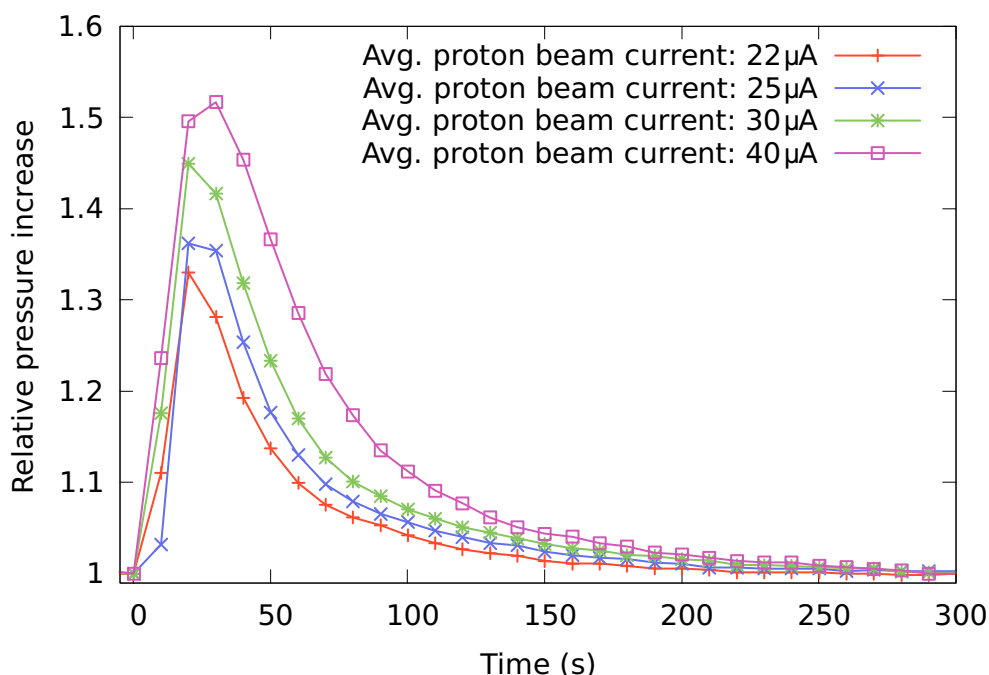
Figure 4.24: *Relative deuterium pressure behaviour in the moderator vessel for four different proton beam kick duty cycles during and after one single kick. Normalised to the baseline pressure. The measurement took place long after starting a sequence with each duty cycle, so the equilibrium baseline pressure had been reached already. It is obvious that the longest kick, corresponding to the highest duty cycle, results in the largest relative pressure increase.*

Chapter 5

Transmission of Ultracold Neutrons through Deuterium Gas

5.1 Motivation

The solid deuterium in the moderator vessel does not occupy the full volume of the vessel, but only the lower part. Thus UCN produced in the deuterium will always have to traverse a volume filled with deuterium gas until they exit through the moderator's aluminium lid towards the storage vessel.

The gas pressure above the cold solid deuterium should be very low (the vapour pressure for solid deuterium at low temperature decreases exponentially with temperature, at solid deuterium
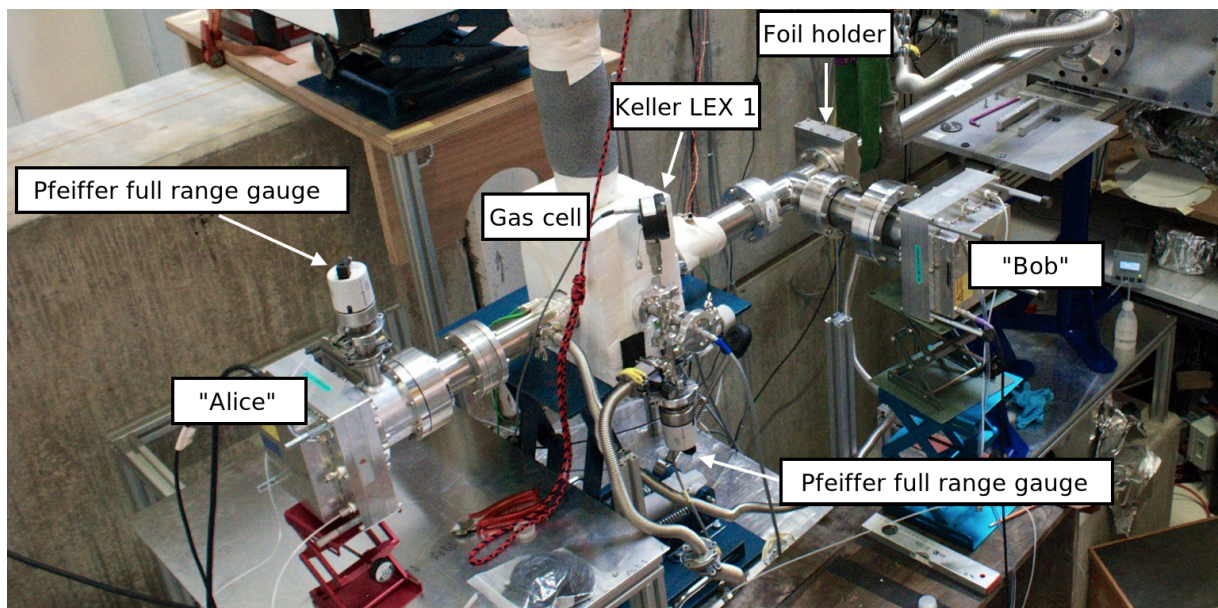
Figure 5.1: *Top view of the measurement setup. Photo by Z. De Hua.*

temperatures of 10 K and 6 K it is given as 6.5 Pa and 2×10^{-4} Pa respectively by [Souers, 1986]). Therefore effects on the UCN output of the source in normal operating conditions should be negligible. Additional motivation stems from the fact that measurements were performed with a pure deuterium gas moderator e.g. in 2013, where UCN production and transmission have to be considered for a quantitative interpretation of the measurement.

UCN cross sections in deuterium gas were measured previously in a dedicated setup, however with smaller volume and not in the full UCN energy range, see [Atchison et al., 2005b].

In order to measure the total cross section of UCN in deuterium gas at various temperatures and pressures, the following measurements were done in October 2014 at the West-1 beam port.

5.2 Setup

5.2.1 General

The gas is contained in a cell made of stainless steel with a length of 5.3(1) cm. Gas can be brought in to the cell through a KF16 connection in the center of the cell. Both ends of the cell are terminated by 100 μm thick AlMg3 aluminium foils with a supporting grid.

The UCN guides are Nocado stainless steel guides with an outer diameter of 70 mm. The only exception is the connection to the Bob detector, which is a stainless steel guide with an outer diameter of 80 mm and a length of 300 mm. The guide between the second VAT shutter and the foil holder is a 1 m long Nocado guide. The T-piece has a through-going piece of 200 mm length. The connection guide to the cell is a 500 mm guide welded to the support grid of the cell window on this side and a 300 mm long guide on the detector side. The remaining guide to the Alice detector is a 300 mm long guide piece. A photo of the setup is shown in Fig. 5.1.

Two copper pipes are wound tightly around the gas cell and lead to a container which is positioned approximately 0.5 m above the gas cell. This container can be manually filled with liquid nitrogen, such that the cell gets cooled to a temperature of approximately 85 K. Alternatively the container can be filled with boiling water in order to heat the gas cell to temperatures above the ambient temperature. Both UCN guides as well as the KF16 gas tube are equipped with heaters in order to keep them at room temperature even if the cell is cooled down to liquid nitrogen temperatures in order to prevent ice formation.

The gas was brought into the cell through a needle valve, which was connected to the KF16 gas inlet of the cell on one side and to the pressure reducer of a pressurised gas cylinder on the other side. No feedback mechanism was implemented, the needle valve had to be adjusted manually in order to compensate for small leakage and to hold the desired gas pressure constant.

The deuterium gas cylinder had been at room temperature for several years. Thus the room temperature ortho- to para-deuterium ratio of 2:1 can therefore be assumed.

Two small Cascade type UCN detectors dubbed "Alice" for the signal detector and "Bob" for the monitor detector at the T-piece in front of the gas cell were used. A third small Cascade type UCN detector ("Charlie") was connected directly to the West-2 beam port for monitoring

purposes. All detectors were kept running throughout the whole measurement time, and were not modified or moved during temperature changes or changes of gas pressure inside the cell.

The setup was modified from the existing setup without temperature control as described in [Hua, 2014].

. First test measurements were done while the UCN source's moderator vessel was only filled with room temperature deuterium gas, because of a prior failure of the cooling plant. Therefore, UCN statistics were very low.

After the source was back to regular conditions, the measurements were redone with significantly better statistics and due to the upgrade of the Klappentrigger control (see Sec. 4.2) with less fluctuations between individual proton beam kicks.

5.2.2   Pressure and temperature sensors

The pressure inside the cell is measured after a KF16 cross using a Pfeiffer PKR 251 full range gauge for pressures far below ambient and a Keller LEX 1 pressure gauge for larger pressures up to 2 bar. A photograph of the gas handling system is shown in Fig. 5.2. The Keller LEX 1 gauge is a piezoresistive pressure sensore and therefore independent of the gas type. It has a specified precision of 0.05 % of the full scale, or 1 mbar in this case. Measurements of the ambient air pressure are compatible within this errors with other atmospheric pressure sensors, when the cell is evacuated the sensor reads small negative values.

The temperature of the gas is measured by two independent PT100 temperature transducers read out via a "Lake Shore 340" temperature controller and were calibrated to below 0.1 K error. A photograph of the open gas cell showing the temperature sensors is shown in Fig. 5.3. It is important to note that the sensors are hanging inside the gas and have no thermal contact to the cell wall.

5.3   Determination of the Loss Cross Section

The loss cross section σ can be calculated as

$$\sigma = -\frac{k_B T}{Lp} \ln(\mathrm{Tr}) \tag{5.1}$$

where T is the temperature of the D_2 gas, L is the length of the gas cell, p is the pressure of the D_2 gas and Tr is the measured UCN transmission:

$$\mathrm{Tr} = \frac{\#\mathrm{counts}_{\mathrm{Alice},p>0}/\#\mathrm{counts}_{\mathrm{Bob},p>0}}{\#\mathrm{counts}_{\mathrm{Alice},p=0}/\#\mathrm{counts}_{\mathrm{Bob},p=0}} \tag{5.2}$$

5.4   Systematic Checks

5.4.1   Temperature independence of the transmission of the empty setup

The transmission of the empty gas cell setup was measured during cooldown. The measurement was started with the cell evacuated and at room temperature. One transmission measurement was done every 5 min for about 6 h until a temperature of approximately 85 K inside the cell was reached. The counts per measurement for all three detectors and the ratio between counts in the "Alice" and "Bob" detectors can be seen in Fig. 5.4.

The ratio does not change significantly throughout the whole time, so temperature dependent changes of the empty cell transmission can be neglected.

5.4.2   Long term measurements at low temperatures

In order to check for systematic effects due to e.g. freezing of water to the gas cell foils when the cell is cooled down with liquid nitrogen, a measurement was done with the empty cell constantly cooled down for four hours, measuring the ratio between the signal and monitor detector counts every 5 min. The results of this measurement are shown in Fig. 5.5.
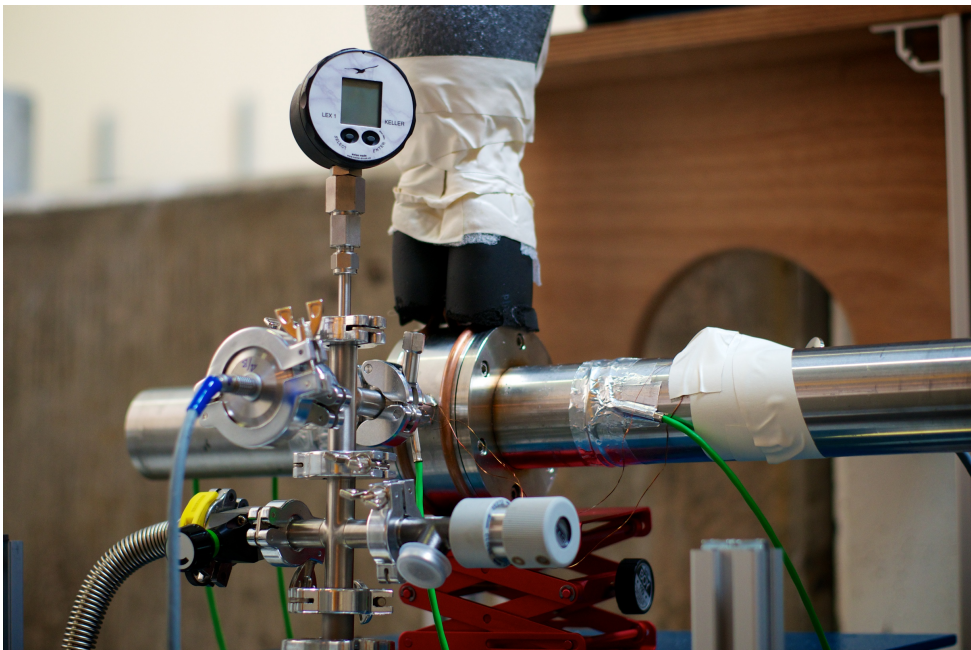
Figure 5.2: *View of the gas cell without thermal insulation. The green cables are heating cables to ensure the outside gas periphery and UCN guides stay at room temperature. Gas is intruduced through the (gray) needle valve on the right hand side, gas pressure below* 1 mbar *is measured with a full range vacuum gauge (not visible), while pressures above* 1 mbar *are measured by the KELLER LEX 1 absolute pressure gauge at the top. Photo by Z. De Hua.*

Fitting a line to the data points yields a decline of the ratio of $-0.042(36)$ % per kick, with a reduced χ^2 of 0.83. Neglecting the one high outlier in the fifth kick and repeating the fit yields a decline of $-0.02(3)$ % per kick, with a reduced χ^2 of 0.65. Considering that the latter decline is compatible with zero and that typical measurement times at liquid nitrogen temperatures were limited to less than two hours, effects of a changing empty cell transmission over time while cooled down can be neglected.

5.4.3 Cooldown pT diagram

A simple two-vessel model for the gas in the cell and the feeding / gauge lines is used to estimate possible influences of the gas temperature and pressure measurements. It is assumed, that the cell will have the temperature read by the two sensors inside, whereas the feeding lines stay at room temperature. The index $i = 0$ indicates the full system of the gas cell and the feeding lines, all at room temperature and in thermodynamical equilibrium. Indices $i = 1$ and $i = 2$ indicate the gas cell alone and the feeding lines alone respectively.

Using

$$p_i = \frac{n_i k_{\mathrm{B}}}{V_i} T_i \tag{5.3}$$

where p_i, V_i, T_i are pressure, volume, and temperature, k_{B} is the Boltzmann constant, and using the conditions
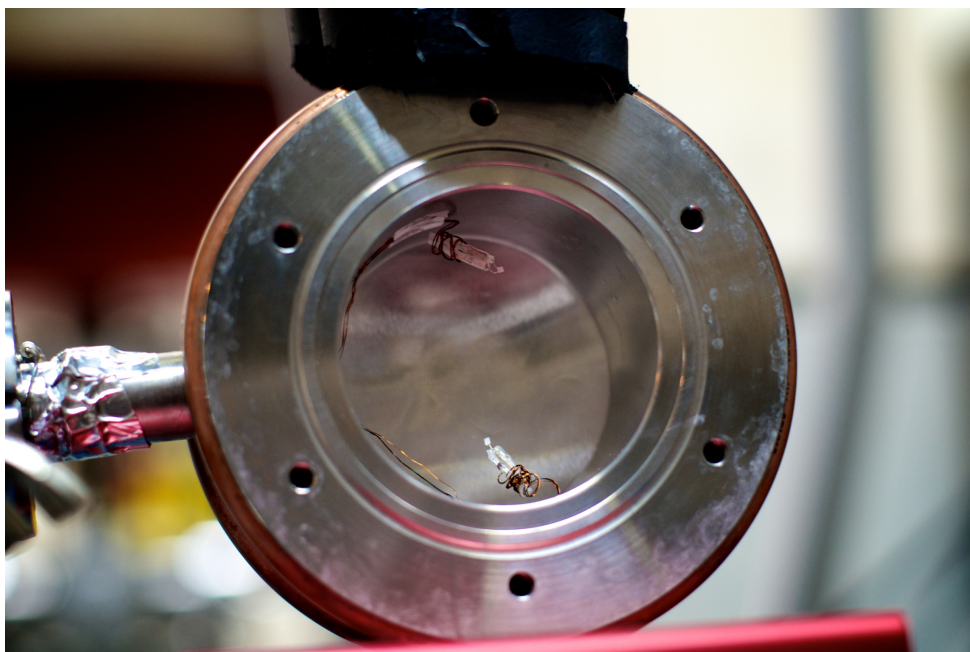
Figure 5.3: *Inside view of the gas cell. Both PT100 temperature sensors can be seen. They are mounted such that they are not thermally coupled to the cell walls. Photo by Z. De Hua.*

$$n_1 + n_2 = n_0 \tag{5.4}$$

$$V_1 + V_2 = V_0 \tag{5.5}$$

$$p_1 = p_2 \tag{5.6}$$

it can be deduced that

$$p_1 = p_0 \frac{V_1 + V_2}{V_1} \frac{T_1}{T_0} \frac{1}{\left[\frac{V_2 T_1}{V_1 T_2} + 1\right]} \tag{5.7}$$

The volume of the gas cell is about $200\,\text{cm}^3$, the internal volume of all feeding lines and gauges was estimated to be about $100\,\text{cm}^3$.

Fixing the gas cell volume and fitting the datapoints to this formula while cooling the setup from room temperature to liquid nitrogen temperature gives an estimate of the warm volume V_2.

The fit shown in Fig. 5.6 yields a warm volume of about $147.6\,\text{cm}^3$, which is reasonable and confirms that the measured data is sound.
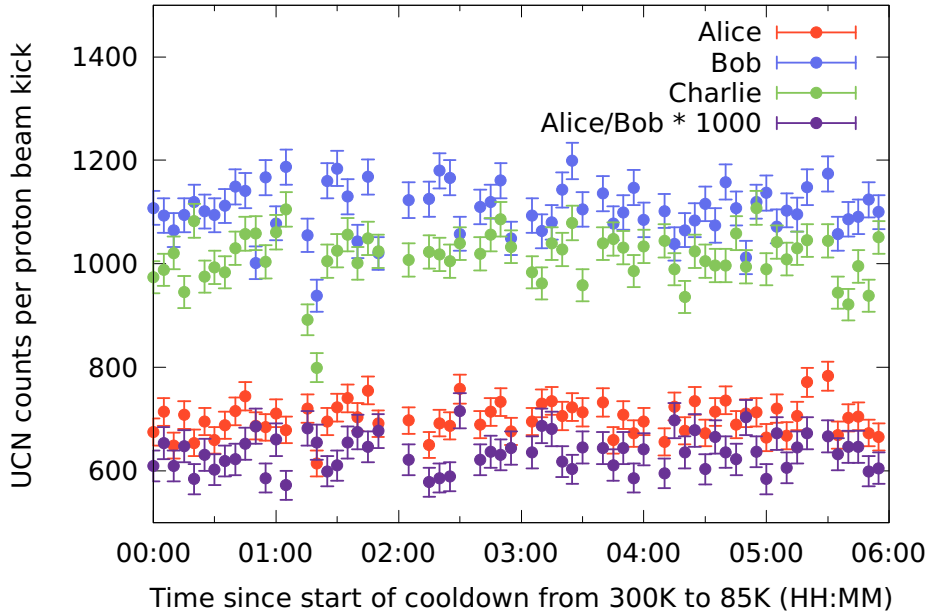
Figure 5.4: *Plot of the UCN transmission through the empty gas cell setup during cooldown from room temperature to liquid nitrogen temperature. All three detector counts (red, blue, green) as well as the ratio between "Alice" and "Bob" stay constant within their normal fluctuations.*

5.5   Transmission Measurements

5.5.1   Temperature control

The gas temperature could not be controlled precisely, as this would need a much more refined cooling or heating system.

Data was taken at 3 different temperatures:

- Room temperature: $T = 301(2)$ K

    - The gas cell was neither heated nor cooled.

    - No temperature stabilisation was applied.

    - The ambient temperature drifts were slowed down by insulation materials.

- Cooled with liquid nitrogen (LN_2): $T = 85(2)$ K

    - The gas cell was cooled with LN_2 flowing in copper tubes around the cell.

    - The LN_2 reservoir was kept filled with boiling nitrogen.

    - The ambient temperature drifts lead to a drift of the equilibrium temperature.
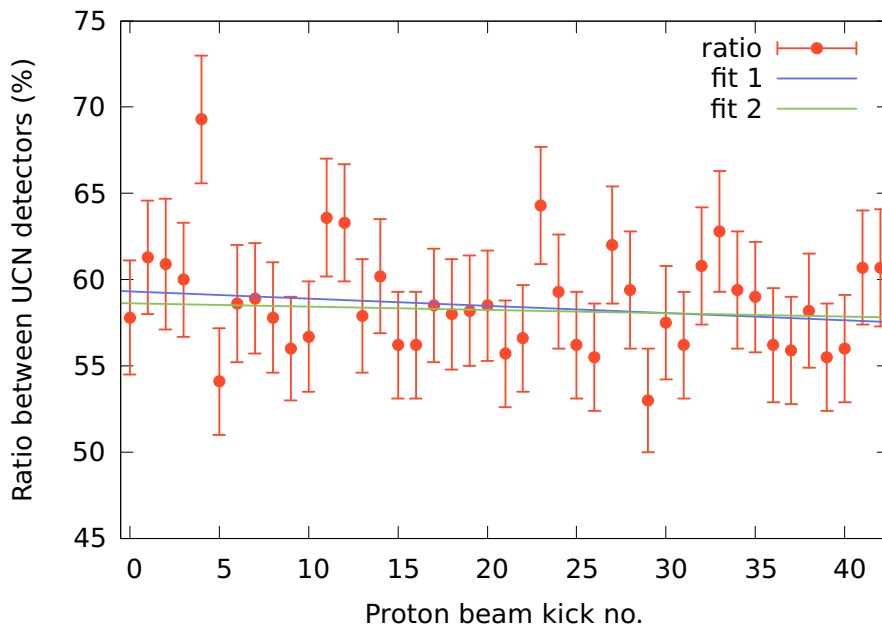
Figure 5.5: *Plot of the count ratio between "Alice" and "Bob" measured with the empty gas cell over four hours. Two fits are indicated, the first (blue line) takes all points into account and indicates a small decline in detection ratio. The second fit (green line) neglects the high outlier in the fifth measurement and is compatible with no decline within errors.*

- Heated with boiling water: $T+333(2)$ K

    – Water was kept boiling in the (nominal) LN_2 reservoir.

    – No pumps were mounted, convection was not working as the heater was at the highest point.

    – No stable equilibrium was reached at reasonably high temperatures.

The temperatures measured with both sensors during the measurements are shown in Fig. 5.7 for LN2 temperatures and Fig. 5.8 at room temperature and elevated temperature. Two measurement sessions at LN_2 temperatures were done.
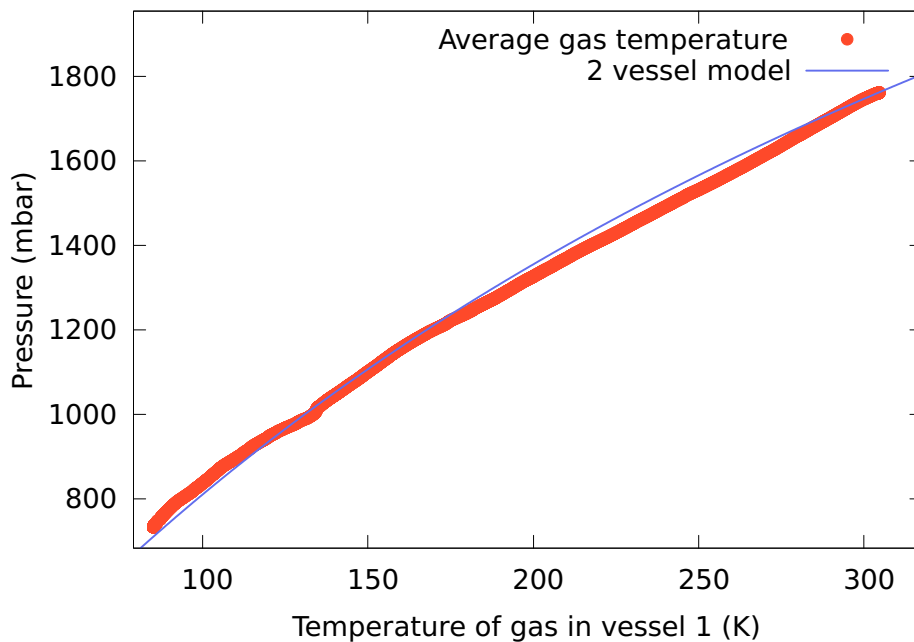
Figure 5.6: *Cooldown pV diagram for the gas cell plus periphery. The fit of the 2 vessel model results in a warm volume V_2 of 147.6 cm^3 with a reduced chi^2 of 1.24.*
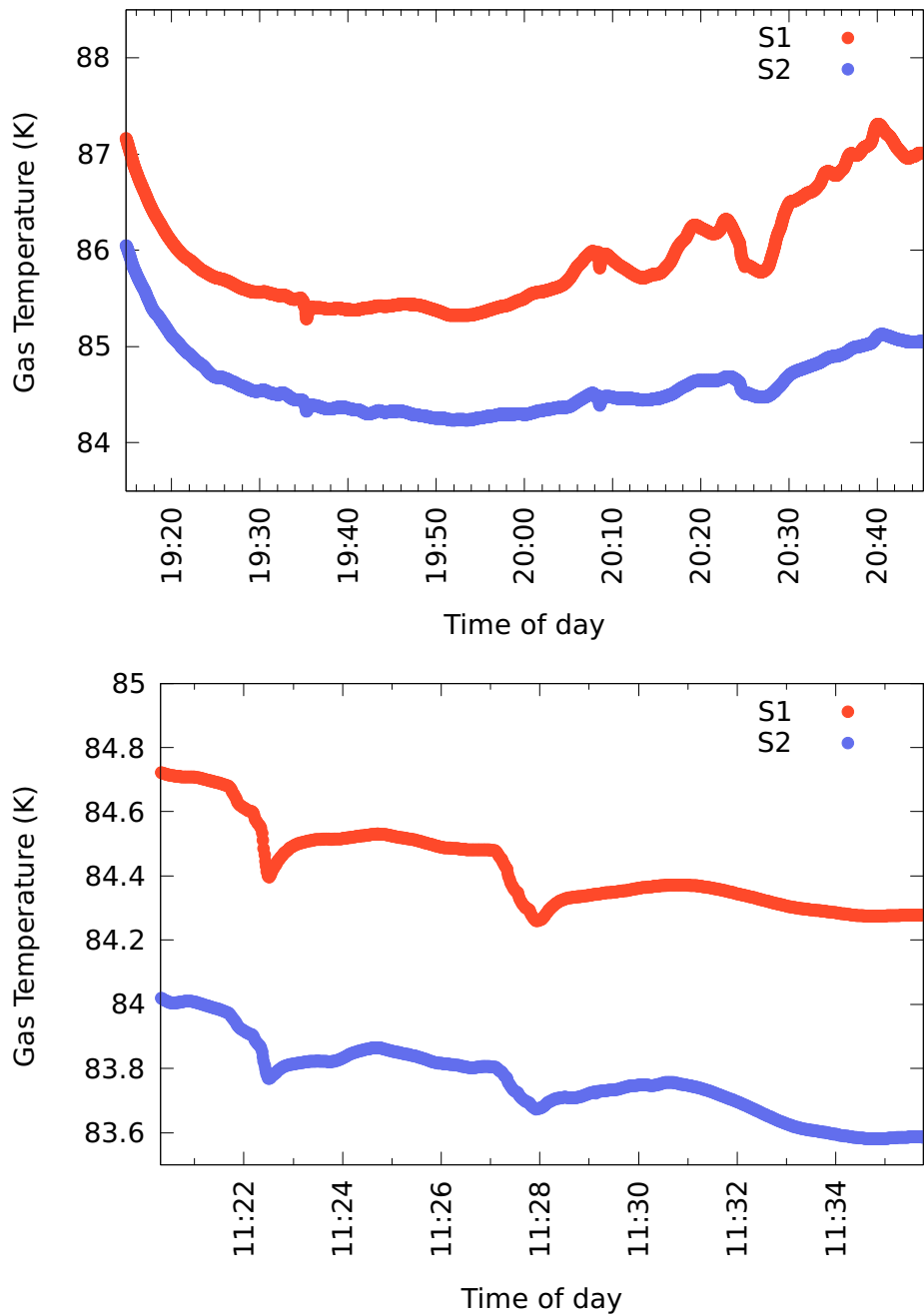
Figure 5.7: *Temperatures during transmission measurements with the cell cooled with liquid nitrogen. S1 and S2 are the two temperature sensors inside the cell.*
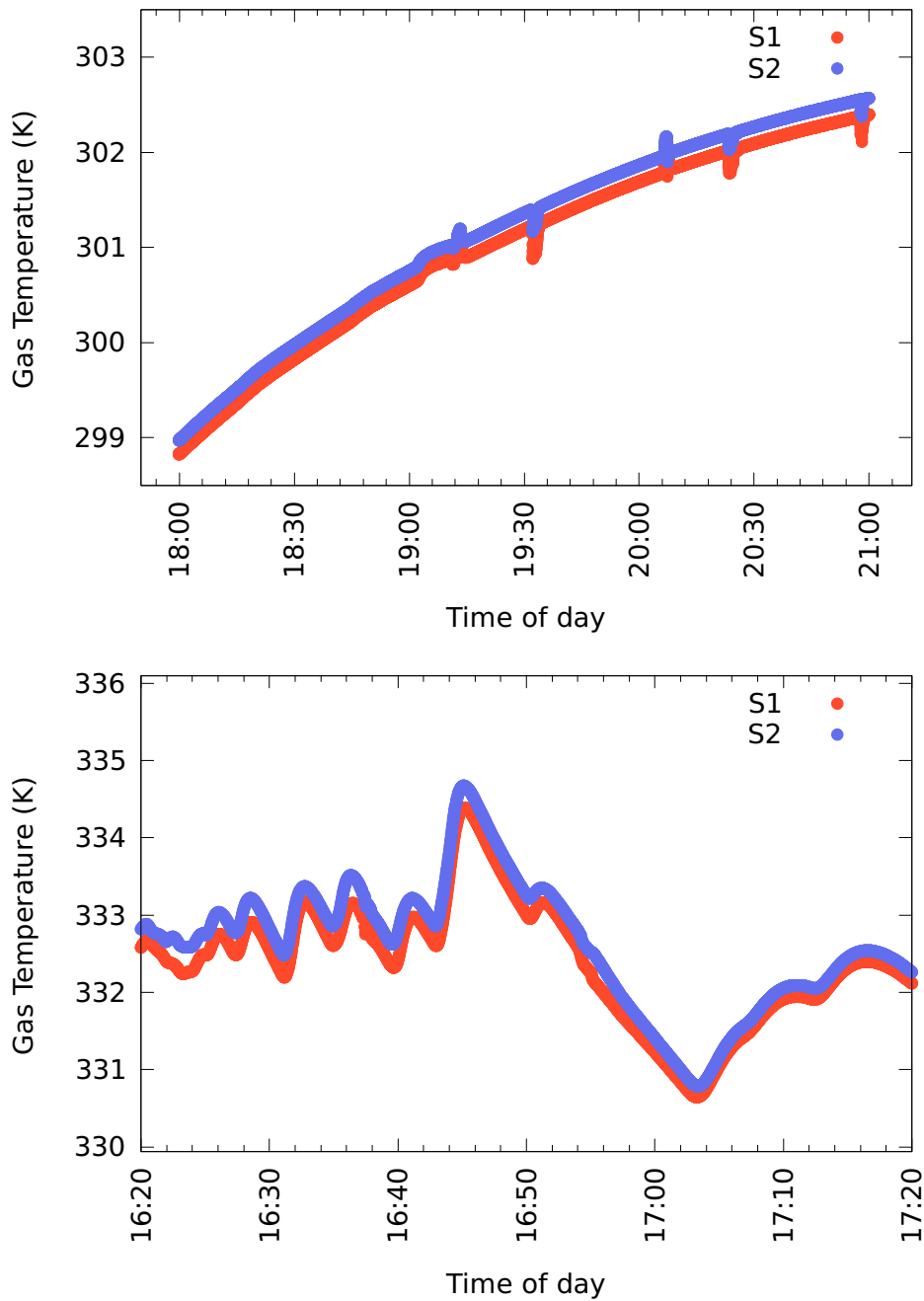
Figure 5.8: *Temperatures during transmission measurements with the cell at room temperature (top) and heated with boiling water (bottom). S1 and S2 are the two temperature sensors inside the cell.*

5.5.2   Measurements at various gas temperatures

The gas transmission was measured during a three day period. The gas cell was cooled down to LN$_2$ temperatures twice, both times for approximately 2 h. Afterwards the cooling was stopped and the cell warmed up to room temperature again. It was heated to about 30 degrees above ambient temperature for about 1.5 h.

For all temperatures, measurements with evacuated cell were performed as well in order to determine the transmission, which was calculated according to Eqn. 5.2.

Data at T ≃ 333 K

T (K)	p (mbar)	#	Counts Alice	Counts Bob	Transm.	Transm. (no mon.)
333(2)	0	3	1 081 553(1040)	1 907 364(1381)	—	—
333(2)	550(2)	3	808 531(899)	1 908 011(1381)	0.747(1)	0.748(1)
333(2)	1100(2)	3	614 340(784)	1 866 537(1366)	0.580(1)	0.568(1)

Data: T ≃ 301 K

T (K)	p (mbar)	#	Counts Alice	Counts Bob	Transm.	Transm. (no mon.)
301(2)	0	3	1 187 325(1090)	2 069 893(1439)	—	—
301(2)	500(2)	6	1 749 016(1323)	4 077 437(2019)	0.748(1)	0.737(1)
301(2)	1000(2)	5	1 134 586(1065)	3 391 297(1842)	0.583(1)	0.573(1)
301(2)	1760(2)	5	777 627(882)	3 350 098(1830)	0.405(1)	0.393(1)

Data: T ≃ 85 K

T (K)	p (mbar)	#	Counts Alice	Counts Bob	Transm.	Transm. (no mon.)
85(2)	0	3	1 114 102(1056)	1 882 630(1372)	—	—
85(2)	500(2)	5	1 643 551(1282)	3 326 562(1824)	0.835(1)	0.885(1)
85(2)	1000(2)	4	1 120 375(1059)	2 629 759(1622)	0.720(1)	0.754(1)
85(2)	131(2)	4	870 394(933)	2 612 058(1616)	0.563(1)	0.586(1)
85(2)	262(2)	4	696 042(834)	2 621 027(1619)	0.449(1)	0.469(1)

Table 5.1: *Measured transmission data for deuterium gas at various temperatures. Average gas temperature (T) and pressure (P), number of repetitions (#), and counts per detector are given. Transmission rates both with and without correction using the monitor detector "Bob" are tabulated as well. Errors on T and p are systematical errors from calibration and fluctuations, errors on counts and transmissions are statistical only.*

Counts in all detectors are integrated from bin 150 to bin 3000, i.e. from approximately 4.3 s after the end of the proton beam kick until shortly before the next one.

The beginning of the integration window was chosen well after the proton beam kick end in order to make sure that no faster neutrons could be left in the source and guide system.

5.5.3 Simple fit to the data

In the simplest model, for each gas temperature, the UCN transmission should follow an exponential decay with respect to the gas pressure:

$$\mathrm{Tr}(p) = e^{-Lp\sigma(E_{\mathrm{kin}})/(k_{\mathrm{B}}T)} \tag{5.8}$$

where L is the length of the gas cell, p is the gas pressure, $\sigma(E_{\mathrm{kin}})$ the total cross section for UCN of a given kinetic energy, k_{B} the Boltzmann constant and T the gas temperature. This is valid only for monoenergetic UCN. Fig. 5.9 shows a plot of the natural logarithm of the UCN transmission and linear fits. It is obvious that the measured data at all temperatures agrees very well with an exponential decay. However, the y-intercepts of all fits are clearly below zero.

Consequently, global fits for all gas temperatures, assuming a calculated total cross section, yield average UCN energies of 91(3) neV, but with a reduced χ^2 value of 240! Such a fit is shown in Fig. 5.10.

Assuming a single average kinetic energy for the UCN traversing the gas cell therefore has to be considered an oversimplification.
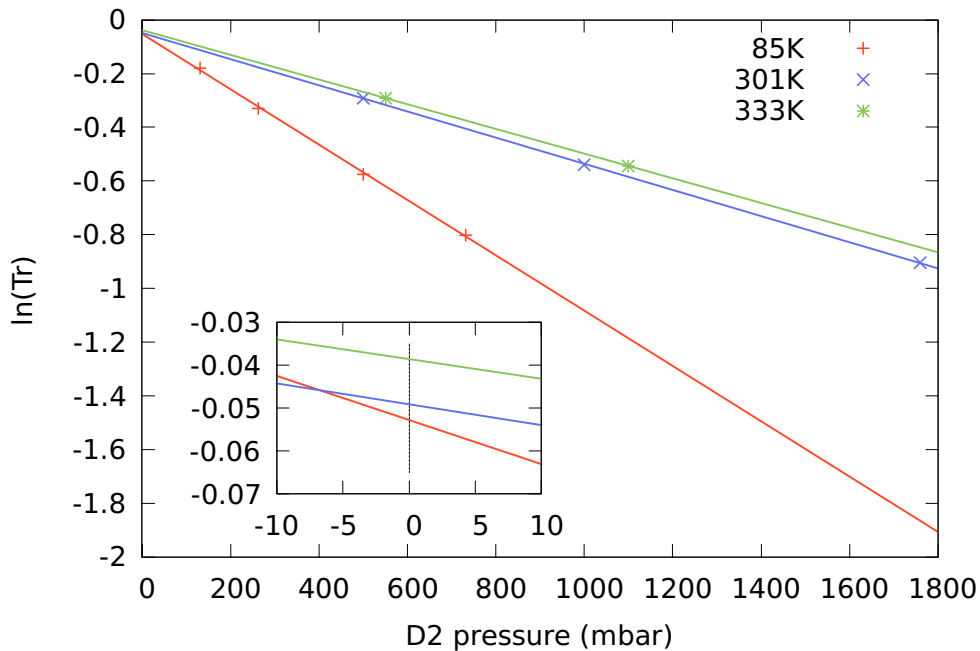
Figure 5.9: *Logarithmic representation of the measured transmission data. The lines represent linear fits to the data. A zoom of the y-intercept is shown in the box.*

5.5.4   Parametrisation of calculated total cross sections

In order to investigate the pressure dependence of the UCN transmission through deuterium gas, calculated cross sections for various gas temperatures were used in order to be able to do global fits.

Total cross sections per molecule for Hydrogen and Deuterium were calculated by Dr. Geza Zsigmond according to [Young and Koppel, 1964] (YK). The results can be found in table 5.2. These values assume an incoming UCN energy of 250 neV.

In the transmission measurements, the deuterium gas had been at room temperature for a long time, so it can be assumed that the spin state population is in equilibrium, i.e. two thirds ortho-D_2, one third para-D_2. The short cooling cycles did not change this spin-state ratio.

The calculated weighted average cross sections per molecule can be found in table 5.3.

The measurements were not taken at the precise gas temperatures for which calculations were made. In order to interpolate, a simple functional dependence was fitted to the calculated values. Fig. 5.11 shows that the resulting parametrisation resembles the calculated values well.

The parametrisation which was used is:

$$\sigma_{\text{param}} = 827.167\,\text{b} \times (T/\text{K})^{0.25} - 982.48\,\text{b}$$
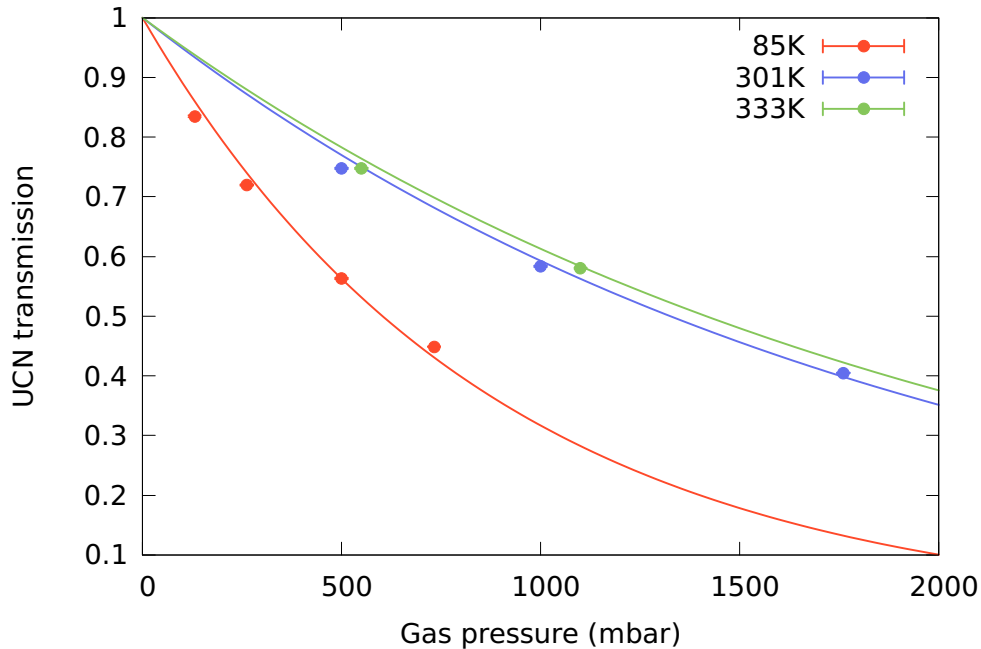
Figure 5.10: *Transmission data with global fit to the average kinetic energy. $\chi^2/n_{d.o.f} = 240$. Statistical errors are smaller than the data points. Obviously the fit systematically misrepresents the data, as it is higher than the measured data for low pressures and lower for high pressures.*

Using this parametrisation to interpolate the cross section with respect to the gas temperature, the total loss cross section for a specific kinetic energy of the incoming UCN can now be calculated as

$$\sigma_{\text{YK}} = \sigma_{\text{param}}(T) \times \frac{\sqrt{250\,\text{eV}}}{E} \times d \times \frac{p}{k_B T}$$

where

- T is the gas temperature in Kelvin

- E is the kinetic energy of the incoming UCN in neV

- d is the length of the gas cell in m

- p is the gas pressure in Pa

- k_B is Boltzmann's constant

5.5.5   Fits with binned incoming UCN energy spectrum

The dependence of the average UCN transmission through the gas cell, or likewise the cross section, on the gas pressure inside the cell varies with the energy spectrum of the incoming UCN.

The incoming UCN energy spectrum is not precisely known. Therefore a generic spectrum with discrete energy classes E_i and weights k_i is assumed, with the normalisation condition $\sum_i^n k_i = 1$. For the number of energy classes n values smaller than the number of measured data points (i.e. smaller than 9) were chosen in order to be able to fit.

The energies E_i were typically distributed equidistant between 0 neV and 300 neV.

A binned energy spectrum like the one shown in Fig. 5.12, consisting of discrete UCN energies of 2, 52, 102 and 152 neV with the relative weights as indicated in the graph, leads to a rather good agreement of calculation and data, as shown in Fig. 5.13. However, k_2, the population of the

T (K)	σ oD$_2$ (b)	σ pD$_2$ (b)	σ pH$_2$ (b)	σ oH$_2$ (b)
25	902.6	837.2	223.5	8053.2
50	1239.8	1140.9	304.5	10671.3
75	1485.8	1357.8	417.1	12475.7
100	1683.2	1532.2	746.8	13846.8
200	2214.9	2026.8	4566.8	17441.3
300	2548.9	2337.9	8623.8	20018.0
400	2781.9	2552.5	11840.9	22098.6

Table 5.2: *Calculated cross sections for ortho- and para- hydrogen and deuterium molecules at an incoming E_{kin}=250 neV [Zsigmond, 2015].*
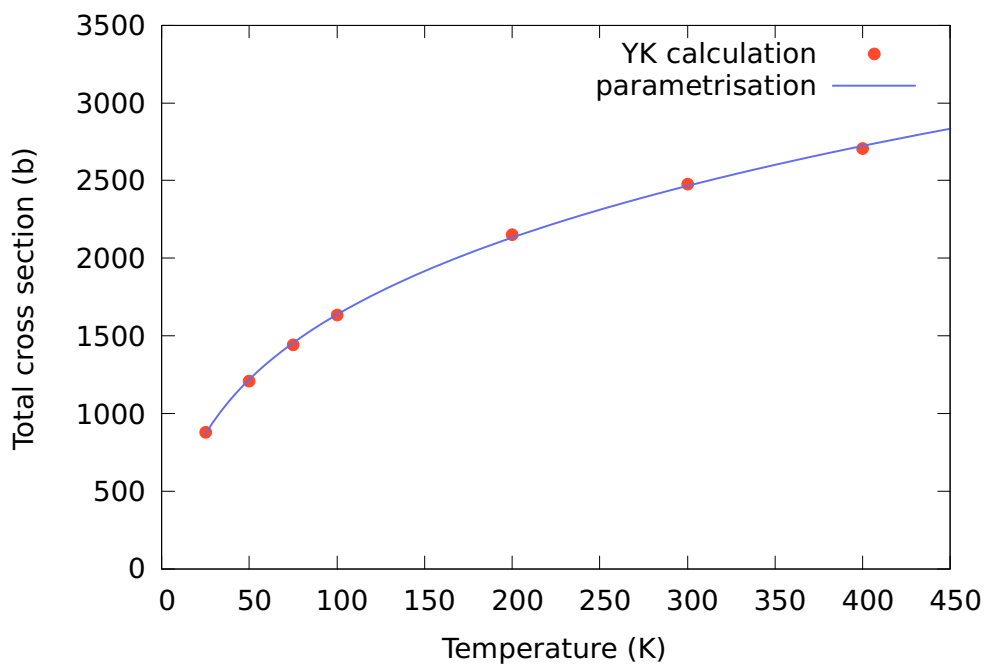
Figure 5.11: *Functional parametrisation of the total loss cross section, see Tab. 5.3.*
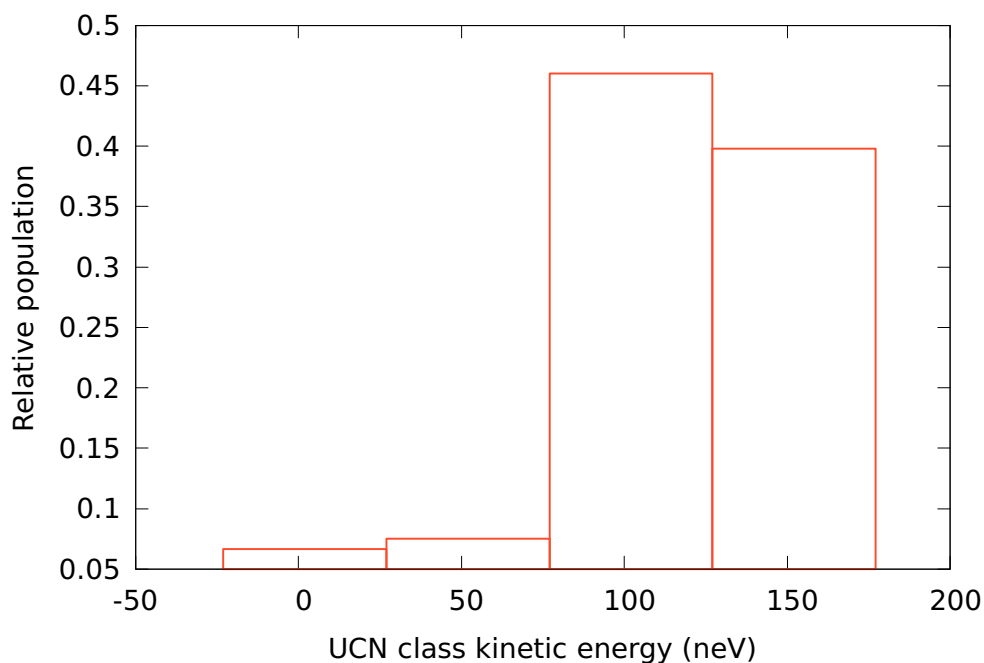
Figure 5.12: *Binned UCN energy spectrum used to model transmission. The four energy classes have discrete energies of 2, 52, 102 and 152 neV. UCN with energies below 54 neV cannot exit the UCN sources vacuum safety window made from AlMg3. Therefore this specrum is not physical.*

energy class with 52 neV, has to be limited towards lower values in order to prevent a gap in the energy population. The reduced χ^2 value of this fit is 0.3

Unfortunately, no UCNs with kinetic energies below ~ 50 neV should be able to traverse the aluminium entrance window of the gas cell and as such the model is unphysical.

Shifting the energy bin centers E_i up to values above 50 neV results in the plot shown in Fig. 5.14, which does not resemble the measured data anymore. The reduced χ^2 value of this fit is 2.8 The fit converges for k_4 going to the smalles allowed value above zero.

No incoming binned UCN energy spectrum could be found which would fit the measured transmission data and satisfies the two least strict conditions of being realistic:

- No UCN with energies below cutoff energy of the AlMg3 vacuum window (approximately 50 neV)

- Continuity of the spectrum, i.e. no unpopulated energy bins surrounded by populated bins.

All fit results showed the consistent feature of an underestimated UCN transmission for small gas pressures. In order to "pull" the fit to 100 % transmission at $p = 0$, a small but not negligible amount of UCN with energies far below 50 neV would be necessary.

5.6   Further Systematic Checks

The energy spectrum of the UCN source changes with time during every production cycle.

- At the beginning of the proton beam kick, the first measurable neutrons reaching the detector are so-called very cold neutrons (VCN), which are faster than UCN.

- During and right after the proton beam kick, a large portion of the UCN have energies up to the Fermi potential of NiMo, i.e. 220 neV.

T (K)	σ_{tot} (b)
25	880.8
50	1206.8
75	1443.2
100	1632.8
200	2152.2
300	2478.6
400	2705.4

Table 5.3: *Total weighted loss cross section for neutrons on deuterium molecules at room temperature for E_{kin}=250 neV.*
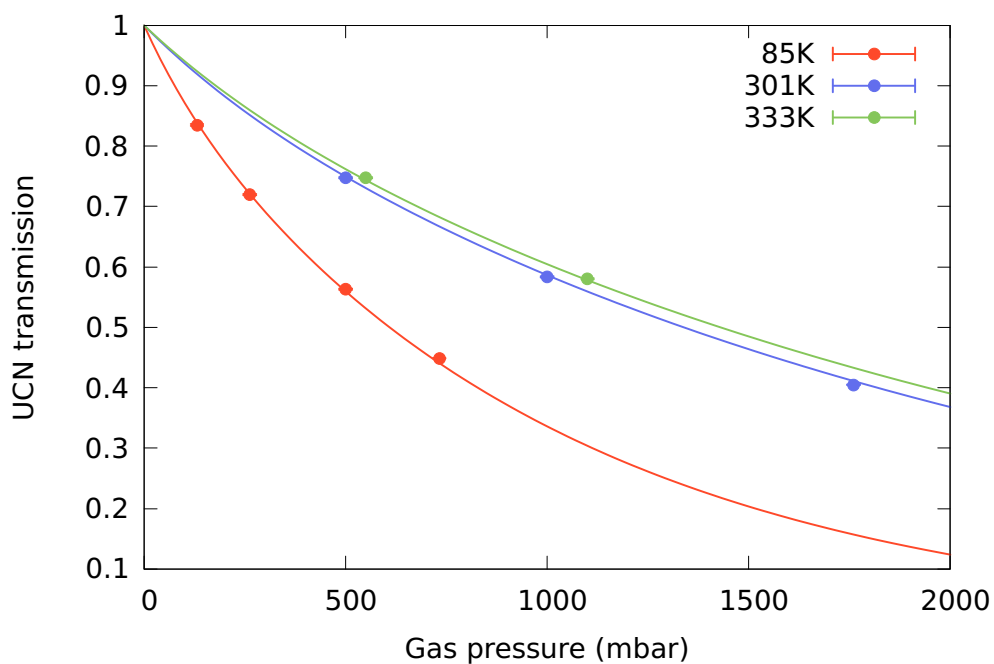
Figure 5.13: *Global fit to the UCN transmission against a theoretical binned energy spectrum from Fig. 5.12.*
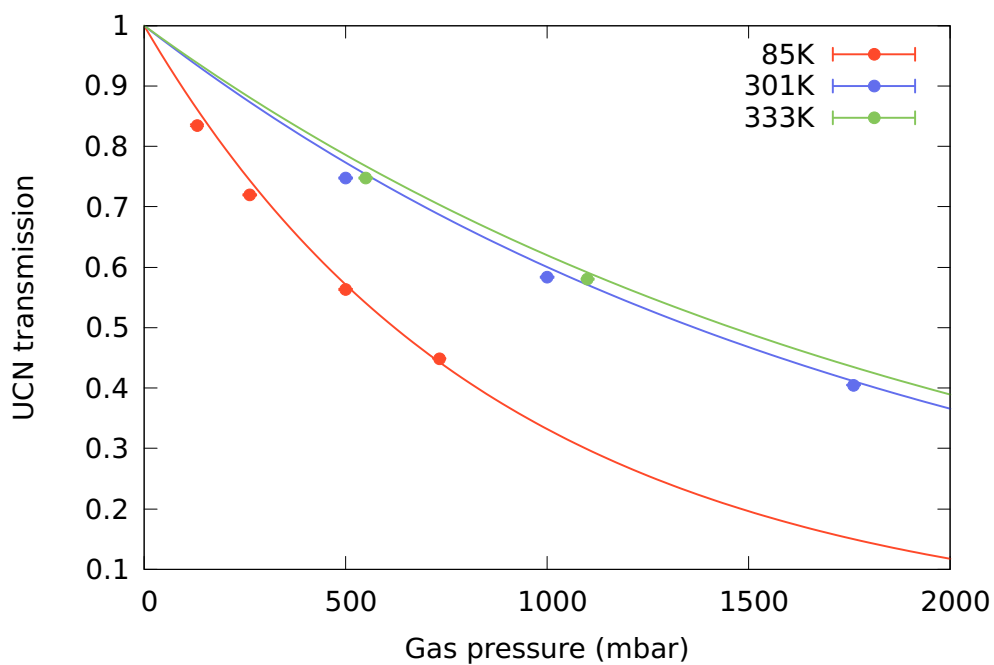
Figure 5.14: *Global fit to the UCN transmission as Fig. 5.13, UCN energy bins shifted by* 48 neV.

- The more time has elapsed since the end of the proton beam kick, the softer the energy spectrum gets.

Fig. 5.15 shows a time spectrum of neutron counts in the detector with the proton beam kick indicated.

Typically, throughout this work only neutrons counted between a few seconds after the end of the proton beam kick and until shortly before the next kick have been taken into account.

In order to investigate the energy dependence of the UCN transmission through deuterium gas and if the issue with fitting the data is a systematic effect due to the particularities of the energy spectrum, the integration window has been varied.

Fig. 5.16 shows a comparison of various first cuts for count integration with the cell filled with deuterium gas at 85 K. Other gas temperatures show identical behaviour.

For even more drastic spectral changes, checks were made for very short integration windows as well. Fig. 5.17 shows transmission data integrated for various long windows, but also counting only the first one to five seconds of neutron arrival during and shortly after the proton beam kick. Neutrons counted in the first second have velocities in excess of 10 m s^{-1}. For the first 1 s and 2 s
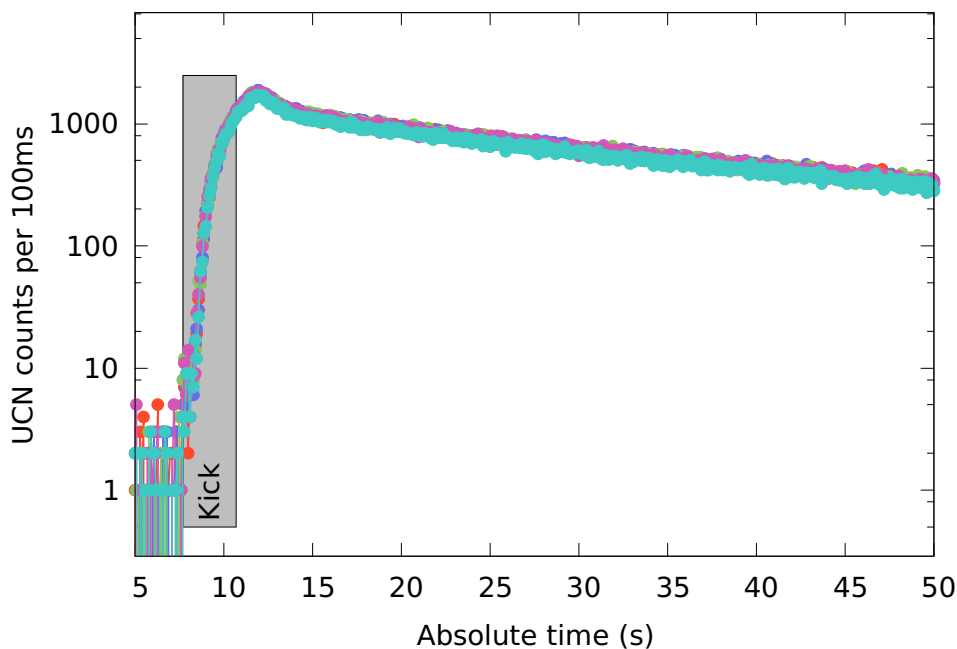
Figure 5.15: *UCN count time spectrum for multiple measurements with the gas cell setup. The absolute timescale starts at t = 0 when the Cascade type UCN detectors are triggered. During the first few seconds, low UCN count rates due to the 7 ms long pilot kick are visible. Shortly after the beginning of the proton beam kick (inserted rectangle) the count rate rises steeply, when first VCN and later UCN arrive at the detector. The count rate peaks shortly after the end of the proton beam kick, and settles to a slow exponential decay after a few seconds. The figure also demonstrates the stability of the timing and UCN counting during the measurements with the gas cell.*
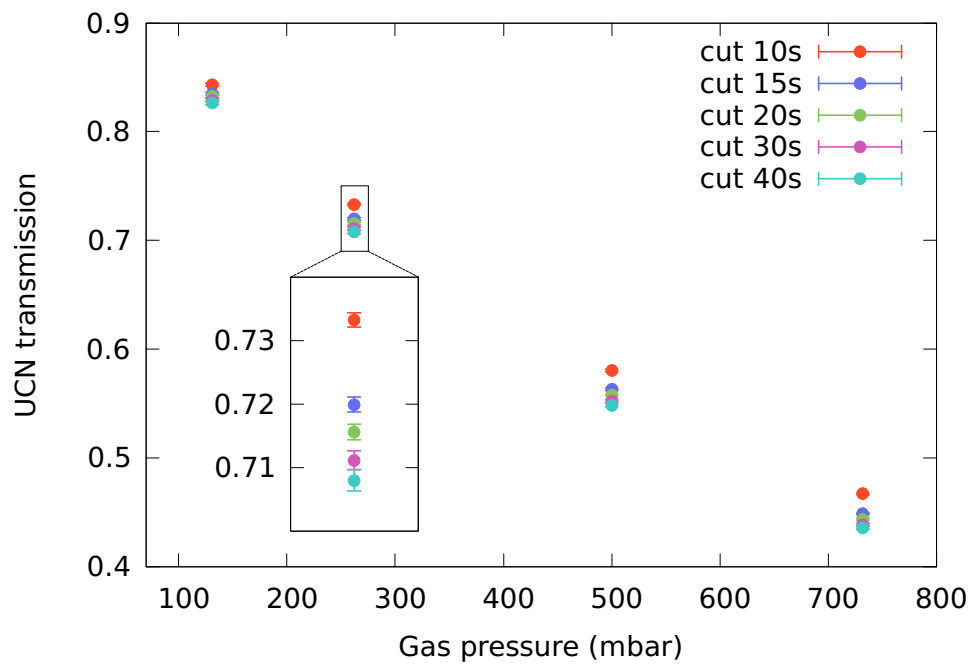
Figure 5.16: *UCN transmission through deuterium gas at 85 K for various starting times of the integration window (10, 15, 20, 30 and 40 s). The end of the integration interval stayed constant at t = 300 s, which includes all UCN until shortly before the next proton beam kick. Starting the integration at t = 10 s ("cut 10s") includes part of the proton beam kick and the peak in neutron count rate (see Fig. 5.15), and thus shows a transmission slightly offset from the group of other integration windows. All other values with later cuts, up to about 30 s after the end of the proton beam kick, show only slightly less transmission for later integration windows.*

in the kick, the statistical error bars are still rather large. Using short integration windows during the proton beam kick generally yields larger transmission, but a flatter slope towards large gas pressures as well. Fitting the first 3 s of arriving neutrons to s single exponential shows the same behaviour as for all UCN measurements, namely the fit does not reach a transmission of 100 % for zero gas pressure.

Varying the integration window cuts for the transmission measurements did not result in a better understanding of the observed behaviour of the transmission with respect to gas pressure.

5.7 Conclusion

Although the cross section calculations for the transmission of UCN through deuterium gas at various temperatures yielded results of approximately the right magnitude, no conclusive result could be obtained from the transmission measurements due to some unknown systematic effect which seemed to vary the transmission with respect to the absolute gas pressure inside the cell.

It is obvious, that the UCN transmission must approach 1 for gas pressures approaching zero, by definition. As shown e.g. in Fig. 5.17, this is not the case for all measurements and data treatments. Generally, too low UCN transmission for low gas pressures was observed.

Extensive investigations to identify the cause for this systematic problem were performed. This included the used sensors for pressure and temperature measurements, where calibrations were
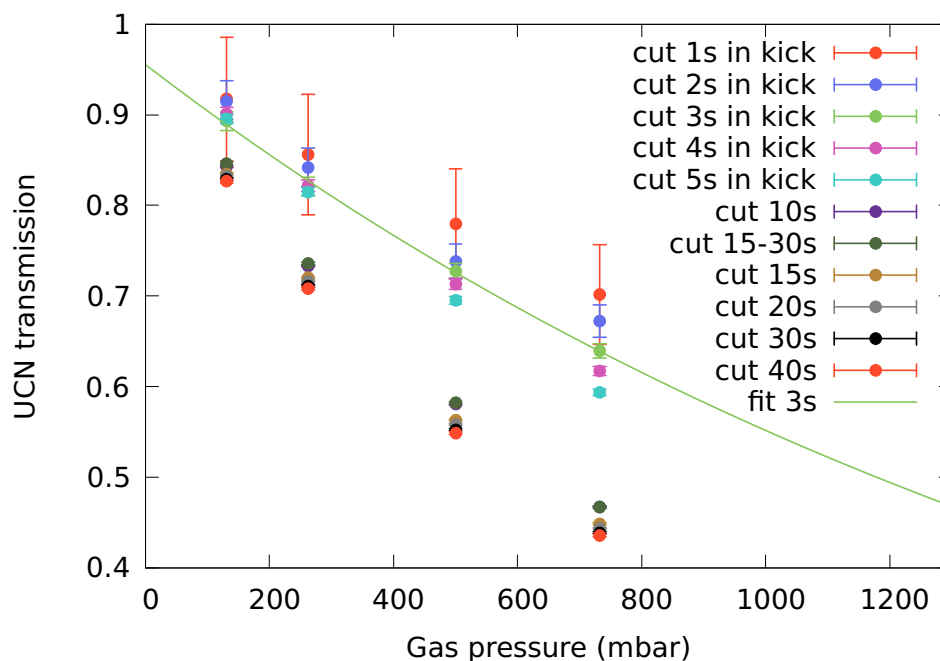
Figure 5.17: *UCN transmission through deuterium gas at 85 K for various integration windows. The first windows are just a few seconds long and start as soon as UCN are arriving in the detectors during the pulse.*

checked and validated for both. The detectors used for UCN counting and monitoring were operated continuously throughout the whole data taking and were not affected by any manipulations of gas pressure or temperature. The detectors are capable to measure up to incident neutron rates on the order of 1 MHz. The incident rates in these measurements were well below such rates, which excludes pileup or detector dead time. Analyses without using the monitor detector were done and gave compatible results. Many different data cuts were performend. Possible effects caused by bulging of the cell windows were studied and excluded. Separate measurements with empty cell were performed for all conditions, therefore eventual effects of the foils which could change with temperature should have been taken into account. Possible efffect due to gas density differences between warm and cold parts of the setup were studied and excluded.

All of our detailed investigations have failed to identify the cause for the systematic effect.

Chapter 6

Construction of a Robust Mobile UCN Storage Experiment

6.1 Motivation

In order to measure the UCN density available at the beamports of the PSI UCN source we have previously used a UCN storage bottle made of the "Strahlwegventil" beamline shutter, a 1 m long UCN guide of 180 mm inner diameter, made of glass and coated with NiMo, and a second shutter identical to the beamline shutter.

This bottle had the following shortcomings due to the use of the beamline shutters made by VAT:

- Slow opening and closing time on the order of 1 s.

- Large slits open during opening and closing, through which UCN loss occurs.

- Large size and heavy weight.

- Only 1 mobile shutter unit exists, all beamline shutters are fixed to the UCN guides and are part of the vacuum safety system of the source.

Therefore a UCN storage experiment was developed with the following main goals:

- Indepence of the UCN source system.

- Fewer UCN losses.

- Shorter shutter actuation times.

- Mobility of the setup.

6.2   Fast UCN Shutters

Two butterfly-type shutters with 200 mm inner diameter were designed and built at PSI. All parts which can be in contact with UCN are made from stainless steel. The shutter blades were polished at PSI. They can be connected to DIN 11866 standard tubes of inner diameter 200 mm and outer diameter 204 mm. A photo of one of the shutters is shown in Fig. 6.1.

The mechanical feedthroughs can be differentially pumped through an additional tubing system terminated by a KF16 flange.

Using a pneumatic actuator made by Festo (Type DSNU-16-50-PPV-A), which delivers a force greater than 100 N along a stroke of 50 mm, opening and closing times of less than 300 ms and less than 100 ms respectively were measured using a high speed camera, see Fig. 6.2.

The shutters add an average length of 10.0(5) mm between the end surface of a connected tube and the shutter blade surface in the closed state.

Using a duration t of the movement of 100 ms and a radius r of the bottle of 100 mm, the maximum speed of the outer edge of the shutter blade during movement is

$$\frac{1}{4} \times \frac{2\pi r}{t} = \frac{157.1\,\text{mm}}{0.1\,\text{s}} \simeq 1.57\,\text{m s}^{-1}.$$

This is still slower than most of the confined UCN, and equivalent to a kinetic energy of 12.9 neV.
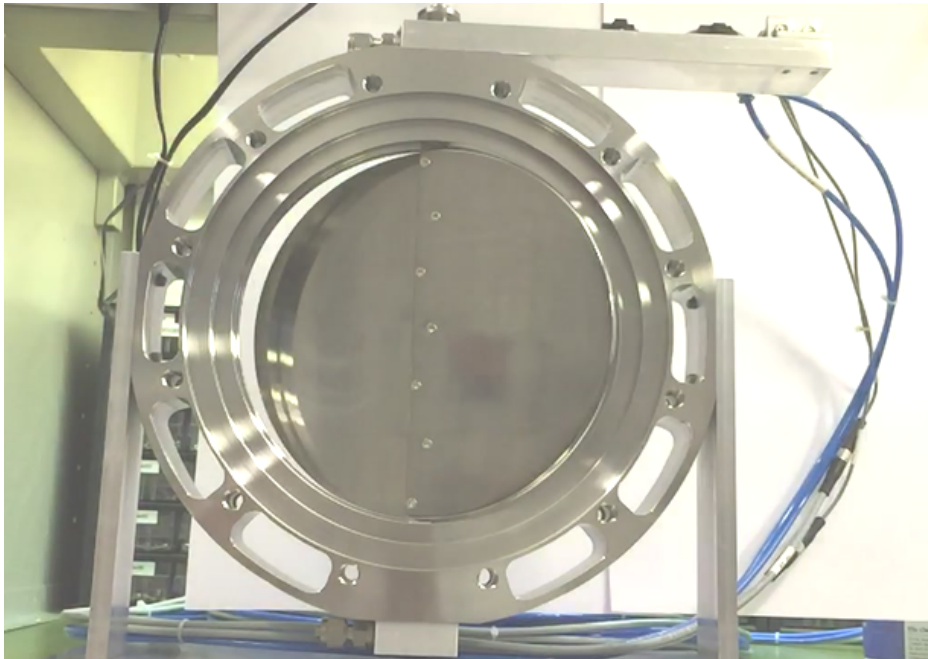
Figure 6.1: *Photograph of one of the shutters. Pressurised air and limit switch feedback lines are visible on the right hand side. Cutouts from the stainless steel body for weight reduction are well visible.*

6.3   The Storage Bottle

A 1000.0(5) mm long stainless steel tube, complying with DIN 11866 ("Rohre aus nichtrostendem Stahl für Aseptik, Chemie und Pharmazie"), made by Herrli AG in Kerzers, Switzerland, with a specified inner surface roughness of R_a < 0.8 µm, ID=200 mm, OD=204 mm, is sandwiched between two UCN shutters described above.

This results in a cylindrical UCN storage bottle of length 1020.0(11) mm, with an inner diameter of 200.0(5) mm, and therefore with a volume of 32 044(164) cm^3.

The shutters are being held in a support structure made from aluminium profiles to make the assembly easier to handle and to provide a solid flat pedestal. At the sides of both shutters which point outwards, 150(1) mm long pieces of stainless steel tube are attached, with KF16 vacuum flanges welded on in the center, in order to pump the experimental volume and to measure the pressure. One of the two KF16 flanges is connected to the inside through a hole with 2 mm diameter, the other one is using the full 16 mm. These two tubes also guarantee that the shutter blades, which protrude by about 50 mm from the shutter housing, can not be blocked by connecting flanges etc. All ID 200 mm stainless steel tube parts have been electropolished after a first test, as discussed below. Fig. 6.3 shows photographs of the assembled storage bottle. A technical drawing of the assembled storage bottle including the small Cascade detector is shown in Fig. 6.4.
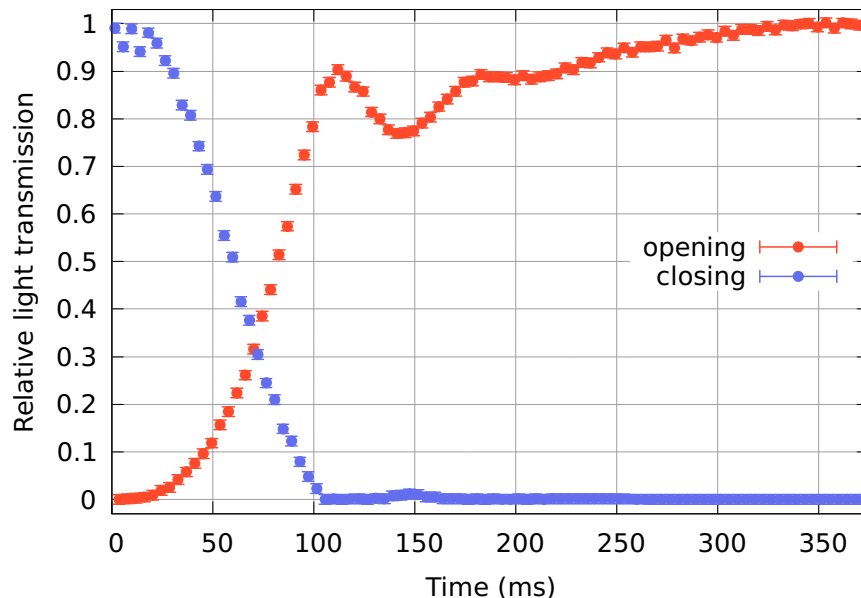
Figure 6.2: *Opening and closing behaviour of the UCN shutters measured by comparing the visible white area of the background behind the shutter with the area visible in fully opened position. Opening from zero to 90 % open takes about 110 ms. The break of the pneumatic cylinder causes a swinging motion towards the open position and the fully open position is then reached within 300 ms. Closing from fully open to 95 % closed takes less than 100 ms.*
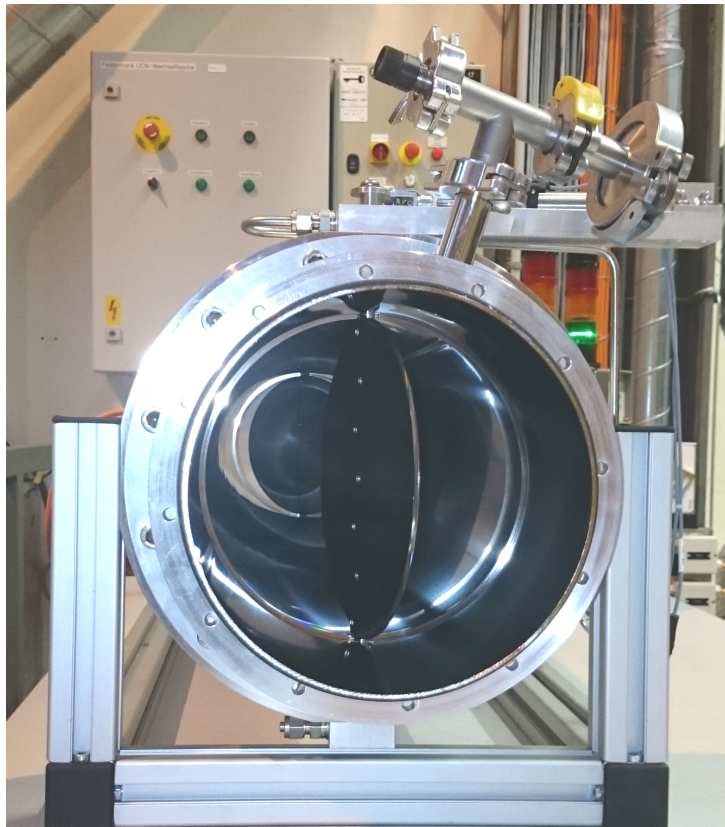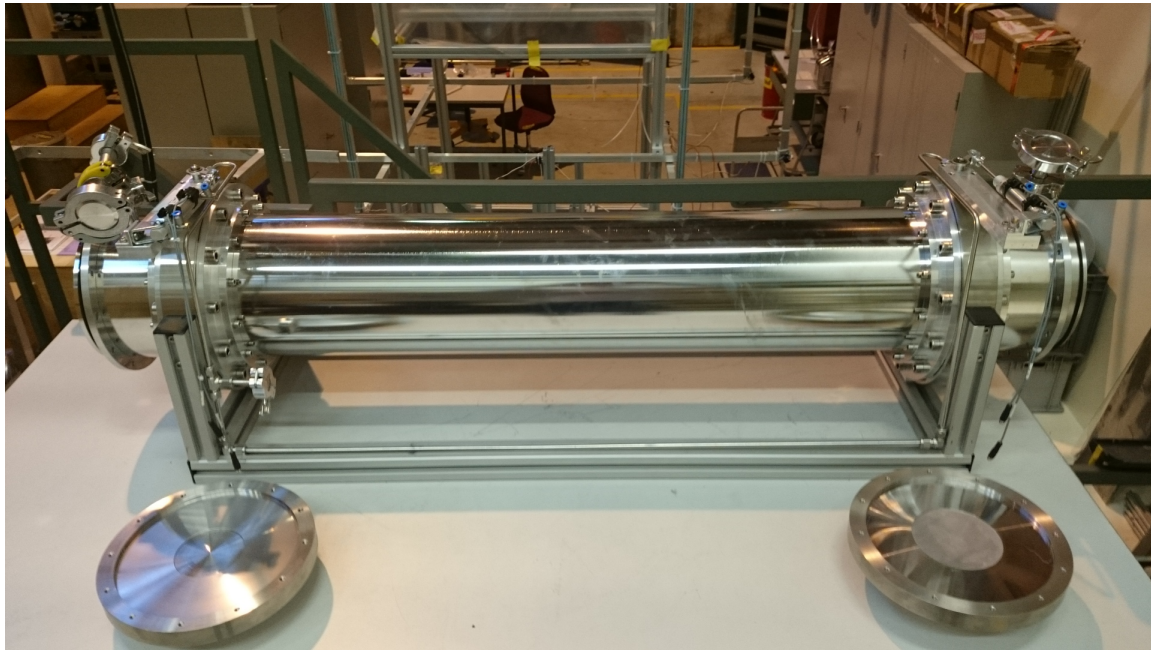
Figure 6.3: *The assembled stainless steel UCN storage bottle. Top: Side view with two NiMo coated aluminium adapter flanges for different guide diameters. Bottom: View into the storage bottle. The KF16 flange is visible at the top right, connected to a manual venting valve and a KF40 adapter.*

6.4   Timing Control for Storage Measurements

The opening and closing sequence for the two shutters needs to be configurable and well repro-
ducible in order to perform UCN storage measurements with a storage bottle.

To simplify the apparatus no timing system was built directly into the pneumatic valve system,
but instead 5V TTL signals are used to control the air flow which moves the shutter blades. The
shutters are open while 5 V are connected to their corresponding input. If there is no voltage
present, the shutters are closed.

An "Arduino Due" board is used for the timing logic. The board is based on a 32-bit microcon-
troller running at a clock speed of 84 MHz and can be programmed using the C programming
language and a hardware abstraction layer provided as open source software. This makes it very
simple to implement a deterministic real-time capable digital controller. Due to the high clock
speed, cycle times of 100 µs are easily accomplished.

Except for peripheral code and handling of serial communication used to configure and control
the software, the relevant C code which is evaluated every cycle is given in Listing 6.1 and uses
the following definitions:

- `storageMeasurement`: Boolean variable specifying if an automatic measurement is active
  (TRUE) or not (FALSE). If no automatic measurement is ongoing, the two shutters can be
  controlled manually.

- `triggered`: Boolean variable, set to TRUE on a rising edge on the digital trigger input,
  typically indicating the start of UCN production. Reset to FALSE when one storage mea-
  surement is done and the next measurement is ready to start.

- `bottleCounter`: unsigned long integer variable counting the cycles since the trigger signal
  was given.

- `fillingTimePreset`: unsigned long integer variable containing the desired filling time in
  multiples of the cycle time.
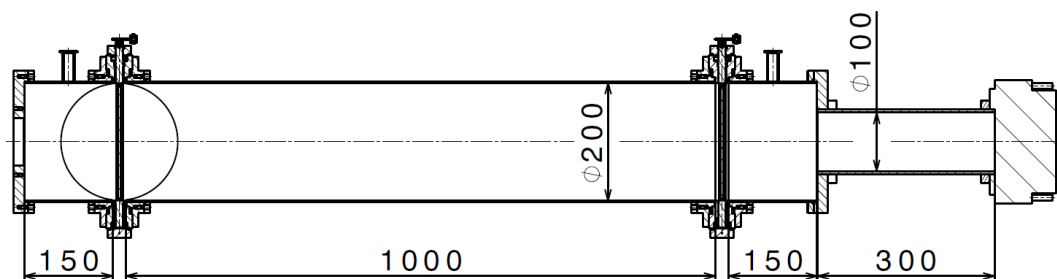
Figure 6.4: *Technical drawing of the assembled storage bottle. The leftmost flange, where the storage bottle
can be connected to a UCN source, has been produced multiple times with varying inner diameters to acco-
modate for UCN guide diameters used at various UCN sources. The KF16 vacuum flange tubes on the left
and right hand side are used to pump the storage bottle and measure the rest gas pressure.*

- `storageTimePreset`: as `fillingTimePreset` but for the storage time, i.e. the time when both shutters are closed.

- `countingTimePreset`: as `fillingTimePreset` but for the counting time before the system accepts triggers again.

- `Pin1State`, `Pin2State`: Boolean variable containing the state of the two shutters.

- `digitalWrite(pin, state)`: function to change the output pin numbered `<pin>` to the state HIGH or LOW, corresponding to 3.3 V or 0 V.

- `PinExtern1`, `PinExtern2)`: unsigned integer variable containing the number of the output pin connected to shutter one or two, respectively.

Summary of the program flow:

1. A counter is being increased every 100 µs as soon as a rising flank on the trigger input was detected.

2. In the first cycle after the trigger, the shutters are set to the filling position.

3. When the counter reaches the predefined filling time, the shutters are set to the storage position.

4. When the counter reaches the sum of the predefined filling and storage times, the shutters are set to the emptying position.

5. When the counter reaches the sum of the predefined filling, storage, and counting times, the shutters are set to the waiting (vacuum pumping) position, the counter is reset to zero and the trigger flag is set to false, waiting to be triggered again.

Commands which can be sent through a serial connection are:

- `manual`: Manual mode.

- `auto`: Automatic (measurement) mode.

- `o1`, `c1`, `o2`, `c2`: (Only effective in manual mode) Open/close shuter 1/2.

- `ft=<time>`, `st=<time>`, `ct=<time>`: Set filling-, storage- or counting time in milliseconds.

- `go`: Manual trigger override.

- `stop`: Immediate stop of an ongoing triggered measurement.

- `reset`: Reset of the system to trigger-ready state.

```
if(storageMeasurement)
{
  if(triggered)
  {
    bottleCounter++;
  }
  if(bottleCounter==1)
  {
    digitalWrite(PinExtern1, HIGH);
    Pin1State=0;
    digitalWrite(PinExtern2, LOW);
    Pin2State=1;
  }
  if(bottleCounter==fillingTimePreset)
  {
    digitalWrite(PinExtern1, LOW);
    Pin1State=1;
    digitalWrite(PinExtern2, LOW);
    Pin2State=1;
  }
  else if(bottleCounter==(fillingTimePreset+
                          storageTimePreset))
  {
    digitalWrite(PinExtern1, LOW);
    Pin1State=1;
    digitalWrite(PinExtern2, HIGH);
    Pin2State=0;
  }
  else if(bottleCounter==(
                          fillingTimePreset+
                          storageTimePreset+
                          countingTimePreset))
  {
    digitalWrite(PinExtern1, HIGH);
    Pin1State=0;
    digitalWrite(PinExtern2, HIGH);
    Pin2State=0;
    triggered=false;
    bottleCounter=0;
  }
}
```

Listing 6.1: *Main part of the control logic for UCN storage experiments, implemented on an Arduino Due board, repeated every cycle, fixed cycle duration* $100\,\mu s$

All timing parameters are set through a serial connection from a PC. Direct operation of the two shutters is also possible.

A custom-made 10 channel isolated TTL driver card is used to convert the 3.3 V output of the microcontroller board to 5 V and galvanically decouple it.

The decoupled 5 V outputs then drive the TTL inputs of the two UCN shutters.

6.5   First Characterisation Measurements

The storage bottle was produced, cleaned in a large ultrasonic bath at PSI and assembled for a first set of test measurements at the West-1 beamport in November 2014. The measurements were conducted on November 17 - 20, 2014. The *big* cascade detector (see Sec. 2.4) was used in this measurement.

6.5.1   UCN transmission

The UCN transmission of the storage bottle, shutters, and connecting tubes (for pumping) was measured. At this time, both the main part of the bottle and the two connecting tubes were not yet electropolished and optically matte.

Fig. 6.5 shows a sketch of the setup.

The transmission is calculated as

$$T = \frac{N_{\text{UCN,b}}}{N_{\text{UCN,o}}}$$

where $N_{\text{UCN,b}}$ is the total number of UCN counts in the detector *with* the bottle connected, and $N_{\text{UCN,o}}$ the total number of counts in the detector *without* the bottle connected, i.e. with the detector connected directly to the beam port.

Errors are derived from the standard deviation of the mean value of three to four proton beam kicks.
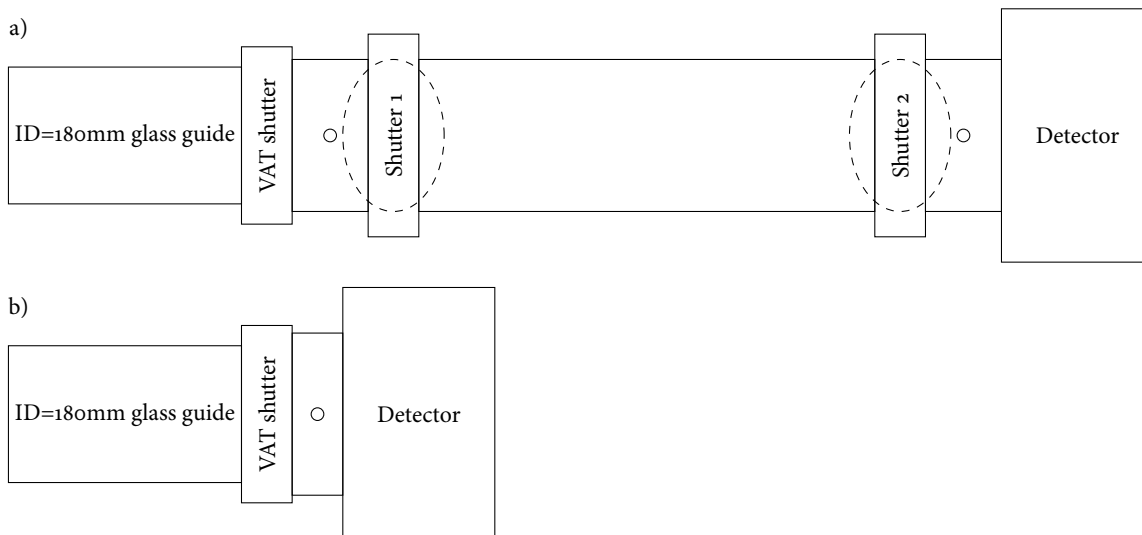
Figure 6.5: *a) Setup: Storage bottle connected to the "Strahlwegventil" VAT shutter at beam port West-1, b) Setup: Detector connected directly to the beam port*

Unfortunately, the Cascade detector showed some anomaly during the time of the measurement, maybe related to the HV supply, such that the measured values are inconclusive.

Right after mounting the setup to the beamline, the transmission in 3 s long proton beam kicks was measured to be 35.05(15) %, whereas when changing back to the setup without bottle, the measured UCN counts corresponded to a UCN transmission of 53.10(27) % initially, falling to 42.62(7) % during the next ~ 17 h.

For "Normkicks", the transmission was measured only once, just after mounting the storage bottle. The result was 23.73(5) %.

Even assuming the highest measured value, the transmission was worse than expected, which led to the decision to electropolish all stainless steel tubes.

6.5.2 Shutter leakage

The two buttefly type shutters are not completely tight with respect to UCN. Fig. 6.6 shows the leakage rate of the two shutters over time. Comparing the UCN rate in the detector measured with both shutters open to the UCN rate with one shutter closed, one finds a leakage between 1 % and 2 % for both shutters.

Fitting single exponential decays to the three count rates, one obtains emptying times of the UCN source of 36.0 s for both shutters open and emptying times of 40.0(3) s and 40.8(3) s for shutter 1 or shutter 2 closed, respectively. This change in emptying time leads to an apparent slow rise of the leakage rate over time.

6.5.3 UCN storage

Although the UCN transmission was not as high as anticipated, a UCN storage and UCN density measurement was done in order to commission the storage bottle. The measured UCN counts had to be corrected for additional UCN which leaked through the closed first shutter. The UCN counts in the detector were integrated starting from the time when the second shutter was opened until about 260 s after the proton beam kick. Then, the counts measured in the same time interval in a measurement where the first shutter stayed closed are subtracted.

The measurements were done using 3 s long proton beam kicks.

Fig. 6.7 shows the storage curve of the bottle. A single exponential fit to the data yields a storage time constant of 26.6 s.

6.5.4 UCN density

Taking the measured amount of UCN in the bottle after a storage time of 2 s and dividing by the volume of the bottle, which is $32\,044(164)$ cm^3, a UCN density of 4.78(3) UCN/cm^3 was measured.

For comparison: In the 2.5×10^4 cm^3 glass storage bottle, using two VAT vacuum shutters, a density of ~ 21 UCN/cm^3 was measured in July 2013. This measurement however was performed

using 6 s long proton beam kicks during a period in which a "Normkick" yielded more than 3×10^6 UCN, while the measurements with the new bottle were performed with a "Normkick" yield of about 1.8×10^6 UCN.

Taking these two factors into account linearly, a density of about 7 UCN/cm^3 should be expected. Furthermore, as the wall potential of stainless steel is lower than the wall potential of glass coated with NiMo, only a lower density can be expected.

6.6 Commissioning Measurements with Electropolished Storage Bottle using the Big Cascade Detector

All stainless steel tubes of the storage bottle were electropolished on the inside at an external company to optimise UCN transmission. Afterwards, all surfaces were optically reflective, in contrast to being matte before. The *big* cascade detector (see Sec. 2.4) was used in this measurement. The measurements with both detectors were taken on December 13 - 14, 2014.
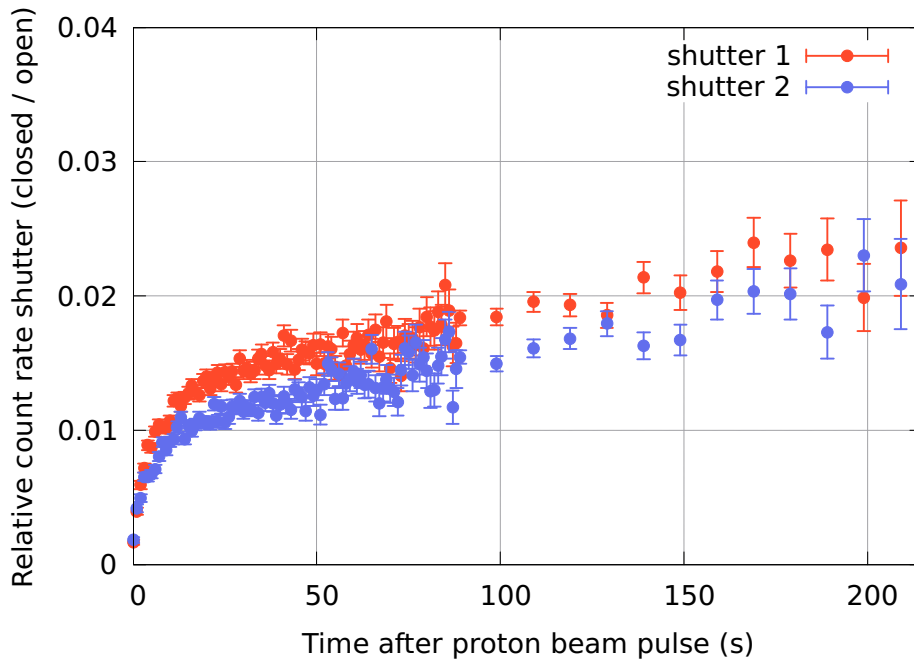
Figure 6.6: *Leakage rate of the two shutters. Bin-wise ratio between UCN counts with opened and closed shutters. Bins of size 1 s during the first 90 s, bins of size 10 s later. The leakage rate rises quickly from 0 to between 1.0 and 1.5 % after the beginning of UCN production, because the rise time of the UCN rate with open shutters is much faster than the one with one shutter closed. Afterwards the leakage rate increases to between 2.0 and 2.5 %, which is likely caused by the shorter emptying time of the source with shutters opened.*

6.6.1   UCN transmission

The setup for transmission and storage measurements was the same as in the first campaign, sketched in Fig. 6.5. Both before and after the bottle was mounted, the big Cascade detector had been running in nEDM monitoring mode for at least one night, such that the count rate should have enough time to stabilise after ramping up the high voltage. Before the bottle was mounted, the proton beam current was 2180 µA, afterwards it was slightly lower at 2170 µA. This is being corrected for in the transmission result. The kick length in this measurement campaign was always 3.2 s with a repetition rate of 340 s. The UCN counts were integrated from bin 200 to bin 2500, which means that only UCN reaching the detector between 10 s after the proton beam kick and 240 s after the kick were taken into account.

Before mounting the bottle to the beam port, out of about 1×10^7 UCN in the total time range, about 7.00×10^6 UCN were recorded in the cut window. After mounting the bottle, out of about 8×10^6 UCN in the total time range, about 5.70×10^6 UCN were recorded in the cut window. This results in a transmission (after correction for the beam current difference) of 81.72(3) % (statistical error only).

6.6.2   Leakage

The leakage rates of the first measurement campaign given in Sec. 6.5 were confirmed.
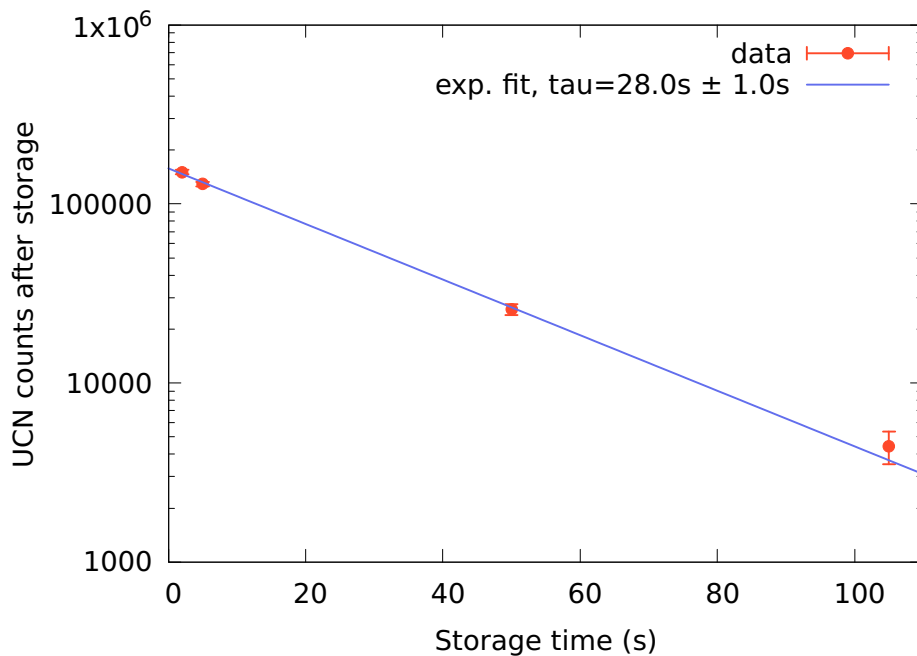
Figure 6.7: *Storage curve (UCN counts per measurement, after storage) measured with the storage bottle, not yet electropolished, at the West-1 beam port during commissioning of the setup in November 2014.*

6.6.3   UCN storage

After optimising the filling time of the bottle to 15 s after beginning of the proton beam kick, which is equal to a set time of 16 s with respect to the WK TTL signal, a background measurement with shutter 1 closed and 4 measurements with storage times of 2, 5, 25, and 105 seconds were performed.

Fig. 6.8 shows an overlay of the measured time spectra in the detector. The background curve well resembles the shape and intensity of the counts in the respective storage measurements long after the shutter 2 was opened. This is confirmed by the residuals after subtracting the background from the data, as shown in Fig. 6.9.

Fig. 6.10 shows the fitted storage curve. Depending on the model, a (long) storage time constant of 25.7 s (single exponential fit) or 39.8 s (double exponential fit) can be extracted. Statistical errors on the individual points are well below 1 % and are therefore smaller than the symbols in the figure.

6.6.4   UCN density

After 2 s of storage, 234 551(484) UCN were counted in the detector.

Using a bottle volume of 32 044(164) cm^3, a UCN density of 7.32(4) UCN/cm^3 can be deduced. For reference: This is measured with a D_2 crystal which yields about 2×10^6 UCN per Normkick, and only 3.2 s long proton beam kicks were used for filling the storage bottle.
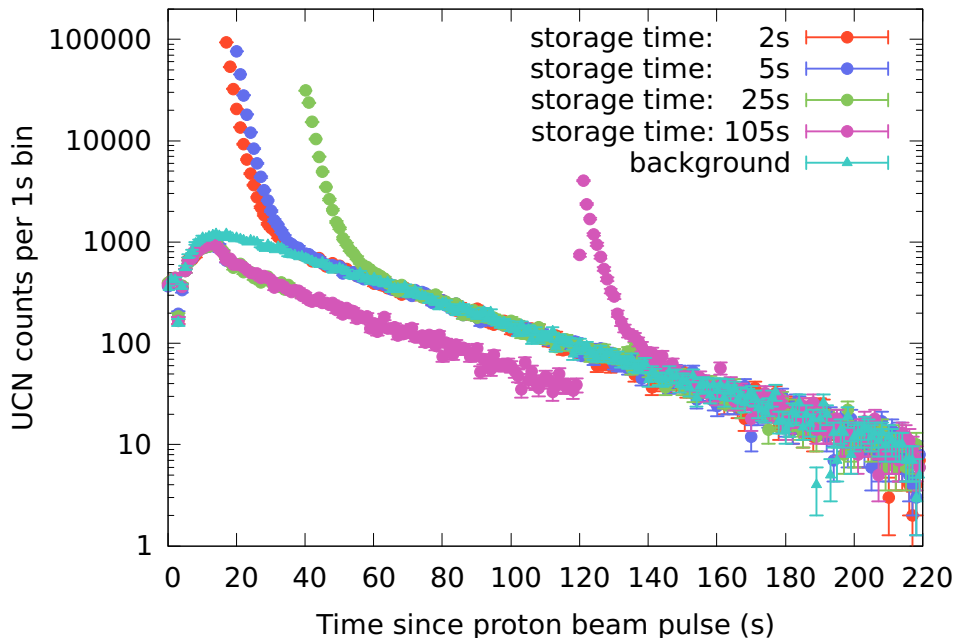
Figure 6.8: *Time spectra of the UCN counts for different storage times using the big Cascade detector. The background curve is the lowest one without the emptying peak, indicated by triangles.*

6.7 Commissioning Measurements with Electropolished Storage Bottle using the Small Cascade Detector

The measurements were subsequently repeated with a *small* Cascade detector (see Sec. 2.4) which was connected to the bottle using a straight 300 mm long piece of acrylic tube, coated with NiMo. As these measurements were taken only two hours after the measurements with the big Cascade detector, the UCN source performance can be considered constant.

6.7.1 UCN storage

Measurements with identical filling and storage times as previously with the *big* Cascade detector were performed and the measured data treated in the same way. The behaviour was found to be identical to the situation with the *big* Cascade detector.

The fitted storage time constants of 26.4 s(single exponential fit) or 39.7 s (double exponential fit) are compatible with the previous ones. The resulting time spectra (Fig. 6.11), residuals (Fig. 6.12), and storage curve (Fig. 6.13) are shown below. Again, statistical errors were small and errorbars are therefore smaller than the symbols in the figure.
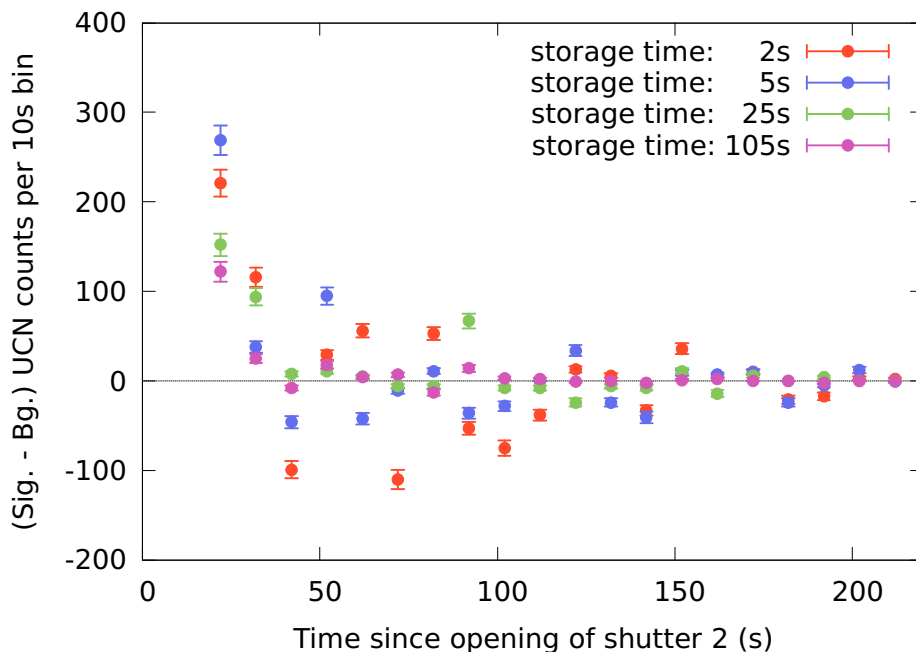
Figure 6.9: *Time spectra residuals of the storage measurement shown in Fig. 6.8 using the big Cascade detector.*

6.7.2   UCN density

After 2 s of storage, 183 349(428) UCN were counted in the detector.

Using a bottle volume of 32 044(164) cm^3, a UCN density of 5.72(3) UCN/cm^3 can be deduced.

The difference of a factor of 0.78 in comparison to the density measured with the big detector in Sec. 6.6.4 can be explained by the different sized detection area and hence a longer "emptying time" of the storage bottle when the small detector is used. Fitting the emptying peaks of the 2 s storage time measurements in both configurations with the sum of two decaying exponentials yields empting time constants of $\tau_1 = 1.4(1)$ s, $\tau_2 = 3.1(1)$ s for the big detector and $\tau_1 = 4.6(9)$ s, $\tau_2 = 9(8)$ s for the small detector respectively. Fig. 6.14 shows both fitted emptying curves for the first 20 s after the opening of shutter 2.
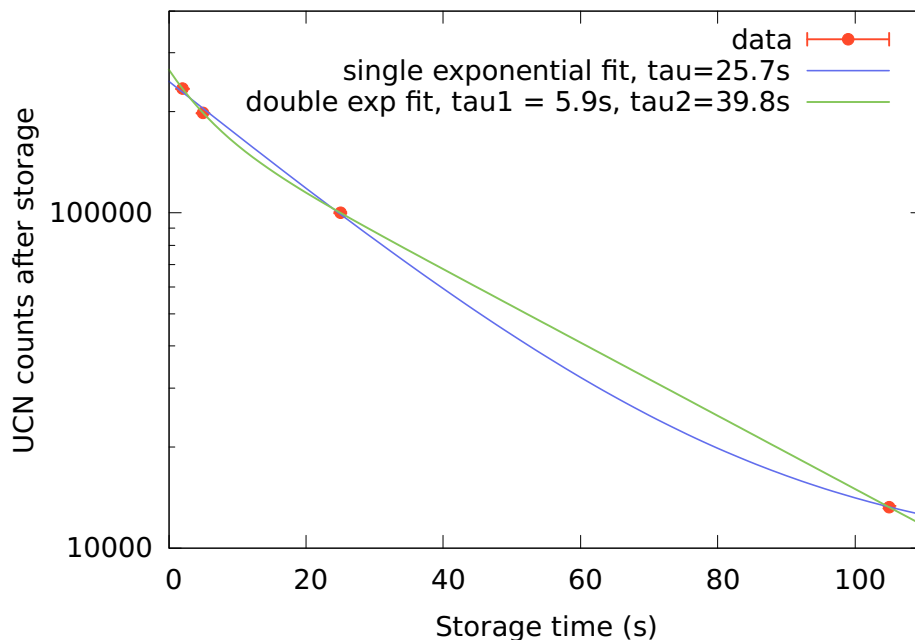
Figure 6.10: *Measured UCN counts after a given storage time (circles) and curves displaying a fit with either a single or double exponential function (using the big Cascade detector).*
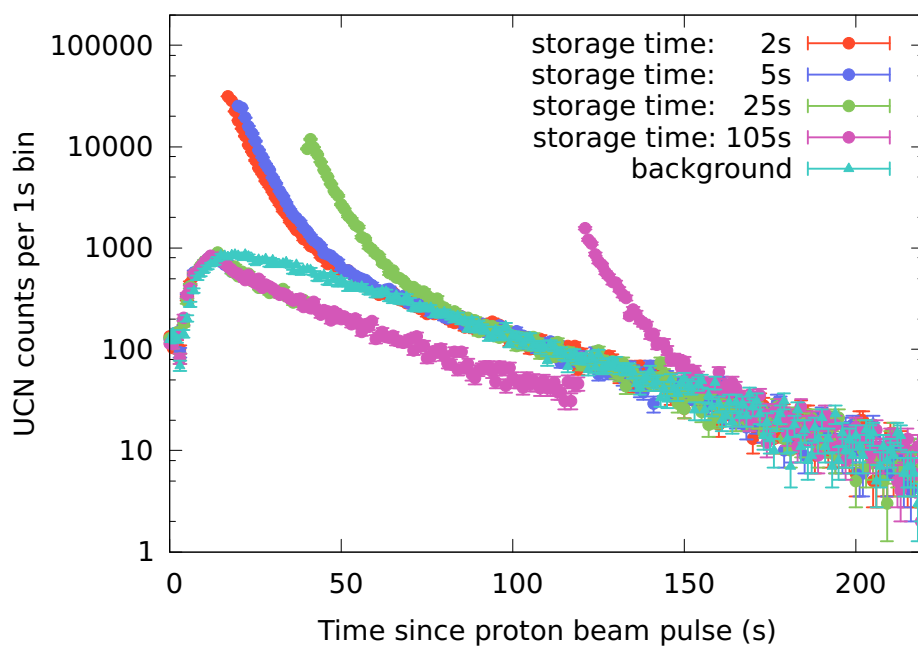
Figure 6.11: *Time spectra of the UCN counts for different storage times using the small Cascade detector. The background curve is the lowest one without the emptying peak, indicated by triangles. Time zero is at the beginning of the proton beam kick.*
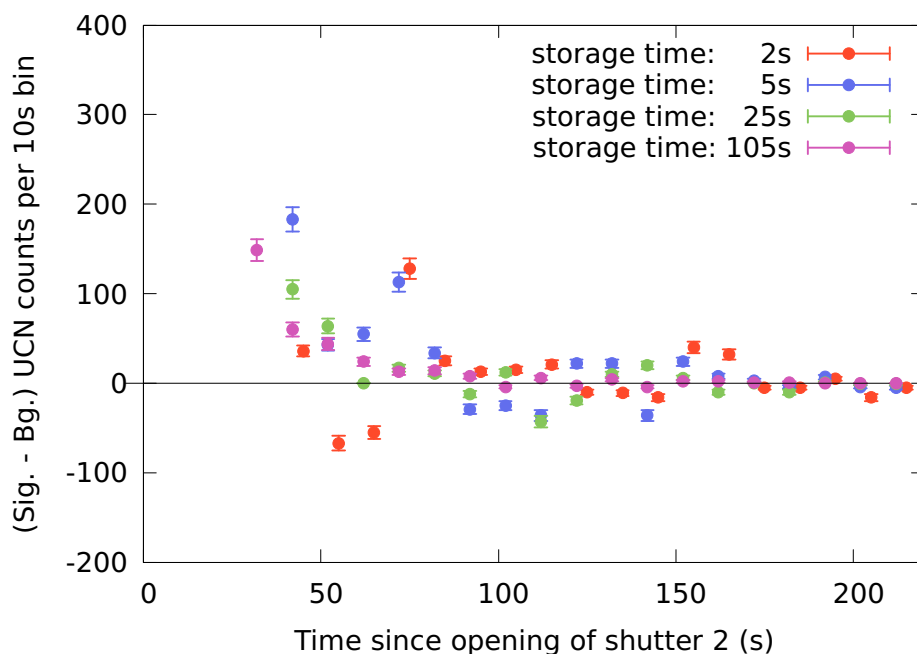
Figure 6.12: *Time spectra residuals of the storage measurement shown in Fig. 6.11 using the small Cascade detector.*
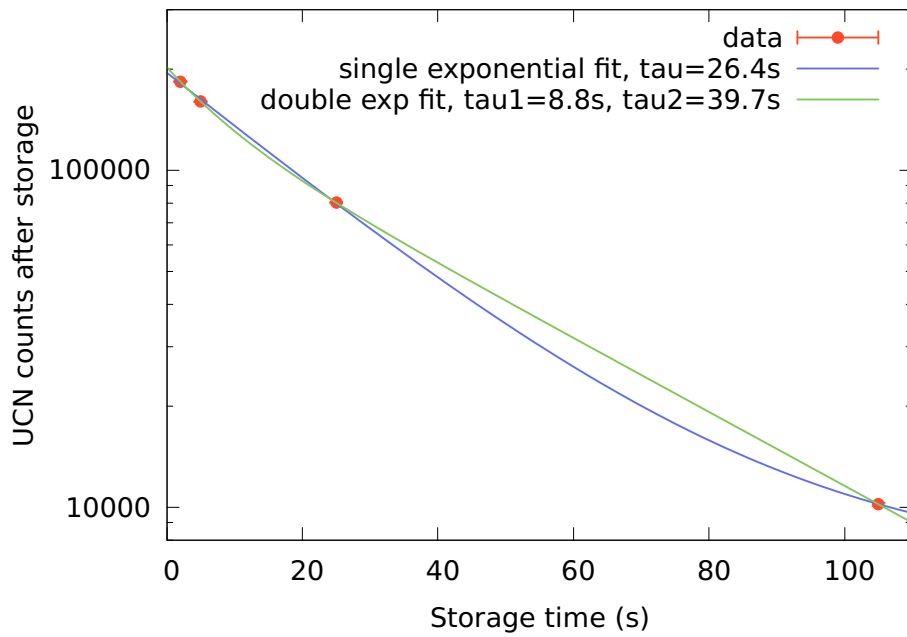
Figure 6.13: *Measured UCN counts after a given storage time (circles) and curves displaying a fit with either a single or double exponential function (using the small Cascade detector).*
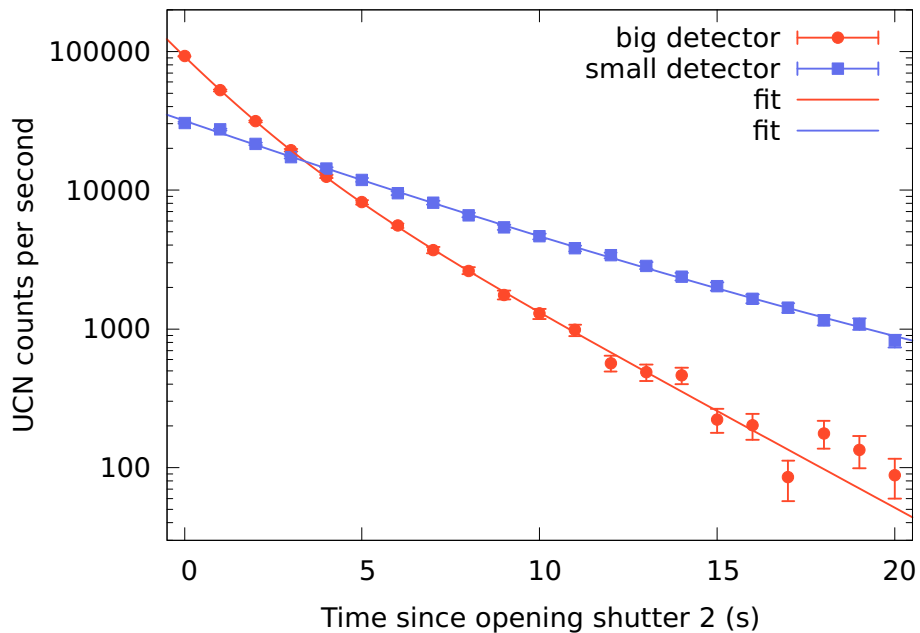
Figure 6.14: *Fitted emptying curves after 2 s storage, measured with the big (red circles) and the small Cascade detector (blue squares) both in horizontal position as shown in Figs. 6.4 and 6.5. Double exponential fits to the data are shown as well. At t = 0 s, the second shutter of the storage bottle opens after storage. It is clearly visible that the emptying time is much shorter with the big detector than compared with the small detector.*

Chapter 7

World-wide Comparison of UCN Densities at Operating UCN Sources

7.1 Motivation

Flagship UCN experiments, like searches for an electric dipole moment of the neutron [Pendlebury et al., 2015, Serebrov et al., 2015, Ito, 2007, Baker et al., 2011], discrete gravitational quantum states of neutrons [Nesvizhevsky et al., 2002, Jenke et al., 2011, Baessler et al., 2011] or asymmetries in the neutron beta decay [Mendenhall et al., 2013, Broussard et al., 2013] , or precision determinations of the free neutron lifetime [Serebrov et al., 2005, Ezhov et al., 2014, Salvat et al., 2014], typically have their experimental geometries defined by the specific requirements of the respective measurements.

They are also limited significantly by counting statistics.

This makes the *UCN density* available to fill an experiment's vessel at a UCN source one of the most important parameters of the source. The UCN density is the parameter quoted for every UCN source, and densities are being projected for future sources. Unfortunately, the determination of the UCN density at a UCN source is strongly dependent on various factors, such as:

- The type of measurement

    - Storage experiment in a storage setup outside of the source

    - Flux measurement and subsequent calculation of the density

- The position of the measurement

    - Inside the source's UCN production volume

    - Outside, available to experiments

- Material and apparatus

    - Fermi potentials of surfaces in contact with UCN

– Size of the storage bottle

- Detector used in the measurement

  – ^{3}He proportional counters

  – ^{10}B based counters, e.g. commercially available "Cascade" UCN detectors based on GEM technology[1]

  – ^{6}Li doped scintillation counters [Ban et al., 2016, Göltl et al., 2013].

  – Activation measurements

- Treatment of data

  – Extrapolation of data to storage time zero

  – Correction for detector efficiency

  – Extrapolation of initial neutron flux

  – Correction of UCN transmission

This leads to the fact that at the start of this work, no quantitative comparison of the available UCN densities at the UCN sources in operation is possible.

In order to change this unsatisfactory situation, a world-wide collaboration of all groups operating UCN sources was formed. A simple, robust, and mobile UCN storage experiment was constructed and used to measure UCN densities at all operating UCN sources world wide. The experimental setup, including the UCN detector, was identical for all measurements and the resulting data was analysed in one consistent way.

This eliminates all of the limiting factors listed above, and allows for a quantitative comparison of UCN densities for a given reasonably large UCN storage experiment. It does not, however, provide an optimised measurement for the maximally reachable UCN density at any UCN source.

7.2   Experimental Setup

The stainless-steel storage bottle described in detail in Sec. 6 was used in two variants for measurements at each source and location.[2] While the beamline towards the storage bottle, the bottle itself and the UCN detector stayed exactly the same, the guide used between the bottle and the detector was either a straight, 300 mm long acrylic tube coated with NiMo or an L-shaped acrylic tube with a short arm of 410 mm and a long arm of 1110 mm length. By connecting the detector to the long arm and pointing it downwards, UCN in the guide are being accelerated by gravity and gain about 110 neV of kinetic energy. This increased energy allows the UCN to pass through the detector's entrance window, which is made of an aluminium foil of 100 μm thickness and has a calculated reflective wall potential of 54 neV.

---

[1]http://n-cdt.com/products/cascade-detector-systems/cascade-u-systems/

[2]At the LANL UCN source, only the horizontal extraction guide was used.

Comparing measurements done with the two different extraction guides towards the detector allows for a rough discrimination between the population of UCN stored in the storage bottle with kinetic energies below and above 54 neV.

In order to keep the possibilities for systematic errors in the comparison to a minimum, almost all peripheral hard- and software was identical in all measurements. This includes the UCN detector and all of it's periphery, i.e. readout electronics, trigger electronics, cables, high voltage power supply, data acquisition computer and software. Except for the measurement at the Los Alamos source, the vacuum pumps and pressure gauges used were shipped along with the experiment setup. After vacuum pumping with an external turbomolecular pump (TMP) through a KF40 vacuum bellow resulted in long pump-down times at LANL, the diameter of one of the holes inside the KF16 pump flanges was increased from 2 mm to 16 mm and a TMP was mounted immediately on top of the flange, protected by a manual vacuum shutter.

After arrival and before the measurements at each source started, the storage bottle was checked for slits between individual components, which could have opened up during transport. If such slits were observed, affected parts were reconnected with minimal slits. During these inspections, the surfaces of the experiment were checked for dust or other contaminations and cleaned if necessary, although this was rarely necessary as the setup was transported in a closed state.

Cascade detectors need a gas mixture of Ar and CO_2 with a volume ratio of 70-90 % Ar to 30-10 % CO_2. The detector gas flow through the detector was established at least 24 h before the first measurements at all sources. The gas flow was manually adjusted and checked in the same fashion. At all UCN sources, gas from the local supplier was used. The specified volume ratios were similar but not identical:

- LANL: 81.2 % Ar to 18.8 % CO_2.

- ILL: "AIR LIQUIDE argon-CO_2 90/10", 90 % Ar to 10 % CO_2.

- TRIGA: "Westfalen Gase Gasgemisch", 80 % Ar to 20 % CO_2.

- PSI: "Messer Ferroline C18", 82 % Ar to 18 % CO_2.

During all measurements, the high voltage used for the detector was set to 1350 V. The voltage was ramped directly to the target voltage without additional conditioning at higher voltages. The settings of the Cascade detectors were identical in every measurement. The reference voltages `Vref0` and `Vref1` were both set to a value of 110 a u throughout all measurements.

7.3 Standard Measurement Sequence

A single storage measurement consists of the following segments:

- Start: An electonic trigger signal, approximately coincident with the start of UCN delivery, starts the timing sequence in the storage experiment electronics.

- Filling: The source-side storage bottle shutter (shutter 1) is in the open position to let UCN coming from the source into the bottle. The detector-side storage bottle shutter (shutter 2) stays in the closed position. This state lasts for the configurable *filling time*, which is defined in the experiment electronics via the command

  ```
  ft=nnnn
  ```

  where "nnnn" is the desired time in milliseconds.

- Storage: When the filling time is over, shutter 1 gets closed, and both shutters stay closed for the configurable *storage time*, which can be set in the electronics via

  ```
  st=mmmm
  ```

  ("mmmm" being the storage time to be used in milliseconds) analogue to the filling time.

- Counting: The third and last configurable time period is the so-called *counting time*, set by

  ```
  ct=kkkk
  ```

  where again "kkkk" is the counting time in milliseconds. During this period, shutter 1 stays closed, while shutter 2 is opened in order to empty the stored UCN into the detector.

- Trigger Ready: After the counting time is over, the electronics are reset to the initial state and then wait for the next trigger signal.

The standard measurement sequence was the following for each extraction variant of the storage setup:

1. Optimise the filling time for the given source and measurement position using a storage time of 5 s. This was done by performing multiple storage measurements where the filling time was varied, but the storage and counting times stayed constant. The optimal filling time was the shortest time with the highest output of UCN after 5 s of storage.

2. Measure the amount of stored UCN in the bottle after storage times of 2, 5, 10, 20, 50 and 100 s using the optimal filling time. The order in which the storage times were measured was typically randomised in order to prevent possible linear drifts from resulting in a systematic effect.

3. Measure background and leakage rates if possible. This part was different for any given UCN source, as the time structure of UCN delivery as well as the possibilities to close off the source varied widely.

7.4 Standard Analysis Steps

The analysis of the measured UCN storage data has two objectives.

- Maximum UCN density: The main objective of this measurement campaign was the *maximum UCN density* achievable under similar conditions at any UCN source. The number of measured UCN after a storage time of 2 s (after a suitable subtraction of leaked UCN) divided by the volume of the storage bottle is considered to be the maximum UCN density. No extrapolations or scalings for inefficiencies in the measurement process were applied. Leakage of UCN from the source into the storage bottle during the storage- and counting time had to be subtracted from the raw counted values because the shutters are not perfectly UCN tight. True background in the detector was measured at all sources and was found to be below 1 Hz and therefore negligible. At all reactor based UCN sources, cadmium shielding around the detector was used.

- Storage time constant: Another observable of interest is the UCN lifetime inside the storage bottle, expressed via the *storage time constant*. This is primarily depending on the surface materials and quality and on the construction of the storage bottle, namely slits and cavities between individual pieces. It is also dependent on the kinetic energies of the stored UCN.

  As the storage bottle was exactly the same for all measurements, only the dependence on kinetic energies of the UCN leads to variations in the lifetime of UCN in the bottle. It can give a qualitative estimate of the average kinetic energies of UCN delivered by the respective source. The lower the average energy, the larger the storage time constant.

  In order to estimate the storage time constant, the leakage of UCN through the detector side shutter needed to be investigated, too. During any storage measurement, UCN leak from the closed storage bottle into the detector. The rate of leakage is proportional to the amount of UCN inside the bottle itself. By measuring the time dependence of this leakage rate for long storage times, the time dependence of the UCN density inside the bottle and therefore the storage time constant can be found. The rate of UCN leakage is fitted to a model function

$$N(t) \propto R(t) = A_1 \times e^{-t/\tau_1} + A_2 \times e^{-t/\tau_2} \tag{7.1}$$

  where $N(t)$ is the total amount of UCN inside the storage bottle, $R(t)$ the rate of leaked UCN as measured in the detector, A_1 and A_2 population constants and τ_1 and τ_2 exponential decay time constants. The parameters A_1, A_2, τ_1, and τ_2 are determined by the fit. A_1 and τ_1 are considered to correspond to the population and lifetime of UCN with kinetic energies too high to be stored properly in the stainless steel bottle. τ_1 is typically below 10 s. A_2 and τ_2 correspond to storable UCN, therefore τ_2 is for this analysis treated as the storage time constant to be compared between UCN sources.

It is worth noting that the scope of this measurement campaign is a comparison of UCN sources, and neither a precision measurement of the maximally reachable UCN density in an optimised storage volume for each given source nor a precision determination of the UCN lifetime in general or in the used storage bottle.

7.5   Measurement at Los Alamos National Laboratory, Feb. 4 + 5, 2015

The storage bottle setup was shipped to Los Alamos National Laboratory (LANL) in January 2015.

7.5.1   The UCN source at LANL

The LANL UCN source is described in detail in [Saunders et al., 2013].

The UCN source at LANL uses neutrons created by spallation when the 800 MeV proton beam of the Los Alamos Neutron Science Center (LANSCE) accelerator hits a helium vapour cooled tungsten target.

The neutrons are then moderated to become cold neutrons in a 1 mm thick layer of polyethylene beads, which are cooled to a temperature of ~ 150 K. This layer of polyethylene is located above the spallation target.

Encased in the polyethylene is a helium cooled container filled with solid deuterium at a temperature below 10 K, where the neutrons can lose almost all their kinetic energy in an inelastic single-phonon scattering process.

The top side of the deuterium container is open, while all other walls are coated with ^{58}Ni. As such, the now ultracold neutrons can only exit upwards. When passing from the solid deuterium into vacuum, they get a boost in kinetic energy of 105 neV [Altarev et al., 2008] due to the material potential of the solid deuterium.

Protons are typically delivered to the target in short bursts every 5 s. Right above the solid deuterium surface a fast acting butterfly valve coated with ^{58}Ni is used to allow UCN to travel upwards when the beam is on target (valve opened). It prevents UCN from falling down from the guide system towards the solid deuterium while the beam is not on target (valve closed).

The target and deuterium container are surrounded by a beryllium neutron reflector in order to optimise the neutron flux inside the deuterium.

In order to compensate for the boost in kinetic energy by the deuterium surface, the UCN guide system towards experiments is situated 1 m above the surface of the solid deuterium.

About 6 m of stainless-steel UCN guides with an outer diameter of 101.6 mm are used to transport the produced UCN through the biological shielding and through a gate valve to the experiments. The experiment side of the gate valve in closed state is coated with polymethylpentene in order to quickly absorb UCN between the gate valve and a given experiments entry port after closing the gate valve.

7.5.2 Setup of the storage bottle

The storage bottle was attached to the LANL UCN source on Feb 4. It was positioned at the main beam port behind the superconduction pre-polarising magnet. A copper guide, approximately 500 mm long, with a 30° bend of bending radius 500 mm, was used to guide the UCN guides to the left. The guide's outer diameter was 76.2 mm, with a wall thickness of 1.5 mm. After the bent copper guide, an additional 200 mm long stainless-steel UCN guide with a 25.4 mm wide vacuum pump connection was installed, which was then connected to the front flange of the storage bottle.

The vacuum in the bottle was measured to be below a pressure of 2×10^{-4} mbar during the whole measurement.

A sketch of the setup can be seen in Fig. 7.1, details of the setup are also shown in the photographs of Figs. 7.2, 7.3, 7.4.

7.5.3 Operating conditions during the measurements

During the density measurements, the proton accelerator delivered proton pulses to the spallation target of the UCN source every 10 s.

7.5.4 Determination of the optimal filling time

The filling time was optimised as described in Sec. 7.3.

An examplary time spectrum of UCN arriving in the detector in a single measurement can be seen in Fig. 7.5. The stored number of UCN versus filling time is shown in Fig. 7.6. It stays constant at times greater than 40 s, therefore this was chosen as the optimal filling time for the density and storage curve measurement.

The leakage rate through the first shutter of the storage bottle saturates at about 130 Hz towards the end of the filling time, as can be seen in Fig. 7.5 between 40 and 50 s.
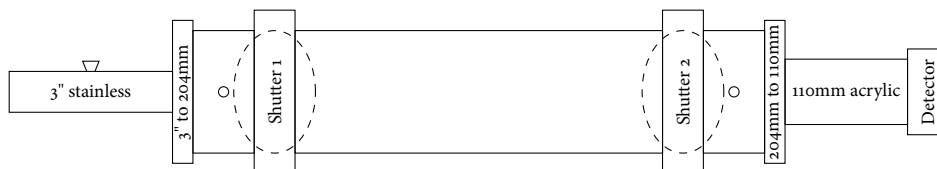
Figure 7.1: *Setup: Storage bottle connected to the beamline at LANL. Given diameters are outer diameters. The wall thickness of the 3" guide piece is 1.65 mm which results in an inner diameter of 72.9 mm. The inner diameters of the storage bottle and connecting tubes is 200 mm, the inner diameter of the acrylic guide to the detector is 100 mm.*
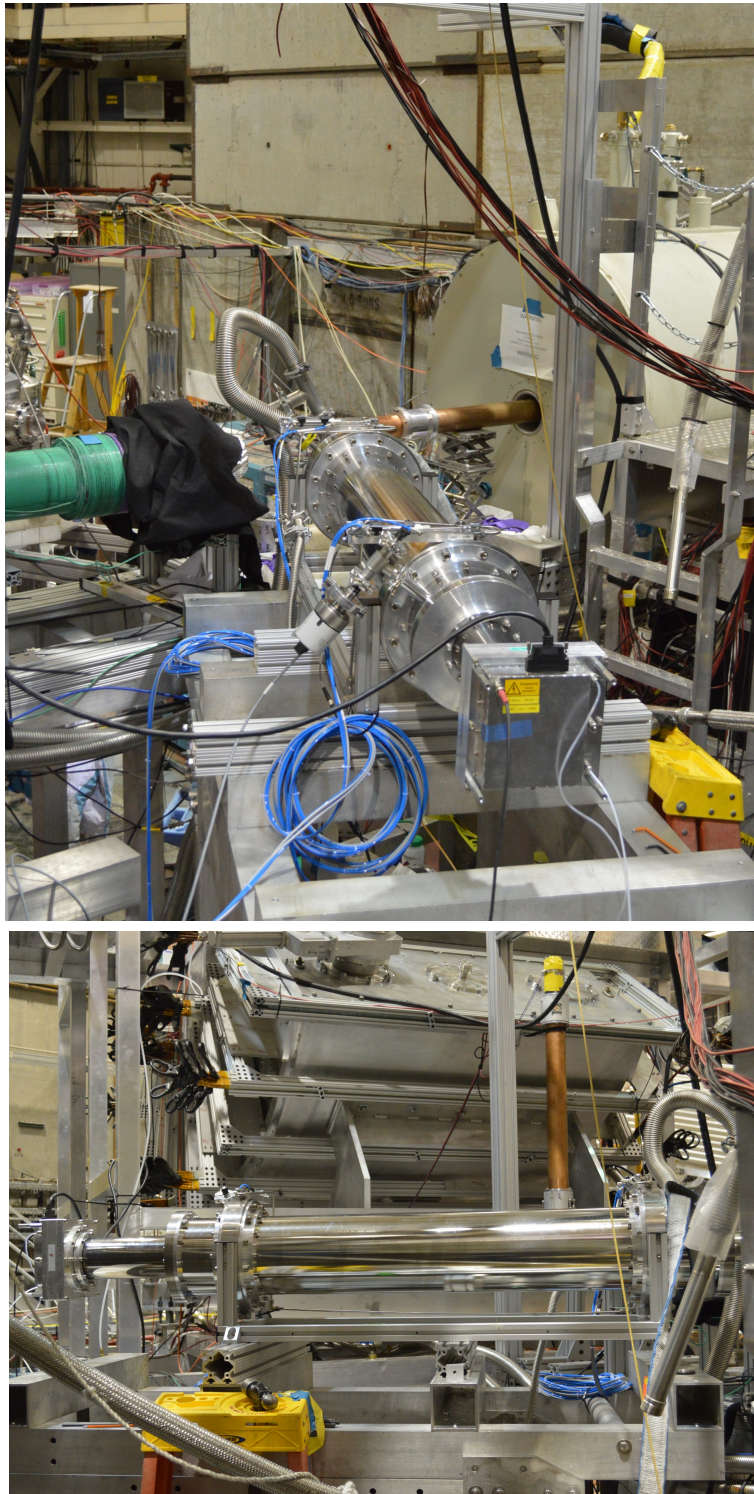
Figure 7.2: *Photos of the setup at the LANL UCN source. Top: The storage bottle and UCN detector with the superconducting magnet and the biological shielding of the source in the background. Bottom: Side view of the storage bottle, the UCNτ experiment in the background.*
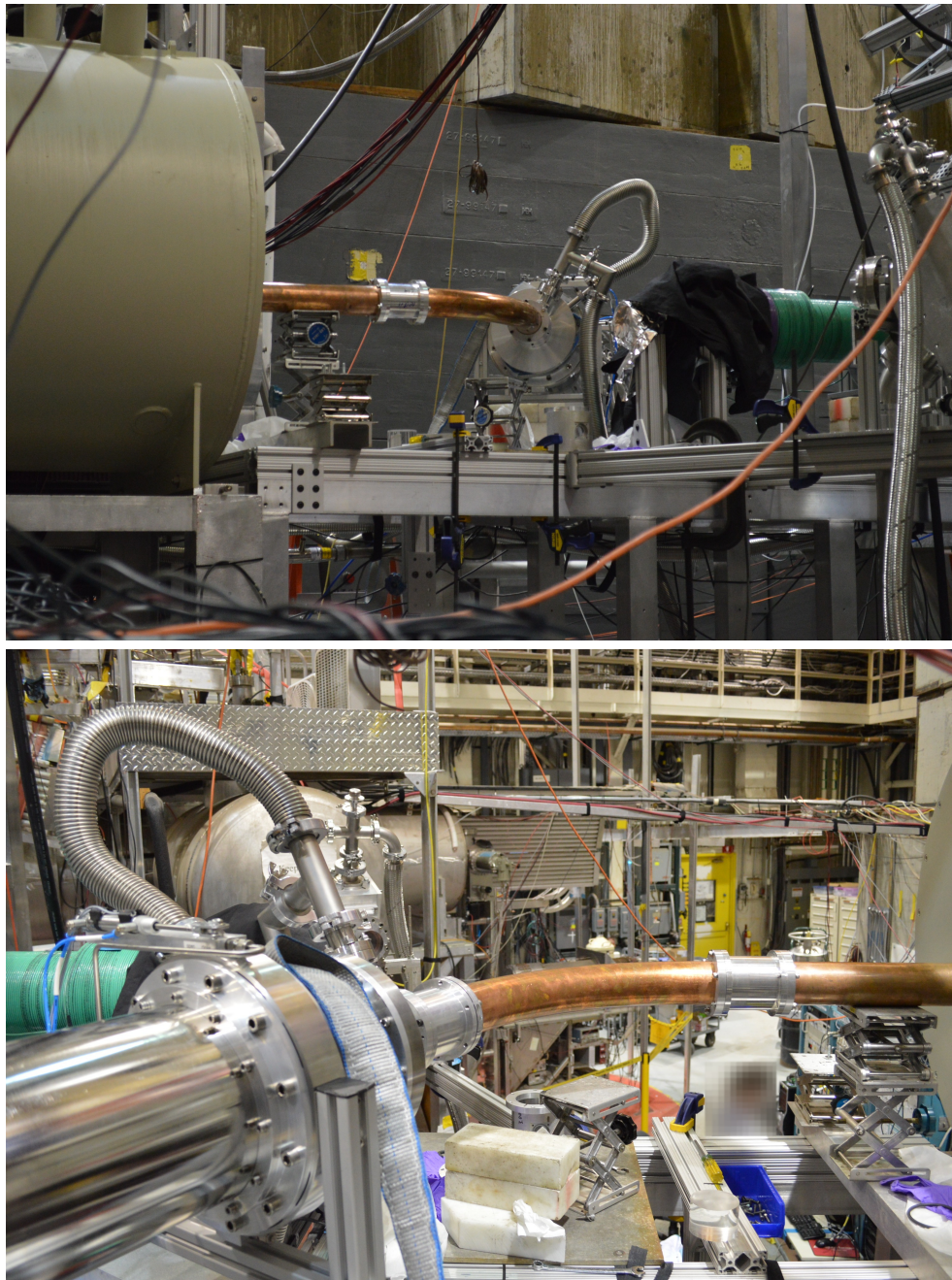
Figure 7.3: *Top: Superconducting magnet on the left hand side, copper guide and bend towards the storage bottle. Bottom: Detailed view of the copper UCN guide used to attach the storage bottle to the beamline.*
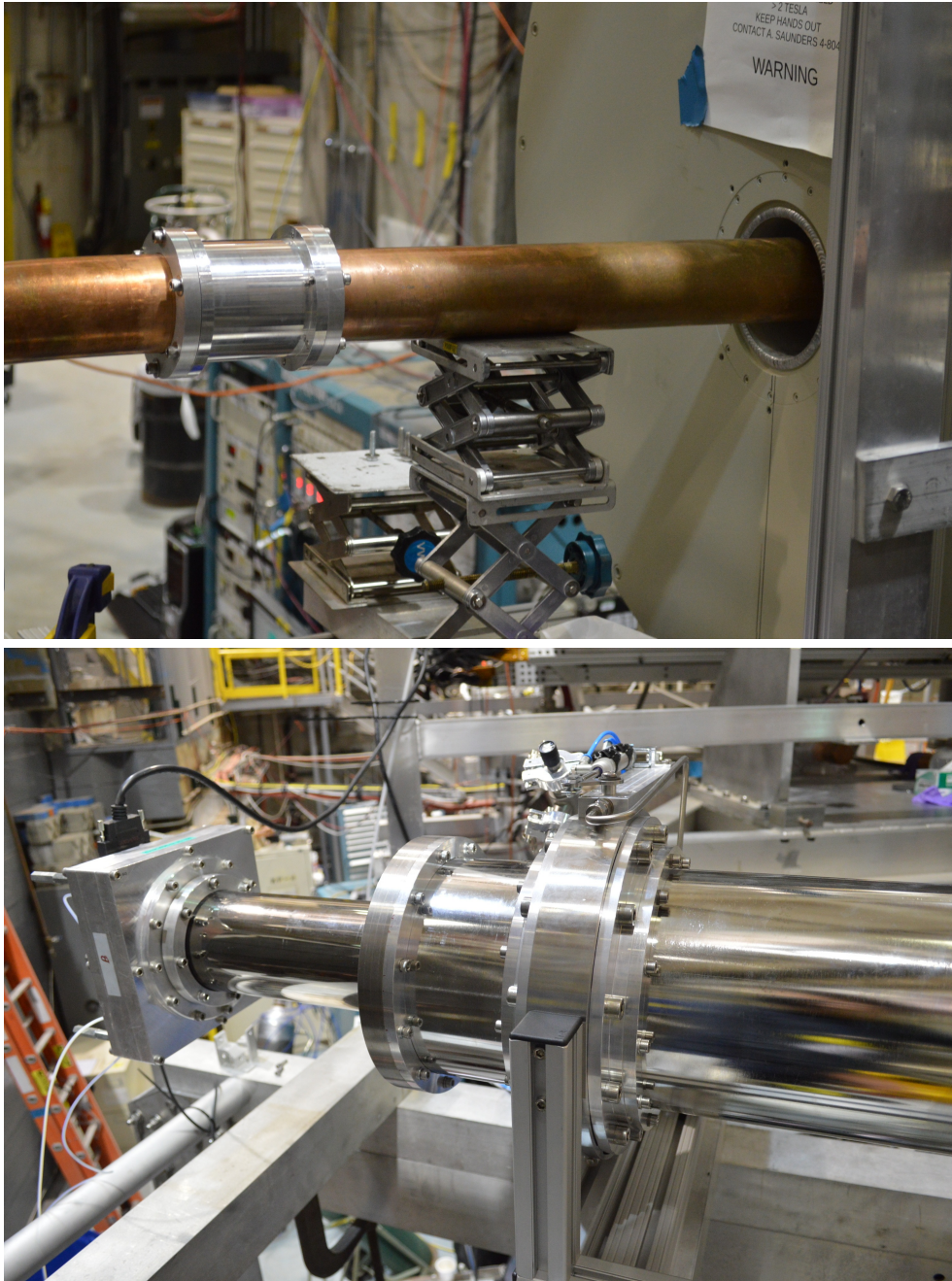
Figure 7.4: *Top: Detailed view of the copper guide exiting the superconduction magnet. Bottom: Detailed view of the detector mounted to the storage bottle.*

7.5.5 UCN storage measurements

The storage curve was recorded with fixed 40 s of filling time and a counting time of 100 s.

In order to find the storage time constant, the time spectra of 6 measurements with storage times of 100 s and 450 s, which corresponds to a storage measurement without infinite storage time, i.e. without ever opening the detecetor side shutte, were added and the UCN rate leaking through the detector side shutter fitted in a 95 s time window during the storage period.

The result is a short storage time constant τ_1 of 18(6) s and a long storage time constant τ_2 of 56(7) s. The reduced χ^2 of the fit was 0.92. The results of the fit are given in Tab. 7.1. The fitted time spectrum is shown in Fig. 7.7.

UCN counts measured after different storage times together with the storage time result from the fitted leakage rate, scaled by an arbitrary factor to match the initial amount of UCN in the bottle, are shown in Fig. 7.8 and demonstrate the compatibility of the two measurements.
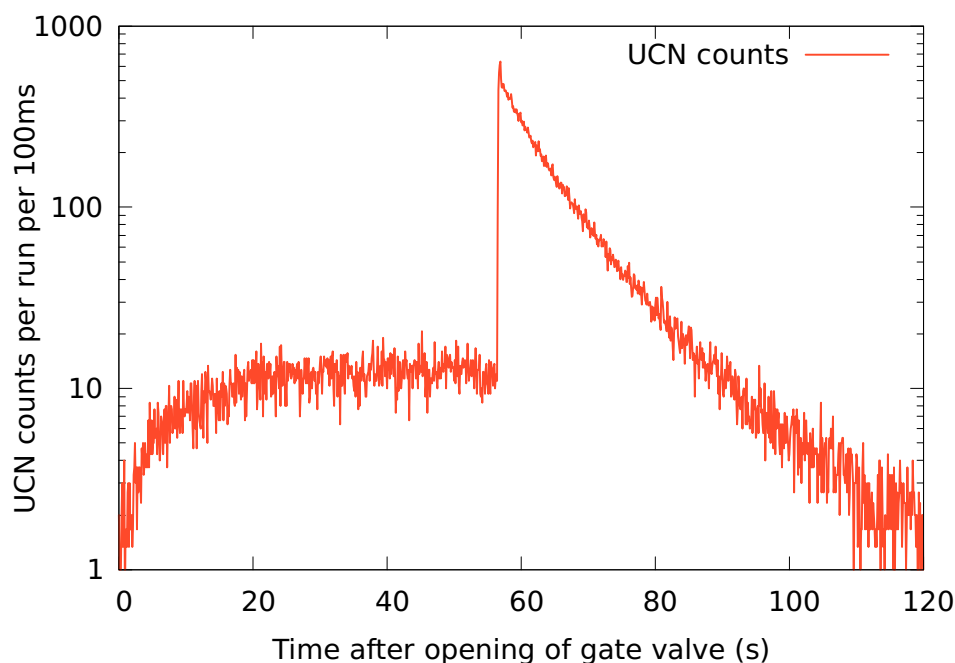
Figure 7.5: *UCN count rates in a single measurement for a filling time of* 50 s *and a storage time of* 5 s *at LANL. The leaked UCN rate during the filling time (visible in the first* 50 s *is flat for times larger than* 40 s, *which means that the maximum UCN density in the bottle has been reached.*

7.5.6 UCN density

- Important difference to all other measurements in this campaign: The measured UCN density at the LANL UCN source was measured using *polarised* UCN, as the storage bottle was mounted behind a 6 T magnet.

- After 2 s of storage, 40 622(205) UCN were counted in the detector after subtraction of the measured detector background of 0.5 Hz in the counting time window and a conservative estimate of the leakage of UCN into the bottle during the storage time of 130 Hz, as measured for the second shutter. In total, 310 UCN are subtracted from the sum of UCN counts in the counting time window.

- With a storage volume of 32 044(164) cm^3, this results in a UCN density after 2 s of storage of 1.27(1) UCN/cm^3.

- We have to assume a scaling factor on the order of 0.6, taking into account a factor of 2 reduction due to neutron polarization, and an increased UCN transmission through the vacuum safety foil located in the center of the magnet. In UCN transmission measurements through comparable foils in strong magnetic fields at PSI, a factor of 0.57(1) was measured (see Ch. 3.5). The UCN transmission of the actually used foil was questioned, as it appeared to be worse than previously. Such a behavior could be caused by surface contamination.
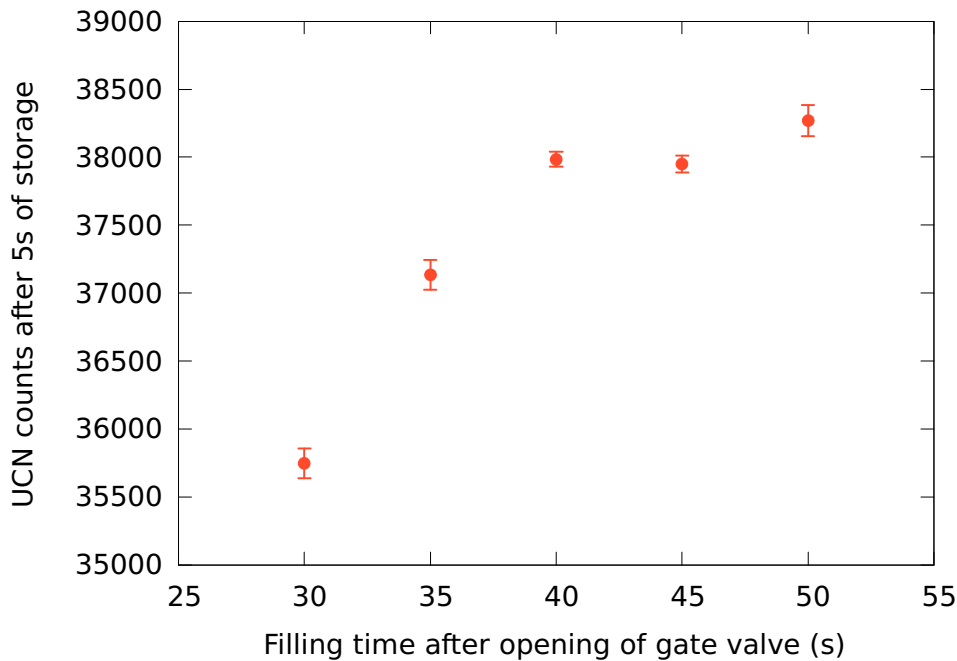
Figure 7.6: *UCN counts after a storage time of 5 s for various filling times at LANL.*

- An additional difference to the measurements at the other UCN sources is the fact, that only measurements with the detector connected to the storage bottle horizontally, i.e. with the straight 300 mm acrylic guide piece, were made. This reduces the detection efficiency with respect to measurements with the L-piece, because of transmission losses in the entrance window of the detector. In order to get a handle on this inefficiency, an measurement with a ^{10}B coated scintillation counter was performed, which does not have such an entrance window but a surface with negative (attractive) Fermi potential. Unfortunately DAQ problems and beam time restrictions made it impossible to record a storage curve with this detector, but a comparison between the number of stored UCN after 2 s measured with the two detectors yielded a factor of about 0.6, which is compatible with earlier measurements of the Cascade detector's foil transmission made by PSI [Göltl, 2008]. In addition one can compare the ratio of counted UCN between horizontal and vertical extraction at Mainz and at PSI (500 mm above beam port), the most comparable sources measured in this campaign, is 0.66 in both cases.

- Using the values measured at PSI for magnet and foil transmissions (0.57(1)), and the factor derived from the other two solid-deuterium-based sources in this comparison, with a large systematic uncertainty (0.66(10)), a factor of 2.7(4) can be calculated for comparison with non-polarized measurements.

- A scaling factor on the order of 0.6 can be assumed between the non-polarised and the polarised case. This factor is an estimation taking into account not only the reduction in UCN intensity by a factor of 2 (polarisation), but also the increasing transmission through the vacuum safety foil caused by higher kinetic energies of the transmitted UCN, which is assumed to be around 20 %.

- An additional difference to the measurements at the other UCN sources is the fact, that only measurements with the detector connected to the storage bottle horizontally, i.e. with the straight 300 mm acrylic guide piece, were made. This reduces the detection efficiency with respect to measurements with the L-piece, because of transmission losses in the entrance window of the detector. In order to get a handle on this inefficiency, an measurement with a ^{10}B coated scintillation counter (comparable to the one described in [Wang et al., 2015]) was performed, which does not have such an entrance window. Unfortunately DAQ problems and beam time restrictions made it impossible to record a storage curve with this detector, but a comparison between the number of stored UCN after 2 s measured with the two detectors yielded a factor of about 0.6, which is compatible with earlier measurements of the foil transmission made at PSI. The ratio of counted UCN between horizontal and

Extr.	A_1	τ_1(s)	A_2	τ_2(s)	red.χ^2
horiz.	244(95)	18(6)	453(101)	56(7)	0.92

Table 7.1: *Fit results for the storage time constants at the LANL UCN source.*

vertical extraction at Mainz and at PSI (500 mm above beam port), the most comparable sources measured in this campaign, is 0.66 in both cases.

- Using the values measured at PSI for magnet and foil transmissions (0.57(1)), and the factor derived from the other two solid-deuterium-based sources in this comparison, with a large systematic uncertainty (0.66(10)), a factor of 2.7(4) can be calculated for comparison with non-polarized measurements.
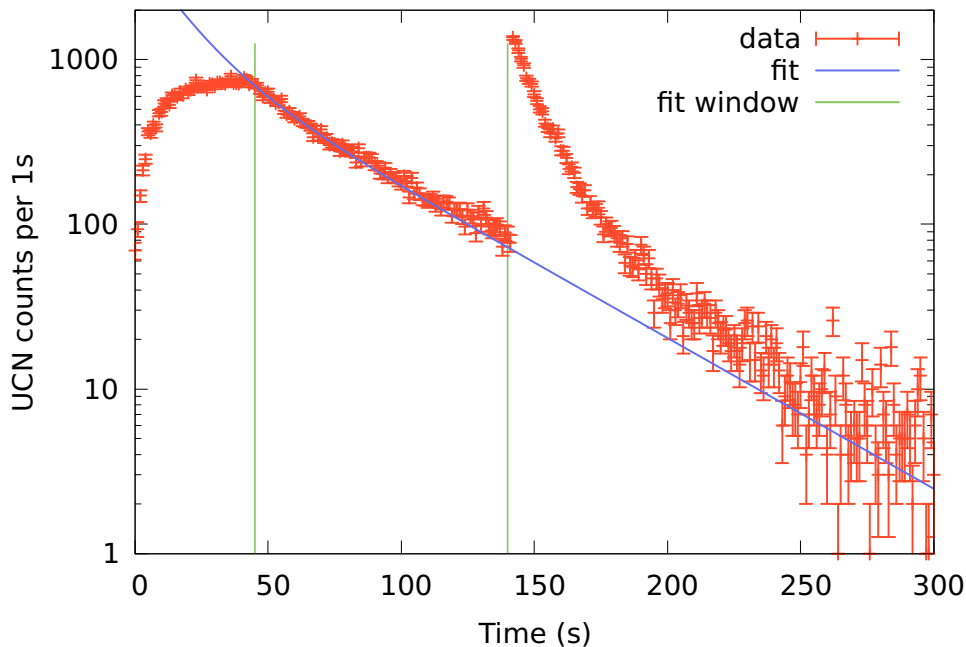
Figure 7.7: *Fit to leakage rate of UCN during storage measurements at LANL. Six measurements with storage times of* 100 s *are summed up binwise. The fit window is indicated by the vertical green lines. The blue line indicates the double exponential fit.*
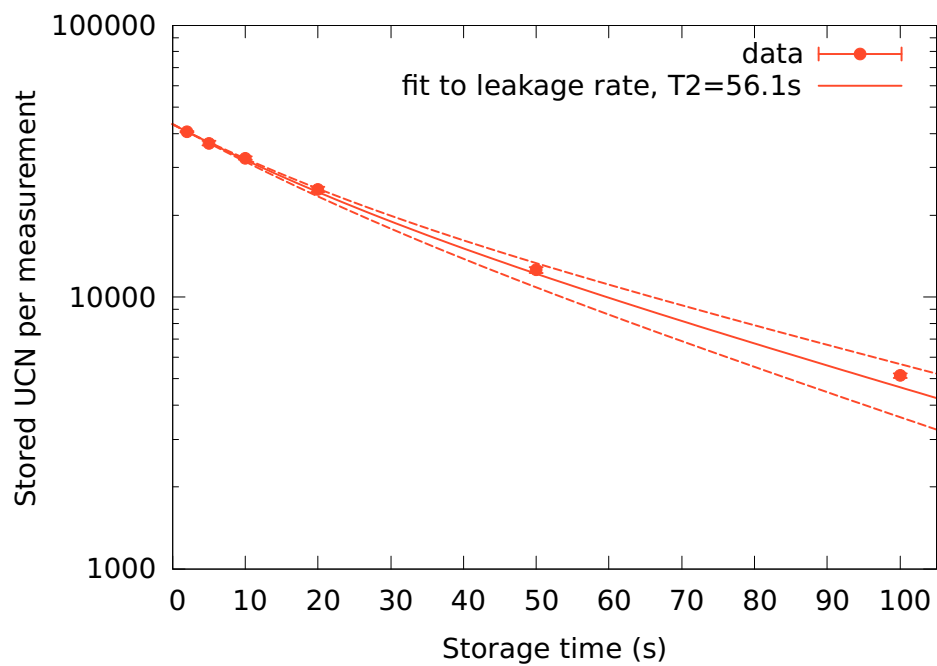
Figure 7.8: *Measured UCN counts after various storage times, measured with a filling time of* 40 s *at LANL. The results of the fit to the leakage rate, arbitrarily scaled, is indicated by the continuous line, with an error band indicated by the dashed lines.*

7.6   Measurement at SUN-2, Jul 17 - 20 2015

After shipping the entire setup back to PSI, small changes to the vacuum system, as described in Sec. 7.2 were applied. Then the experiment was transported to the Institut Laue Langevin, ILL, in Grenoble, France, in July 2015.

7.6.1   The SUN-2 UCN source at ILL

The SUN-2 UCN source is described in detail in [Leung et al., 2016].

The SUN-2 UCN source uses a monochromatic 0.89 nm cold neutron beam from the ILL High-Flux Reactor (HFR) as a primary source for neutrons. These are delivered with a flux density of $9 \times 10^8 \, \text{cm}^{-2}\text{s}^{-1}\text{nm}^{-1}$ at the beamline H172b.

The cold neutron beam enters a 1000 by 70 by 70 mm³ converter vessel filled with superfluid helium at a temperature below 1 K. The walls of this vessel are made from beryllium for the front- and endface and beryllium coated aluminium for the larger wall faces. The beryllium coated plates are in addition coated with fomblin grease. Beryllium has a Fermi potential of 250 neV while fomblin grease only has a Fermi potential of 70 neV.

Inside the superfluid helium, neutrons can lose almost all their kinetic energy in an inelastic single-phonon scattering process, and thus become ultracold.

As both the nuclear absorption cross section as well as the upscattering cross section of UCN in superfluid helium are negligibly small, UCN can be produced and accumulated in such a source vessel for very long times comparable to the free neutron lifetime.

After an arbitrary accumulation time, UCN can be extracted upwards from the superfluid helium through a vertical cone which can be opened or closed with a gate valve. The opening towards the helium container has a diameter of 23 mm.

500 mm above the gate valve, the UCN are fed into a horizontal stainless-steel UCN guide with an outer diameter of 70 mm to exit the source. This elevation also compensates for the boost in kinetic energy of 18.5 neV caused by the Fermi potential of the superfluid helium.

7.6.2   Setup of the storage bottle

The storage bottle was mounted directly at the output of the UCN source, using a 141.5 mm long stainless-steel UCN guide with an outer diameter of 70 mm. Fig. 7.9 shows the storage bottle connected to the SUN-2 UCN source, with both UCN extraction options. Fig. 7.10 shows details of the connection and extraction. Note that there is no vacuum separation window between the storage bottle and the extraction guide, which in turn is directly connected to the superfluid helium in the converter vessel.

While the vacuum shutter to the source was closed, the rest gas pressure in the storage bottle was below 2×10^{-4} mbar, as soon as the shutter was opened the vacuum gauge readings were disturbed by the helium coming from the source.

The source was operated with UCN accumulation times of 600 s and 300 s. The accumulation time is the time where the neutron beam is incident on the helium while the gate valve of the source is closed.

The cold neutron beam was only switched off for longer breaks in the measurement, e.g. for modifying the setup. During the measurements itself, the beam stayed on the converter vessel, such that a new measurement could be started every 300 s or 600 s respectively.

7.6.3   Operating conditions during the measurements

During the measurements the HFR was operating in normal conditions with a reactor power of 52.5(3) MW. The reactor cycle no. was 175.

The SUN-2 source was operated at a helium temperature of below 0.7 K.

Except for two interruptions described in Sec. 7.6.4 the source could be operated continuously.

7.6.4   Problems while running the source

The UCN output per accumulation was decreasing rapidly with time. The most probable candidate for the source of this degradation of performance is outgassing from the UCN guide which connects the detector to the storage bottle. This guide is made of acrylic coated with NiMo.

As the storage bottle was not separated from the cold source vacuum wise, any gas in the system could possibly freeze out on the walls of the cold extraction guides, which would result in a reduction of extraction efficiency for UCN produced inside the superfluid helium.

Additionally, blockades in the ^{3}He handling system made a warm-up of the source necessary twice during the measurement time.

7.6.5   Determination of the optimal filling time

The filling time was optimised as described in Sec. 7.3, in the range from 40 s to 80 s as shown in Fig. 7.11.

As it was quickly observed that the UCN output per accumulation was decreasing with time as described in Sec. 7.6.4, the scanning of the filling time was aborted after a course scan, and a filling time of 60 s was chosen. Looking at the time spectrum of UCN leaking through the second shutter during filling, for long filling times, also suggests that after about 50 s the maximum density is reached and only very slowly declines for longer filling times (Fig. 7.12).

Figure 7.9: *Photos of the setup installed at the SUN-2 source. Top: Vertical extraction, bottom: horizontal extraction.*

Figure 7.10: *Details of the setup at SUN-2: Top: The vertical extraction guide plus detector. Bottom: Connection of the storage bottle to the UCN source.*

7.6.6   UCN storage measurements

For both accumulation times storage curves were recorded. The corresponding results are shown in Fig. 7.13 and Fig. 7.14.

An upper bound of the amount of UCN leaking in through the first bottle shutter after the end of the filling period was determined by one measurement with the first shutter permanently closed and the second shutter permanently opened, and then applying the same time cuts as for a storage measurement with a storage time of 2 s.

In order to find the storage time constants, for each detector setup and accumulation time the time spectra of 4 measurements with storage times of 100 s and 200 s were added and the UCN rate leaking through the detector side shutter fitted in a 95 s time window during the storage period, as described in Sec. 7.4.

For 600 s accumulation and horizontal extraction, a double exponential fit didn't converge. Here, a fifth measurement with a storage time of 300 s was added and a single exponential fit was made with a good convergence and storage time constant.

The fitted storage time constants for the various setups are shown in Table 7.2.

7.6.7   UCN density

The following UCN densities after 2 seconds of storage have been deduced for the various setups:
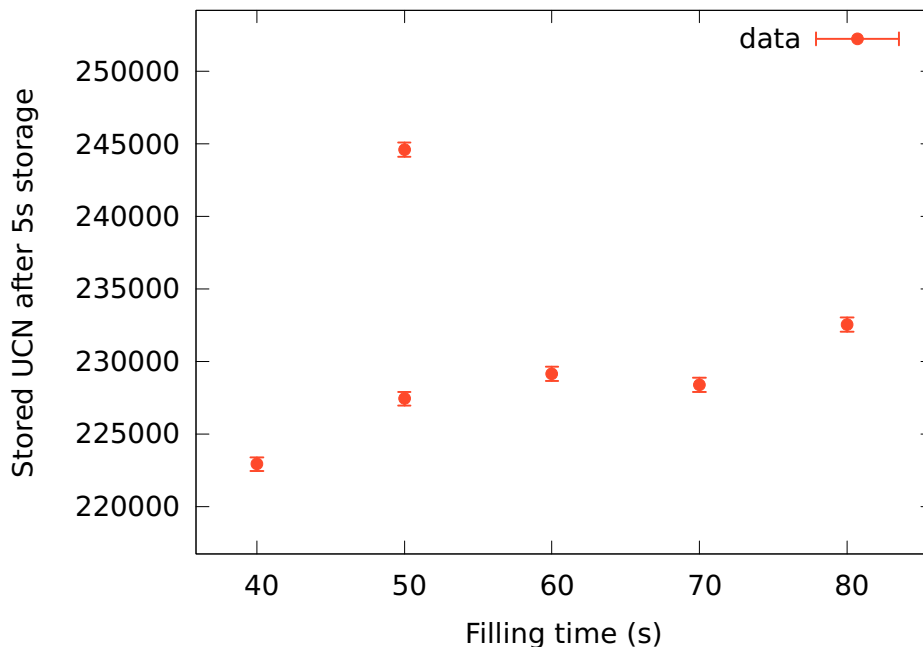
Figure 7.11: *UCN counts after a storage time of* 5 s *for various filling times at SUN-2. The data points at* t =50 s *differ because of the decline in UCN output per accumulation, as described in Sec. 7.6.4*

- Accumulation time 600 s:

    - vertical extraction: 6.47(4) UCN/cm^3
    - horizontal extraction: 0.87(1) UCN/cm^3

- Accumulation time 300 s:

    - vertical extraction: 4.62(3) UCN/cm^3
    - horizontal extraction: 0.76(1) UCN/cm^3

Measured UCN counts for 2 s storage time, subtracted leakage, and densities are listed in Table 7.3.
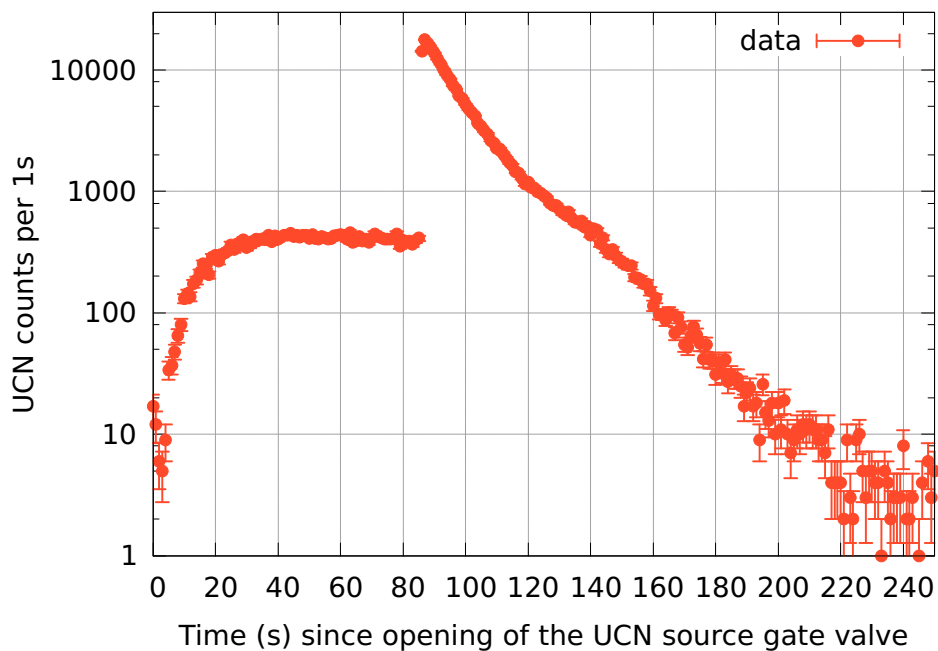
Figure 7.12: *UCN counts versus time after opening the UCN source gate valve, for a filling time of 80 s at SUN-2. It is obvious that the leakage rate while filling grows up to about 40 s and then stays constant.*
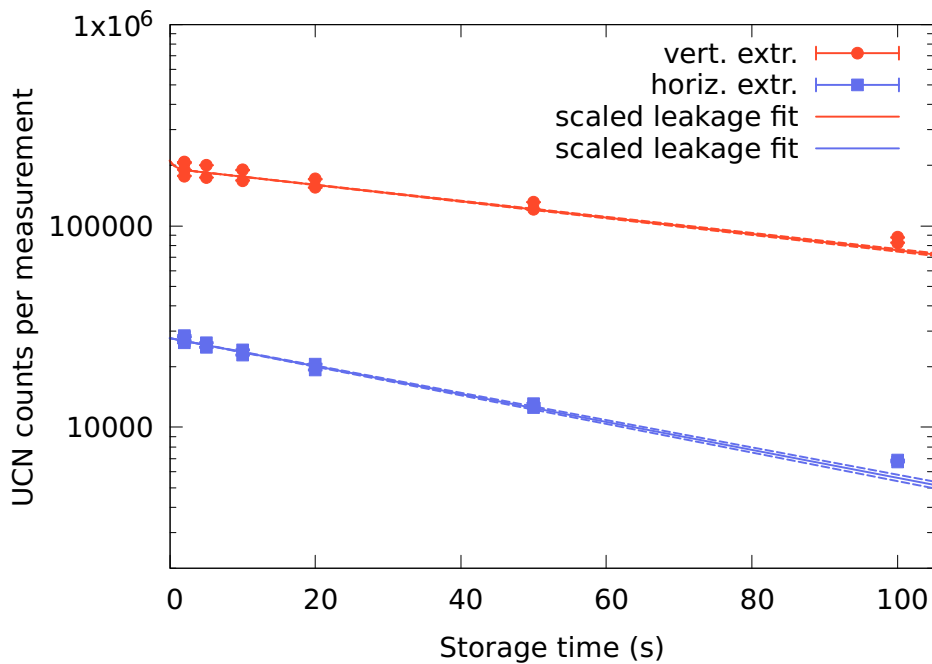
Figure 7.13: *Measured UCN counts after various storage times at the SUN-2 source for a UCN accumulation time of 600 s. The measurements were done starting with a storage time of 2 s and increasing up to 200 s, then one more measurement was done at 2 s before the times were decreased from 200 s to 2 s again. The results of the fits to the leakage rate, arbitrarily scaled, are indicated by the continuous lines, with error bands indicated by the dashed lines.*

Acc.(s)	Extr.	A_1	τ_1(s)	A_2	τ_2(s)	red.χ^2
300	horiz.	3(2)	4(5)	24(1)	59.7(21)	1.28
300	vert.	—	—	107(1)	103.7(22)	1.32
600	horiz.	—	—	35(1)	62.6(14)	1.53
600	vert.	14(10)	1(1)	145(1)	107.0(17)	1.34

Table 7.2: *Fit results: Storage time constants at the SUN-2 UCN source. A double exponential fit did not converge for 600 s accumulation and horizontal extraction as well as for 300 s and vertical extraction.*

Acc. (s)	Extr.	UCN counts after storage	Leakage subtr. (counts)	Density (UCN/cm^3)
600	vert.	207 215(484)	13 384(116)	6.47(4)
600	horiz.	28 015(181)	2409(49)	0.87(1)
300	vert.	148 132(408)	9066(95)	4.62(3)
300	horiz.	24 352(169)	2162(46)	0.76(1)

Table 7.3: *Results of storage measurements with 2 s storage time at the SUN-2 UCN source*
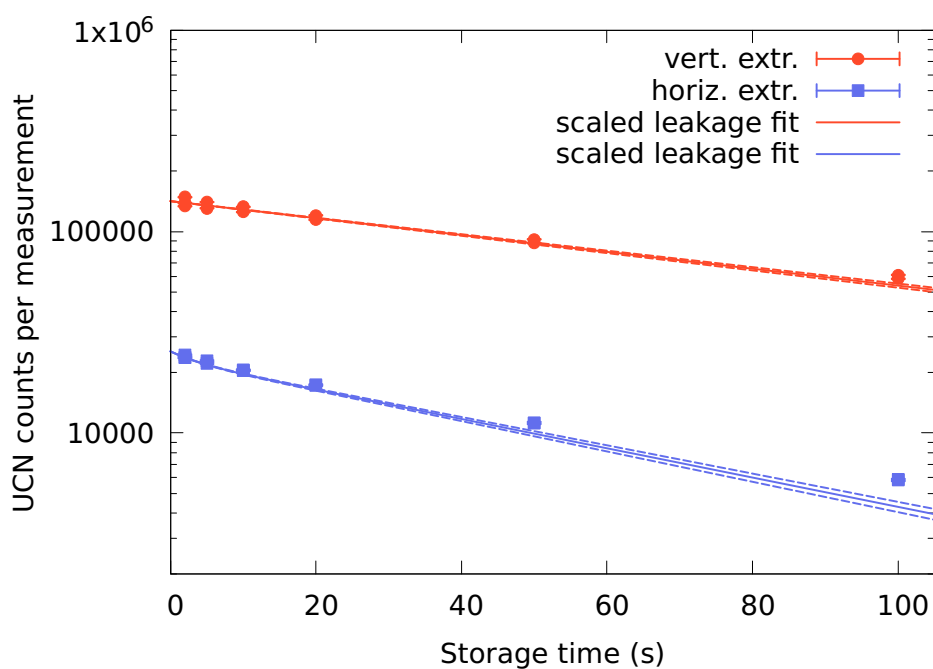
Figure 7.14: *Measured UCN counts after various storage times at the SUN-2 source for a UCN accumulation time of* 300 s. *The measurements were done starting with a storage time of* 2 s *and increasing up to* 200 s, *then one more measurement was done at* 2 s *before the times were decreased from* 200 s *to* 2 s *again. The results of the fits to the leakage rate, arbitrarily scaled, are indicated by the continuous lines, with error bands indicated by the dashed lines.*

7.7   Measurement at PF2, Aug 04 - Sep 09 2015

Two separate measurements were performed at the turbine UCN source at PF2, ILL Grenoble, at the height of the beam port, and at the height of the former RAL-Sussex-ILL nEDM experiment [Baker et al., 2014].

7.7.1   The PF2 UCN source at ILL

The PF2 UCN source is described in detail in [Steyerl et al., 1986].

From the vertically serviced cold neutron source in the 58 MW High Flux Reactor (HFR) at the ILL, a vertical cold neutron guide guides neutrons with wavelengths between 70 and 90 Å to a UCN turbine about 15 m above the cold source.

The UCN turbine features 690 nickel turbine blades which rotate in neutron flight direction with half the incoming neutron velocity ($\sim 50\,\mathrm{m\,s^{-1}}$ neutrons, $\sim 25\,\mathrm{m\,s^{-1}}$ turbine blades). Neutrons incident on the turbine blades are Doppler shifted to UCN velocities. They can exit through four UCN guides (UCN, EDM, MAMBO, TEST), of which three can be selected via a moving guide piece which connects one of the three to the turbine, while the fourth, so-called test-beam port, which has the smallest UCN flux, is permanently connected.

The UCN density measurements were performed at the so-called EDM beamline, which has the highest UCN flux at PF2.

7.7.2   Setup of the storage bottle

The first measurement was done at the height of the EDM beamline exit from the turbine. In the second measurement UCN were guided to the EDM platform and the storage vessel was 2200 mm above the beamline exit.

Both measurements were not only done in the standard configuration with a vacuum separation foil made of aluminium (AlMg3) with 100 µm thickness between the experiment and the turbine vacuum, but also without this safety foil.

All UCN guides used in the measurements at PF2 were stainless-steel guides with an outer diameter of 81.5 mm, with an internal Ni coating. One additional 540 mm long guide piece, also made from stainless-steel and coated with Ni, but with an outer diameter of only 80 mm, was used to connect the storage bottle to the beamline. The inner diameter of all guides is 78 mm.

For the measurements at the turbine level, one 1 m long, UCN guide was attached to the turbine's vacuum shutter. This guide was followed either by a regular guide coupler or by a coupler also housing the vacuum separation foil. One more 1 m guide piece and finally the 80 mm diameter guide completed the beamline to the storage bottle.

For the measurements on top of the platform, an S-shaped construction made of two 30° angled pieces and four straight guides of about 1 m length each, was added between the foil position and the 80 mm diameter guide. This resulted in the bottle being 2200 mm above beam exit height measured from guide center to guide center.

Fig. 7.17 shows photographs of the storage bottle setup at turbine exit height and the aluminium vacuum safety foil. Fig. 7.15 shows photographs of the storage bottle setup on top of the nEDM platform. Fig. 7.16 shows details of the S-shaped beam line.

7.7.3 Operating conditions during the measurements

During the measurements directly at the turbine exit the HFR was operating in normal conditions with a reactor power of 52.5(3) MW. The reactor cycle no. was 175. The measurements on top of the nEDM platform took place on the first two days of reactor cycle 176. The reactor was still ramping to it's final power.

The two measurements without vacuum safety foil were taken with a reactor power of about 49.0(5) MW while the measurements with vacuum safety foil were taken with a reactor power of about 50.8(5) MW. Rest gas pressure inside the storage bottle was below 2×10^{-4} mbar for all measurements.

During all measurements, the UCN and MAMBO beamlines of the PF2 turbine were also in use, such that UCN had to be requested in order to fill the storage bottle. After requesting UCN, the turbine switch moves the extraction guide towards the EDM beamline, but the extraction tube cannot be actively moved away. Thus, the UCN intensity on the first shutter of the storage bottle stays high even after filling the bottle is finished. It can then either be kept high by forcing the beamline switch to stay at its current position, or it can be called to a different beamline at any given time.

The storage bottle shutters are not completely UCN tight, and the vacuum shutters at the turbine can only be opened and closed from the turbine control panel but not using a timing system, and can therefore not be closed during our measurement. Larger amounts of UCN therefore leak into the bottle during the storage time at PF2 than at any other UCN source. For consistency it was chosen to always keep the beamline switch at the EDM beamline until the counting time of the measurement was finished rather than have it move away at arbitrary times to an unknown position. This does not much influence the measurement of the UCN density after short storage times of a few seconds, because the effect can easily be measured and subtracted. But for comparing various storage times in order to determine the storage time constant this is unfortunately not the case.

7.7.4 Determination of the optimal filling time

In both positions, on top of the platform and at turbine height, the filling time was optimised as described in Sec. 7.3. The results are shown in Fig. 7.18. A filling time of 70 s was chosen for the measurements.

The filling time was chosen to be rather long instead of being optimised for many repetitions. It was measured once at the turbine exit and once on top of the platform. It was assumed that especially as it was initially chosen to be rather long, it would not be too short for any of the four measurements at each position.

Figure 7.15: *Photos of the setup on the EDM platform at PF2. Top: Storage bottle setup with vertical extraction. Bottom: UCN beamline up to the platform.*
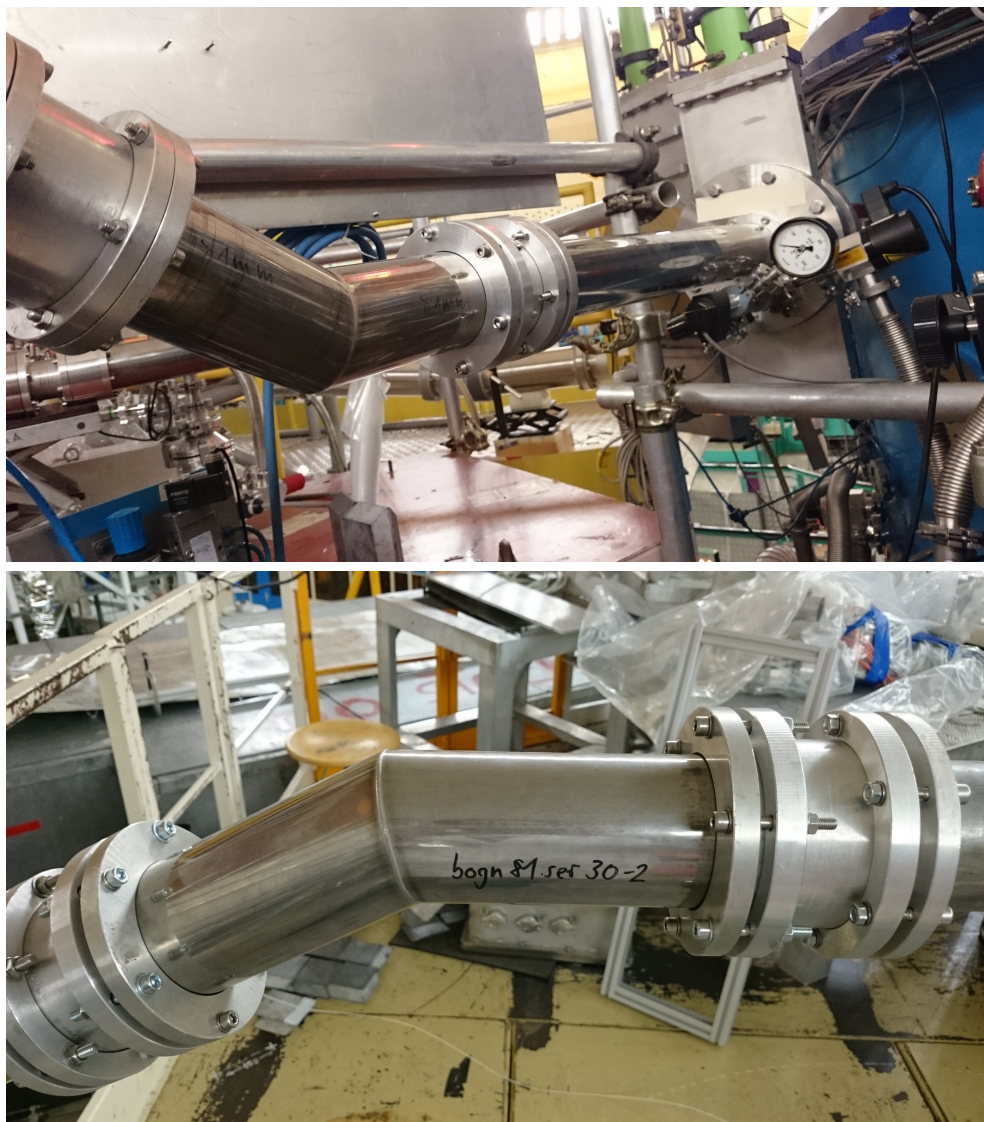
Figure 7.16: *Details of the beamline to the EDM platform at PF2. Top: First UCN guide between the turbine and the foil position. Bottom: One of the 30° angle pieces.*
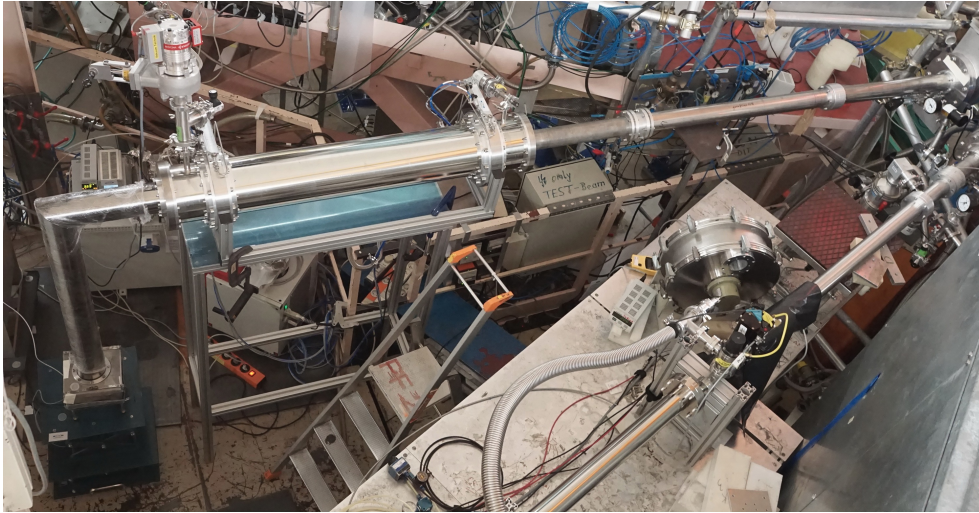
Figure 7.17: *Top: Photos of the setup at turbine exit height at PF2, vertical extraction into the detector. The TEST beamline can be seen on the bottom right hand side. Bottom: Unmounting the vacuum safety foil. The blue turbine housing can be seen in the background.*
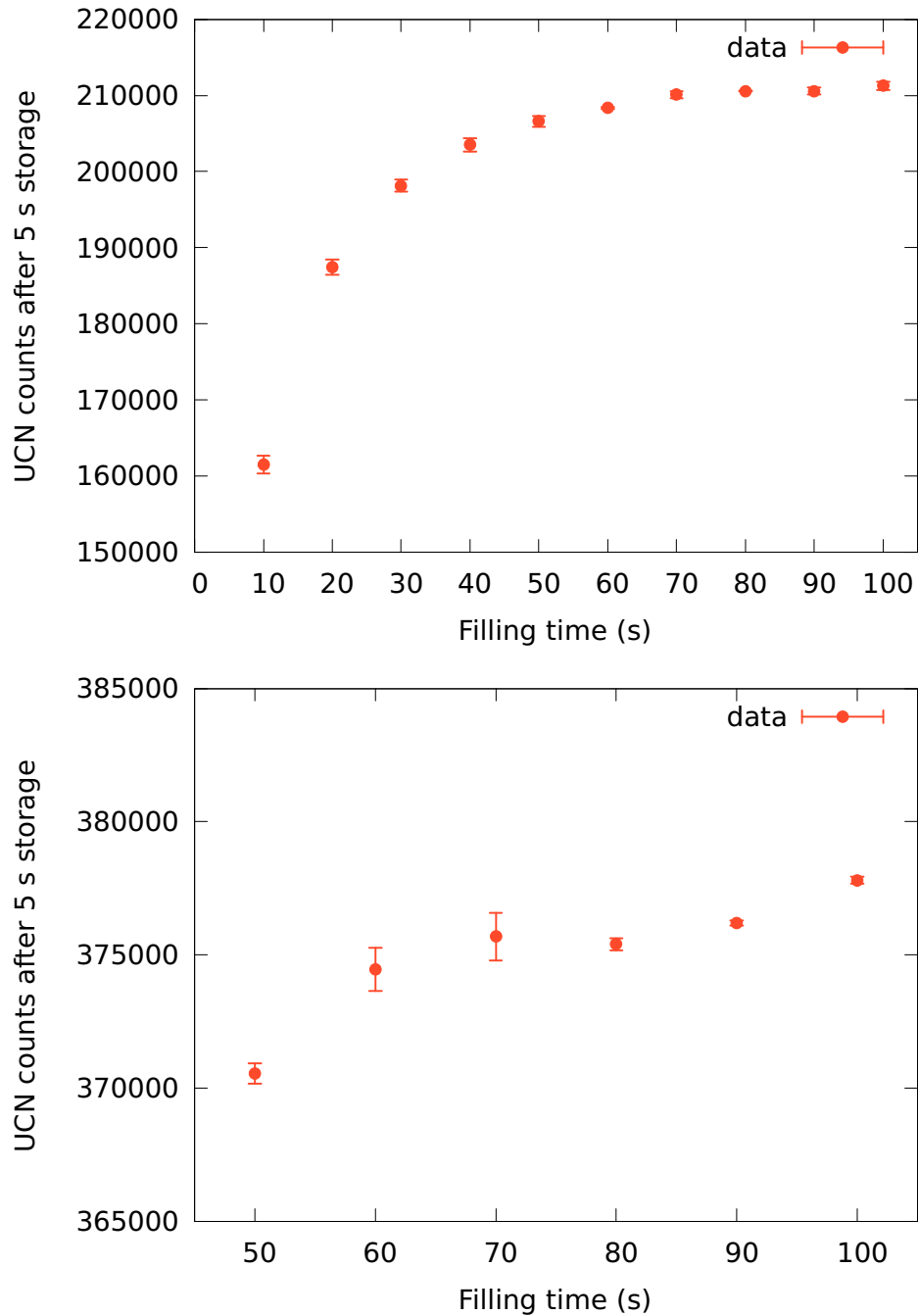
Figure 7.18: *UCN counts after* 5 s *of storage using various filling times. Top: Measured at turbine exit height with vertical extraction and with the vacuum separation foil in place. Bottom: Measured on top of the platform with vertical extraction, without vacuum separation foil. A filling time of* 70 s *was chosen for both cases.*

7.7.5 UCN storage measurements

Storage curves were recorded in both positions. The results are shown in Fig. 7.20 and Fig. 7.21 respectively. It is worth noting that while at turbine exit height both measurements without vacuum separation foil are higher than their counterparts with foil, on top of the platform the measurements with vertical extraction into the detector are consistently the highest, both with and without foil. This can be explained by the gravitational lowering of the average kinetic energies of UCN stored in the bottle on top of the platform. A significant fraction of the stored UCN is too slow to overcome the Fermi potential of the detector entrance window (50 neV), and thus can only be detected with the detector mounted lower using the L-shaped UCN guide.

An example of a typical time spectrum of UCN counts for measurements at the PF2 source is shown in Fig. 7.19. Time spectra of all measured setups, both at the turbine exit and on top of the platform, are qualitatively similar, and differ only in the absolute counts leaking through with closed shutters and at the emptying peak.

The UCN rate incident on the first shutter of the storage bottle during storage- and counting times was very high at the PF2 UCN source, as described in Sec. 7.7.3. Due to the fact that the shutters are not perfectly UCN tight, as described in Sec. 6.5.2, this made a modification of the fit function used for evaluating the storage time constants necessary. Instead of Eqn. 7.1, the
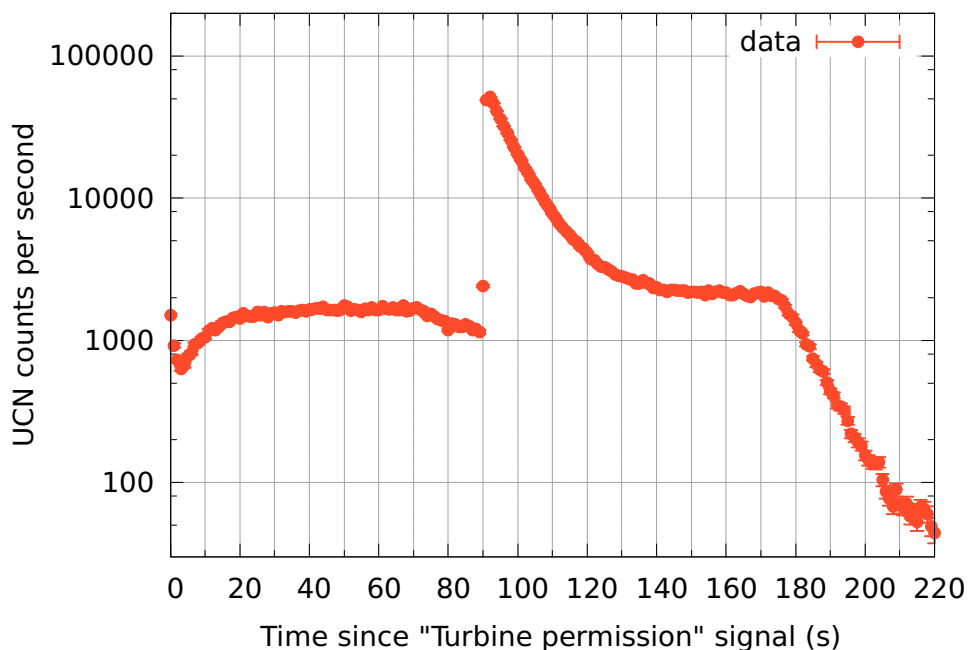
Figure 7.19: *Time spectrum of UCN counts for a measurement with* 20 s *storage time, measured using vertical extraction, without a vacuum safety foil, directly at the turbine exit. Starting from a very low UCN rate when the turbine's extraction tube is not at the EDM position, the rate of UCN leaking through the second shutter during filling rises and saturates after about* 50 s. *After the first shutter is closed at t = 70 s, the rate drops for the storage time of* 20 s *until the emptying peak. Afterwards the count rate stabilises at the high leakage rate of about* 2 kHz *until the extraction tube moves away at t = 170 s.*

leakage rate during storage measurements with storage times larger than 100 s was fitted using the following formula:

$$N(t) \propto R(t) = A_1 \times e^{-t/\tau_1} + A_2 \times e^{-t/\tau_2} + L \times \tau_1 \tag{7.2}$$

where $N(t)$ is the total amount of UCN inside the storage bottle, $R(t)$ the rate of UCN leaking through shutter 2 as measured in the detector, A_1 and A_2 population constants and τ_1 and τ_2 exponential decay time constants, as described in Sec. 7.7.3. Additionally, the leakage rate L is introduced as the constant amount of UCN leaking through shutter 1 into the bottle. This has been measured for every setup and is given in Table 7.6 and Table 7.7. Furthermore, it is assumed that the UCN leaking into the bottle are dominated by faster UCN for which only the decay time constant τ_1 is relevant.

Using this model and the additional input from the measured leakage rates, the storage time constants could be fitted with reduced χ^2 between 1.25 and 1.35, which is comparable to the reduced χ^2 values obtained for all other UCN sources, where the simpler model without constant leakage term is used.

The fitted storage time constants for the UCN density measurements at the turbine exit height are shown in Table 7.4, the storage time constants for the measurements on top of the platform are shown in Table 7.5
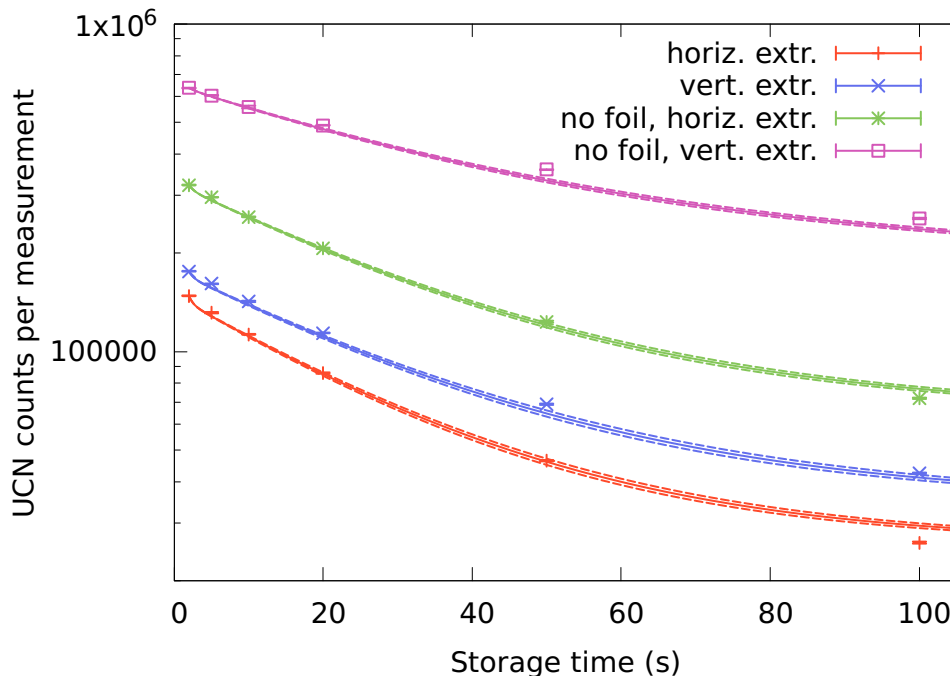
Figure 7.20: *Measured UCN counts after various storage times, measured with a filling time of* 70 s *at turbine exit height. The results of the fits to the leakage rate, arbitrarily scaled, are indicated by the continuous lines, with error bands indicated by the dashed lines. Both measurements without aluminium foil are higher than measurements with foil.*

7.7.6   UCN density

The following UCN densities were obtained using the UCN counts from storage measurements with a storage time of 2 s and the storage bottle volume of $32\,044(164)$ cm^3 as given in Sec. 6.3.

At turbine exit height:

- With vacuum separation foil:

    - Horizontal extraction: $4.61(2)$ UCN/cm^3
    - Vertical extraction: $5.48(3)$ UCN/cm^3

- Without vacuum separation foil:

    - Horizontal extraction: $10.04(6)$ UCN/cm^3
    - Vertical extraction: $19.90(11)$ UCN/cm^3

On top of the platform:

- With vacuum separation foil:

    - Horizontal extraction: $3.45(2)$ UCN/cm^3
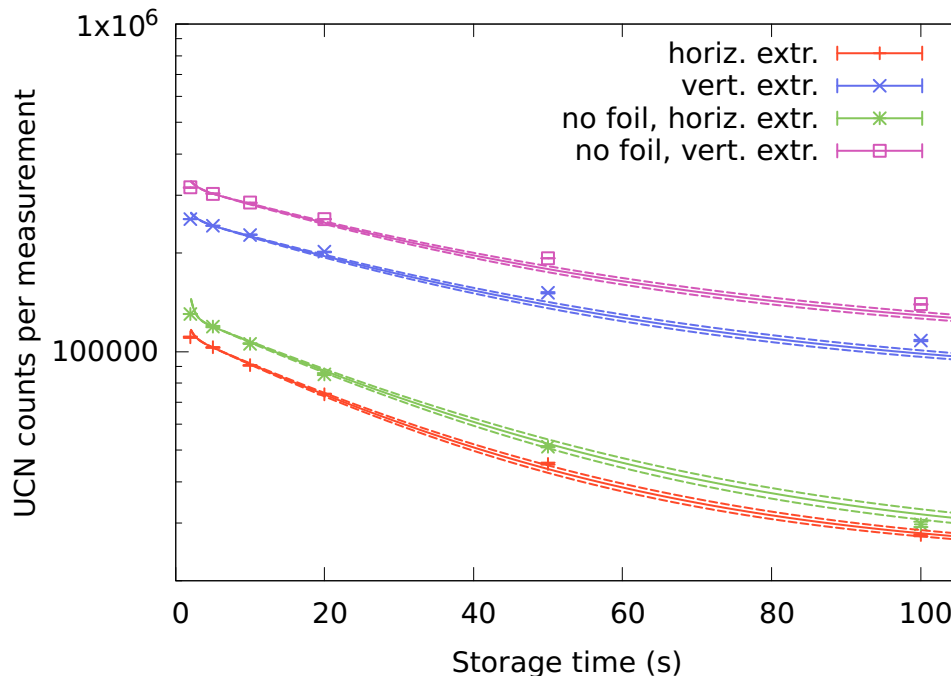
Figure 7.21: *Measured UCN counts after various storage times, measured with a filling time of 70 s, measured on top of the EDM platform. The results of the fits to the leakage rate, arbitrarily scaled, are indicated by the continuous lines, with error bands indicated by the dashed lines. Measurements with and without aluminium foil are interspersed.*

    – Vertical extraction: 7.91(4) UCN/cm^3

- Without vacuum separation foil:

    – Horizontal extraction: 4.06(2) UCN/cm^3

    – Vertical extraction: 9.88(6) UCN/cm^3

Measured net UCN counts, subtracted UCN leakage counts, and UCN densities at turbine height are listed in Table 7.6, the corresponding results for the measurements on top of the EDM platform are listed in Table 7.7.

Foil	Extraction	A_1	τ_1 (s)	A_2	τ_2 (s)	red.χ^2
Yes	horiz.	13(10)	0.6(1)	186(2)	27.6(6)	1.32
Yes	vert.	11(10)	0.7(1)	198(2)	32.0(8)	1.26
No	horiz.	17(14)	0.7(1)	380(3)	32.1(6)	1.35
No	vert.	10(14)	1.1(1)	519(4)	41.8(10)	1.26

Table 7.4: *Fit results: Storage time constants at the PF2 UCN source at ILL, measured at turbine exit height.*

Foil	Extraction	A_1	τ_1 (s)	A_2	τ_2 (s)	red.χ^2
Yes	horiz.	8(7)	0.6(1)	102(1)	33.1(12)	1.27
Yes	vert.	12(8)	1.0(1)	158(2)	44.8(21)	1.25
No	horiz.	25(9)	0.5(1)	122(1)	36.5(13)	1.31
No	vert.	15(9)	1.0(1)	189(3)	45.9(21)	1.24

Table 7.5: *Fit results: Storage time constants at the PF2 UCN source at ILL, measured on top of the EDM platform.*

Foil	Extr.	Net UCN counts	Leakage rate (Hz)	Subtracted leakage counts	Density (UCN/cm^3)
Yes	horiz.	147 740(232)	750(8)	60 000	4.61(2)
Yes	vert.	175 459(444)	760(9)	60 800	5.48(3)
No	horiz.	321 730(777)	1400(12)	112 000	10.04(6)
No	vert.	637 795(1166)	2050(9)	164 000	19.90(11)

Table 7.6: *Results at the PF2 UCN source, at turbine exit height.*

Foil	Extr.	Net UCN counts	Leakage rate (Hz)	Subtracted leakage counts	Density (UCN/cm^3)
Yes	horiz.	110 636(497)	434(5)	34 720	3.45(2)
Yes	vert.	253 502(392)	750(7)	60 000	7.91(4)
No	horiz.	130 182(213)	555(17)	44 400	4.06(2)
No	vert.	316 709(944)	904(12)	72 320	9.88(6)

Table 7.7: *Results at the PF2 UCN source, on the EDM platform.*

7.8   Measurement at the TRIGA Reactor, Mainz, Nov 12 - 19 2015

At the UCN source of the Mainz TRIGA reactor at Johannes-Gutenberg-University Mainz, in beamtube D, measurements were performed in November 2015.

7.8.1   The UCN source in beamtube D of the TRIGA reactor, Mainz

The UCN source in beamtube D of the TRIGA reactor in Mainz is described in detail in [Karch et al., 2014, Lauer and Zechlau, 2013].

The TRIGA reactor is used in pulse mode, with a pulselength of about 30 ms. Pulses of about 9.5 MW s were produced every ~ 12 min. Beamtube D is horizontally directed straight at the reactor core. The UCN source can be inserted into the beamtube.

Neutrons from the reactor core first enter a premoderator vessel, which is filled with either H_2 or CH_4 at a temperature of 6 K. There the neuetrons are moderated to becomme cold. Subsequently, they enter the converter vessel filled with sD_2, also at a temperature of 6 K.

Inside the solid deuterium, cold neutrons can lose all kinetic energy in a single inelastic phonon process, after which they end up as ultracold neutrons (see [Atchison et al., 2005a]. Afterwards they can diffuse out of the solid deuterium

UCN are extracted horizontally using a stainless-steel UCN guide with an inner diameter of 66 mm which connects to the converter vessel. When exiting the solid deuterium, UCN experience a horizontal boost in kinetic energy of 105 neV as observed in Mainz for the first time [Altarev et al., 2008]. At the beamport, the source vacuum is separated from the experiment vacuum by an $AlMg_3$ foil of 100 µm thickness.

In contrast to the other two sD_2 based sources measured in this campaign, i.e. at LANL and at PSI, the boost in kinetic energy by the solid deuterium is not being compensated for inside the source but the beamport is at the same height as the converter vessel.

7.8.2   Setup of the storage bottle

In order to compensate for the horizontal boost in kinetic energy, the height of the density measurement outside of the UCN source was optimised prior to the measurements.

The storage bottle was connected to the beamport port via an S-shape beamline made from two stainless-steel bends of 800 mm bending radius and a outer diameter of 70 mm, with straight UCN guides of various lengths inbetween. Fig. 7.22 shows the measured UCN counts after 2 s of storage for various heights. The best result was achieved using a 1200 mm long glass guide between the two bends. This resulted in a total elevation of 1300 mm above the beam port. A picture of the setup, although with a shorter glass guide, is shown in Fig. 7.23.

Between the source output port and the S-shaped beamline, an additional fast UCN shutter was installed. It was kept open during all density measurements except for the leakage measurements.

To start the storage measurements, a TTL pulse approximately 1.2 s before the start of the reactor pulse was used.

### 7.8.3   Operating conditions during the measurements

The average pulse energy of the so-called "2$" reactor pulses during the measurements was 9.5(1) MW s. The amount of deuterium in the source was 8 mol. H_2 was used as a premoderator. Both premoderator and moderator were kept at a temperature of about 6 K.

Every storage time setting was measured with three reactor pulses, which were then averaged. The operating personnel was optimising the timing between subsequent reactor pulses for comparable beam power.

The timing system was started by a TTL pulse approximately 1.2 s before the start of the reactor pulse.

7.8.4   Determination of the optimal filling time

The filling time was optimised as described in 7.3. In contrast to the continuous sources at ILL and LANL, the production pulses at the TRIGA reactor source are very short (30 ms FWHM) resulting in short UCN pulses. This results in a pronounced sharp peak in the filling time optimisation curves, which are shown for both extraction schemes in Fig. 7.24. For the vertical
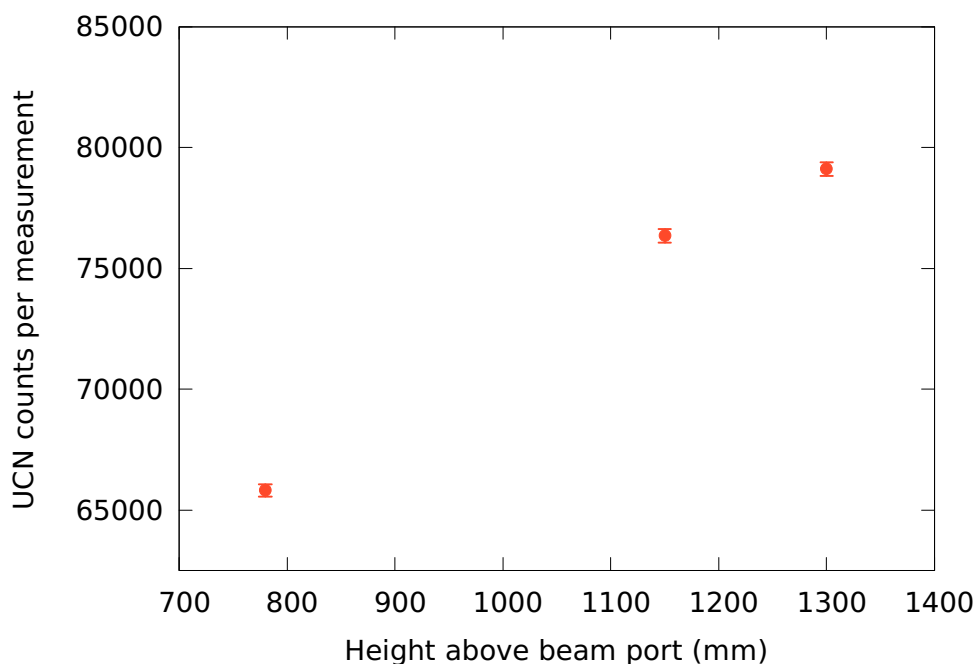
Figure 7.22: *UCN counts after 2 s of storage for mounting positions of the storage bottle at various heigths above the beam port.*

extraction scheme, a filling time of 4 s was chosen for the final measurement. For the horizontal extraction scheme, the filling time was reduced to 3 s.

The observed difference in optimal filling time can be qualitatively explained by the fact that the horizontal extraction has a threshold on detectable UCN energies because of the Fermi potential of the detector entrance window (54 neV), and is therefore insensitive to slower UCN.

7.8.5   UCN storage measurements

The storage curves recorded with vertical and horizontal extraction at a height of 1300 mm above the beam port are shown in Fig. 7.26.

Three UCN production pulses were averaged for every storage time. In order to measure the amount of UCN leaking into the storage bottle during the counting time, the additional shutter at the source output port was closed for the duration of the filling- and storage time of a measurement with a storage time of 2 s.

A total leakage of about 1000 UCN was measured, and was subtracted from the data for the density measurements.

The storage time constants were extracted from fitting the leaking UCN during 100 and 200 s storage measurements, as described in 7.4, and are shown in Table. 7.8. A typical UCN count time spectrum for storage times of 100 and 200 s is shown in Fig. 7.25.

7.8.6   UCN density

After 2 s of storage the UCN counts corresponded to the following UCN densities when using the vessel volume of $32\,044(164)$ cm^3 as given in Sec. 6.3:

- Horizontal extraction: $1.60(1)$ UCN/cm^3

- Vertical extraction: $2.43(2)$ UCN/cm^3

These values together with the corresponding subtracted leakage counts are shown in Tab. 7.9.

| Extraction	A_1	$\tau_1(s)$	A_2	$\tau_2(s)$	red.χ^2
horizontal	246(40)	12(4)	443(40)	48(3)	0.86
vertical	336(70)	18(4)	545(80)	76(9)	0.92

Table 7.8: *Fit results: Storage time constants and amplitudes at the TRIGA UCN source.*

| Extraction	Net UCN counts	Subtracted leakage counts	Density (UCN/cm³)
horizontal	51 299(215)	722(30)	1.60(1)
vertical	77 941(383)	1229(30)	2.43(2)

Table 7.9: *Results at the TRIGA Mainz: Net UCN counts in* 2 s *storage measurements, subtracted UCN leakage counts, and determined UCN density.*


Figure 7.23: *Photos of the setup at the TRIGA Mainz, beamport D. Top: Storage bottle setup with vertical extraction. Bottom: Beamline from the source port upwards to the storage bottle, shorter straight guide than in the final measurement.*
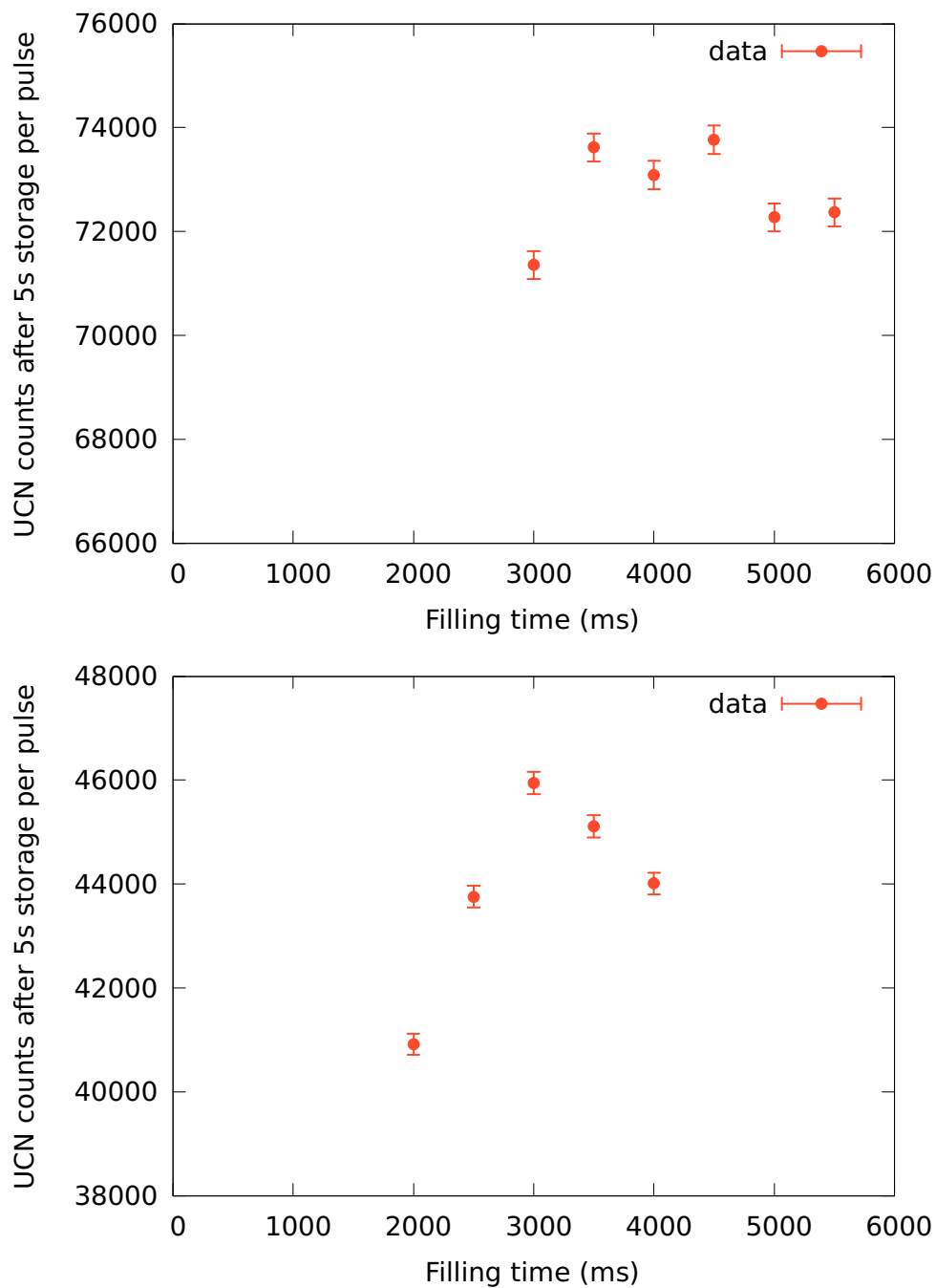
Figure 7.24: *UCN counts after* 5 s *storage vs filling time at the TRIGA source in Mainz. Top: Vertical extraction, bottom: Horizontal extraction.*
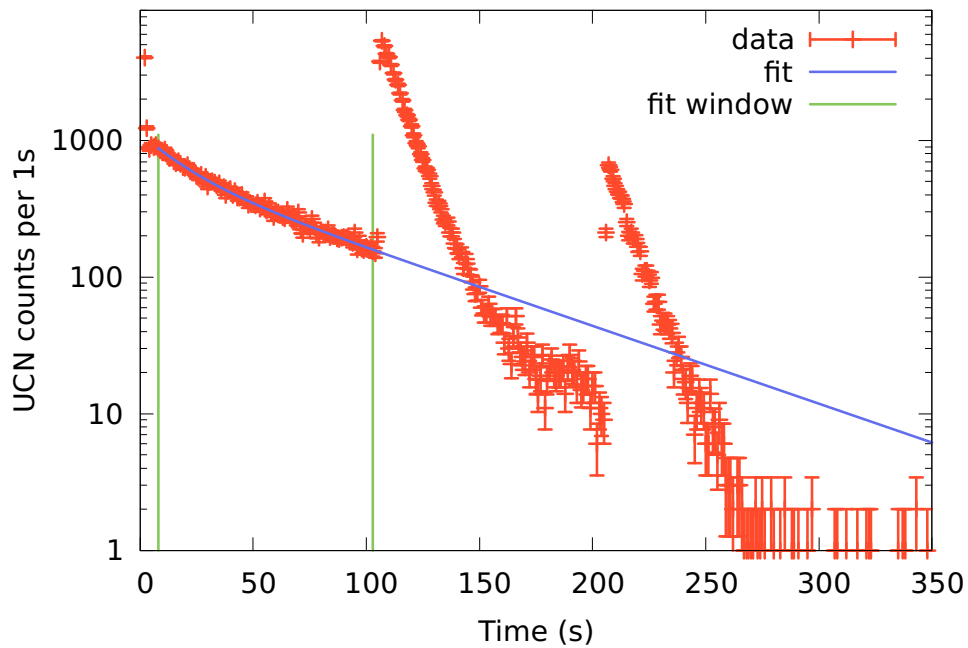
Figure 7.25: *UCN counts per* 1 s *bin, sum of four measurements with* 100 *and* 200 s *of storage time. The fit window for the evaluation of the storage time constants is indicated with vertical green lines.*
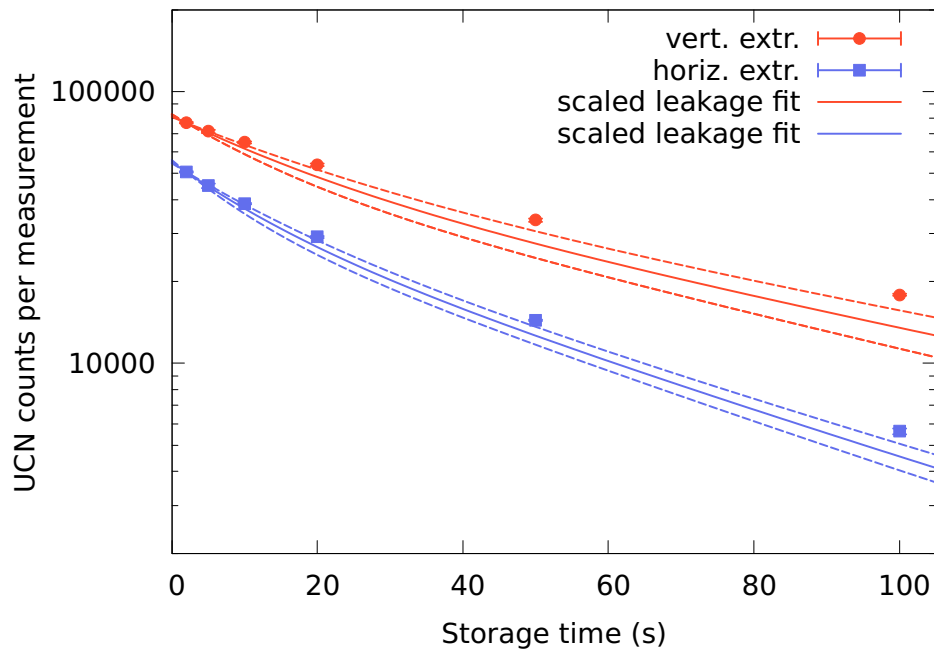
Figure 7.26: *Measured UCN counts after various storage times, measured with filling times of* 4 s *(vertical extraction) and* 3 s *(horizontal extraction) at the TRIGA UCN source. The results of the fits to the leakage rate, arbitrarily scaled, are indicated by the continuous lines, with error bands indicated by the dashed lines.*

7.9   Measurement at PSI, Dec 10 + 15 2015

At the PSI UCN source, measurements were performed at beamport West-1. In order to compensate for the influence of the built-in AlMg3 vacuum separation foil at beamport height, measurements were not only done at beamport height but also at a height of 500 mm above.

The UCN source at PSI is described in detail in Sec. 2.2.

7.9.1   Operating conditions during the measurements

Measurements at the beam height were done using 8 s long proton beam kicks every 500 s with a nominal proton beam current of 2400 μA.

At the elevated position, 8 s long kicks were repeated every 440 s with a nominal proton beam current of 2200 μA.

The trigger input for the shutter control system was connected to the WK signal, which triggers 1 s before the rising edge of the proton beam kick.

The beamline shuttern NLK-South to the South beam port was closed, NLK-W-2, to the higher beam port, was open,

7.9.2   Setup

At the West-1 beamline shutter, a 1 m long glass guide with an inner diameter of 180 mm and coated with NiMo was mounted, followed by a vacuum shutter of the same type as the beamline shutter.

For the measurements at beam height, the storage bottle was directly connected to the second shutter. For the measurements at a height of 500 mm above the beam port, the second shutter was followed by an electropolished stainless-steel 45° bend (bending radius 300 mm) with a nominal inner diameter of 200 mm, mounted at an angle of about 30° out of the horizontal plane. Attached to this bend was an electropolished stainless-steel tube of 1 m length, inner diameter 200 mm as well, and a second identical bend, to which the storage bottle was then connected parallel to the beam port. This setup is identical, except for the length of the straight stainless-steel tube, to the one described in Sec. 3.6.

Both setups can be seen in Figs. 7.27 and 7.28. The shiny guide half hidden by concrete shielding is the NiMo coated glass guide.

### 7.9.3   Determination of the optimal filling time

The filling time was optimised as usual, the resulting filling time plots are shown in Fig. 7.29. At beam height, a filling time of 26 s, was chosen, while at the elevated position, a filling time of 24 s was chosen.
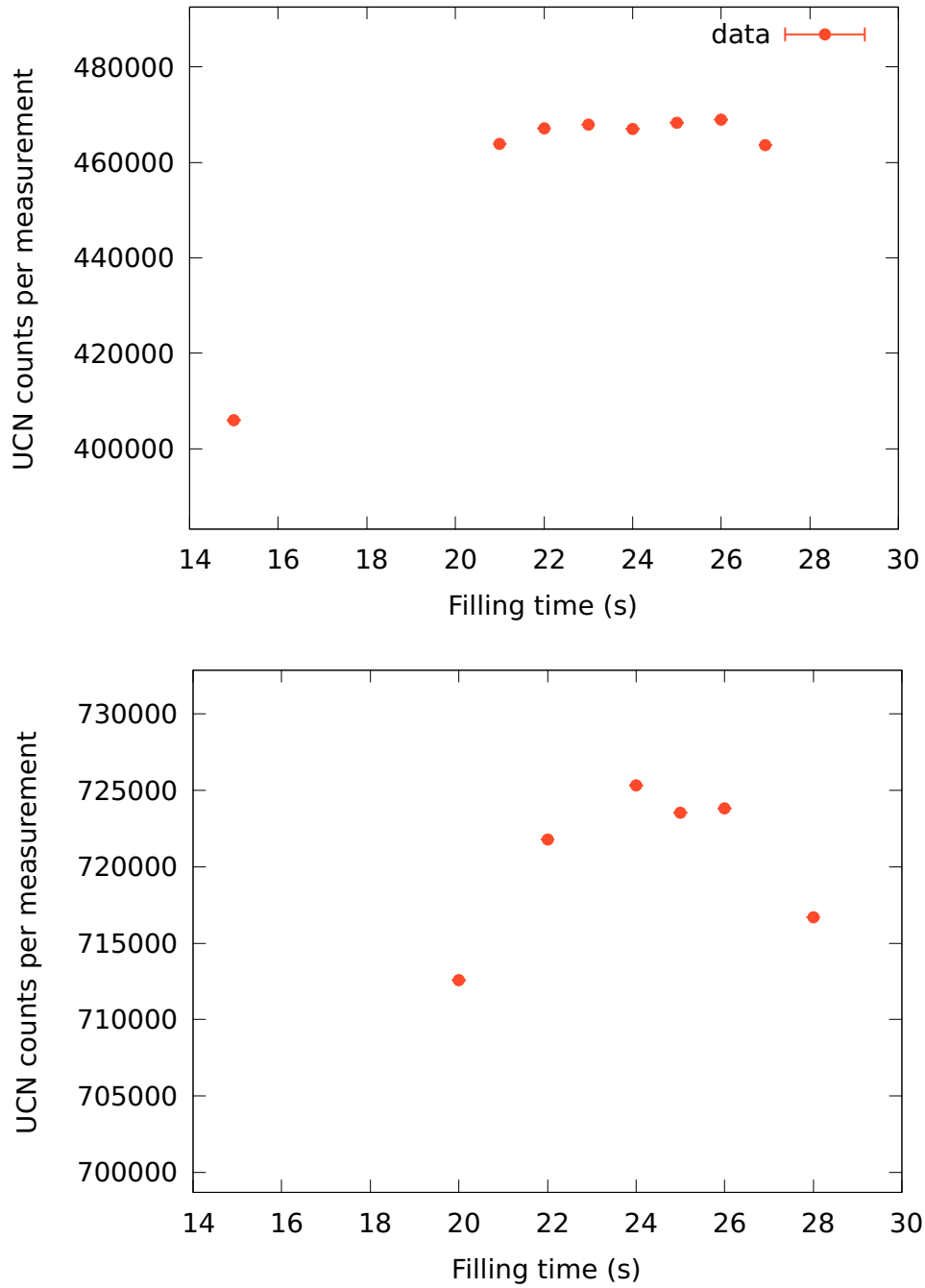
Figure 7.27: *Setup at the West-1 beamport at the PSI UCN source. Top: Setup with horizontal extraction. Bottom: Vertical extraction.*
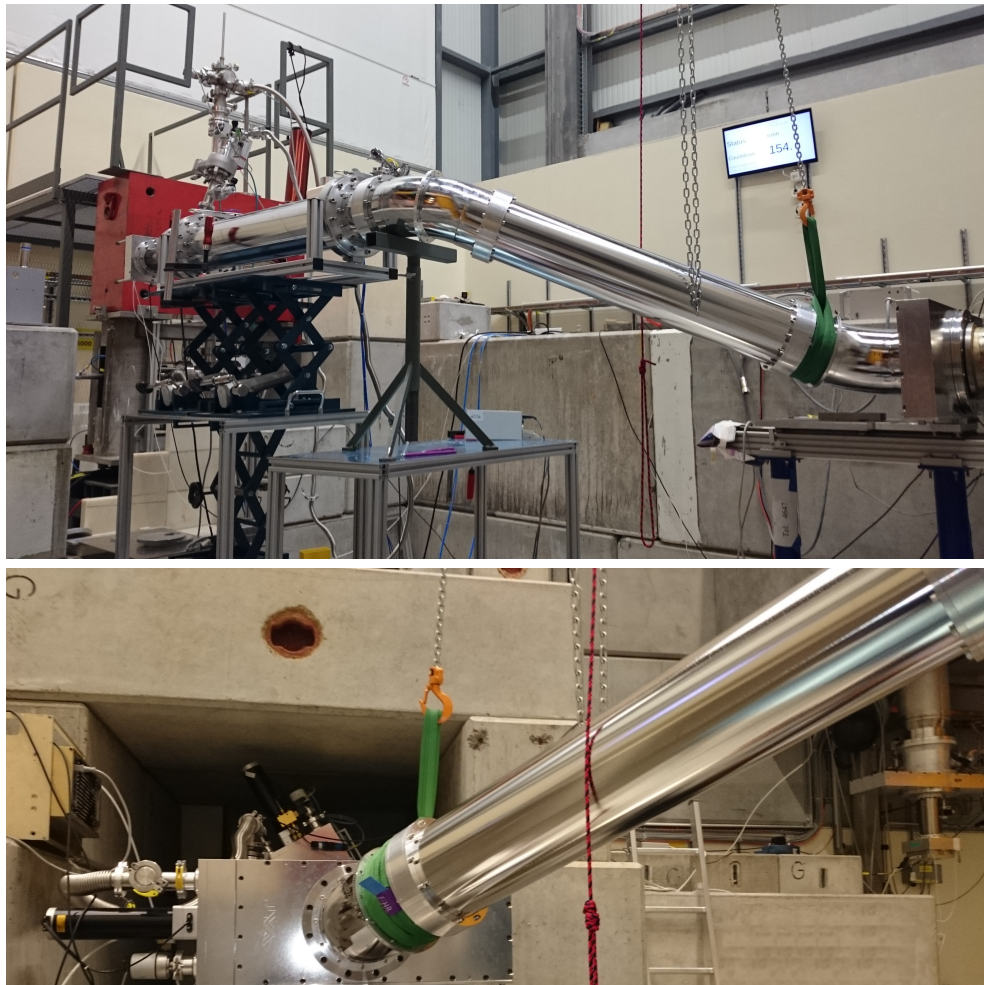
Figure 7.28: *Setup at 500 mm above the West-1 beamport at the PSI UCN source. Top: Setup with horizontal extraction. Bottom: Detailed view from below the storage bottle towards the VAT shutter.*

Figure 7.29: *Stored UCN vs filling time PSI, West-1 beamport. Top: Vertical extraction, at beam height, bottom: Vertical extraction, 500 mm above beam height.*

7.9.4   Storage

In order to keep leakage through shutter 1 to a minimum, the external VAT shutter was closed together synchronous to the bottle shutter.

An upper bound on the remaining leakage was determined by doing a measurement identical to a measurement with 2 s storage time, but with the bottle shutter 1 (and not the VAT shutter) manually set to be permanently closed. In addition, the second bottle shutter was manually kept open during the filling period in order not to accumulate UCN in the bottle. This measurement was then analysed in the same manner as a regular 2 s storage measurement.

For points measured at longer storage times, this background estimate was exponentially lowered with the long time constant determined by the fit to the leakage rate, see below. The resulting storage curves are shown in Fig. 7.31.

The storage time constants extracted from fitting the leakage rates during 100 and 200 s storage measurements, as described in 7.4, are shown in Table. 7.10. An example UCN count spectrum together with the leakage rate fit is shown in Fig. 7.30.

7.9.5   UCN density

The UCN densities corresponding to the 2 s storage measurements using the vessel volume of $32\,044(164)$ cm^3 as given in Sec. 6.3 are:
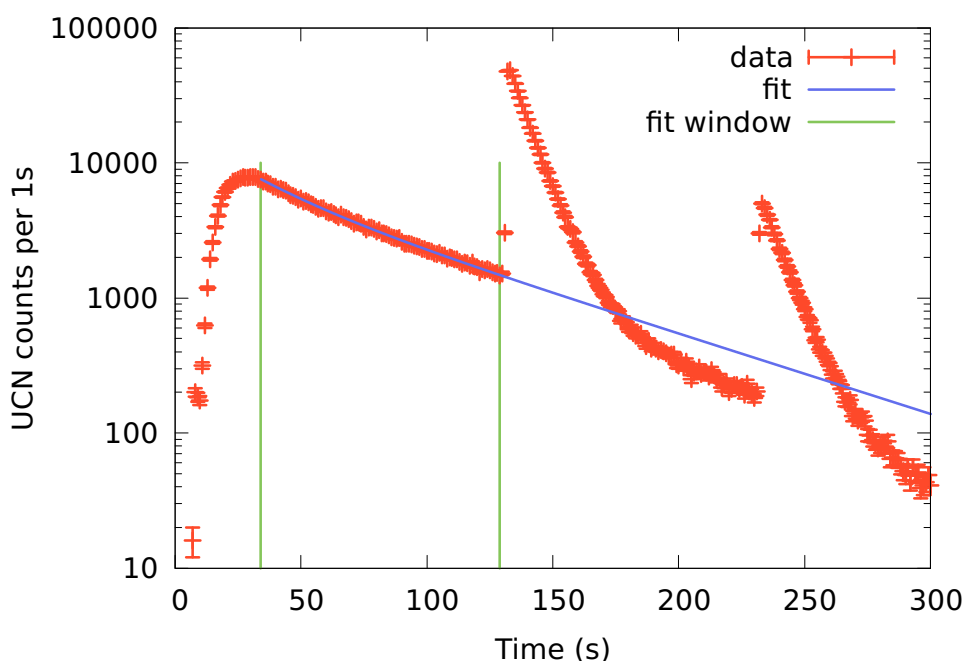
Figure 7.30: *Time spectrum of UCN counts in the detector, measured at an elevation of* 500 mm*, with vertical extraction. The double-exponential fit to the leakage rate of UCN during storage measurements with* 100 s *and* 200 s *storage time is indicated (blue line), the vertical green lines show the fit window.*
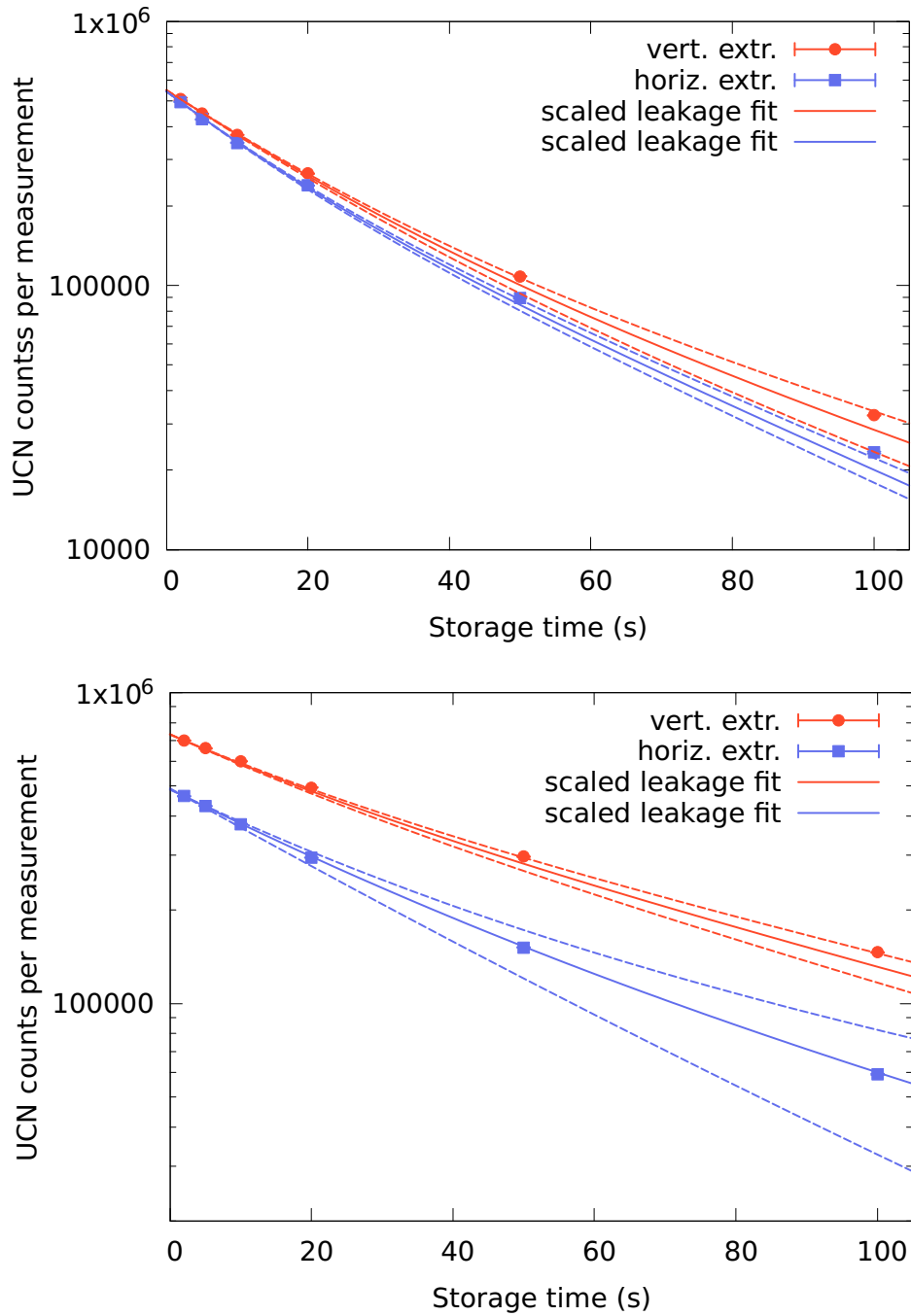
Figure 7.31: *Measured UCN counts after various storage times, measured with filling times of 26 s (at beam height) and 24 s (elevated) at the PSI UCN source. The results of the fits to the leakage rate, arbitrarily scaled, are indicated by the continuous lines, with error bands indicated by the dashed lines. Top: At beam height. Bottom: Elevated by 500 mm*

- At beamport height:

  - Horizontal extraction: 15.45(9) UCN/cm^3
  - Vertical extraction: 15.83(18) UCN/cm^3

- At 500 mm above beamport height:

  - Horizontal extraction: 14.47(8) UCN/cm^3
  - Vertical extraction: 21.87(12) UCN/cm^3

Measured UCN counts, subtracted leakage, and densities are listed in Table 7.11. Given errors are the standard deviations of the mean averaged over typically three proton beam pulses per setting.

Height (mm)	Extr.	A_1	τ_1 (s)	A_2	τ_2 (s)	red. χ^2
0	vert.	394(51)	19.7(15)	245(53)	49.0(46)	1.05
0	horiz.	211(26)	14.5(13)	275(28)	37.0(15)	1.00
500	vert.	226(66)	23.7(46)	520(68)	73.1(60)	1.11
500	horiz.	153(81)	28.7(76)	117(82)	71.9(257)	1.13

Table 7.10: *Fit results: Storage time constants of the storage bottle installed at the PSI UCN source, measured at beam height and elevated by* 500 mm.

Height (mm)	Extr.	UCN counts after storage	Leakage subtr. (counts)	Density (UCN/cm^3)
0	horiz.	510 687(1320)	15 531(125)	15.5(1)
0	vert.	523 977(5198)	16 625(129)	15.8(2)
500	horiz.	505 138(711)	41 345(203)	14.5(1)
500	vert.	767 268(925)	66 466(258)	21.9(1)

Table 7.11: *Storage results at the PSI UCN source.*

7.10   Summary and Outlook

The UCN density at all UCN sources in operation world-wide was measured. The same setup, detector, and analysis was used at all sources (with very few exceptions mentioned above). No extrapolations or corrections have been made to the tabulated results. Data from these measurements is the first complete set of comparable UCN density values, which can be used for quantitative comparison between the sources. However, the various UCN sources are so different in concept, size, and UCN energy spectrum, that a single set of such comparison measurements cannot by itself provide the full picture. For example for non-continuous sources with a production volume smaller than the bottle volume of approximately 32 L, a dilution of the available UCN density is inevitable.

The presented comparison data should therefore only be interpreted as a snapshot of any UCN source in combination with the used UCN storage bottle.
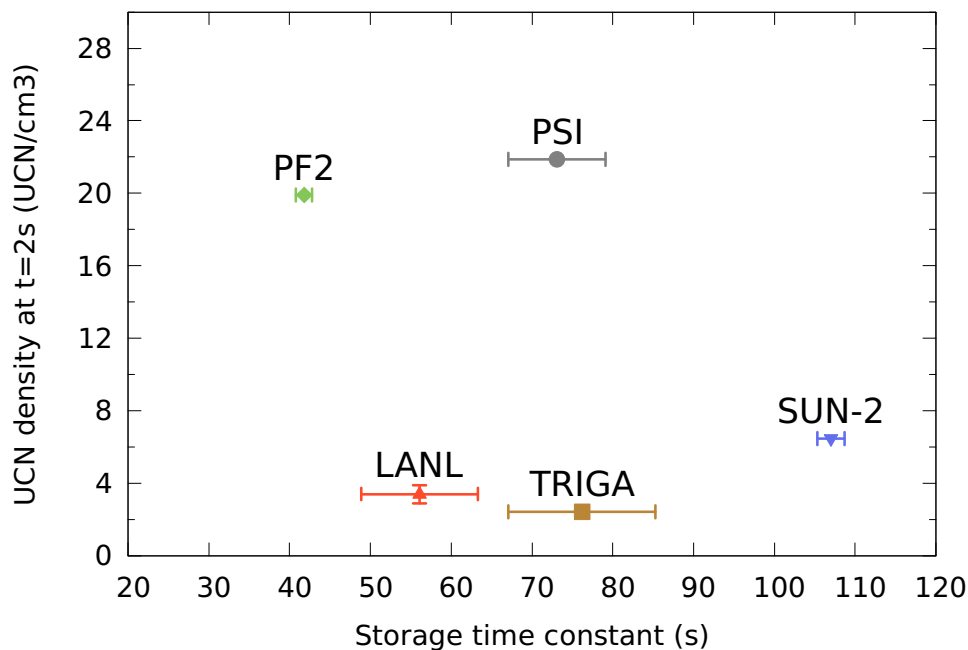
Figure 7.32: *Best measured UCN density per source versus long storage time constant. The magnitude of the long storage time constant can be interpreted as inversely correlated with the average kinetic energy of UCN at a given source. The data point for the Los Alamos source has been scaled with the factors mentioned in Sec. 7.5.6.*

The fact that the same setup was used everywhere also allows a more qualitative assessment of the UCN energy spectrum at a given source. Fig. 7.32 shows the highest measured UCN density per source versus the long storage time constant τ_2 evaluated by fitting the leakage rate through shutter 2 during long storage measurements.

Because of the kinetic energy dependence of the loss rate for UCN in a given bottle, this long storage time constant can be viewed as a measure of the average kinetic energy of the UCN.

This successful measurement campaign also provides the insight that in a small community as the operators of UCN sources are, it is possible to collaborate on a world-wide basis and provide the necessary benchmarks to the slightly larger community of UCN users.

It would be beneficial for both communities, if the now started spirit of collaboration would grow further, and would for example result in more "standard" measurements. More measurements of this kind, possibly with very different setups than the one used here, would enable experimenters to judge which source might be a good place for a given experiment on more than just the one or two parameters presented in this work.

Chapter 8

Optimisation of the UCN Source Environment at PSI

8.1 Synchronous Data Taking in Experiment Area West

8.1.1 Trigger signals

The UCN source at PSI is a pulsed source. This results in UCN intensity variations of several orders of magnitude over a time of a few hundred seconds after each proton beam kick. The energy spectrum of the UCN exiting the beam port during this period is also varying, but UCN have higher average energies close to the proton beam kick when the UCN are being produced, and lower average energies for later times, see also [Komposch, 2012].

Most UCN experiments profit from high counting statistics, however their performance and results are potentially energy spectrum dependent. Therefore, experiments acquire statistics in integer multiples of kicks and exploit the reproducible time behaviour of observed UCN counts. This requires a well defined zero-time in the recorded UCN data per kick which has to be set by external means.

Three UCN related trigger signals provided by the accelerator control system are available in the experimental areas. The signals are transmitted to the experimental areas using optical fibres, and are locally converted and fanned out to positive 5 V TTL signals on 50 Ω terminated transmission lines using Lemo 00 standard plugs.

The signal definitions are the following:

- Signal "KICK": HIGH whenever the proton beam is impinging on the UCN target, LOW when the beam is not on target.

- Signal "WK": Rising edge LOW to HIGH 1 s before the start of the main proton beam pulse for UCN production, falling edge HIGH to LOW at the end of the main proton beam kick.

- Signal "WWK": Rising edge LOW to HIGH 5 s before first pilot pulse[1], falling edge HIGH to LOW at the end of the main proton beam kick.

Fig. 8.1 shows the signals for a typical 4 s long proton beam kick, preceded by a single 7 ms pilot kick.

8.1.2   Trigger setup 2013-2015

The Cascade UCN detectors can be operated in batch mode, which means that new measurements and data files are started on external electrical or optical trigger signals. This is our chosen way to organise measurements at a pulsed source, as it results in one data file per proton beam pulse, where theoretically the time zero is always the same.

Unfortunately, for this mode of operation not one but two signals are necessary, as the last measurement has to be stopped to read all remaining data from the FPGA, before a new measurement can be started. This process takes multiple seconds to complete, depending for example on the performance of the connected read-out computer. Thus it is not possible to simply trigger on e.g. the WK signal, because only every second proton beam kick would be recorded.

Starting in 2013, the following logic was used to trigger all measurements done with Cascade detectors:

The WWK signal was split in two separate signals, where one would trigger a NIM TTL Trigger module, which in turn would send a trigger signal to stop the last measurement to the detector. The second signal would start a Lecroy "Model 222 NIM Dual Gate and Delay Generator" set to a delay of about 7 s, which was empirically found to be long enough for all used computers to stop a measurement and be ready to start again. The signal at the end of the delay would trigger the same NIM TTL Trigger module as before, which in turn would start the next measurement. As the WWK signal changes state approximately 15 s before the main proton beam kick, this

---

[1]Every main proton beam pulse is is preceded by at least one 7 ms long "pilot" pulse which is used to make sure the proton beam is centered in the beamline, or to adjust the centering if not. See Section 2.2.10 for a detailed description.
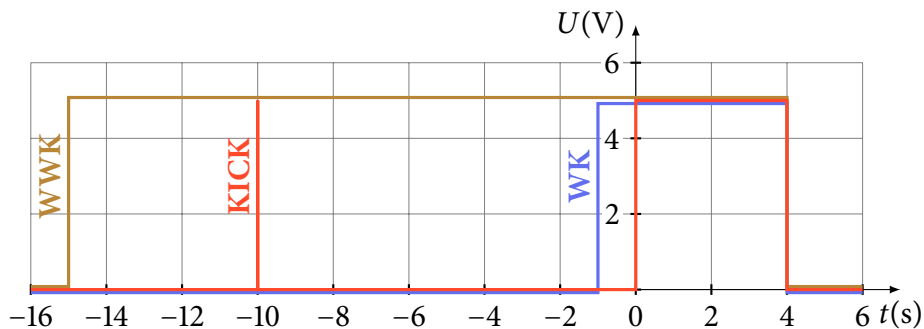
Figure 8.1: *Timing diagram of the voltage U on the trigger lines for a 4 s long proton beam kick starting at t = 0 s. WWK goes HIGH at t = −15 s, KICK goes HIGH for 7 ms during the pilot kick at t = −10 s and for 4 s at t = 0 s. WK goes HIGH at t = −1 s. All Signals go LOW at t = 4 s.*

results in about 8 s of measurement time before the start of UCN production, during which the remaining count rate due to the 7 ms long pilot pulse can be measured. Unfortunately, not the complete pilot pulse is recorded.

8.1.3   Problems with the trigger setup

The scheme explained in Sec. 8.1.2 has three major drawbacks:

1. In case of issues with centering the proton beam, multiple pilot kicks can be needed before a main kick happens. This does not happen frequently, but it is possible.

2. The precision of the WWK signal with respect to the start of the proton beam kick is reduced as optimisation processes of the proton beam line control system prior to the kick vary in execution time.

3. The WWK signal is generated by a PC in the accelerator control room, which subsequently starts the real-time proton beam kick sequence. As the PC itself is not a real-time system, the timing precision is even more reduced.

In 2015 it was found that the third listed drawback was creating problems, where the WWK signal would be off by 1 s at irregular intervals. This lead to timing offsets in the data files created by Cascade detectors, which resulted in additionally needed manual steps during analysis of kick to kick data. Fig. 8.2 shows such an issue, where one out of three measurements in the same setup has a different UCN arrival time with respect to the starting time of the detector.

8.1.4   Real-time reimplementation of the WK signal

The cause of the 1 s signal offsets was not directly investigated. Instead, the generation of the WK signal, which until that time had been implemented on the same PC, was reimplemented in a high precision real-time timing system which was in use for other timing aspects of the proton accelerator anyway.

As a result, the WK signal could be implemented in such a way, that all three drawbacks listed above are eliminated, and the WK signal switches from LOW to HIGH at the required 1 s before the main proton pulse, with sub-microsecond accuracy.

Multiple tests had to be done in order to accomplish this, but since October 2015 the new system is fully operational.

8.1.5   Conclusion and outlook

Since Autumn 2015 a high quality trigger signal 1 s before the main proton beam kick is available at all three beam ports in the experimental area at the UCN source.

From Spring 2016, this trigger signal has been used to trigger the Cascade detector in area West.

It is not possible to simply use a combination of WK and WWK in an OR configuration to trigger the detector, because it can happen that after the WWK signal has gone from LOW to HIGH, the proton beam stops, such that no proton beam kick is possible.

In this case, the detectors are stopped, but not restarted, which results in them being started and immediately stopped in all subsequent proton beam kicks.

Instead the WWK signal can be used to stop the last measurement, and the logical combination of signals shown in Fig. 8.3 to start the next measurement.

Like this, the detector is started in any case, be it on the rising edge of the WK signal or, missing any proton beam kick, at the falling edge of the WWK signal. A logic simulation for this combination of logic gates is shown in Fig. 8.4.

A prototype implementation of this trigger logic was deployed on May 17 2016.

Using the rising flank of UCN detected in a small Cascade detector directly attached to beam port West-2 as a measure of synchrony between the start of the detector and the starting time of UCN production during the proton beam kick yields the noticable result displayed in Fig. 8.5.
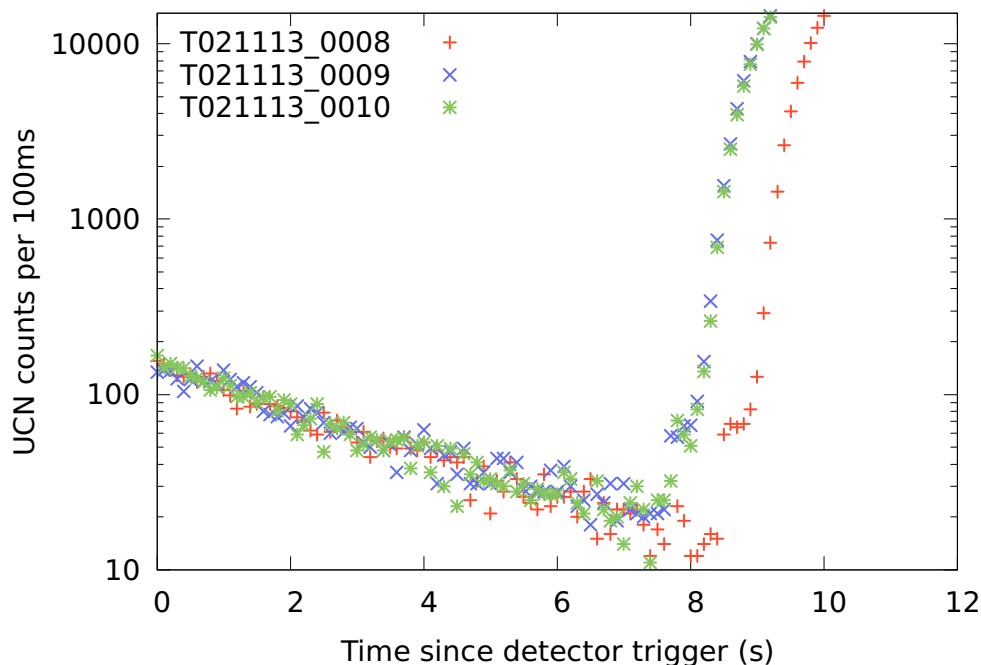

Figure 8.2: *Detector timing issue due to timing variations in the generation of the WWK signal. Three subsequent measurements with identical detector setup were recorded, in measurement 8 the rising flank of UCN counts is visible about 1 s later than in measurements 9 and 10.*
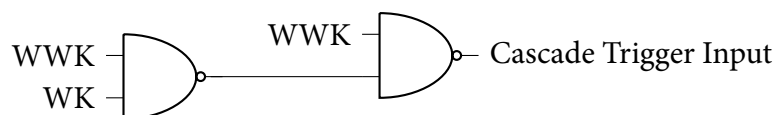
Figure 8.3: *Boolean logic diagram for a combination of WWK and WK signal to be used to start the Cascade detectors, after they have been stopped by the bare WWK signal.*
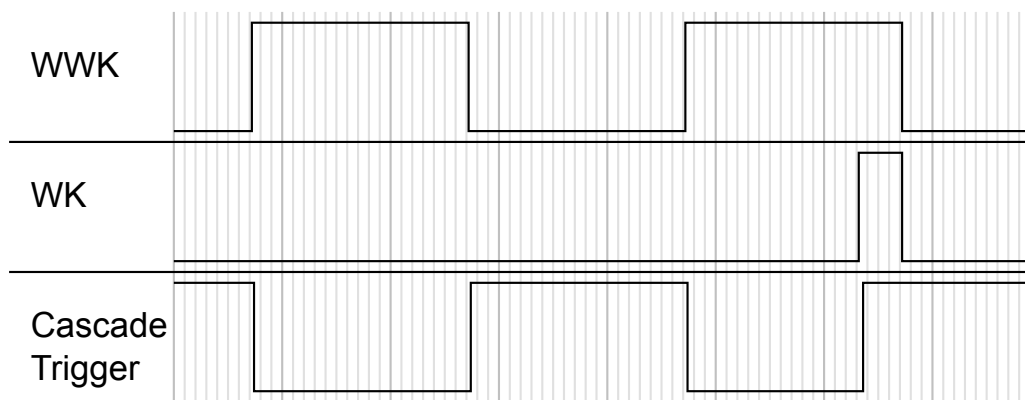
Figure 8.4: *Simulation of the Boolean logic for two trigger signals with some separation time for the Cascade detectors. Every period where WWK is HIGH simulates one sequence to produce UCN. In the left case, something goes wrong and neither WK changes to HIGH nor are UCN produced. In this case the detectors get started on the falling edge of WWK in order to be ready to be stopped again for the next kick. On the right hand side, everything works and while the WWK signal is still HIGH, the WK signal changes from LOW to HIGH and immediately triggers the detectors.*
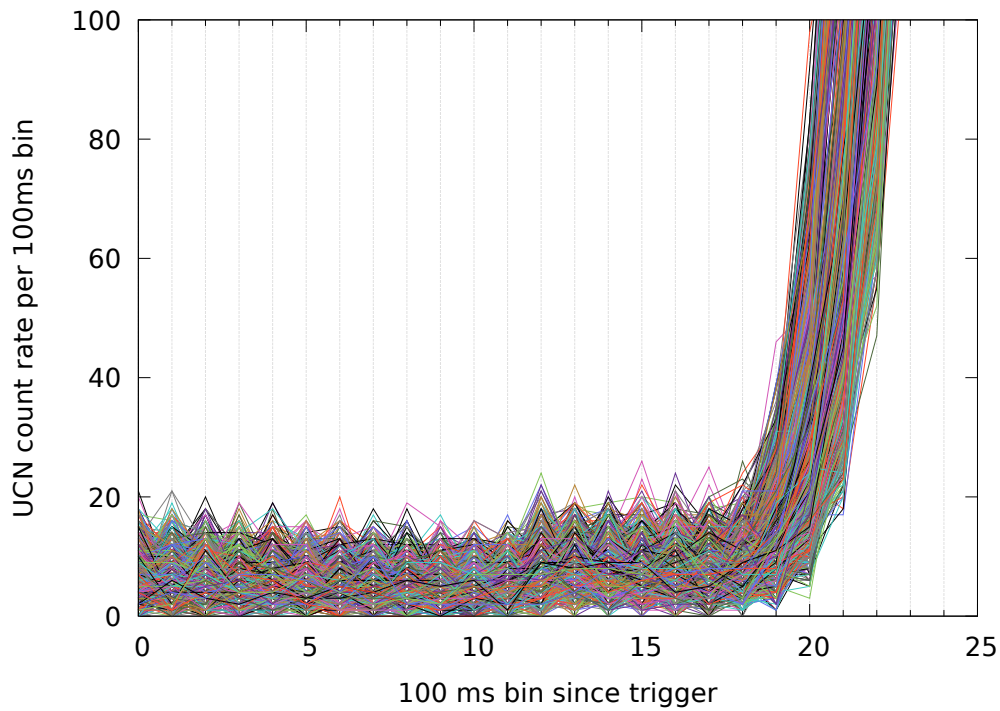
Figure 8.5: *Rising edge of the UCN count rate with respect to absolute time of the Cascade detector's data file. The detector was mounted at the West-2 beam port. More than 3000 proton beam kicks are plotted. These are all measured UCN in May 2016 starting on May 18, with the only cut being on the total amount of counts being larger than 9×10^5. The rising flank is less than 4 bins of 100 ms width wide. Not a single time-wise outlier is visible.*

8.2   Proton Beam Kick Countdown Displays

8.2.1   Motivation

UCN production at the PSI UCN source is typically done 24/7. Proton beam kicks are started automatically with a given repetition frequency. However, many experiments require manual intervention, be it to change a setting or to modify the experimental setup itself.

With typical repetition frequencies of one proton beam kick every 300 s, missing out on the first kick after a change of setup out of ignorance for when the next kick is scheduled costs counting statistics and reduces the amount of useable UCN each day.

In addition, although the UCN source is operated with radiation safety as a key requirement, the dose rate close to the beam ports is higher while the beam is on target than when the beam is away.

All this calls for a well visible proton beam kick indicator system, including the information that automatic proton beam kicks are being delivered, and when the next one is going to be.

8.2.2   Implementation

Signal handling

At the PSI proton accelerator, the Experimental Physics and Industrial Control System (EPICS) [EPICS, 2016] is used for information distribution and soft real-time signaling.

There are two EPICS channels of interest for a UCN proton beam kick indicator:

- `UCNQ:BEAMREQ:STATUS` is a status variable with the options "Running" or "Stopped", indicating whether the system which automatically generates proton beam kicks to the UCN target is active or not.

- `UCNQ:BEAMREQ:COUNTDOWN` is a numerical variable counting the seconds until the proton beam kick sequence will be initiated the next time. It is being updated every second.

The EPICS base software, which among much more provides tools to query and monitor the value of given channels, is compatible with computers running e.g. the Linux® operating system.

Hardware

Raspberry Pi model B computers are chosen as the hardware platform, together with various large computer monitors. This choice was made based on the following criteria:

- Prerequisites: Linux operating system, wired ethernet connection, monitor connection.

- Form factor: The Raspberry Pi computers are small with respect to any monitor usable for a large display. No more space than the size of the monitor dictates is needed for the installation.

- Ease of use and installation: Typical computer monitors are equipped with video input methods directly compatible with the Raspberry Pi video output. Today many computer monitors also feature USB sockets which can be used to supply the Raspberry Pi with power.

- Cost and scalability: The installation cost of an instance of the proton beam kick monitor is entirely dominated by the cost of a suitable monitor, making it feasible to install many instances.

Most later models of the Raspberry Pi computers can be used as well.

Software

A computer program was written in the Python programming language, using the pyQt bindings to the Qt graphics framework, which queries both relevant EPICS channels and displays the results on the attached screen in a prominent way. It is making use of the pyEpics interface to EPICS for Python.

The relevant code for the display of EPICS channels is shown in Listing 8.1. Apart from this, some peripheral code is used to display text in the largest possible font for any given screen size.

```python
class myEpicsDisp(myResizableQLabel):
    def __init__(
        self,
        parent,
        ca,
        defaultFontSize,
        fontScale1,
        fontScale2
    ):
        super(myEpicsDisp, self).__init__(
            parent,
            defaultFontSize,
            fontScale1,
            fontScale2
        )
        tmpvar = epics.caget(ca, timeout=10)
        epics.camonitor(ca, writer=None, callback=self.cbPrint)
        if(tmpvar == None):
            self.setText("NAN")
        else:
            self.setText(str(tmpvar))

    def cbPrint(self, value, **kwargs):
        self.setText(str(value)[:4])
```

Listing 8.1: *Definition of the "myEpicsDisp" class used to display the value of an EPICS channel, including later updates through the callback function "cbPrint".*

Fig. 8.6 shows a screenshot of one of the monitors.

8.2.3   Limitations

Unfortunately, as stated in Section 8.1.3, the time between the beginning of a proton beam kick sequence and the actual kick is not deterministic.

It is therefore intrinsically impossible to display a precise countdown to the proton beam kick.

When the countdown shared via the `UCNQ:BEAMREQ:COUNTDOWN` EPICS channel reaches zero, it takes approximately 10 s until the first pilot kick is released, and if the beam centering is OK, another 10 s until the main proton beam kick starts.

This is indicated on the displays as well.

8.2.4   Conclusion

Since 2013, multiple proton beam kick countdown monitors are in operation in the experimental areas around the UCN source. They have become a valuable tool to experimentators when planning accesses to the experimental setup changes of configuration.
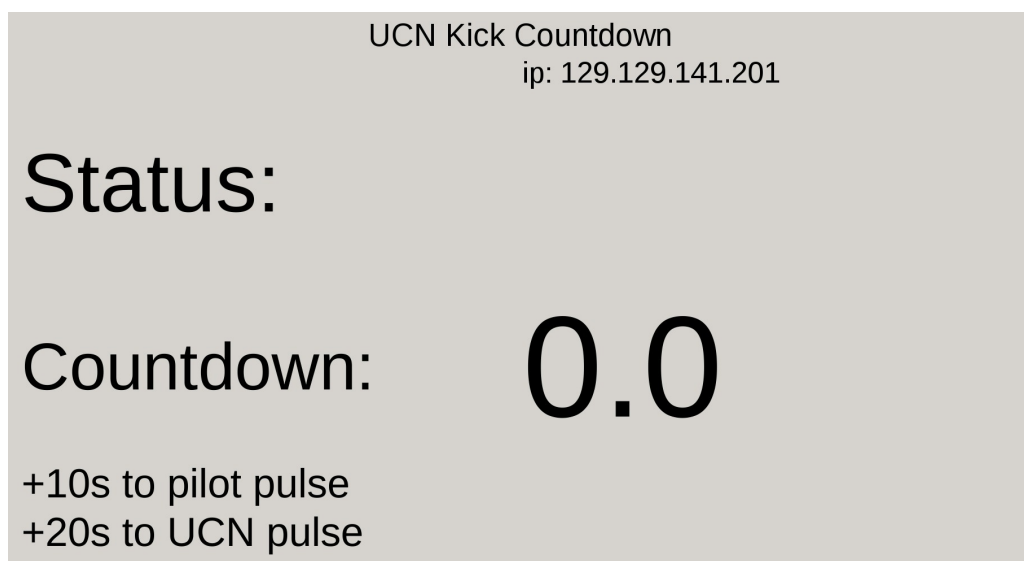
Figure 8.6: *Screenshot of a proton beam kick countdown monitor. Typically, "Status:" is either followed by "Running" or "Stopped", while "Countdown':" shows the time until the next initiation of the proton beam kick sequence in seconds.*

Chapter 9

Summary and Outlook

The source for ultracold neutrons at Paul Scherrer Institute has developed into a reliable and world-leading facility in the course of the last four years. I am grateful to have been involved in this process, and to have shaped it to a certain extent.

In this thesis, major steps on this journey, as well as the international comparison with other UCN facilities are documented.

9.1 Summary of Chapters 1 to 9

9.1.1 Chapter 1

A historical introduction to the subject of ultracold neutrons.

9.1.2 Chapter 2

A functional description of parts of the PSI UCN source and terminology relevant for the scope of this thesis.

9.1.3 Chapter 3

Several characterisation measurements have been performed in order to understand and verify the various source subsystems.

The thermal flux produced by the spallation target and heavy water tank was measured along the full height of the source vacuum tank, and found to be consistent with Monte Carlo simulations. The results are published in [Becker et al., 2015].

The production of UCN in thin films of solid deuterium was studied up to almost 8 mm thickness. A linear dependence of the UCN output on the layer thickness was found for thin layers, while for thicker layers deviations from this behaviour were found.

The storage time constant of the central storage vessel was measured, and previous measurements were re-analysed using the same analysis method. Earlier suspected trends towards decreasing storage time constants were disproven.

The transport of UCN through the guide system and central storage vessel was studied in the "Ping-Pong" measurements, which were optimised with respect to background rejection and timing reproducibility. The absolute transmission ratios were found to be consitent with analytical and Monte Carlo calculations, while for time-resolved comparison to Monte Carlo simulations more detailed modeling of the source is necessary.

The transmission of UCN through the polarising magnet was measured for field strengths up to 5 T. At the highest field strength, the transmission was found to be 0.57(1).

The UCN densitiy at beamport West-1 was measured using two different storage bottles. With a NiMo coated glass bottle, a UCN density of 21.0(1) UCN/cm³ was measured in 2013. Using a mobile storage bottle made from stainless steel, the density was measured for multiple heights above the beamport, and a peak density of 22.3(7) UCN/cm³ was measured at an elevation of approximately 500 mm above the beamport.

The dependence of UCN output to the length of the proton beam kick was measured at all three beam ports. It was also found that very long proton beam kicks, around 8 s long, can lead to a slower decrease in UCN rate from proton beam kick to proton beam kick, or can under special circumstances even lead to an increase from kick to kick.

9.1.4   Chapter 4

Optimization of the proton beam spot on the spallation target increased the UCN output by about 10 %.

The peak to peak intensity fluctuations of the UCN output from proton beam kick to proton beam kick were reduced by a factor of 3, replacing the electronics and signaling paths for the trigger of the central storage vessel flaps with a more precise system.

The average proton beam current on the UCN target was increased from 20 µA to 40 µA with the prospect of further increasing it to 60 µA in the second half of 2016. It was shown that the deuterium and cryogenic system can handle the increased heat load without issues.

9.1.5   Chapter 5

Transmission of UCN through a 5.3 cm long cell filled with deuterium gas at various pressures and temperatures was measured in a dedicated setup. The measured UCN transmissions with respect to gas pressure deviate systematically from the expected curves. Extensive systematic checks of the setup and analysis were performed, but no systematic effect could be identified.

9.1.6   Chapter 6

A robust, transportable UCN storage bottle made from stainless steel was designed, built, and characterised. The results are published in [Bison et al., 2016].

9.1.7 Chapter 7

The mobile UCN storage bottle was used to measure the UCN density at all operating UCN sources world wide. The PSI UCN source was found to be the source with the highest UCN density of 22.3(7) UCN/cm^3 after 2 s of storage time in this specific stainless steel storage bottle.

9.1.8 Chapter 8

Several optimisations to the UCN source environment have been implemented.

Trigger signals indicating the start of a proton beam kick for UCN production have been reimplemented in the proton accelerator timing system, making them reliable on the microsecond level.

Countdown displays showing the remaining time until the next proton beam kick is expected during automatic UCN production have been designed and built and are in operation at multiple points in the UCN experimental areas.

9.2 An Ongoing Journey...

Although the source for ultracold neutrons at the Paul Scherrer Institute is one of the leading UCN sources world wide, as shown in this thesis, its development is far from over.

Subsystems such as the solid deuterium can offer significant potential for improvement in UCN output. Ideas for possible upgrades are already present, but will need to be modeled and systemically evaluated more precisely in order to offer a feasible improvement at some point in the future. Models of the UCN source and attached experiments need to become as detailed as possible. The source environment for users remains an important, if often underestimated part of the UCN source ecosystem and needs to stay competitive as well.

And so I remain hopeful that someday a PhD student will happily report the first Norm-Kick with more than 50 million UCN to the group, only saddened by the fact that once again an apero is due.

Appendix

A   Storage Time Fit Graphics

A.1   LANL
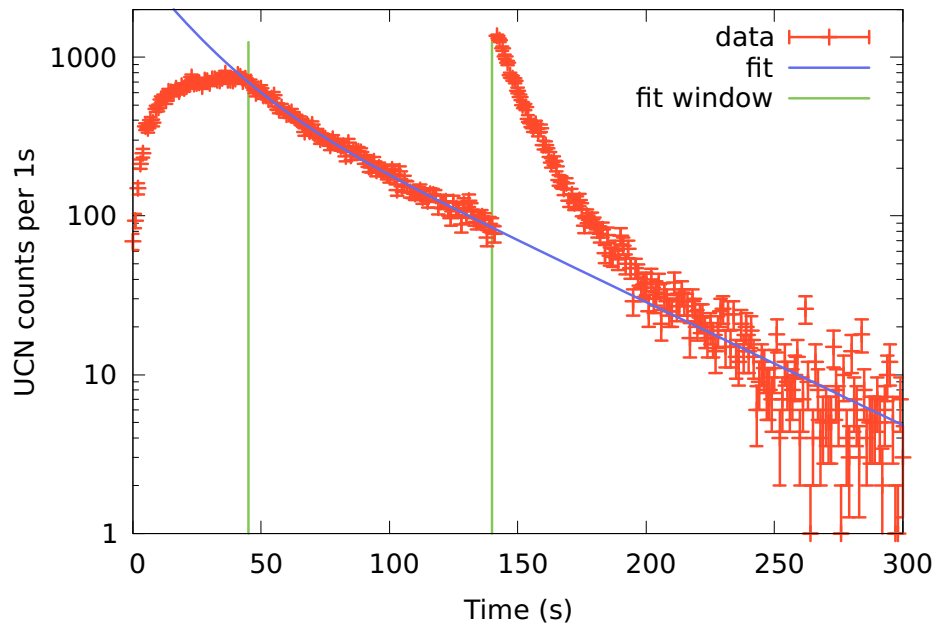
Figure 1: *Fit to Leakage Rate of UCN during* 100 s *or longer Storage Measurements at LANL. Horizontal Extraction of UCN to the Detector.*

A.2 SUN2, UCN Accumulation Time: 600 s
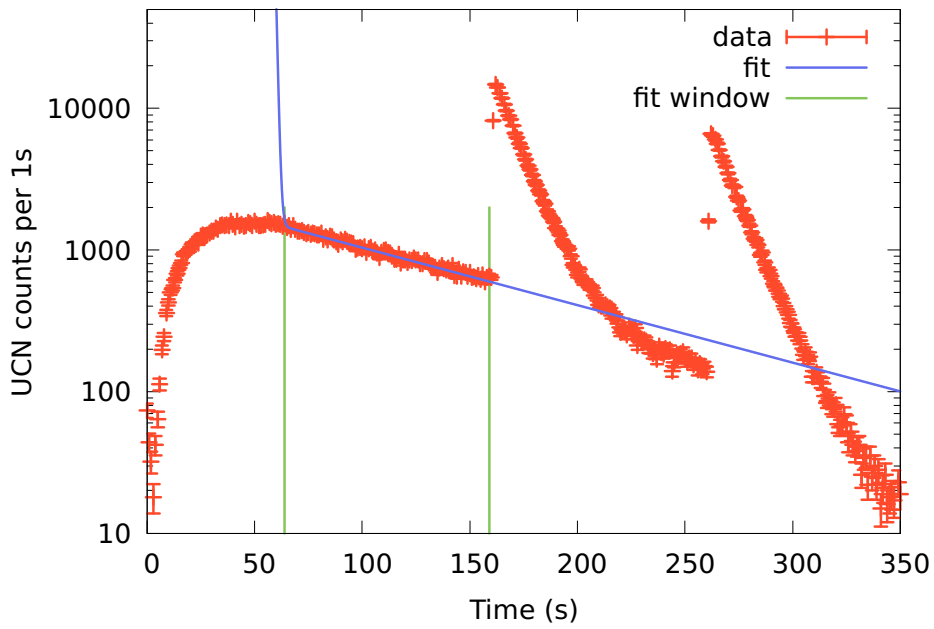
Figure 2: *Fit to Leakage Rate of UCN during* 100 s *or longer Storage Measurements at SUN2. Vertical Extraction of UCN to the Detector.*
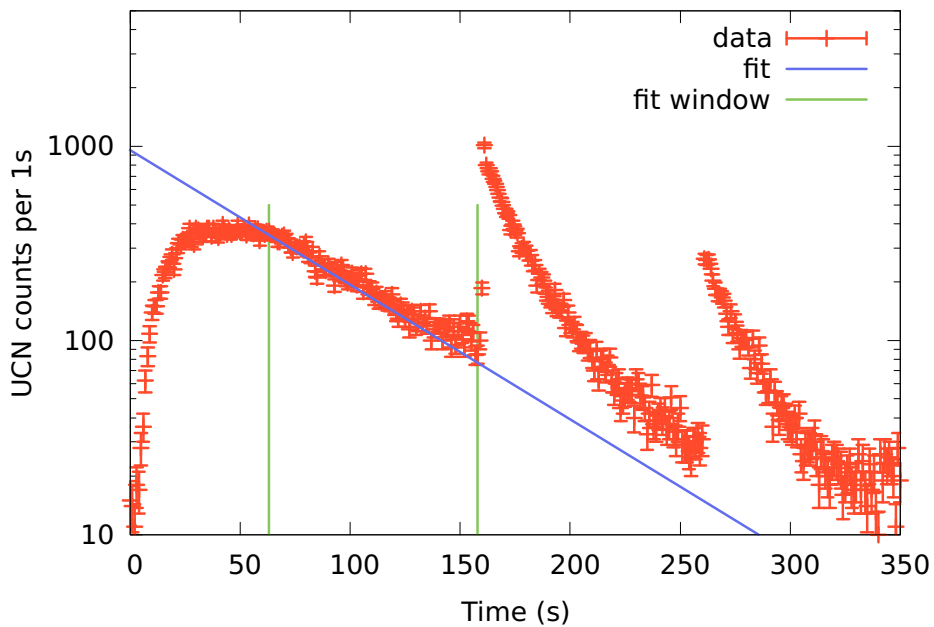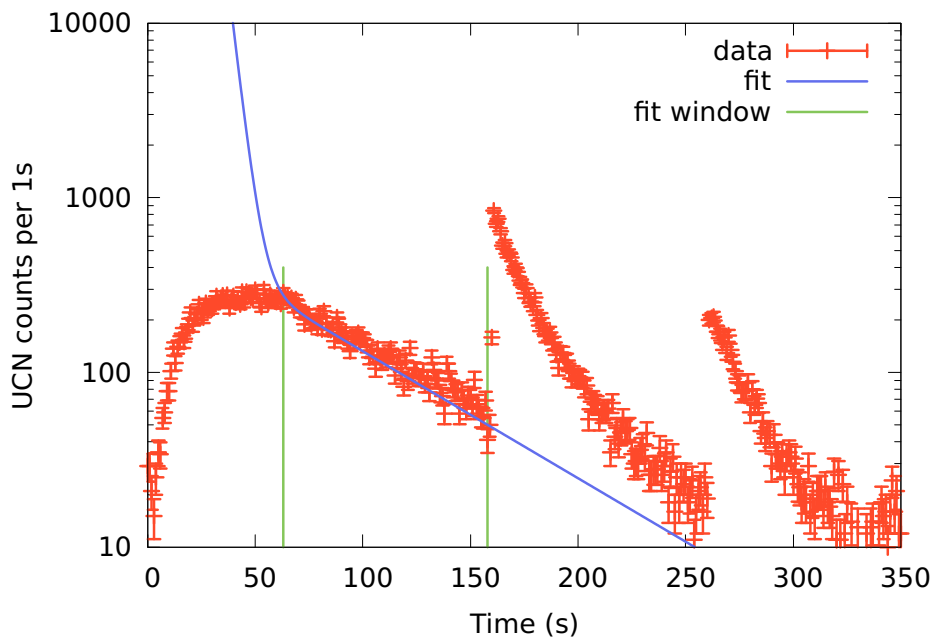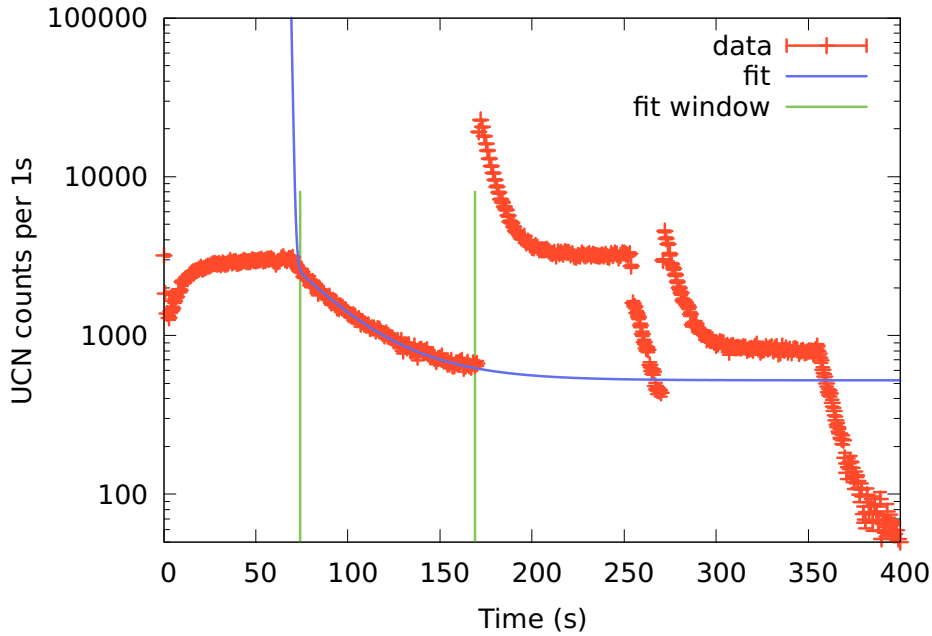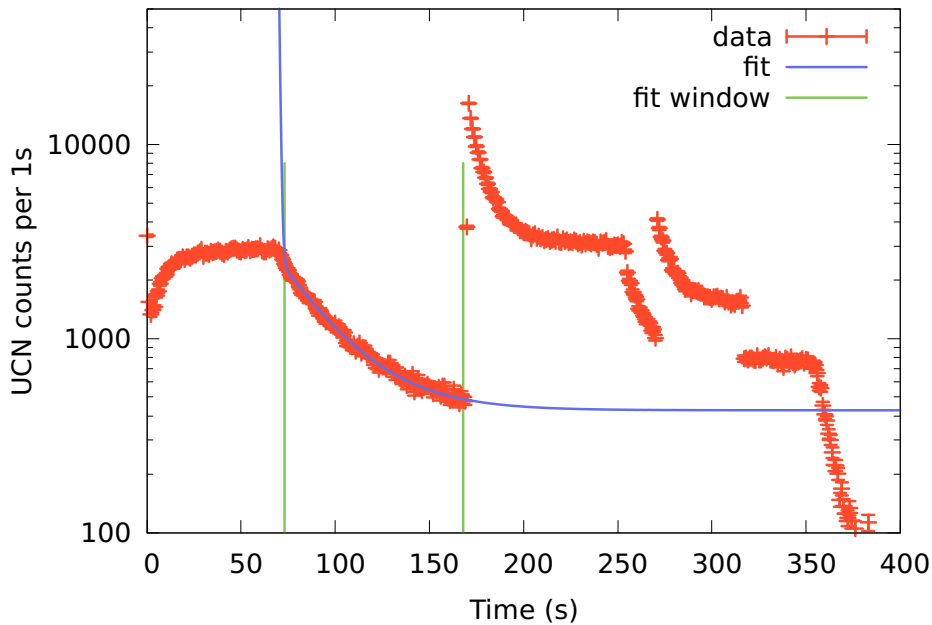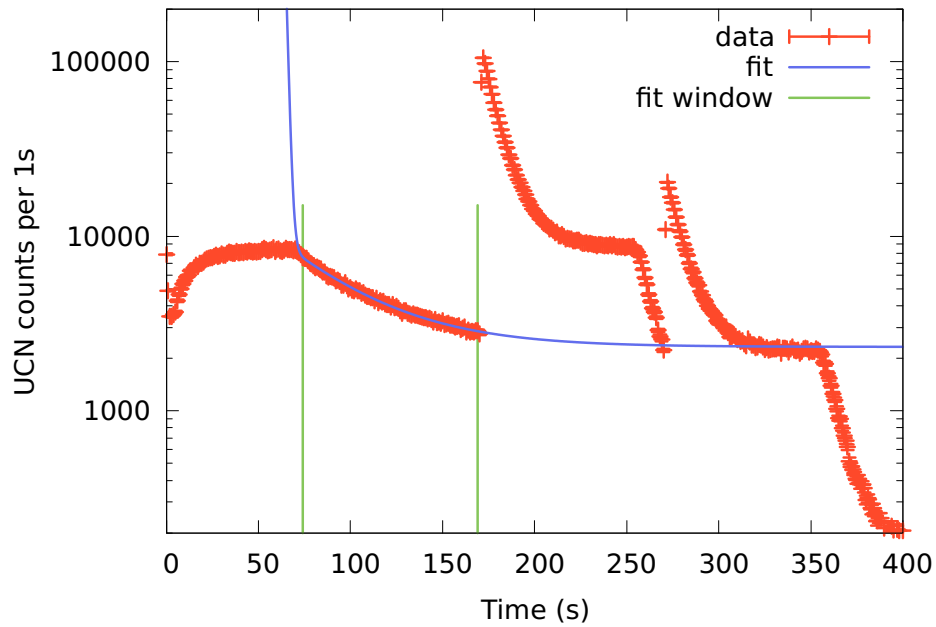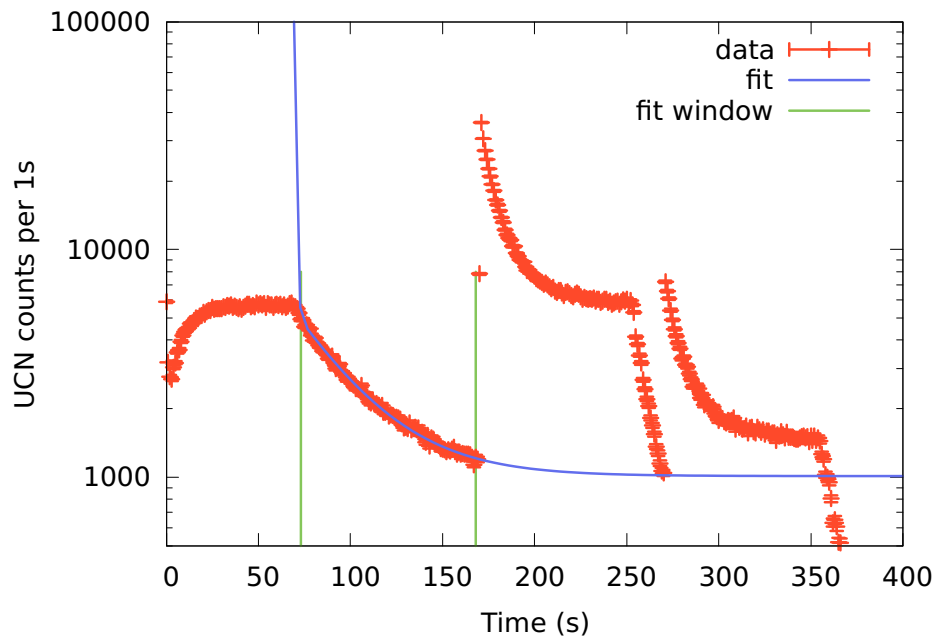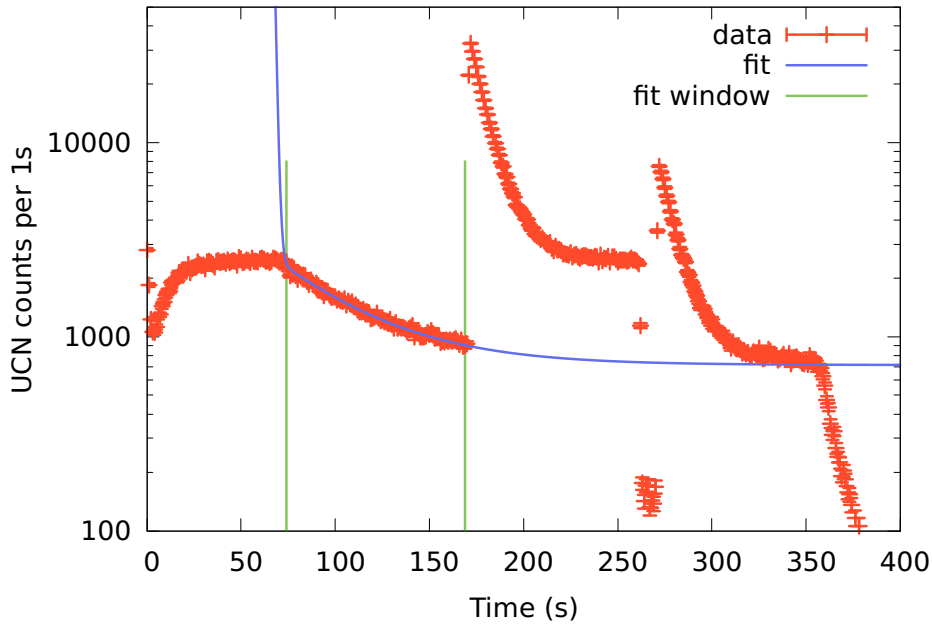

Figure 3: *Fit to Leakage Rate of UCN during* 100 s *or longer Storage Measurements at SUN2. Horizontal Extraction of UCN to the Detector.*

A.3   SUN2, UCN Accumulation Time: 300 s
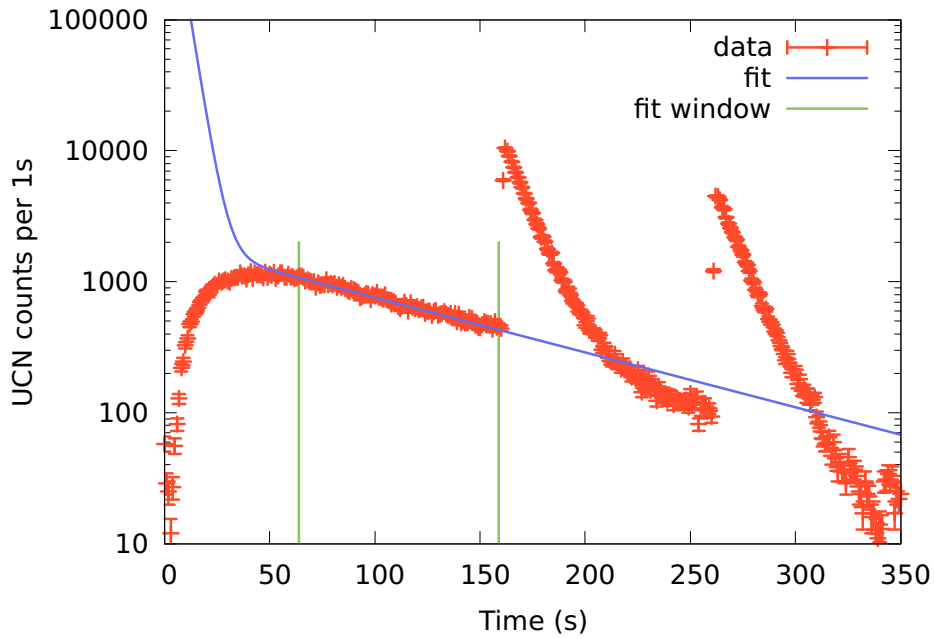
Figure 4: *Fit to Leakage Rate of UCN during* 100 s *or longer Storage Measurements at SUN2. Vertical Extraction of UCN to the Detector.*
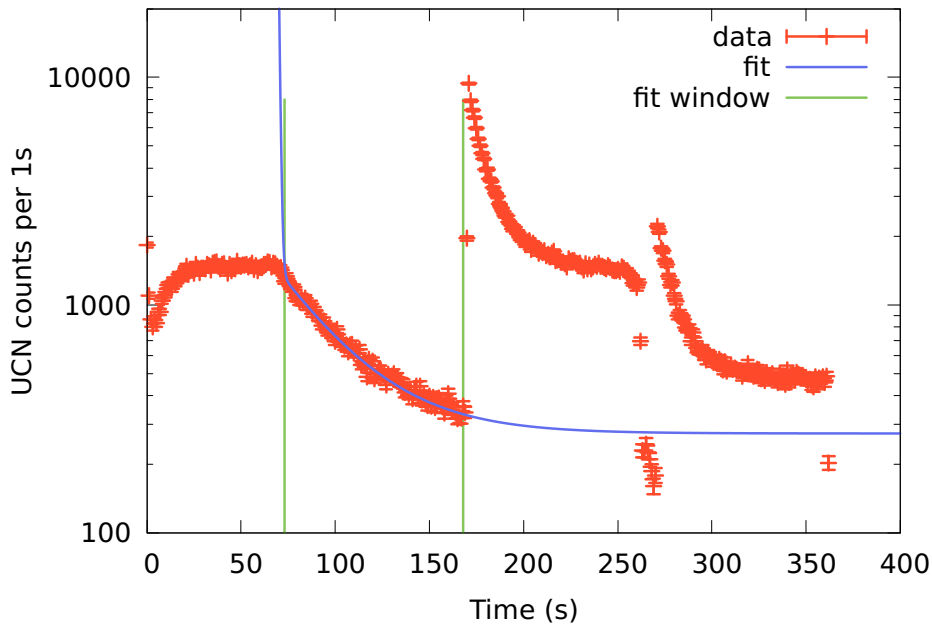

Figure 5: *Fit to Leakage Rate of UCN during* 100 s *or longer Storage Measurements at SUN2. Horizontal Extraction of UCN to the Detector.*

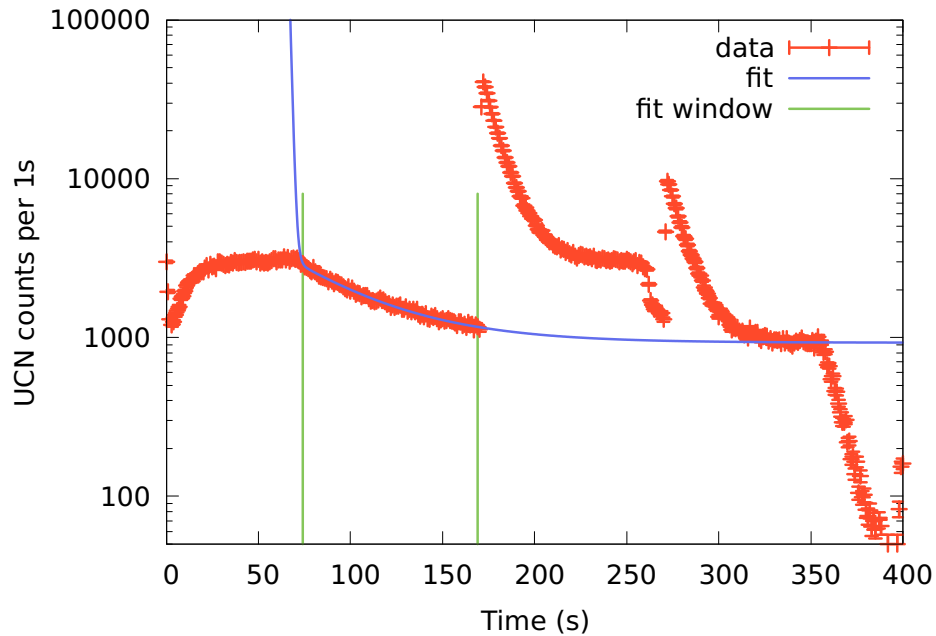## A.4 PF2, At Turbine Height, With Vacuum Safety Foil

Figure 6: *Fit to Leakage Rate of UCN during* 100 s *or longer Storage Measurements at PF2. With Vacuum Safety Foil, Vertical Extraction of UCN to the Detector.*
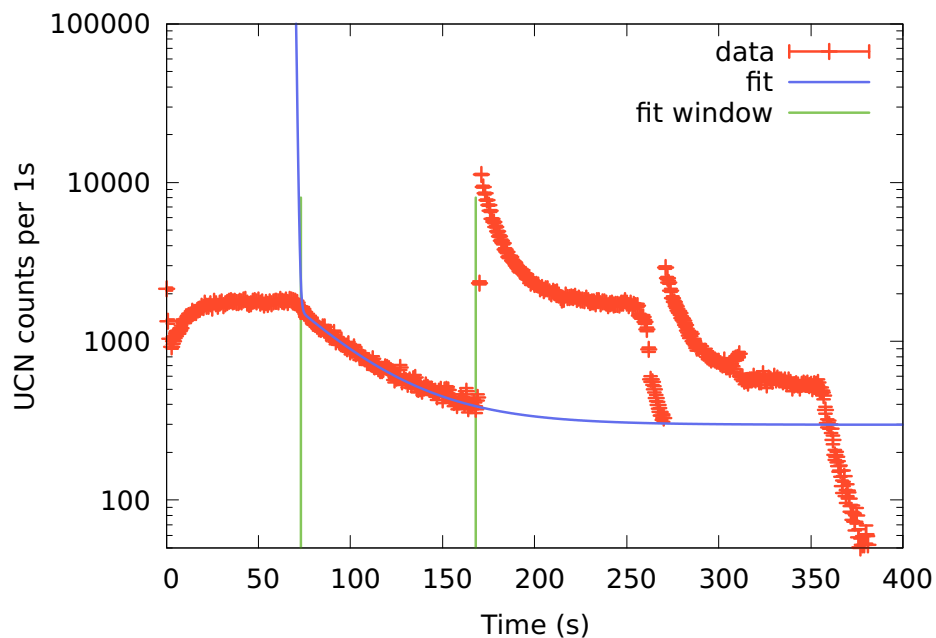

Figure 7: *Fit to Leakage Rate of UCN during* 100 s *or longer Storage Measurements at PF2. With Vacuum Safety Foil, Horizontal Extraction of UCN to the Detector.*

## A.5   PF2, At Turbine Height, Without Vacuum Safety Foil

Figure 8: *Fit to Leakage Rate of UCN during* 100 s *or longer Storage Measurements at PF2. Without Vacuum Safety Foil, Vertical Extraction of UCN to the Detector.*

Figure 9: *Fit to Leakage Rate of UCN during* 100 s *or longer Storage Measurements at PF2. Without Vacuum Safety Foil, Horizontal Extraction of UCN to the Detector.*

A.6   PF2, At the Top of the Platform, With Vacuum Safety Foil

Figure 10: *Fit to Leakage Rate of UCN during* 100 s *or longer Storage Measurements at PF2. With Vacuum Safety Foil, Vertical Extraction of UCN to the Detector.*
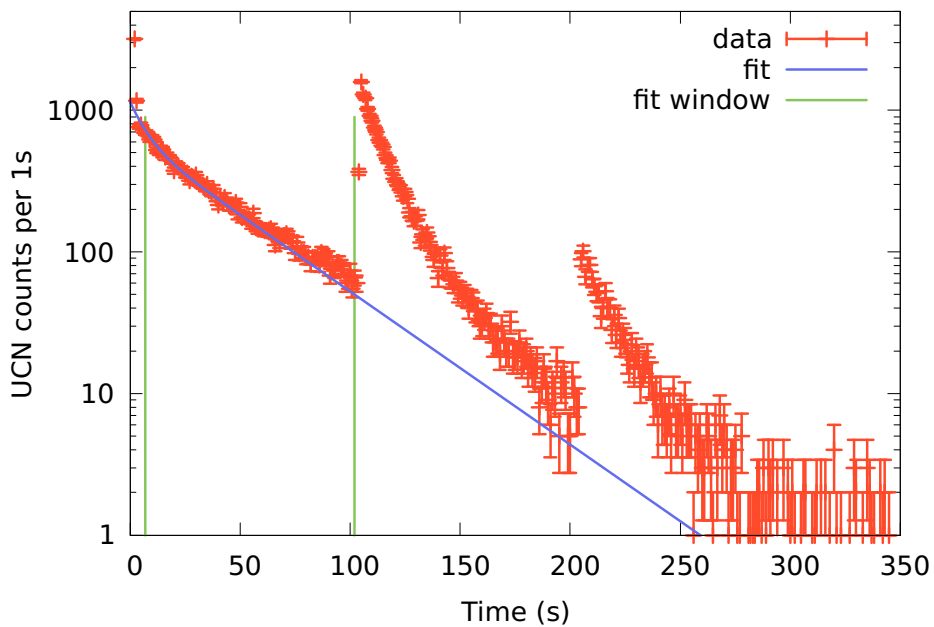

Figure 11: *Fit to Leakage Rate of UCN during* 100 s *or longer Storage Measurements at PF2. With Vacuum Safety Foil, Horizontal Extraction of UCN to the Detector.*

A.7   PF2, At the Top of the Platform, Without Vacuum Safety Foil

Figure 12: *Fit to Leakage Rate of UCN during* 100 s *or longer Storage Measurements at PF2. Without Vacuum Safety Foil, Vertical Extraction of UCN to the Detector.*

Figure 13: *Fit to Leakage Rate of UCN during* 100 s *or longer Storage Measurements at PF2. Without Vacuum Safety Foil, Horizontal Extraction of UCN to the Detector.*

A.8 TRIGA
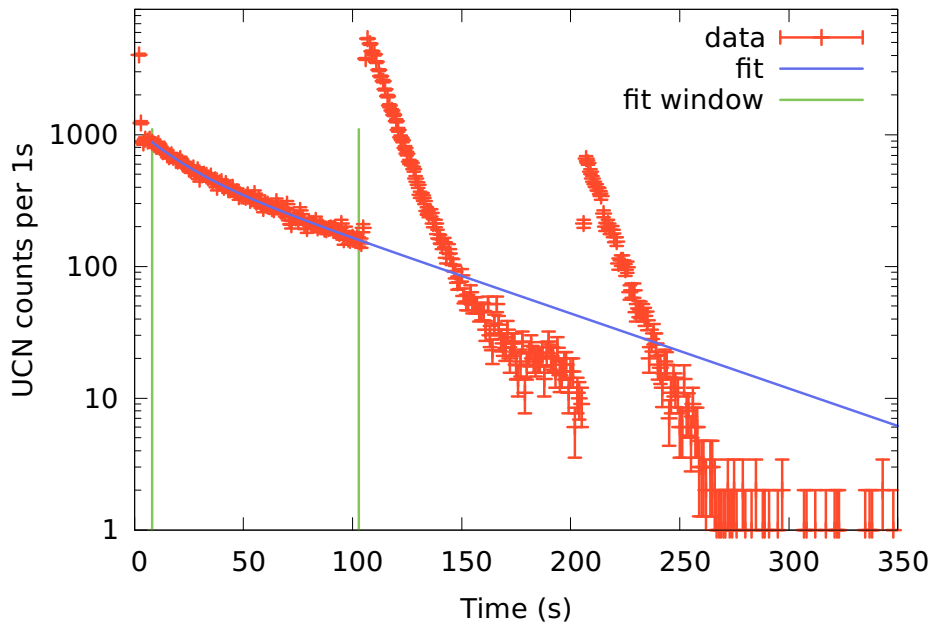
Figure 14: *Fit to Leakage Rate of UCN during* 100 s *or longer Storage Measurements at TRIGA. Vertical Extraction of UCN to the Detector.*
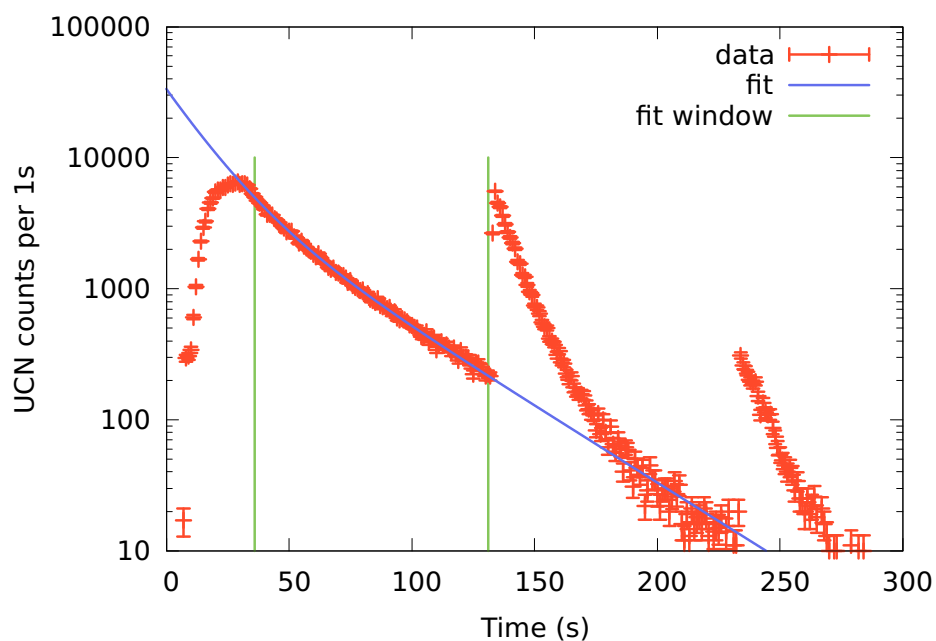

Figure 15: *Fit to Leakage Rate of UCN during* 100 s *or longer Storage Measurements at TRIGA. Horizontal Extraction of UCN to the Detector.*
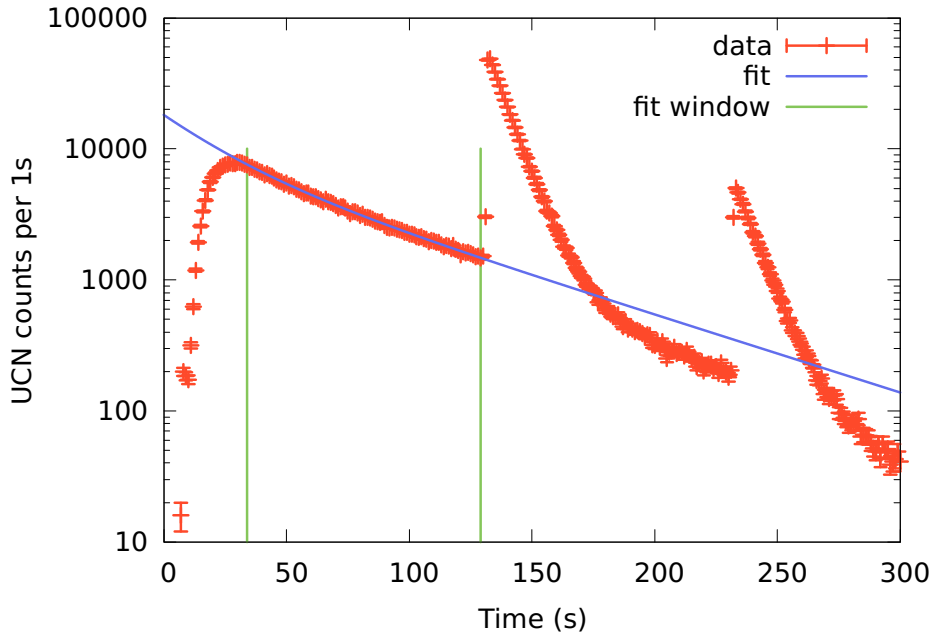
A.9   PSI, At Beam Height
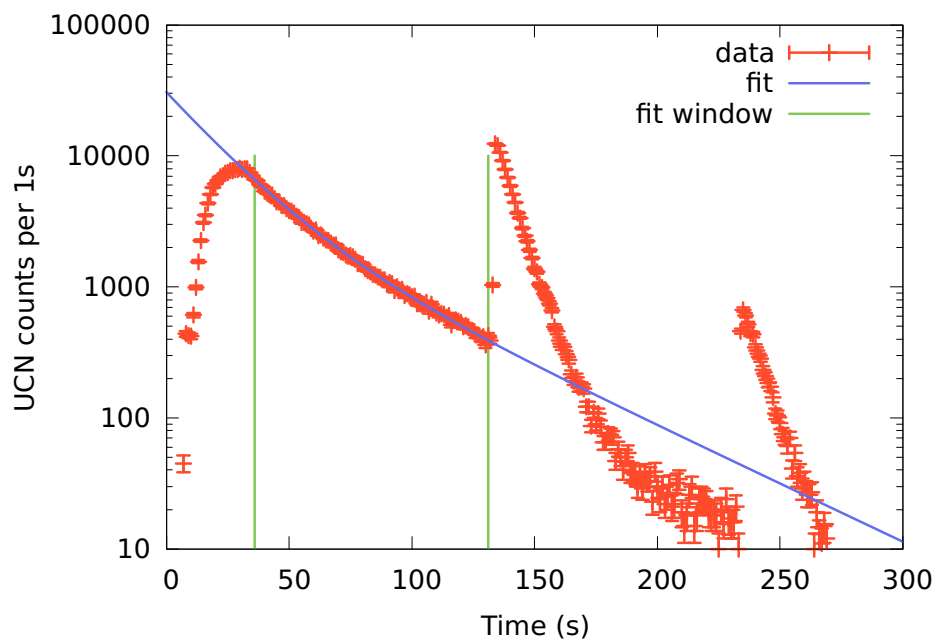
Figure 16: *Fit to Leakage Rate of UCN during* 100 s *or longer Storage Measurements at PSI. Vertical Extraction of UCN to the Detector.*
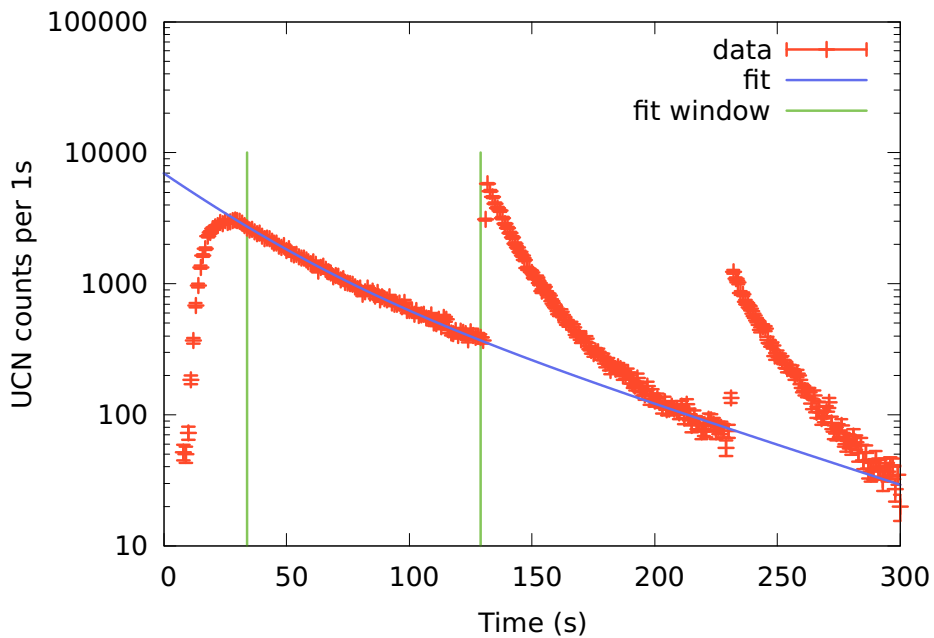

Figure 17: *Fit to Leakage Rate of UCN during* 100 s *or longer Storage Measurements at PSI. Horizontal Extraction of UCN to the Detector.*

A.10 PSI, Elevated by 500 mm

Figure 18: *Fit to Leakage Rate of UCN during* 100 s *or longer Storage Measurements at PSI. Vertical Extraction of UCN to the Detector.*

Figure 19: *Fit to Leakage Rate of UCN during* 100 s *or longer Storage Measurements at PSI. Horizontal Extraction of UCN to the Detector.*

# B	Acknowledgements

Bibliography

[Afach et al., 2015] Afach, S., Ban, G., Bison, G., Bodek, K., Chowdhuri, Z., Daum, M., Fertl, M., Franke, B., Geltenbort, P., Grujić, Z. D., Hayen, L., Hélaine, V., Henneck, R., Kasprzak, M., Kermaïdic, Y., Kirch, K., Komposch, S., Kozela, A., Krempel, J., Lauss, B., Lefort, T., Lemière, Y., Mtchedlishvili, A., Naviliat-Cuncic, O., Piegsa, F. M., Pignol, G., Prashanth, P. N., Quéméner, G., Rawlik, M., Ries, D., Rebreyend, D., Roccia, S., Rozpedzik, D., Schmidt-Wellenburg, P., Severijns, N., Weis, A., Wursten, E., Wyszynski, G., Zejma, J., and Zsigmond, G. (2015). A device for simultaneous spin analysis of ultracold neutrons. *Eur. Phys. J.*, A51(11):143. `arXiv:1502.06876, doi:10.1140/epja/i2015-15143-7`. 74

[Altarev et al., 2008] Altarev, I., Daum, M., Frei, A., Gutsmiedl, E., Hampel, G., Hartmann, F., Heil, W., Knecht, A., Kratz, J., Lauer, T., Meier, M., Paul, S., Schmidt, U., Sobolev, Y., Wiehl, N., and Zsigmond, G. (2008). Neutron velocity distribution from a superthermal solid sd_2 ultracold neutron source. *The European Physical Journal A - Hadrons and Nuclei*, 37:9–14. 10.1140/epja/i2008-10604-8. URL: `http://dx.doi.org/10.1140/epja/i2008-10604-8`. 150, 179

[Anicic et al., 2005] Anicic, D., Daum, M., Dzieglewski, G., George, D., Horvat, M., Janser, G., Jenni, F., Jirousek, I., Kirch, K., Korhonen, T., Künzi, R., Mezger, A. C., Rohrer, U., and Tanner, L. (2005). A fast kicker magnet for the PSI 600 MeV proton beam to the PSI ultra-cold neutron source. *Nuclear Instruments and Methods in Physics Research A*, 541:598–609. `doi:10.1016/j.nima.2004.12.032`. 30, 34

[Arzumanov et al., 2012] Arzumanov, S. S., Bondarenko, L. N., Morozov, V. I., Panin, Y. N., and Chernyavsky, S. M. (2012). Analysis and correction of the measurement of the neutron lifetime. *JETP Letters*, 95(5):224–228. `doi:10.1134/S0021364012050025`. 22

[Atchison et al., 2007a] Atchison, F., Blau, B., Bodek, K., van den Brandt, B., Bryś, T., Daum, M., Fierlinger, P., Frei, A., Geltenbort, P., Hautle, P., Henneck, R., Heule, S., Holley, A., Kasprzak, M., Kirch, K., Knecht, A., Konter, J. A., Kuźniak, M., Liu, C.-Y., Morris, C. L., Pichlmaier, A., Plonka, C., Pokotilovski, Y., Saunders, A., Shin, Y., Tortorella, D., Wohlmuther, M., Young, A. R., Zejma, J., and Zsigmond, G. (2007a). Cold neutron energy dependent production of ultracold neutrons in solid deuterium. *Phys. Rev. Lett.*, 99:262502. URL: `http://link.aps.org/doi/10.1103/PhysRevLett.99.262502, doi:10.1103/PhysRevLett.99.262502`. 31

[Atchison et al., 2005a] Atchison, F., Blau, B., Brandt, B. v. d., T., B., Daum, M., Fierlinger, P., Hautle, P., Henneck, R., Heule, S., Kasprzak, M., Kirch, K., Kohlbrecher, J., Kuehen, G., Konter, J. A., Pichlmaier, A., Wokaun, A., Bodek, K., Geltenbort, P., and Zmeskal, J. (2005a). Measured total cross sections of slow neutrons scattered by solid deuterium and implications for ultracold neutron sources. *Phys. Rev. Lett.*, 95:182502. URL: `http://link.aps.org/doi/10.1103/PhysRevLett.95.182502`, `doi:10.1103/PhysRevLett.95.182502`. 41, 179

[Atchison et al., 2007b] Atchison, F., Blau, B., Daum, M., Fierlinger, P., Geltenbort, P., Gupta, M., Henneck, R., Heule, S., Kasprzak, M., Knecht, A., Kuźniak, M., Kirch, K., Meier, M., Pichlmaier, A., Reiser, R., Theiler, B., Zimmer, O., and Zsigmond, G. (2007b). Measurement of the fermi potential of diamond-like carbon and other materials. *Nuclear Instruments and Methods in Physics Research Section B: Beam Interactions with Materials and Atoms*, 260(2):647 – 656. `doi:http://dx.doi.org/10.1016/j.nimb.2007.04.253`. 31

[Atchison et al., 2005b] Atchison, F., Brandt, B. v. d., T., B., Daum, M., Fierlinger, P., Hautle, P., Henneck, R., Heule, S., Kasprzak, M., Kirch, K., Konter, J. A., Michels, A., Pichlmaier, A., Wohlmuther, M., Wokaun, A., Bodek, K., Szerer, U., Geltenbort, P., Zmeskal, J., and Pokotilovskiy, Y. (2005b). Measured total cross sections of slow neutrons scattered by gaseous and liquid $^2H_2$. *Phys. Rev. Lett.*, 94:212502. `doi:10.1103/PhysRevLett.94.212502`. 108

[Baessler et al., 2011] Baessler, S., Beau, M., Kreuz, M., Kurlov, V. N., Nesvizhevsky, V. V., Pignol, G., Protasov, K. V., Vezzu, F., and Voronin, A. Y. (2011). The GRANIT spectrometer. *Comptes Rendus Physique*, 12(8):707 – 728. `doi:http://dx.doi.org/10.1016/j.crhy.2011.04.010`. 24, 145

[Baker et al., 2011] Baker, C., Ban, G., Bodek, K., Burghoff, M., Chowdhuri, Z., Daum, M., Fertl, M., Franke, B., Geltenbort, P., Green, K., van der Grinten, M., Gutsmiedl, E., Harris, P., Henneck, R., Iaydjiev, P., Ivanov, S., Khomutov, N., Kasprzak, M., Kirch, K., Kistryn, S., Knappe-Gruneberg, S., Knecht, A., Knowles, P., Kozela, A., Lauss, B., Lefort, T., Lemiere, Y., Naviliat-Cuncic, O., Pendlebury, J., Pierre, E., Piegsa, F., Pignol, G., Quemener, G., Roccia, S., Schmidt-Wellenburg, P., Shiers, D., Smith, K., Schnabel, A., Trahms, L., Weis, A., Zejma, J., Zenner, J., and Zsigmond, G. (2011). The search for the neutron electric dipole moment at the paul scherrer institute. *Physics Procedia*, 17(0):159 – 167. 2nd International Workshop on the Physics of fundamental Symmetries and Interactions - PSI2010. 145

[Baker et al., 2014] Baker, C., Chibane, Y., Chouder, M., Geltenbort, P., Green, K., Harris, P., Heckel, B., Iaydjiev, P., Ivanov, S., Kilvington, I., Lamoreaux, S., May, D., Pendlebury, J., Richardson, J., Shiers, D., Smith, K., and van der Grinten, M. (2014). Apparatus for measurement of the electric dipole moment of the neutron using a cohabiting atomic-mercury magnetometer. *Nuclear Instruments and Methods in Physics Research Section A: Accelerators, Spectrometers, Detectors and Associated Equipment*, 736:184 – 203. `doi:http://dx.doi.org/10.1016/j.nima.2013.10.005`. 168

[Ban et al., 2016] Ban, G., Bison, G., Bodek, K., Chowdhuri, Z., Geltenbort, P., Griffith, W., Helaine, V., Henneck, R., Kasprzak, M., Kermaidic, Y., Kirch, K., Komposch, S., Koss, P.,

Kozela, A., Krempel, K., Lauss, B., Lefort, T., Lemiere, Y., Mtchedlishvili, A., Musgrave, M., Naviliat-Cuncic, O., Piegsa, F. M., Pierre, E., Pignol, G., Quemener, G., Rawlik, M., Ries, D., Rebreyend, D., Roccia, S., Rogel, G., Schmidt-Wellenburg, P., Severijns, N., Wursten, E., Zejma, J., , and Zsigmond, G. (2016). Ultracold neutron detection with ^{6}Li-doped glass scintillators. *The European Physical Journal A - Hadrons and Nuclei*. 146

[Becker et al., 2015] Becker, H., Bison, G., Blau, B., Chowdhuri, Z., Eikenberg, J., Fertl, M., Kirch, K., Lauss, B., Perret, G., Reggiani, D., Ries, D., Schmidt-Wellenburg, P., Talanov, V., Wohlmuther, M., and Zsigmond, G. (2015). Neutron production and thermal moderation at the psi ucn source. *Nuclear Instruments and Methods in Physics Research Section A*, 777(0):20–27. `doi:10.1016/j.nima.2014.12.091`. 30, 39, 40, 205

[Bison et al., 2016] Bison, G., Burri, F., Daum, M., Kirch, K., Krempel, J., Lauss, B., Meier, M., Ries, D., Schmidt-Wellenburg, P., and Zsigmond, G. (2016). An ultracold neutron storage bottle for ucn density measurements. `arXiv:1606.01804`. 206

[Broussard et al., 2013] Broussard, L. et al. (2013). UCNB: The Neutrino Asymmetry in Polarized Ultracold Neutron Decay. In Fleming, B, editor, *11TH CONFERENCE ON THE INTERSECTIONS OF PARTICLE AND NUCLEAR PHYSICS (CIPANP 2012)*, volume 1560 of *AIP Conference Proceedings*, pages 149–151. AMER INST PHYSICS. `doi:10.1063/1.4826741`. 24, 145

[Brys, 2007] Brys, T. (2007). *Extraction of ultracold neutrons from a solid deuterium source*. PhD thesis, ETH Zürich, No.17350. 48

[Chupp and Ramsey-Musolf, 2015] Chupp, T. and Ramsey-Musolf, M. (2015). Electric dipole moments: A global analysis. *Phys. Rev. C*, 91:035502. `doi:10.1103/PhysRevC.91.035502`. 23

[Cyburt et al., 2016] Cyburt, R. H., Fields, B. D., Olive, K. A., and Yeh, T.-H. (2016). Big bang nucleosynthesis: Present status. *Rev. Mod. Phys.*, 88:015004. `doi:10.1103/RevModPhys.88.015004`. 23

[D.B. Pelowitz, Ed., 2011] D.B. Pelowitz, Ed. (2011). Mcnpx users manual version 2.7.0. *LA-CP-11-00438*. 39

[Dölling et al., 2005] Dölling, R., Duperrex, P. A., Erne, R., Frei, U., Graf, M., Müller, U., Rezzonico, R., Rohrer, U., and Thomsen, K. (2005). Beam diagnostics at the high power proton beam lines and targets at PSI. In *7th European Workshop on Beam Diagnostics and Instrumentation for Particle Accelerators (DIPAC 2005) Lyon, France, June 6-8, 2005*, pages 226–230. URL: `http://accelconf.web.cern.ch/AccelConf/d05/PAPERS/ITTA02.PDF`. 81

[Engel et al., 2013] Engel, J., Ramsey-Musolf, M. J., and van Kolck, U. (2013). Electric dipole moments of nucleons, nuclei, and atoms: The standard model and beyond. *Progress in Particle and Nuclear Physics*, 71:21 – 74. Fundamental Symmetries in the Era of the {LHC}. URL: `http://www.sciencedirect.com/science/article/pii/S0146641013000227`, `doi:http://dx.doi.org/10.1016/j.ppnp.2013.03.003`. 23

[EPICS, 2016] EPICS (2016). Experimental physics and industrial control system. `http://www.aps.anl.gov/epics/index.php`. Accessed: 2016-02-14. 201

[Ezhov et al., 2014] Ezhov, V. F. et al. (2014). Measurement of the neutron lifetime with ultra-cold neutrons stored in a magneto-gravitational trap. `arXiv:1412.7434`. 145

[Fermi, E. and Amaldi, E, 1936] Fermi, E. and Amaldi, E (1936). On the Motion of Neutrons in Hydrogeneous Substances. *Ricerca Scientifica*, 7:13–52. English translation: G. M. Tenner, 'ENRICO FERMI - COLLECTED PAPERS (NOTE E MEMORIE) VOLUME 1 ITALY 1921-1938', The University of Chicago Press, (1962), 980-1016. URL: `http://www.lincei.it/modules.php?name=Content&pa=showpage&pid=125`. 22

[Fermi, E. and Zinn, W, 1944] Fermi, E. and Zinn, W (1944). COLLIMATION OF NEUTRON BEAM FROM THERMAL COLUMN OF CP-3 AND THE INDEX OF REFRACTION FOR THERMAL NEUTRONS. *Not published*. Excerpt from Report CP-1965 for Month Ending July 29, 1944, 'Enrico Fermi. Note e Memorie (Collected Papers), vol. II, United States 1939-1954', Roma 1965, published by the Accademia Nazionale dei Lincei, 425-427. URL: `http://www.lincei.it/modules.php?name=Content&pa=showpage&pid=125`. 21

[Fermi, E. and Zinn, W.H., 1946] Fermi, E. and Zinn, W.H. (1946). Reflection of neutrons on mirrors. *Phys. Rev.*, 70:103. 21

[Frank et al., 2009] Frank, A., Geltenbort, P., Jentschel, M., Kulin, G., Kustov, D., Nosov, V., and Strepetov, A. (2009). New test of the weak equivalence principle for neutrons. *Nuclear Instruments and Methods in Physics Research Section A: Accelerators, Spectrometers, Detectors and Associated Equipment*, 611(2–3):314 – 317. Particle Physics with Slow Neutrons. `doi:http://dx.doi.org/10.1016/j.nima.2009.07.088`. 24

[Göltl, 2008] Göltl, L. (2008). Measurements and procedures for the construction and characterization of ultra-cold neutron guides. Master's thesis (Diplomarbeit), University of Heidelberg and University of Mainz. 157

[Göltl et al., 2013] Göltl, L., Chowdhuri, Z., Fertl, M., Gray, F., Henneck, R., Kirch, K., Lauss, B., Lefort, T., Mtchedlishvili, A., Schmidt-Wellenburg, P., and Zsigmond, G. (2013). An endoscopic detector for ultracold neutrons. *The European Physical Journal A*, 49(1):1–9. `doi:10.1140/epja/i2013-13009-8`. 146

[Golub and Boenig, 1983] Golub, R. and Boenig, K. (1983). New type of low temperature source of ultra-cold neutrons and production of continous beams of ucn. *Z. Phys. B*, 51:95. `doi:10.1007/BF01308763`. 42

[Golub, R. and Richardson, D. and Lamoreaux, S.K., 1991] Golub, R. and Richardson, D. and Lamoreaux, S.K. (1991). *Ultra-Cold Neutrons*. Adam Hilger. 32

[Grillenberger et al., 2013] Grillenberger, J., Humbel, M., Mezger, A., Seidel, M., and Tron, W. (2013). Status and further development of the PSI high intensity proton facility. *Proceedings of Cyclotrons2013, Vancouver, BC, Canada*, MOPPT004:1. 101

[Göltl, 2012] Göltl, L. (2012). *Characterization of the PSI ultra-cold neutron source.* PhD thesis, ETH Zürich, No.20350. 29, 49, 53, 55, 67, 68, 74

[Hahn and Strassmann, 1939] Hahn, O. and Strassmann, F. (1939). Über den nachweis und das verhalten der bei der bestrahlung des urans mittels neutronen entstehenden erdalkalimetalle. *Naturwissenschaften*, 27(1):11–15. URL: `http://dx.doi.org/10.1007/BF01488241`, `doi:10.1007/BF01488241`. 25

[Hua, 2014] Hua, Z. D. (2014). The Total Scattering Cross Section of Ultracold Neutrons in Gaseous Deuterium. Master's thesis, ETH Zürich. 109

[Ito, 2007] Ito, T. M. (2007). Plans for a neutron edm experiment at sns. *Journal of Physics: Conference Series*, 69(1):012037. URL: `http://stacks.iop.org/1742-6596/69/i=1/a=012037`. 145

[Jenke et al., 2014] Jenke, T., Cronenberg, G., Burgdörfer, J., Chizhova, L. A., Geltenbort, P., Ivanov, A. N., Lauer, T., Lins, T., Rotter, S., Saul, H., Schmidt, U., and Abele, H. (2014). Gravity resonance spectroscopy constrains dark energy and dark matter scenarios. *Phys. Rev. Lett.*, 112:151105. `doi:10.1103/PhysRevLett.112.151105`. 24

[Jenke et al., 2011] Jenke, T., Geltenbort, P., Lemmel, H., and Abele, H. (2011). Realization of a gravity-resonance-spectroscopy technique. *Nat Phys*, 7(6):468–472. `doi:10.1038/nphys1970`. 24, 145

[Karch et al., 2014] Karch, J., Sobolev, Y., Beck, M., Eberhardt, K., Hampel, G., Heil, W., Kieser, R., Reich, T., Trautmann, N., and Ziegner, M. (2014). Performance of the solid deuterium ultra-cold neutron source at the pulsed reactor TRIGA mainz. *Eur. Phys. J. A*, 50(4):78. `doi:10.1140/epja/i2014-14078-9`. 179

[Komposch, 2012] Komposch, S. (2012). Untersuchungen zur Charakterisierung der Quelle fuer ultrakalte Neutronen am Paul Scherrer Institut. Master's thesis (Diplomarbeit), Johannes Gutenberg Universitaet Mainz. 49, 195

[Lamoreaux and Golub, 2009] Lamoreaux, S. K. and Golub, R. (2009). Experimental searches for the neutron electric dipole moment. *Journal of Physics G: Nuclear and Particle Physics*, 36(10):104002. `doi:10.1088/0954-3899/36/10/104002`. 23

[Lauer and Zechlau, 2013] Lauer, T. and Zechlau, T. (2013). A prospective pulsed source of ultra-cold neutrons for experiments in fundamental neutron physics. *The European Physical Journal A*, 49(8):1–6. `doi:10.1140/epja/i2013-13104-x`. 179

[Lauss, 2016] Lauss, B. (2016). personal communication. 60

[Leung et al., 2016] Leung, K. K. H., Ivanov, S., Piegsa, F. M., Simson, M., and Zimmer, O. (2016). Ultracold-neutron production and up-scattering in superfluid helium between 1.1 k and 2.4 k. *Phys. Rev. C*, 93:025501. `doi:10.1103/PhysRevC.93.025501`. 160

[Lushikov et al., 1969] Lushikov, V. I., Pokotilovskii, Y. N., Strelkov, A. V., and Shapiro, F. L. (1969). Observation of ultracold neutrons. *JETP Letters*, 9:23 – 26. URL: `http://www.jetpletters.ac.ru/ps/1639/article_25024.shtml`. 22

[Marciano and Sirlin, 2006] Marciano, W. J. and Sirlin, A. (2006). Improved calculation of electroweak radiative corrections and the value of V_{ud}. *Phys. Rev. Lett.*, 96:032002. `doi:10.1103/PhysRevLett.96.032002`. 23

[Meitner and Frisch, 1939] Meitner, L. and Frisch, O. R. (1939). Disintegration of uranium by neutrons: a new type of nuclear reaction. *Nature*, 143(3615):239–240. `doi:10.1038/143239a0`. 25

[Mendenhall et al., 2013] Mendenhall, M. P., Pattie, R. W., Bagdasarova, Y., Berguno, D. B., Broussard, L. J., Carr, R., Currie, S., Ding, X., Filippone, B. W., García, A., Geltenbort, P., Hickerson, K. P., Hoagland, J., Holley, A. T., Hong, R., Ito, T. M., Knecht, A., Liu, C.-Y., Liu, J. L., Makela, M., Mammei, R. R., Martin, J. W., Melconian, D., Moore, S. D., Morris, C. L., Pérez Galván, A., Picker, R., Pitt, M. L., Plaster, B., Ramsey, J. C., Rios, R., Saunders, A., Seestrom, S. J., Sharapov, E. I., Sondheim, W. E., Tatar, E., Vogelaar, R. B., VornDick, B., Wrede, C., Young, A. R., and Zeck, B. A. (2013). Precision measurement of the neutron β-decay asymmetry. *Phys. Rev. C*, 87:032501. `doi:10.1103/PhysRevC.87.032501`. 24, 145

[Morris et al., 2002] Morris, C. L., Anaya, J. M., Bowles, T. J., Filippone, B. W., Geltenbort, P., Hill, R. E., Hino, M., Hoedl, S., Hogan, G. E., Ito, T. M., Kawai, T., Kirch, K., Lamoreaux, S. K., Liu, C.-Y., Makela, M., Marek, L. J., Martin, J. W., Mortensen, R. N., Pichlmaier, A., Saunders, A., Seestrom, S. J., Smith, D., Teasdale, W., Tipton, B., Utsuro, M., Young, A. R., and Yuan, J. (2002). Measurements of ultracold-neutron lifetimes in solid deuterium. *Phys. Rev. Lett.*, 89:272501. `doi:10.1103/PhysRevLett.89.272501`. 31, 41

[Nesvizhevsky et al., 2002] Nesvizhevsky, V. V., Borner, H. G., Petukhov, A. K., Abele, H., Baeszler, S., Ruesz, F. J., Stoferle, T., Westphal, A., Gagarski, A. M., Petrov, G. A., and Strelkov, A. V. (2002). Quantum states of neutrons in the earth's gravitational field. *Nature*, 415(6869):297–299. `doi:10.1038/415297a`. 24, 145

[Olive et al., 2014] Olive, K. A. et al. (2014). Review of Particle Physics. *Chin. Phys.*, C38:090001. `doi:10.1088/1674-1137/38/9/090001`. 23

[Pendlebury et al., 2015] Pendlebury, J. M., Afach, S., Ayres, N. J., Baker, C. A., Ban, G., Bison, G., Bodek, K., Burghoff, M., Geltenbort, P., Green, K., Griffith, W. C., van der Grinten, M., Grujić, Z. D., Harris, P. G., Hélaine, V., Iaydjiev, P., Ivanov, S. N., Kasprzak, M., Kermaidic, Y., Kirch, K., Koch, H.-C., Komposch, S., Kozela, A., Krempel, J., Lauss, B., Lefort, T., Lemière, Y., May, D. J. R., Musgrave, M., Naviliat-Cuncic, O., Piegsa, F. M., Pignol, G., Prashanth, P. N., Quéméner, G., Rawlik, M., Rebreyend, D., Richardson, J. D., Ries, D., Roccia, S., Rozpedzik, D., Schnabel, A., Schmidt-Wellenburg, P., Severijns, N., Shiers, D., Thorne, J. A., Weis, A., Winston, O. J., Wursten, E., Zejma, J., and Zsigmond, G. (2015). Revised experimental upper limit on the electric dipole moment of the neutron. *Phys. Rev. D*, 92:092003. `doi:10.1103/PhysRevD.92.092003`. 23, 145

[Pichlmaier et al., 2010] Pichlmaier, A., Varlamov, V., Schreckenbach, K., and Geltenbort, P. (2010). Neutron lifetime measurement with the {UCN} trap-in-trap {MAMBO} {II}. *Physics Letters B*, 693(3):221 – 226. `doi:http://dx.doi.org/10.1016/j.physletb.2010.08.032.` 22

[Plonka-Spehr et al., 2010] Plonka-Spehr, C., Kraft, A., Iaydjiev, P., Klepp, J., Nesvizhevsky, V., Geltenbort, P., and Lauer, T. (2010). An optical device for ultra-cold neutrons—investigation of systematic effects and applications. *Nuclear Instruments and Methods in Physics Research Section A: Accelerators, Spectrometers, Detectors and Associated Equipment*, 618(1–3):239 – 247. `doi:http://dx.doi.org/10.1016/j.nima.2010.02.110.` 24

[Ramsey, 1982] Ramsey, N. F. (1982). Electric-dipole moments of particles. *Annual Review of Nuclear and Particle Science*, 32(1):211–233. `doi:10.1146/annurev.ns.32.120182.001235.` 23

[Sakharov, A. D., 1967] Sakharov, A. D. (1967). Violation of CP Invariance, C Asymmetry, and Baryon Asymmetry of the Universe. *JETP Letters*, 5:24. URL: `http://www.jetpletters.ac.ru/ps/1643/article_25089.shtml.` 23

[Salvat et al., 2014] Salvat, D. J., Adamek, E. R., Barlow, D., Bowman, J. D., Broussard, L. J., Callahan, N. B., Clayton, S. M., Cude-Woods, C., Currie, S., Dees, E. B., Fox, W., Geltenbort, P., Hickerson, K. P., Holley, A. T., Liu, C.-Y., Makela, M., Medina, J., Morley, D. J., Morris, C. L., Penttilä, S. I., Ramsey, J., Saunders, A., Seestrom, S. J., Sharapov, E. I., Sjue, S. K. L., Slaughter, B. A., Vanderwerp, J., VornDick, B., Walstrom, P. L., Wang, Z., Womack, T. L., and Young, A. R. (2014). Storage of ultracold neutrons in the magneto-gravitational trap of the UCNτ experiment. *Phys. Rev. C*, 89:052501. `doi:10.1103/PhysRevC.89.052501.` 145

[Saunders et al., 2013] Saunders, A., Makela, M., Bagdasarova, Y., Back, H. O., Boissevain, J., Broussard, L. J., Bowles, T. J., Carr, R., Currie, S. A., Filippone, B., Garcia, A., Geltenbort, P., Hickerson, K. P., Hill, R. E., Hoagland, J., Hoedl, S., Holley, A. T., Hogan, G., Ito, T. M., Lamoreaux, S., Liu, C.-Y., Liu, J., Mammei, R. R., Martin, J., Melconian, D., Mendenhall, M. P., Morris, C. L., Mortensen, R. N., Pattie, R. W., Pitt, M., Plaster, B., Ramsey, J., Rios, R., Sallaska, A., Seestrom, S. J., Sharapov, E. I., Sjue, S., Sondheim, W. E., Teasdale, W., Young, A. R., VornDick, B., Vogelaar, R. B., Wang, Z., and Xu, Y. (2013). Performance of the los alamos national laboratory spallation-driven solid-deuterium ultra-cold neutron source. *Review of Scientific Instruments*, 84(1). `doi:10.1063/1.4770063.` 150

[Seaborg, 1937] Seaborg, G. T. (1937). *The interaction of fast neutrons with lead*. PhD thesis, University of California, Berkeley, USA. 25

[Seidel et al., 2010] Seidel, M., Adam, S., Adelmann, A., Baumgarten, C., Bi, Y., Dölling, R., Fitze, H., Fuchs, A., Humbel, M., Grillenberger, J., Kiselev, D., Mezger, A., Reggiani, D., Schneider, M., Yang, J., Zhang, H., and Zhang, T. (2010). Production of a 1.3 mw proton beam at psi. *Proceedings of IPAC'10, Kyoto, Japan*, TUYRA03:1309. 30, 101

[Seiffert, 1970] Seiffert, W.-D. (1970). Messung der streuquerschnitte von flüssigem und festem wasserstoff, deuterium und deuteriumhydrid für thermische neutronen. *Euratom Report NO. EUR 4455d.* 41

[Serebrov et al., 2005] Serebrov, A., Varlamov, V., Kharitonov, A., Fomin, A., Pokotilovski, Y., Geltenbort, P., Butterworth, J., Krasnoschekova, I., Lasakov, M., Taľdaev, R., Vassiljev, A., and Zherebtsov, O. (2005). Measurement of the neutron lifetime using a gravitational trap and a low-temperature fomblin coating. *Physics Letters B*, 605(1–2):72 – 78. `doi:http://dx.doi.org/10.1016/j.physletb.2004.11.013.` 22, 145

[Serebrov et al., 2015] Serebrov, A. P., Kolomenskiy, E. A., Pirozhkov, A. N., Krasnoshekova, I. A., Vasiliev, A. V., Polyushkin, A. O., Lasakov, M. S., Murashkin, A. N., Solovey, V. A., Fomin, A. K., Shoka, I. V., Zherebtsov, O. M., Geltenbort, P., Ivanov, S. N., Zimmer, O., Alexandrov, E. B., Dmitriev, S. P., and Dovator, N. A. (2015). New measurements of the neutron electric dipole moment with the petersburg nuclear physics institute double-chamber electric dipole moment spectrometer. *Physics of Particles and Nuclei Letters*, 12(2):286–296. `doi:10.1134/S1547477115020193.` 145

[Shapiro, 1968] Shapiro, F. L. (1968). Electric dipole moments of elementary particles. *Soviet Physics Uspekhi*, 11(3):345. URL: `http://stacks.iop.org/0038-5670/11/i=3/a=A11`, `doi:10.1070/PU1968v011n03ABEH003840.` 22

[Souers, 1986] Souers, P. C. (1986). *Hydrogen properties for fusion research.* Univ. of California Press, Berkeley-Los Angeles-London. 41, 108

[Steyerl et al., 1986] Steyerl, A., Nagel, H., Schreiber, F.-X., Steinhauser, K.-A., Gaehler, R., Glaeser, W., Ageron, P., Astruc, J., Drexel, W., Gervais, G., and Mampe, W. (1986). A new source of cold and ultracold neutrons. *Physics Letters A*, 116(7):347 – 352. `doi:10.1016/0375-9601(86)90587-6.` 168

[Wang et al., 2015] Wang, Z., Hoffbauer, M., Morris, C., Callahan, N., Adamek, E., Bacon, J., Blatnik, M., Brandt, A., Broussard, L., Clayton, S., Cude-Woods, C., Currie, S., Dees, E., Ding, X., Gao, J., Gray, F., Hickerson, K., Holley, A., Ito, T., Liu, C.-Y., Makela, M., Ramsey, J., Jr., R. P., Salvat, D., Saunders, A., Schmidt, D., Schulze, R., Seestrom, S., Sharapov, E., Sprow, A., Tang, Z., Wei, W., Wexler, J., Womack, T., Young, A., and Zeck, B. (2015). A multilayer surface detector for ultracold neutrons. *Nuclear Instruments and Methods in Physics Research Section A: Accelerators, Spectrometers, Detectors and Associated Equipment*, 798:30 – 35. `doi:http://dx.doi.org/10.1016/j.nima.2015.07.010.` 157

[Wietfeldt and Greene, 2011] Wietfeldt, F. E. and Greene, G. L. (2011). *Colloquium* : The neutron lifetime. *Rev. Mod. Phys.*, 83:1173–1192. `doi:10.1103/RevModPhys.83.1173.` 23

[Wohlmuther and Heidenreich, 2006] Wohlmuther, M. and Heidenreich, G. (2006). The spallation target of the ultra-cold neutron source UCN at PSI. *Nuclear Instruments and Methods A*, 564:51. 30

[Young and Koppel, 1964] Young, J. A. and Koppel, J. U. (1964). Slow neutron scattering by molecular hydrogen and deuterium. *Phys. Rev.*, 135:A603–A611. 119

[Yu et al., 1986] Yu, Z.-C., Malik, S., and Golub, R. (1986). A thin film source of ultra-cold neutrons. *Z. Phys. B*, 62:137. `doi:10.1007/BF01323423`. 42

[Zel'dovich, Z. B., 1959] Zel'dovich, Z. B. (1959). Storage of Cold Neutrons. *Sov. Phys. JETP*, 9:1389. URL: `http://www.jetp.ac.ru/cgi-bin/e/index/e/9/6/p1389?a=list`. 22

[Zsigmond, 2015] Zsigmond, G. (2015). personal communication. 30, 60, 120